

**Plastidic Phosphoenolpyruvate:  
Investigations on its role in plant growth and  
development**

**Inaugural-Dissertation**

**zur**

**Erlangung des Doktorgrades  
der Mathematisch-Naturwissenschaftlichen Fakultät  
der Universität zu Köln**

**vorgelegt von**

**Veena Prabhakar**

**aus Bangalore, Indien**

Berichterstatter:

Prof. Dr. Ulf-Ingo Flügge

Prof. Dr. Sabine Waffenschmidt

Tag der mündlichen Prüfung:

1st Februar 2010

## **Dedication**

This thesis is dedicated to my loving mother **Suriyakala**, who has raised me to be the person I am today and to my lovely daughter **Prateeksha**.

Mom, I want to thank you for your constant support, encouragement and instilling in me the confidence that I am capable of doing anything I put my mind to.

**Thank You !**

Two roads diverged in a wood, and I-  
I took the one less traveled by,  
And that has made all the difference.

-Robert Frost

## Index

<b>1.</b>	<b>Introduction</b>	1
1.1	Plant Glycolysis	1
1.2	Phosphoenolpyruvate (PEP)	2
1.3	Enolase	5
1.4	Phosphoglycerate mutase	6
1.5	Phosphoenolpyruvate/phosphate translocator (PPT)	7
1.6	PEP as a substrate for shikimate pathway	9
1.7	PEP via pyruvate as a substrate for fatty acid synthesis (FAS)	10
1.8	PEP via pyruvate as a substrate for the synthesis of branched chain amino acids	13
1.9	PEP as a substrate for plastid methylerythritol-phosphate (MEP) pathway of isoprenoid biosynthesis	14
<b>2.</b>	<b>Materials and methods</b>	17
2.1	Materials	17
2.1.1	Chemicals	17
2.1.2	Enzymes	17
2.1.3	Kits	17
2.1.4	Antibiotics	17
2.1.5	Bacteria	18
2.1.6	Plant lines	19
2.1.7	Software	19
2.1.8	Vectors	20
2.2	Methods	20
2.2.1	Plant methods ( <i>Arabidopsis thaliana</i> )	20
2.2.1.1	Growth conditions	20
2.2.1.1.1	Greenhouse	20
2.2.1.1.2	Temperature controlled climate chamber	20
2.2.1.1.3	Growth of <i>A. thaliana</i> on sterile media	21
2.2.1.1.4	Sterilization of <i>A. thaliana</i> seeds	21
2.2.1.1.5	Dry sterilization of seeds using chlorine gas	21
2.2.1.1.6	Liquid/wet sterilization	21

2.2.1.2	Preparation of media for <i>A. thaliana</i> plants	22
2.2.1.3	Plant selection	22
2.2.1.3.1	Selection on MS agar plates	22
2.2.1.3.2	BASTA Selection	22
2.2.1.4	Transformation of <i>A. thaliana</i> using vacuum infiltration	23
2.2.1.5	GUS staining	23
2.2.1.6	Screening of T-DNA insertion lines	23
2.2.1.7	Crossing of <i>A. thaliana</i> plants	24
2.2.1.8	<i>A. thaliana</i> cell cultures	24
2.2.1.8.1	Maintenance of cell cultures	24
2.2.1.8.2	Cell culture transformation	25
2.2.2	Microbiological methods	25
2.2.2.1	Growth and transformation of <i>Escherichia coli</i>	25
2.2.2.1.1	Media	25
2.2.2.1.2	Growth of <i>E.coli</i>	26
2.2.2.1.3	Preparation of competent cells ( <i>E.coli</i> )	26
2.2.2.1.4	Transformation of <i>E.coli</i>	27
2.2.2.2	Growth and transformation of <i>Agrobacterium tumefaciens</i>	27
2.2.2.2.1	Media	25
2.2.2.2.2	Growth of <i>A. tumefaciens</i>	27
2.2.2.2.3	Preparation of competent cells of <i>A. tumefaciens</i>	27
2.2.2.2.4	Transformation of <i>A. tumefaciens</i> by electroporation	28
2.2.3	Molecular biological methods	28
2.2.3.1	Plasmid isolation	28
2.2.3.1.1	Mini preparation	28
2.2.3.1.2	Midi preparation	28
2.2.3.2	Isolation of <i>A. thaliana</i> genomic DNA	28
2.2.3.2.1	Fast Prep (Edwards et al., 1991)	28
2.2.3.2.2	Standard Prep (Liu et al., 1995)	29
2.2.3.3	Expression analysis	29
2.2.3.3.1	RNA isolation (Trisure method)	29
2.2.3.3.2	RNA isolation (Qiagen method)	30
2.2.3.3.3	DNase digestion	30
2.2.3.3.4	Reverse transcription	30

2.2.3.3.5	Photometric determination of nucleic acid concentration	30
2.2.3.3.6	Gel electrophoresis	30
2.2.3.4	Enzymatic analysis of DNA	31
2.2.3.4.1	Restriction digestion	31
2.2.3.4.2	De-Phosphorylation of Cloning vectors	31
2.2.3.4.3	Ligation of DNA fragments	32
2.2.3.4.4	Gateway cloning	32
2.2.3.4.5	Sequencing	32
2.2.3.5	Polymerase Chain Reaction	33
2.2.3.5.1	Standard PCR	33
2.2.3.5.2	Colony PCR	34
2.2.3.5.3	Semi-quantitative RT-PCR	34
2.2.3.5.4	Real-Time PCR	34
2.2.4	Biochemical methods	34
2.2.4.1	Protein extraction from <i>E. coli</i>	34
2.2.4.2	Protein extraction from <i>A. thaliana</i> seeds	35
2.2.4.3	Enrichment of proteins by Nickel-NTA affinity chromatography	35
2.2.4.4	Separation of proteins by SDS-PAGE	35
2.2.4.5	Staining of Proteins	36
2.2.4.5.1	Protein staining with Coomassie-Brilliant Blue	36
2.2.4.5.2	Protein staining with Silver nitrate	37
2.2.4.6	Western Blotting	38
2.2.4.7	Immunological detection of proteins on PVDF membrane	38
2.2.4.8	Determination of protein concentration	39
2.2.4.8.1	Standard method (Bradford 1976)	39
2.2.4.8.2	Detergent-compatible protein assay	39
2.2.4.9	Enzyme activity assay for enolase	40
2.2.4.10	Total fatty acid analysis in seeds	41
2.2.4.11	Amino acid analysis in mature flowers	41
2.2.4.12	Determination of flavonoids in mature flowers	41
2.2.4.13	Determination of anthocyanins in mature flowers	41
2.2.4.14	Determination of soluble sugars and starch in seeds	42
2.2.5	Histochemical methods	43
2.2.5.1	Alexander's staining	43

2.2.5.2	DAPI staining	43
2.2.5.3	ACN staining	43
2.2.5.4	Histochemical localization of secondary metabolites in pollen	43
2.2.6	Microscopy	44
2.2.6.1	Transmission electron microscopy	44
2.2.6.2	Scanning electron microscopy	44
2.2.6.3	Differential Interference Contrast (DIC) microscopy	44
2.2.6.4	Fluorescence microscopy	44
2.2.7	Weblinks used	45
<b>3.</b>	<b>Results</b>	46
3.1	Identification and sub-cellular localization of <i>Arabidopsis thaliana</i> plastidic enolase (ENO1) and cytosolic enolase (ENOC)	46
3.2	Over-expression of ENO1 in <i>E. coli</i>	48
3.3	Recombinant ENO1 exhibits ENO activity; a kinetic characterization	50
3.4	Tissue- and cell-specific expression profiles of <i>ENO1</i>	53
3.5	Identification and characterization of <i>ENO1</i> T-DNA insertion line <i>Ateno1-2</i>	56
3.6	Distorted trichome morphology of homozygous <i>eno1-2</i>	59
3.7	Double knockout of <i>PPT1</i> and <i>ENO1</i> in genetic crosses of <i>cue1</i> and <i>eno1</i> mutant is lethal	60
3.8	Segregation pattern and transmission efficiency of <i>cue1/eno1</i> (+/-) mutants	61
3.9	Phenotypic analysis of <i>cue1/eno1</i> (+/-) double mutants	64
3.10	Expression profile of <i>ENO1</i> in <i>cue1/eno1</i> (+/-) double mutant shoot apex and young roots	68
3.11	Phenotypic characterization of female gametophyte of the <i>cue1/eno1</i> (+/-) double mutants	69
3.11.1	Ovule analysis	69
3.12	Seed analysis	71
3.13	Phenotypic characterization of male gametophyte of <i>cue1/eno1</i> (+/-) double mutants	74
3.13.1	Cross-section of anthers	74
3.13.2	Analysis of pollen viability and structure	75
3.13.2.1	Pollen viability analysis	75

3.13.2.2	Pollen ultrastructure	77
3.13.2.3	Analysis of phenolic compounds in pollen	79
3.14	Diminished content of aromatic and branched chain amino acids in flowers of <i>cue1/eno1</i> (+/-) mutants	80
3.15	Analysis of secondary plant products in <i>cue1/eno1</i> (+/-) double mutants	83
3.16	Is cuticle wax integrity disturbed in <i>cue1/eno1</i> (+/-) double mutants ?	85
3.17	Expression of <i>KCR1</i> and <i>KCR2</i> in <i>cue1/eno1</i> (+/-) double mutants	86
3.18	Over-expression of <i>ENO1</i> rescues the <i>cue1</i> phenotype	86
3.19	Over-expression of <i>ENO1</i> in <i>los2</i> mutants has no effect	88
3.20	<i>ENO1</i> over-expression restores photosynthetic electron transport in <i>cue1</i> but has no effect in wild-type plants	89
3.21	Does <i>ENO1</i> overexpression lead to overall seed improvement ?	90
3.22	Analysis of seed storage compounds in <i>cue1/eno1</i> (+/-) double mutants	92
<b>4.</b>	<b>Discussion</b>	96
4.1	Phosphoenolpyruvate enolase ( <i>ENO1</i> ) in <i>Arabidopsis thaliana</i> is plastid localized and functional	96
4.2	<i>ENO1</i> is also expressed in trichomes and non-root hair cells	97
4.3	<i>ENO</i> mutants lack a pronounced phenotype in the macroscopic scale	98
4.4	Importance of PEP in plants and the significance of <i>ENO1</i> in plastidic PEP formation	99
4.5	<i>ENO1</i> and <i>PPT1</i> deficiency in plastids leads to partial lethality and aberrant segregation	102
4.6	Limitation of PEP inside plastids leads to gametophyte lethality	103
4.7	Absence of PEP/Pyruvate inside plastids leads to seed abortion	105
4.8	<i>ccEe</i> plants display constraints in vegetative development	106
4.9	Link between cuticle wax biosynthesis and phenotype of <i>ccEe</i> plants	108
4.10	Constitutive overexpression of <i>ENO1</i> rescues the <i>cue1</i> phenotype	109
4.11	Controlling seed production and oil content in <i>A.thaliana</i> : A biotechnological approach	110

<b>5. References</b>	113
<b>Appendix</b>	130
<b>Abbreviations</b>	135
<b>Abstract</b>	139
<b>Zusammenfassung</b>	140
<b>Acknowledgements</b>	142
<b>Erklärung</b>	143
<b>Lebenslauf</b>	144

# 1 Introduction

## 1.1 Plant Glycolysis

Glycolysis is the process responsible for the conversion of monosaccharides to pyruvic acid. It was the first major biochemical pathway to be well characterized and a ubiquitous feature of cellular metabolism (Plaxton, 1996). Various studies of glycolysis have shown, it is the ‘central’ metabolic pathway that is present, at least in part, in all organisms. In plants, glycolysis is the predominant pathway fueling respiration (TCA cycle) because unlike animal mitochondria, plant mitochondria rarely respire fatty acids (ap, Rees 1990). Although a majority of glycolytic enzymes are common to all organisms, glycolysis in higher plants possesses numerous distinctive features. One conspicuous feature of plant glycolysis discovered in the 1970s is the presence of a complete or nearly complete sequence of glycolytic enzymes in plastids (Givan, 1999) which is very distinct and spatially separated from the glycolytic enzymes located in the cytosol. Thus, in plants, glycolysis is both a cytosolic and plastidic process (Fig. 1.1). In the cytosol, glycolysis is involved in catabolism where it degrades sucrose to ultimately form pyruvate which is used as a substrate for fermentation and aerobic respiration (Fernie et al., 2004).

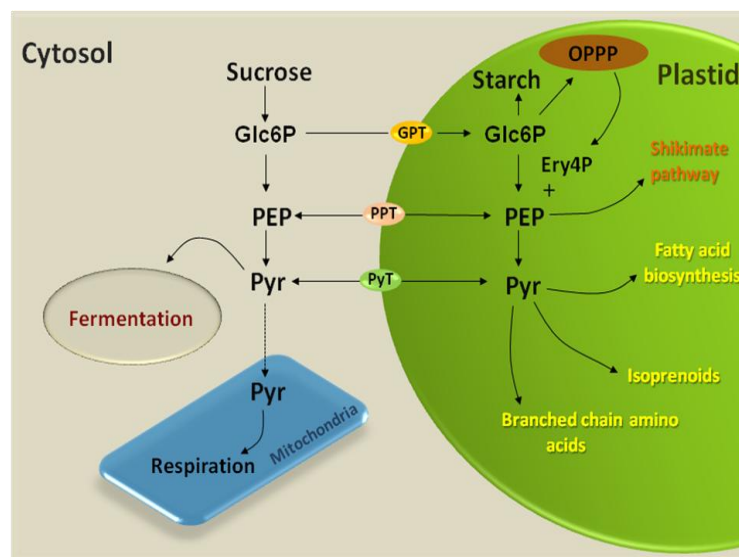


**Figure 1.1: Basic scheme of plant glycolysis in cytosol and plastids.** Glc6P=Glucose 6-phosphate; PEP=Phosphoenolpyruvate; Pyr=Pyruvate; EryP= Erythrose 4-Phosphate; OPPP=Oxidative Pentose Phosphate pathway.

In chloroplasts in dark, as well as plastids in non-photosynthetic tissues, the primary function of glycolysis is to provide metabolites for various biosynthetic pathways such as shikimate pathway, fatty acid biosynthesis, branched chain amino acid synthesis and isoprenoid

biosynthesis, as well as to supply substrates for glycolysis in cytosol (Blakeley and Dennis, 1993; Dennis and Miernyk, 1982; Emes and Tobin, 1993). Plastidic and cytosolic isoenzymes of glycolysis have been shown to differ in their kinetic and regulatory properties suggesting that the two pathways are independently regulated (Givan, 1999). Moreover, these isoenzymes are encoded by distinct nuclear genes (Copeland and Turner, 1987; Hattori et al., 1995; Henze et al., 1994). Compartmentalization of these enzymes and their related metabolites prevents the concurrent occurrence of potentially incompatible metabolic processes (Dennis and Emes, 1990). These pathways can interact with one another through the action of highly selective transporters present in the inner plastid envelope (Emes et al., 1993). Plastidic glycolytic enzymes are thought to be synthesized as inactive precursors on ribosomes in the cytosol followed by their import into the organelle with concomitant cleavage of an N-terminal transit peptide (Dennis and Emes, 1990). Even though plastids from several non-photosynthetic tissues, including developing wheat and castor seeds, have been found to have all the enzymes of glycolysis from glucose to pyruvate, some chloroplasts may lack one or several enzymes of the lower half of the glycolysis pathway (i.e conversion of 3-PGA to PEP via PGyM and ENO ) (Emes and Tobin, 1993). In contrast, the cytosol of many unicellular green algae appears to have either very low activities or are even missing in some of the cytosolic enzymes, whereas their chloroplasts seem to contain the entire sequence of glycolytic enzymes (Huppe and Turpin 1994; Schnarrenberger et al., 1994).

The catabolic role of glycolysis is important to plants with regard to converting potential energy to usable energy during the oxidation of glucose to pyruvate. However, many of the metabolites in the glycolytic pathway are also used by anabolic pathways, and, as a consequence, flux through the pathway is critical to maintain a supply of carbon skeletons for biosynthesis. Thus, an impairment in glycolysis would affect the overall growth and development in plants.

## 1.2 Phosphoenolpyruvate (PEP)

Phosphoenolpyruvate is a central intermediate of metabolism in pro- and eukaryotes. The glycolytic sequence starting from 3-phosphoglycerate (3-PGA), involving phosphoglycerate mutase (PGyM) and enolase (ENO), appears to be the main route for the production of phosphoenolpyruvate (PEP), (Canback et al., 2002). Besides glycolysis (Plaxton, 1996; Givan 1999) in plants, PEP can also be formed from pyruvate by PPDK (pyruvate, orthophosphate dikinase), which is an essential step in C<sub>4</sub>- and crassulacean acid metabolism (CAM)-plants

(Edwards and Nakamoto, 1985) but occurs also in C3-plants (Chastain et al., 2002; Hibberd and Quick, 2002) or from oxaloacetate in gluconeogenesis (Sung et al., 1988) by PEP carboxykinase (PEPCK) (Walker and Chen, 2002; Leegood and Walker 2003). Whereas PPDK in *Arabidopsis thaliana* has been shown to be dually targeted to the cytosol and the plastids (Parsley and Hibberd 2006) PEPCK is localized to the cytosol of plants (Walker and Chen 2002; Leegood and Walker 2003). PEP can also be delivered by the Phosphoenolpyruvate/phosphate translocator (PPT) from the cytosol (Fischer et al., 1997) or generated inside the plastids by a complete glycolytic pathway (Fig. 1.2). However, chloroplasts and most non-green plastids lack the ability to form PEP via glycolysis because the essential enzymes, which converts 3-phosphoglycerate (3-PGA) to PEP, phosphoglycerate mutase (PGyM) and enolase (ENO), are either absent or, if present, show low activity (Stitt and ap Rees, 1979; Schulze-Siebert et al., 1984; Journet and Douce, 1985; Bagge and Larsson, 1986; Van der Straeten et al., 1991; Miernyk and Dennis, 1992; Borchert et al., 1993). In contrast, plastids from lipid storing tissues such as seeds of castor bean (*Ricinus communis*) or canola have been demonstrated biochemically to be capable of catalyzing glycolytic PEP formation (Eastmond and Rawsthorne, 2000).

In the catabolic direction, PEP in cytosol is metabolized to pyruvate by the action of pyruvate kinase (PK), yielding pyruvate, which can enter the citric acid cycle to generate NADH and ATP by the respiratory chain in the mitochondria (Fernie et al., 2004). Besides their catabolic function for energy generation in heterotrophic tissues or in leaves during the dark period, both PEP and pyruvate inside the plastids represent essential precursors for anabolic reactions. PEP, together with erythrose 4-phosphate, is fed into the shikimate pathway, which is localized within the plastid stroma (Herrmann 1995; Schmid and Amrhein, 1995; Hermann and Weaver 1999). The shikimate pathway is essential for the production of aromatic amino acids and a huge variety of secondary plant products. In turn, pyruvate can act as a precursor for (i) for fatty acid biosynthesis (Dennis, 1989; Ohlrogge and Jaworski, 1997) (ii) for the synthesis of branched-chain amino acids (Schulze-Siebert et al., 1984), and together with glyceraldehyde 3-phosphate (iii) for the mevalonate-independent pathway (2-C-methyl-D-erythritol 4-phosphate [MEP] pathway) of isoprenoid biosynthesis (Lichtenthaler, 1999). All these pathways are entirely localized to the plastid stroma (Fig. 1.2).

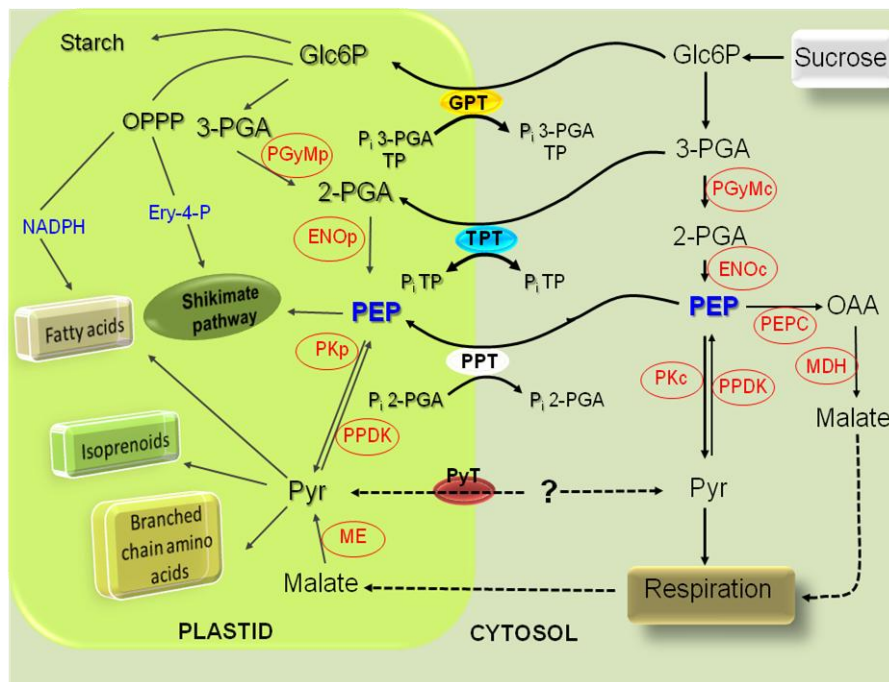


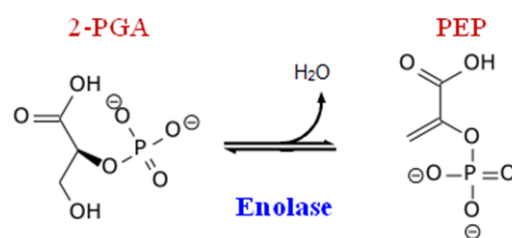
**Figure 1.2: Role of PEP as a central metabolite and its involvement in various biosynthetic pathways.** Glc6P=Glucose 6-Phosphate; OPPP=Oxidative pentose phosphate pathway; 3-PGA=3-phosphoglycerate; 2-PGA= 2-phosphoglycerate; Ery-4-P=Erythrose 4-Phosphate; PEP=Phosphoenolpyruvate; Pyr=Pyruvate; PGyMp=putative plastidic phosphoglycerate mutase; PGyMc=cytosolic phosphoglycerate mutase; ENOp=Putative plastidic enolase; ENOc=cytosolic enolase; PKp=plastidic pyruvate kinase; PKc=cytosolic pyruvate kinase; PPDK=Pyruvate, orthophosphate dikinase; PEPC=PEP carboxylase; MDH=Malate dehydrogenase; ME=Malic enzyme; GPT=Glucose6P/phosphate translocator; PPT=PEP/phosphatetranslocator; TPT=Triosephosphate/phosphate translocator

The supply of PEP to plastids might be a limiting factor determining the biosynthesis of secondary metabolites. A deficiency in the PPT leads to insufficient supply of PEP inside the plastids which affects plant growth and development observed in the *Arabidopsis* mutant *cue1* mutants. Voll et al. (2003) introduced a *PPT* and a *PPDK* respectively into *cue1*, and in both transformants, the mutant phenotype was rescued suggesting that a PEP deficiency within the plastids triggered developmental constraints in *cue1*. In the *cue1/PPT* line, the PEP-specific transport rates increased fivefold above wild-type level, and 24-fold above the *cue1* mutant, whereas total PEP production was not considerably altered compared to the wild type. In contrast, the *cue1/PPDK* lines accumulated substantial amount of PEP (6-fold higher than wild-type plants and mutant) during the photoperiod, indicating that PPDK was active in chloroplasts (Voll et al., 2003). The increase of PEP rescued the synthesis of phenylpropanoids and aromatic amino acids in transgenic plants. In the *cue1* mutant, phenylpropanoids decreased to 25% of wild-type level. Phenylpropanoids seems almost restored to wild-type levels in *cue1/PPDK* and *cue1/PPT* plants. Similarly, a combined deficiency of PPT and plastidic enolase may lead to lethality as they both play an important

role in PEP provision inside plastids. Thus, PEP has a central role in plant metabolism and contributes to various pathways significant for plant development.

### 1.3 Enolase

Enolase (2-phospho-glycerate hydrolase, EC 4.2.1.1) catalyzes the formation of phosphoenolpyruvate from 2-phosphoglycerate (2-PGA). The reaction involves dehydration, the removal of a water molecule, to form the *enol* structure of PEP.



The enzyme has been purified and the genes have been cloned from diverse sources: *E. coli* (Weng et al., 1986), yeast (Chin et al., 1981), spinach (Sinha and Brewer, 1984), tomato and *A. thaliana* (Van der Straeten et al., 1991). Although octameric enzymes have been described, in all eukaryotes and many prokaryotes, enolase is biologically active as a dimer, with subunits having a molecular weight of approximately 45,000 Dalton (Hannaert et al., 2000). Two enolase isozymes, one found in the cytosol and the other localized in the plastid were identified. The cytosolic reaction sequence of glycolysis in plants is well documented (Stitt and ap Rees, 1979), in contrast the occurrence of a complete glycolytic pathway in plastids is still a matter of debate. The plastidic and cytosolic isozymes of enolase from developing endosperm of castor oil seeds, *Ricinus communis* L. cv. *Baker 296*, were separated and partially purified (Miernyk and Dennis 1984) indicating that some plastids contain a complete glycolytic pathway. *A. thaliana* contains three putative enolase genes (TAIR; <http://www.arabidopsis.org/>, Winter et al., 2007), At1g74030 which is, according to *in silico* predictions of an N-terminal target sequence, most likely a plastidic isoform and At2g29560, At2g36530, the putative cytosolic isoforms. (<http://aramemnon.botanik.uni-koeln.de/>; Schwacke et al., 2003). At1g74030 referred to as putative plastidic enolase has a length of 477 amino acids and a molecular mass of 51.5 kDa. *In silico* expression analyzes based on microarray data (<http://bar.utoronto.ca/efp/cgi-bin/efpWeb.cgi>) revealed high expression levels of *ENO1* in roots and siliques (i.e. during embryo development), but a low expression in green tissues, such as leaves or stems (Fig. 1.3).

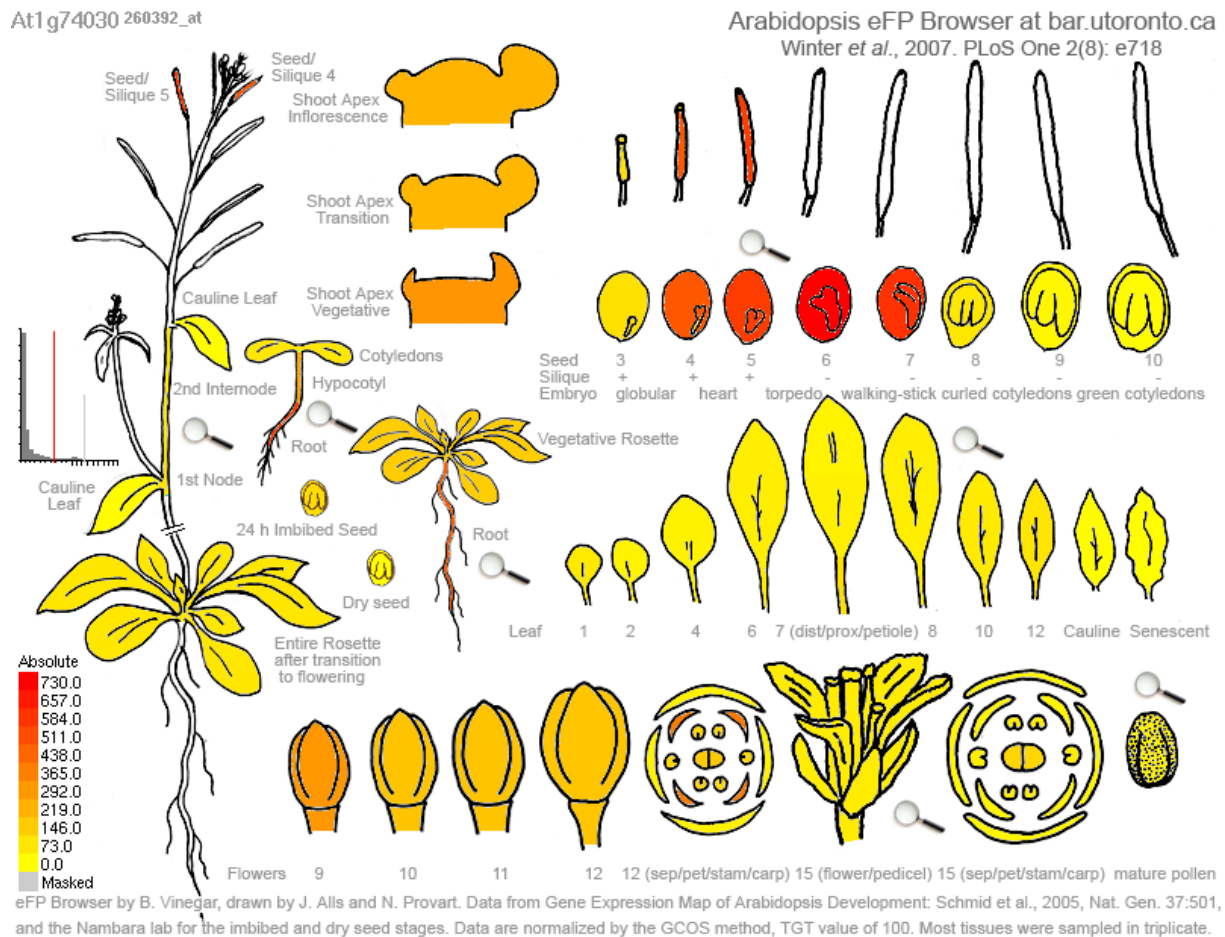
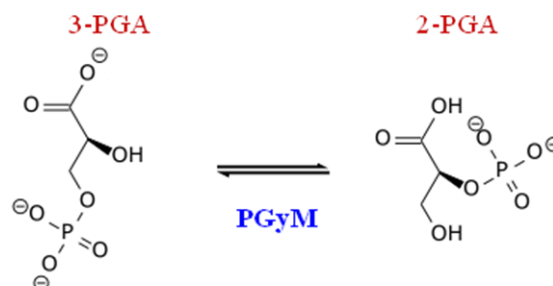


**Figure 1.3:** *In silico* expression analyses of At1g74030 based on microarray data (Arabidopsis eFP browser).

## 1.4 Phosphoglycerate mutase

Phosphoglycerate mutase (EC 5.4.2.1) (PGyM) catalyzes the internal transfer of a phosphate group from C-3 to C-2 which results in the conversion of 3-phosphoglycerate (3-PGA) to 2-phosphoglycerate (2-PGA) through a 2,3-bisphosphoglycerate intermediate.



Two apparently evolutionarily unrelated enzymes with PGyM activity have been characterized. One enzyme (dPGyM) requires the cofactor 2,3-bisphosphoglycerate (2,3-BPGA) for activity, while the other (iPGyM) does not. Vertebrates, budding yeast, and various eubacterial species only have dPGyM, whilst nematodes, archaea, higher plants and various other eubacteria only possess iPGyM. In addition, a small number of eubacteria

appear to encode both enzymes (Fothergill-Gilmore and Watson, 1989). Comparison of kinetic properties and expression levels of the two PGyM of *E. coli* has allowed assessing the metabolic roles of each. Both PGyM isoforms catalyze the interconversion of 2-phosphoglycerate and 3-phosphoglycerate in the glycolytic and gluconeogenic directions, but dPGM has at least a 10-fold higher specific activity for both reactions (Fraser et al., 1999). In plants, two isoenzymes of PGyM have been reported, a cytosolic and a plastidic form. Chloroplasts and some non-green plastids appear to lack PGyM whereas plastids from lipid storing seeds of canola or castor bean, have been shown biochemically to contain a complete set of glycolytic enzymes (Miernyk and Dennis, 1982; 1992; Kang and Rawsthorne, 1994; 1996). The genome of *A. thaliana* contains fifteen putative PGyM genes of which four genes code for proteins with predicted N-terminal transit peptides for plastid targeting (<http://aramemnon.botanik.uni-koeln.de>). At3g50520, At3g05170, At3g08590, At3g26780, At4g09520, At4g38370, At5g04120, At2g17280, At1g09780, At1g08940, At1g12850 are putative cytosolic forms and At1g22170, At5g22620, At5g62840 and At1g78050 are putative plastidic forms. It is not clear whether or not chloroplasts of *A. thaliana* contain a phosphoglycerate mutase, but lack only enolase.

## 1.5 Phosphoenolpyruvate/phosphate translocator (PPT)

Phosphate translocators, in general, catalyze a strict counter exchange of phosphorylated intermediates with either inorganic phosphates or other phosphorylated intermediates. They are divided into four subfamilies, the triosephosphate/phosphate translocators (TPT), the glucose-6P/phosphate translocators (GPT), the phosphoenolpyruvate/phosphate translocators (PPT) and the xylulose-5P/phosphate translocators (XPT). The PPT imports PEP from the cytosol in exchange for inorganic phosphates or 2-PGA (Fischer et al., 1997) (Fig. 1.1). This translocator is able to supply the plastids with PEP even in the presence of triose phosphates and 3-PGA. The *PPT* gene subfamily consists of eight genes, only two of them representing full-length genes (*AtPPT1*, At5g33320; and *AtPPT2*, At3g01550) and six being truncated genes (*AtPPTs1-6*) (Fischer et al., 2003). Both the PPTs show a differential, only partially overlapping tissue-specific expression pattern. *AtPPT1* is mainly expressed in the vasculature of leaves and roots, especially in the xylem parenchyma cells but not in the mesophyll cells, whereas *AtPPT2* is expressed ubiquitously in the leaves, but not in the roots as observed by promoter::GUS or GFP fusions (Knappe et al., 2003). *In silico* expression analyses of *AtPPT1* based on microarray data revealed that it was expressed ubiquitously in the plant especially during early embryo development (Fig. 1.4). The importance of the PPT protein for plant

development became obvious by the analysis of corresponding *A. thaliana* mutants. *AtPPT1* is defective in the *chlorophyll a/b binding protein underexpressed (cue1)* mutant (Li et al., 1995). These mutant plants under-express genes for chloroplast components, both in the light and in response to light pulse and they exhibit a pleiotropic leaf phenotype with dark green paraveinal and light green interveinal regions. The *cue1* mutant alleles are impaired in chloroplast and mesophyll development and show inhibited root growth.

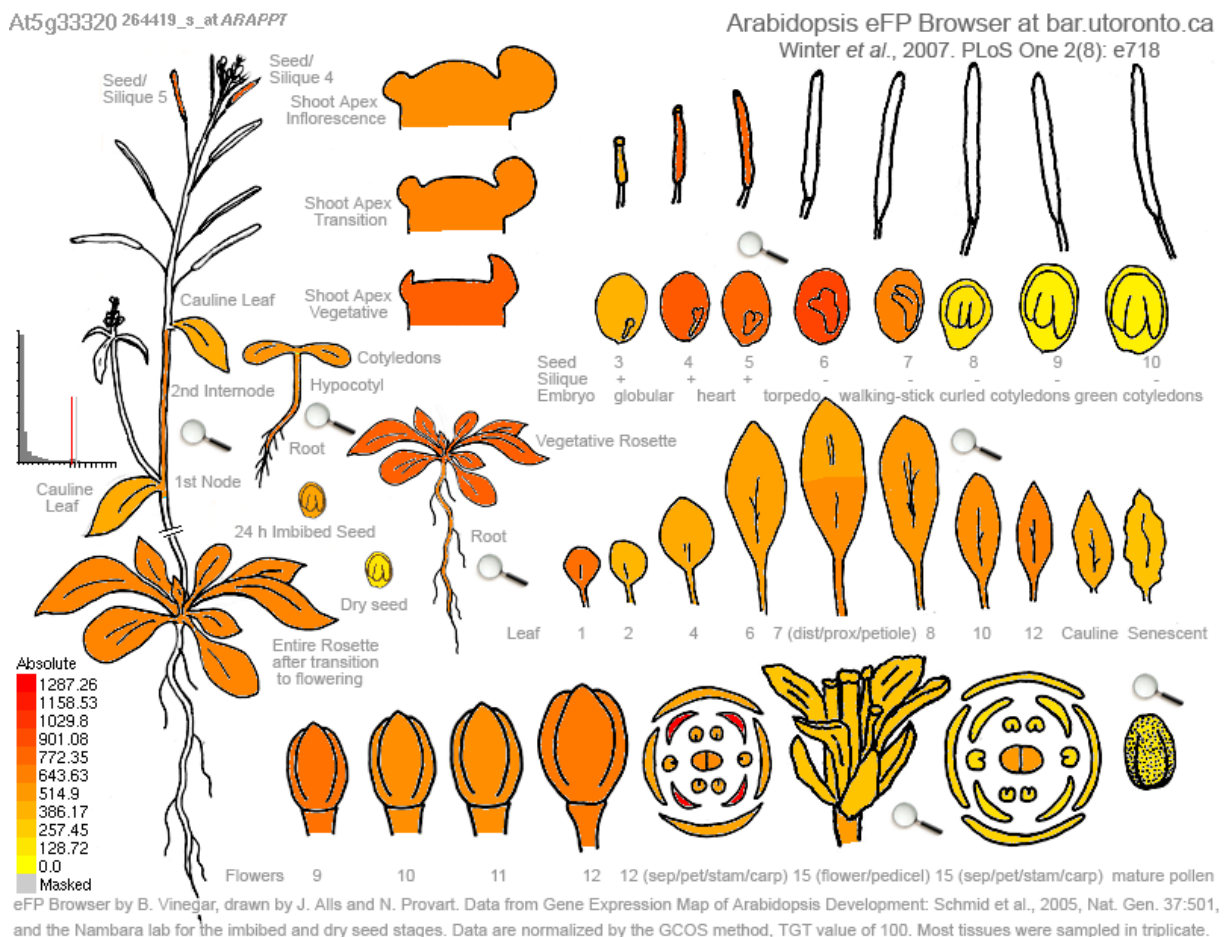


**Figure 1.4:** *In silico* expression analyses of *At5g33320* based on microarray data (Arabidopsis eFP browser).

The proposed physiological role of the PPT in leaves of C3-plants is the supply of PEP to the stroma as a precursor for the shikimate pathway (Voll et al., 2003). It has been reported that the amino acid composition is perturbed in the *cue1* mutants, particularly, Phe was reduced from 20-40% in dark and light respectively, whereas there was a slight increase in Trp and Tyr compared to the wild type (Voll et al., 2003). One can rescue the *cue1* phenotype by feeding a combination of aromatic amino acids to the mutants. The constitutive overexpression of a C4-type pyruvate, orthophosphate dikinase (PPDK), which produces PEP from pyruvate in plastids could rescue the *cue1* phenotype supporting the idea that the

provision of PEP for the shikimate pathway is limiting in certain tissues of the *cue1* mutant (Voll et al., 2003).

## 1.6 PEP as a substrate for shikimate pathway

The shikimate pathway is found only in microorganisms and plants, but not in animals. All enzymes of this pathway have been obtained in pure form from prokaryotic and eukaryotic sources and their respective DNAs have been characterized from several organisms. (Herrmann 1983; Frost et al., 1984; Duncan et al., 1986; Mousdale et al., 1987; Schmidt et al., 1990; Diaz and Merino, 1997; Klee et al., 1987). The immediate substrates for the shikimate pathway are erythrose 4-phosphate (Ery4P) and phosphoenolpyruvate (PEP) (Mousdale and Coggins, 1985; Schmid and Amrhein, 1995). In a sequence of seven metabolic steps, phosphoenolpyruvate (PEP) and erythrose 4-phosphate are converted to chorismate, the precursor of aromatic amino acids and many aromatic secondary plant products, such as lignin, flavonoids and anthocyanins (Fig. 1.5). All pathway intermediates can also be considered branch point compounds (Hermann and Weaver, 1999) that may serve as substrates for other metabolic pathways, for example, the formation of the cyclohexanecarboxylic acid (CHC)-derived moiety of the antifungal agent ansatrienin and the dihydroxycyclohexanecarboxylic acid (DHCHC) starter unit for the biosynthesis of the immunosuppressant ascomycin (Wilson et al., 1998) in *Streptomyces*. Ery4P is an intermediate of both the oxidative and the reductive pentose phosphate pathway of plastids and is generated inside the plastids (ap Rees, 1985). It is provided by transketolase, which converts glyceraldehydes 3-phosphate and fructose 6-phosphate to xylulose 5-phosphate and Ery4P. Unlike Ery4P, PEP cannot be generated in chloroplasts, because most plastids have little or no PGyM and enolase activity, glycolysis cannot proceed further than 3-phosphoglycerate (Bagge and Larsson, 1986; Stitt, 1997). Plastids therefore rely on the supply of cytosolic PEP. The transport of PEP from the cytosol into plastids is mediated by a specific PEP/phosphate translocator (PPT) (Fig. 1.2), which imports cytosolic PEP into the plastids in exchange with inorganic phosphate. (Fischer et al., 1997). The predominant aromatic amino acids formed from the shikimate pathway are phenylalanine, tyrosine and tryptophan. Chorismate, which is the end product of this pathway is the precursor for these three aromatic amino acids (Fig. 1.4) and several other aromatic compounds of primary metabolism. In addition, the three aromatic amino acids are precursors to a large variety of plant secondary metabolites (Dewick, 1998). Phenylalanine is utilized in protein synthesis and as a substrate for the phenylpropanoid pathway (via cinnamic acid), which produces numerous secondary

plant products such as anthocyanins, lignin, growth promoters, growth inhibitors, and phenolics (Ruegger et al., 2001). Tyrosine and tryptophan are also required for protein synthesis. One of the plant hormones, indole acetic acid which is an auxin, is derived from tryptophan and is absolutely necessary for cell expansion, maintenance of apical dominance, and well as other regulatory processes in the plant (Franz, 1997). Tryptophan and tyrosine leads to the production of various alkaloids and cyanogenic compounds.

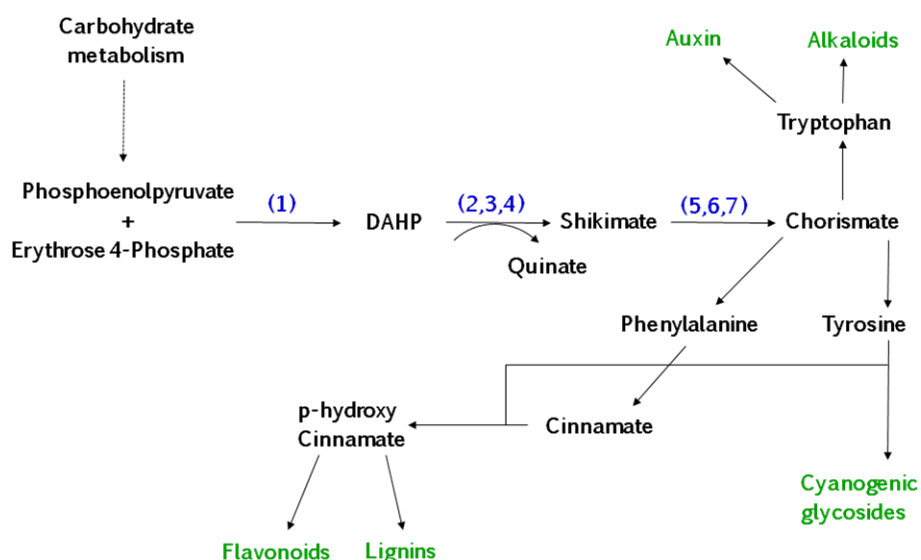


**Figure 1.5: Basic overview of shikimate pathway.** (1) DAHP synthetase (2) 3-dehydroquinate synthetase (3) 3-dehydroquinate dehydratase (4) shikimate-NADP-oxidoreductase (5) shikimate kinase (6) EPSP synthase (7) chorismate synthase.

Since, the shikimate pathway provides precursors for a large number of the primary and secondary metabolites for development of plants, a sufficient supply of PEP in plastids must be guaranteed to provide the aromatic amino acids.

## 1.7 PEP via pyruvate as a substrate for fatty acid synthesis (FAS)

Fatty acid synthesis (FAS) is characteristic of all living organisms. Multi-enzyme complexes referred to as type I fatty acid synthase (Wakil, 1989) carry out the bulk of FAS in animal cells and yeasts (Singh et al., 1985; Chang and Hammes 1989; Smith 1994), whereas in prokaryotes and plants, distinct soluble enzymes referred to as FAS II (Rock and Cronan 1996; Paul et al., 2001; Rawsthorne 2002) carry out the reactions. There are two soluble FAS II systems in plants, one in chloroplasts and another in mitochondria (Caughey and Kekwick 1982; Gueguen et al., 2000; Rawsthorne 2002). The FAS of the chloroplast (plastid) envelope represents the major pathway of plant fatty acid synthesis (Kekwick 1986, Slabas and Fawcett 1992, Rawsthorne 2002), corresponding to the mammalian FAS I (Smith, 1994)

and bacterial FAS II systems (Rock and Cronan, 1996). The plastidial system is regulated at acetyl-CoA carboxylation, analogously to the regulation of *E. coli* FAS II (Davis and Cronan 2001; Rawsthorne, 2002). The rate of FAS in plants depends on the redox state and the energy status. In addition, the diurnal rhythm and the amount of light are regulatory factors affecting lipid synthesis (Browse et al., 1981; Rawsthorne, 2002). Few of the plastidial FAS II enzymes, such as  $\beta$ -ketoacyl-ACP reductase, have been characterized at the molecular level (Fisher et al., 2000). It is known that fatty acids are synthesized within the plastids in plants (Ohlrogge et al., 1978; Ohlrogge and Jaworski, 1997), and exported and modified in the endoplasmic reticulum (ER) (Moore, 1993).

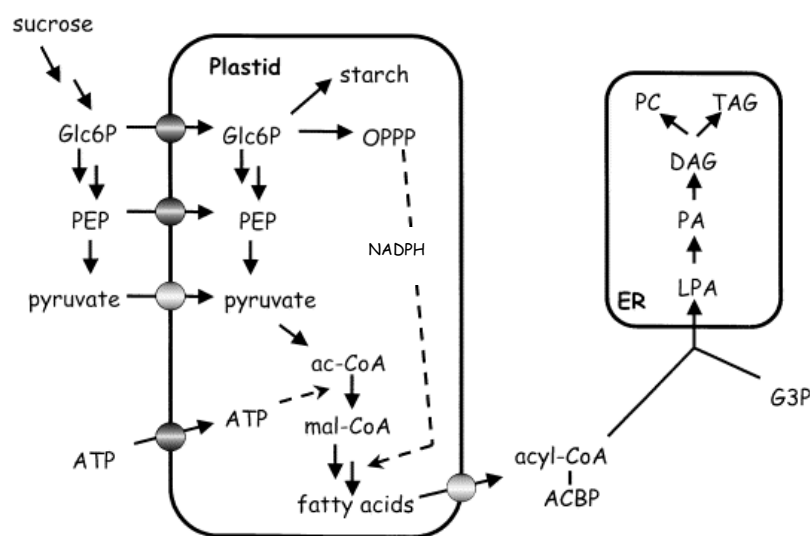


**Figure 1.6: An overview fatty acid synthesis and plastidial carbon partitioning in the developing oilseed rape embryo based on metabolic studies** (Rawsthorne, 2001). The compartmental nature of the metabolism from sucrose to lipids involving the cytosol, plastids and the endoplasmic reticulum is illustrated, as is the interaction between the oxidative pentose phosphate pathway and fatty acid synthesis (dashed arrow). Transporters on the plastid envelope are shown as shaded circles. ac-CoA=acetyl-CoA; mal-CoA=malonyl-CoA; OPPP=oxidative pentose phosphate pathway.

The plastidic fatty acid biosynthesis in heterotrophic tissues is dependent on the supply of carbon skeletons from the cytosol. In principle, fatty acid biosynthesis in non-green plastids could be driven by the import of glucose 6-phosphate (Glc6P) (Fig. 1.6), triose phosphates (TP), malate or pyruvate (Smith et al., 1992; Kang and Rawsthorne, 1994; Qi et al., 1995; Eastmond and Rawsthorne, 2000). In *Brassicaceae*, such as the crop plant canola (*Brassica napus*) or the model plant *A. thaliana*, PEP is likely to be the predominant precursor for fatty acid biosynthesis in seeds (Schwender and Ohlrogge, 2002; Schwender et al., 2003). Thus, the sufficient supply of PEP within the plastids plays an important role in the smooth flow of plastid fatty acid biosynthesis (Kubis et al., 2004). In principle, pyruvate generated by cytosolic pyruvate kinase (PKc) may be imported as precursor for fatty acid biosynthesis,

which is supported by feeding experiments with  $^{14}\text{C}$ -labeled pyruvate to isolated plastids from *B. napus* embryos and the subsequent incorporation of  $^{14}\text{C}$  into fatty acids (Kang and Rawsthorne, 1994; Eastmond and Rawsthorne, 2000). A plastid  $\text{Na}^+$ -coupled pyruvate transporter has recently been identified and characterized (Furomoto et al., 2009). It is, however, tempting to speculate that stromal PEP serves as a sole precursor for fatty acid biosynthesis in plastids of developing seeds. This notion is supported by disruption of the plastid localized pyruvate kinase, which converts PEP to pyruvate, resulting in a 60% diminished seed oil content (Andre et al., 2007) or a complete depletion of seed oil (Baud et al., 2007). The simplest description of the plastidial pathway of fatty acid biosynthesis consists of two enzyme systems: acetyl-CoA carboxylase (ACCase) and fatty acid synthase (FAS). ACCase catalyzes the formation of malonyl-CoA from acetyl-CoA, and FAS transfers the malonyl moiety to acyl carrier protein (ACP) and catalyzes the elongation of the growing acyl chain with malonyl-ACP (Fig. 1.7).

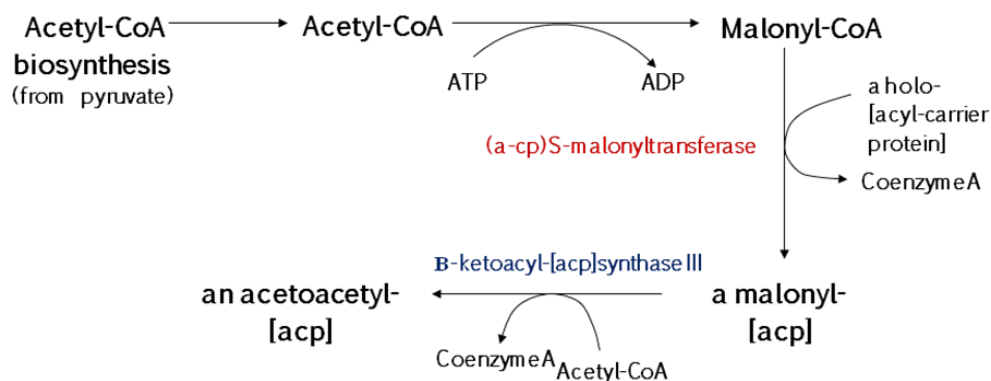


**Figure 1.7: Schematic representation of fatty acid biosynthesis in plants.**

In most plants, the primary products of the fatty acid elongation are 16:0-ACP and 18:0-ACP. The first double bond is then introduced to 18:0-ACP by  $\Delta^9$  18:0-ACP desaturase, which is ubiquitous to all plants. Additional double bonds are inserted to oleate and palmitate after they are incorporated into lipids. Plants also contain very long-chain fatty acids (chain length larger than 18 C atoms). The additional chain elongation occurs via the very long chain fatty acid biosynthesis pathway located in the ER. Free fatty acids are released from acyl-ACPs and are exported out of plastids.

## 1.8 PEP via pyruvate as a substrate for the synthesis of branched chain amino acids

PEP may contribute, through the provision of pyruvate, to the synthesis of branched-chain amino acids which takes place in the stroma of plastids (Schulze-Siebert et al., 1984, Kaneko et al., 1990; Sathasivan et al., 1990, Frisch et al., 1991; Weisemann and Matthews, 1993; Ghislain et al., 1994, Muehlbauer et al., 1994). Pyruvate, which derives from oxidative Malate breakdown by the NADP-malic enzyme or by plastidic pyruvate kinase from PEP can be used as a precursor for the synthesis of the branched-chain amino acids leucine and valine formed from acetolactate (Bonner and Jensen, 1997). Pyruvate can also be imported directly into the plastids (Proudlove and Thurman, 1981; Furomoto et al., 2009). Isoleucine and valine are synthesized in chloroplasts from two parallel pathways with four common enzymes each of which has dual substrate specificity. The exception is the committing enzyme of the isoleucine pathway threonine dehydratase (Samach et al., 1995) which catalyzes the synthesis of the oxoacid 2-ketobutyrate from threonine but has no role in valine metabolism. The first parallel reaction is catalyzed by acetolactate synthase. The intermediates 2-acetohydroxy butyrate and 2-acetolactate and then subjected to alkyl re-arrangement to form the corresponding 2,3-dihydroxyvaleric acids. The next step is catalyzed by dihydroxy-acid dehydratase. The final step in isoleucine and valine biosynthesis is transamination of ketoacids (Fig. 1.8). The synthesis of leucine, valine and isoleucine are subject to control by their end products. The formation of isoleucine is also influenced by complex regulatory mechanisms of amino acids of the aspartate (Galili, 1995). The synthesis of aspartate-derived amino acids methionine, lysine and threonine is also subject to a strong feedback control by their end products. Finally, the branched-chain amino acids serve as precursors to various plant secondary metabolites like cyanogenic glycosides, glucosinolates and acyl-sugars.

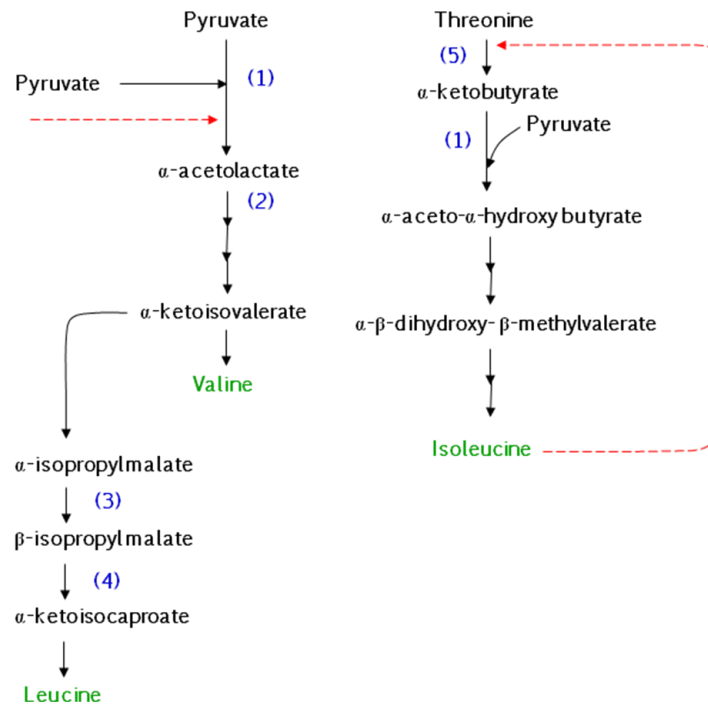


**Figure 1.8: Overview of branched-chain amino acid synthesis.** (1) Acetolactate synthase (2) Ketoacid reducto isomerase (3) Isopropyl malate isomerase (4) Isopropyl malate dehydrogenase (5) Threonine dehydratase

## 1.9 PEP as a substrate for plastid methylerythritol-phosphate (MEP) pathway of isoprenoid biosynthesis

Pyruvate which is generated from PEP inside the plastids or imported directly from the cytosol, is a precursor for the methylerythritol-phosphate (MEP) pathway. Pyruvate, together with D-glyceraldehyde-3-phosphate is the substrate for the isomers isopentenyl pyrophosphate (IPP) and dimethylallyl pyrophosphate (DMAPP). In higher plants, two distinct biosynthetic routes to IPP and DMAPP exist (Laule et al., 2002). The cytosolic mevalonate (MVA) pathway produces sesquiterpenes, triterpenes, homoterpenes and precursors for sterols and ubiquinone via farnesyl diphosphate (FPP) (Disch et al., 1998; Vickers et al 2009). The plastidial MVA-independent pathway, which involves a condensation of pyruvate and glyceraldehyde-3-phosphate via 1-deoxy-D-xylulose 5-phosphate as a first intermediate, is used for the synthesis of isoprene, carotenoids, abscisic acid, and the side chains of chlorophylls and plastoquinone (Arigoni et al., 1997; Lichtenthaler et al., 1997; Schwender et al., 1997; Milborrow et al., 1998; Hirai et al., 2000). Although this subcellular compartmentation allows both pathways to operate independently in plants, there is evidence that they cooperate in the biosynthesis of certain metabolites. For example, the chamomile sesquiterpenes are composed of two C5 isoprenoid units formed via the MVA independent pathway, with a third unit being derived from the MVA-independent pathway (Adam et al.,

1999) (Fig. 1.9). An interaction of both pathways has also been reported for monoterpene and sesquiterpene volatiles emitted by lima beans. Members of the isoprenoid group have an extraordinarily wide range of roles in the plant; these include well-characterized physiological functions in primary metabolism such as growth regulation (for e.g. hormones), photosynthetic components (phytyl side chains of chlorophylls, prenyl side chains of plastoquinones) and structural (for e.g., sterol membrane components) roles, and also secondary functions such as defense (for example, some phytoalexins) and antioxidants (for e.g. tocopherols and carotenoids). In addition to this, isoprenoids fulfill a variety of roles in secondary metabolism, these roles are also very diverse, and many remain to be fully characterized (Harborne 1991; Vickers et al., 2009).

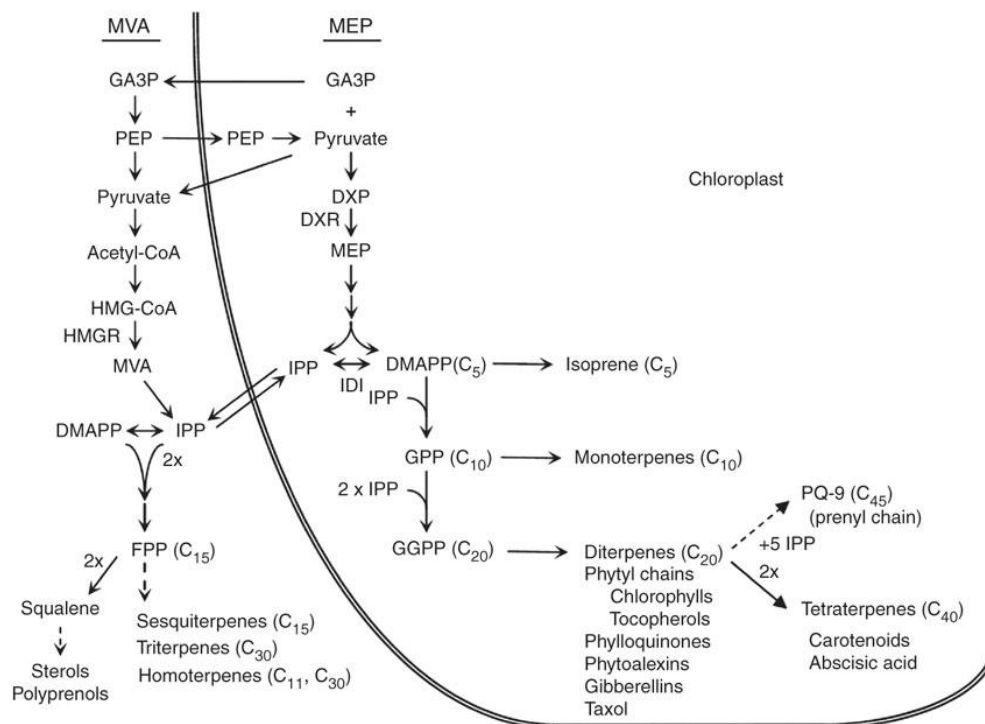


**Figure 1.9: Schematic representation of isoprenoid biosynthetic pathways** (Vickers et al., 2009)

As a final point, it is tempting to speculate, whether a combined absence of *PPT* (*PPT1* or *PPT2*) and plastidic enolase or phosphoglycerate mutase would have detrimental effects on various aspects of plant functions. Indeed, a combined loss in *PPT1* and the putative plastid localised enolase leads to a lethal phenotype (Löttgert, PhD thesis) underlining the importance of stromal PEP. Both genes, *PPT1* and *ENO1*, are co-expressed during certain stages of seed development (<http://www.bar.utoronto.ca/efp/cgi-bin/efpWeb.cgi>) (Fig. 1.2 and 1.3). As neither *PPT2* nor *PPDK* appear to be expressed during

the same developmental stage, it is likely that both *PPT1* and the putative plastidic enolase share similar functions (i.e. the provision of PEP to plastids). It is not entirely clear whether or not metabolic limitations (shikimate pathway, fatty acid biosynthesis) are the main reasons for the lethality of developing seeds in the *cue1/enol* double mutant. The aim of the proposed research was to elucidate the role of a complete plastidic glycolysis in various aspects of plant development and physiology with focus on the *PPT* (*PPT1* and *PPT2*) as well as complete plastidic glycolysis, not only in developing seeds but also in heterotrophic tissues such as roots. The combined loss of *PPT1* and enolase genes or *PPT1* and phosphoglycerate mutase genes would affect the aromatic amino acid pathway. The effect of the combined loss of the above named genes on the fatty acid biosynthesis is unpredictable, because pyruvate could also be fed into fatty acid biosynthesis by a pyruvate transporter (Furomoto et al., 2009). Similarly, in the early globular stage of embryogenesis when only the *PPT2* is expressed but neither *ENO1*, *PPT1* or *PPDK*, a loss of function of *PPT2* would also be detrimental to the plant.

## **2 Materials and methods**

### **2.1 Materials**

#### **2.1.1 Chemicals**

Chemicals were obtained from the following companies:

Biomol (Hamburg, D), Difco (Hamburg, D), Duchefa (Haarlem, NL), Eurobio (Les Ulis Cedex, F), Fluka AG (Buchs, CH), Merck (Darmstadt, D), Roche (Mannheim, D), Roth (Karlsruhe, D), Fisher Scientific GmbH (Schwerte, D), Chromatographie Service GmbH (Langerwehe, D) and Sigma-Aldrich (Deisenhofen, D). Research grade purity was used for all purposes.

#### **2.1.2 Enzymes**

Enzymes for molecular biology were obtained from the companies:

Invitrogen (Karlsruhe, D), MBI Fermentas (St. Leon-Rot, D), Promega (Mannheim, D), Qiagen (Hilden, D), Roche (Mannheim, D) and Sigma (Deisenhofen, D).

#### **2.1.3 Kits**

The following Kits were used according to the manufacturer's protocols:

TRIsure (Bioline)

RNeasy Plant Mini Kit (Qiagen)

DC Protein Assay Kit (Bio-Rad)

Bradford Reagent (Roth)

Big Dye<sup>®</sup> Terminator Cycle Sequencing Kit v3.1 (Applied Biosystems, Foster City, USA)

CompactPrep Plasmid Midi (Qiagen GmbH, Hilden, D)

QIAquick Gel Extraction Kit (Qiagen GmbH, Hilden, D)

Quantum Prep<sup>®</sup> Plasmid Miniprep Kit (BioRad, München, D)

Super Script<sup>™</sup> II - Reverse Transcriptase (Bioline)

#### **2.1.4 Antibiotics**

The following antibiotics were used:

Antibiotic	stock solution		working concentration
Ampicillin	100 mg/mol	in water	100 µg/mol
Carbenicillin	50 mg/mL	in water	50 µg/mL
Kanamycin	50 mg/mL	in water	50 µg/mL
Gentamycin	25 mg/mL	in water	25 µg/mL
Hygromycin	50 mg/mL	in water	50 µg/mL
Chloramphenicol	75 mg/mL	in ethanol	75 µg/mL
Rifampicin	20 mg/mL	in DMSO	100 µg/mL
Rifampicin	30 mg/mL	in DMSO	150 µg/mL

### 2.1.5 Bacteria

The following bacteria strains were used:

#### Escherichia coli:

##### **DH5α**

*F- supE44 ΔlacU169 (Φ80, lacZΔM15) hsdR17 recA1 endA1 gyrA96 thi-1 relA1*  
for plasmid amplification

##### **DH10B**

*F- mcrA Δ(mrr-hsdRMS-mcrBC) φ80lacZΔM15 ΔlacX74 recA1 endA1 araD139*  
*Δ(ara, leu)7697 galU galK λ- rpsL nupG* for plasmid amplification

##### **BL21**

*E. coli* B F<sup>-</sup> *dcm ompT hsdS(rB- mB -) gal λ(DE3)*. Chemically competent *E. coli* used for expression that carries the lambda DE3 lysogen.

##### **XL10-Blue**

*F- supE44, hsdR17, recA1, endA1, gyrA46, thi, relA1, lac, F'[proAB+, lacIq, lacZΔM15, Tn10(tetr)]* for plasmid amplification

##### **Top10**

*F- mcrA Δ(mrr-hsdRMS-mcrBC) Φ80lacZΔM15 ΔlacX74 deoR recA1 araD139 Δ(ara-leu)7697 galU galK rpsL (StrR) endA1 nupG*  
for plasmid amplification

##### **DB3.1**

*F- gyrA462 endA1 (sr1-recA) mcrB mrr hsdS20(rB-, mB-) supE44 ara-14 galK2*  
*lacY1 proA2 rpsL20(SmR) xyl-5 - leu mtI1*  
for amplification of plasmids containing the *ccdB* gene (GATEWAY-cloning)

**Agrobacterium tumefaciens:**

GV3101 (pMP90)

GV3101 containing the helper plasmid pSoup

SV 0 (super virulent strain for cell culture transformation) *LBA4404.pBBR1MCS virGN54D***2.1.6 Plant lines**Wild-type *A. thaliana* plants were of the ecotypes Columbia-0 (Col-0), and Bensheim (Be).

The following T-DNA insertion lines were all in Col-0 background and were obtained from the following sources:

SIGnAL (SALK Institute Genomic Analysis Laboratory, <http://signal.salk.edu>)MPIZ ([http://www.mpiz-koeln.mpg.de/GABI-Kat/GABI-Kat\\_homepage.html](http://www.mpiz-koeln.mpg.de/GABI-Kat/GABI-Kat_homepage.html))NASC (<http://arabidopsis.org.uk/>)

<b>Line</b>	<b>Ecotype/Background</b>
pOCA108	Bensheim
<i>cue1-1</i>	pOCA108
<i>cue1-3</i>	pOCA109
<i>cue1-6</i>	Col-0

Note: pOCA108 is a transgenic line expressing Alcohol dehydrogenase (ADH) under the control of a CAB3 promoter.

<b>Gene</b>	<b>At number</b>	<b>Mutant name</b>	<b>Line</b>
ENO1	At1g74030	<i>Ateno1-1</i>	N521328 (NASC)
ENO1	At1g74030	<i>Ateno1-2</i>	N421734 (NASC)

**2.1.7 Software**

Acrobat Reader Version 7.0	Adobe
Photoshop Version CS3	
DISKUS Software Package	Technisches Büro Hilger
Enhanced Chem Station G1701 CA Dec. 1999	Agilent (USA)
i-Control	Tecan (Austria GmbH)
Magellan v6.3 software	
	TIGR

## Multi Experiment Viewer 4.2

SeqMan II Edit Seq	DNA-Star Inc
Sequence Detection Software v1.4	Applied Biosystems
Sigma Plot Version 10.0	SPSS
Vector NTI Advanced 10.0	Invitrogen

### 2.1.8 Vectors

Vector	Source	Use
pDONOR207	Invitrogen GmbH	Cloning of PCR products in E.coli
pENTR D-TOPO	Invitrogen GmbH	Cloning of PCR products in E.coli
pENTR SD/D-TOPO	Invitrogen GmbH	Cloning of PCR products in E.coli
pET-DEST 42	Invitrogen GmbH	Inducible expression in E.coli
pGWB2	Invitrogen GmbH	Constitutive over-expression in plants
pGWB3	Invitrogen GmbH	GUS expression in plants
pGWB5	Invitrogen GmbH	Transient GFP expression in plants

## 2.2 Methods

### 2.2.1 Plant methods (*Arabidopsis thaliana*)

#### 2.2.1.1 Growth conditions

##### 2.2.1.1.1 Greenhouse

*Arabidopsis* seeds were sown in 9 cm plastic pots on a substrate mixture containing three parts soil and one part Vermiculite. For vernalization, the pots were kept for a minimum of 48 h at 4°C in the dark, and then the pots were transferred to the greenhouse for germination. Approximately 2 weeks after germination, the plants were transplanted to 9 cm or 6 cm pots containing the substrate mixture. In the greenhouse, plants were grown under long day conditions with a light/dark cycle of 16:8 hours, a temperature of 21°/18°C and a relative humidity of approximately 40%.

### 2.2.1.1.2 Temperature controlled climate chamber

*A. thaliana* plants were grown on culture plates in a climate chamber (Percival Scientific, Model CU-36L5 or AR-66LS) with humidity of 50% and a temperature of 22°C during light period and 18°C during dark period respectively. For growth under long day conditions, the plants were subjected to a day/night rhythm of 16:8 hours, for short day conditions of 8:16 hours.

### 2.2.1.1.3 Growth of *A. thaliana* plants on sterile media

Surface sterilized Arabidopsis seeds were used for growth on sterile MS media. The dry seeds were spread on autoclaved paper and transferred onto the plates using a sterile toothpick singly when required or the seeds were carefully and evenly distributed on the plates by gentle tapping of the 1.5mL tube containing the sterile seeds. The seeds on the plates were vernalized for 48 h at 4°C in the dark, and then the plates were transferred to a climate chamber. All plates were sealed using gas permeable adhesive tape.

### 2.2.1.1.4 Sterilization of *A. thaliana* seeds

For growth of Arabidopsis plants on sterile media, the seeds were surface sterilized before sowing on plates. There were two types of surface sterilizations applied: i) Dry sterilization of seeds using Chlor gas ii) Liquid/Wet sterilization of seeds.

### 2.2.1.1.5 Dry sterilization of seeds using chlorine gas

About 100 seeds per line were placed in 1.5 mL reaction tubes, which were then placed open in an exsiccator containing a beaker with 100 mL sodium hypochlorite. 3 mL HCl<sub>conc.</sub> was added and the lid of the exsiccator was kept closed or approximately 4 h. The tubes were closed and transferred to the sterile hood, where they were kept open for one hour to allow remaining chlorine gas to evaporate and the seeds were used for dispersion on sterile media.

### 2.2.1.1.6 Liquid/Wet sterilization

#### **Sterilization solution**

1mL	Sodium hypochloride
6mL	Water
2 drops	Tween 20

70% ethanol (Sterile)

Approximately 50 *A. thaliana* seeds were taken in a sterile 1.5 mL tube and 1 mL of 70% ethanol was added to it and mixed thoroughly by vortexing. The ethanol was discarded and 1 mL of the sterilization solution was added to the seeds and the tubes were placed in a shaker for 20 min. Later, the supernatant was removed and the seeds were rinsed five times with sterile water and used for dispersion on sterile media.

### 2.2.1.2 Preparation of media for *A. thaliana* plants

Sterilized seeds were laid out on MS plates and stratified for two to three days at 4°C. The growth of the plants was carried out in a climate chamber (RUMED 1200; Fa. Rubarth Apparate GmbH, Laatzen) at 22°C under a light-dark cycle of 16:8 h and a photon flux of 36  $\mu\text{mol}\cdot\text{m}^{-2}\cdot\text{s}^{-1}$

#### MS-Plates:

1% (w/v) Sucrose

0.44% (w/v) Murashige & Skoog (Duchefa, Haarlem, NL, Kat.-Nr. M0245)

0.8% (w/v) Agar (Difco)

pH5.6/KOH

The MS-medium was autoclaved and after cooling poured into sterile petri dishes. After solidification of the medium, the set plates were used directly or stored for several days at 4°C.

### 2.2.1.3 Plant selection

#### 2.2.1.3.1 Selection on MS agar plates

For selection of plants on agar plates antibiotic stock solutions (2.1.4) as required were added to the autoclaved medium after cooling.

#### 2.2.1.3.2 BASTA selection

Transgenic plants containing the *bar*-gene, which mediates the resistance to the herbicide phosphinothricin (BASTA), were grown on soil and selected for development of the first primary (four-leaf stage). The plants were sprayed with the herbicide solution from a distance of approximately 30 cm. When the plants were very dense, this process was repeated (after approximately one week).

#### BASTA-solution:

250 mg/l BASTA®

0.1% Tween-20

#### 2.2.1.4 Transformation of *A. thaliana* using vacuum infiltration

Agrobacteria containing the plasmid of interest were grown at 28°C with continuous shaking to an OD 600 of 0.8-1.0 and the culture was centrifuged at 4°C for 15 min at 2500 g. The pellet was dissolved in the infiltration medium (about 1/3 the original volume).

##### **Infiltration medium**

½ MS-Medium with Vitamin

5% Sucrose

Tween-20

pH 5.8/KOH

The *A. thaliana* plants to be infiltrated were grown on soil and the mature and developing siliques from the plants were removed and flowers were retained. The plants were submerged upside down in a vacuum in the agrobacterial-suspension so that flowers and buds were well submerged in the medium. Using a water jet pump, vacuum suction was applied for 5 min and repeated thrice. Further, the flowers were wet again with the agrobacterial-suspension and the plants were covered for the next two days with a plastic lid, which was sprayed sporadically to maintain a high humidity.

#### 2.2.1.5 GUS staining

Plants to be tested for promoter activity were vacuum-infiltrated with GUS staining solution, until plants were completely submerged in the solution (using vacuum suction) and the leaves were translucent. Further, the plants were incubated at 37°C until staining was visible. To enhance visibility of the GUS signal, chlorophyll was extracted by incubating the plants in 80% ethanol at 65°C.

##### **GUS Staining Solution**

0.1 M	NaPO <sub>4</sub> pH7
10 mM	EDTA
0.5 mM	K-Ferricyanid
0.5 mM	K-Ferrocyanid
1 mM	X-Gluc
0,1%	Triton X-100

#### 2.2.1.6 Screening of T-DNA insertion lines

The genotype of T-DNA insertion lines was determined using PCR-based (2.2.3.5.1) methods. Genomic DNA of single plants was isolated (2.2.3.2.1) and used as template for PCR with two gene specific primers or one gene specific primer and one primer complementary to the flanking sequence of the T-DNA in separate reactions (See primer sequence table). Homozygous plants were kept for further analyses.

### **2.2.1.7 Crossing of *A. thaliana* plants**

For crossing of different lines, six week-old homozygous plants were used. All open flowers and developed siliques were removed from the plants to be pollinated and of the remaining flower buds the three largest buds were opened carefully under the binocular and all organs except the carpels were removed. Stamens of the plants donating pollen were isolated and pollen was transferred onto the stigma of the other line cautiously. The flowers used for crossing were labeled, harvested when ripened and were sown on soil. F<sub>1</sub> plants were screened for the occurrence of the respective T-DNA inserts in heterozygous state, these were allowed to set seed, and in the F<sub>2</sub> generation, the offspring was screened in PCR reactions for double homozygous plants.

### **2.2.1.8 *A. thaliana* cell cultures**

#### **2.2.1.8.1 Maintenance of cell cultures**

*A. thaliana* cells were grown in suspension culture in the dark at 18 to 22°C with shaking at about 1560 rpm. Once a week, the cells were diluted 1:4 with fresh, room temperature media. Approximately every four weeks, the cell culture was screened for bacterial contamination and backup plates were prepared. In case of visible bacterial contamination, the diluted cultures were treated with ticarzidin, and hence before using cells for transformation, they need to be diluted twice. For backup plates, 50 mL cell culture was centrifuged (15 min, 500 g), the supernatant discarded, the pellet resuspended in media and spread on plates.

#### **Suspension culture medium**

4.3 g	Duchefa MS basal salt mixture (M 0221)
4 mL	B5 vitamins
400 mg	Myo-inositol
30 g	Sucrose
ad 1L	H <sub>2</sub> O

The pH was adjusted to 5.8 with KOH; for plates, 0.8% Gelrite was added, 0.5 mL 2 mg/mL 2,4D was added after autoclaving and cooling.

### 2.2.1.8.2 Cell culture transformation

For cell culture transformation, *Agrobacterium tumefaciens* strain SV-0 carrying the binary vector and colonies of the anti-silencing strain RK19 were picked from fresh plates and were grown for 24 h at 28°C in 5 mL cultures in YEB containing the appropriate antibiotics (20 µg/mL rifampicin, 75 µg/mol chloramphenicol, 50 µg/mL kanamycin for selection of the binary plasmid). The cells were pelleted by centrifugation (15 min, 4000 rpm) and resuspended in 1mL Arabidopsis cell culture media.

For co-culture, freshly diluted Arabidopsis suspension culture were mixed 50:1 with the different *Agrobacterium* strains containing the plasmid of interest, grown for 3 to 5 days in the dark at 25°C, and then screened for expression of the transgene.

## 2.2.2 Microbiological methods

### 2.2.2.1 Growth and transformation of *Escherichia.coli*

#### 2.2.2.1.1 Media

LB	10 g	Trypton
	5 g	Yeast Extract
	10 g	NaCl
	ad 1L	H <sub>2</sub> O <sub>bd</sub>
2YT	16 g	Trypton
	10 g	Yeast Extract
	5 g	NaCl
	ad 1L	H <sub>2</sub> O <sub>bd</sub>
SOC	20 g	Trypton
	5 g	Yeast Extract
	0.585 g	NaCl
	0.186 g	KCl
	0.953 g	MgCl <sub>2</sub>
	1.2 g	MgSO <sub>4</sub> * 7H <sub>2</sub> O
	36 g	Glucose

ad 1L H2Obd

For preparation of agar plates, 1.5 % (w/v) bacto agar was added. The media were autoclaved and the required antibiotics were added after cooling the media to about 40°C.

### 2.2.2.1.2 Growth of *E. coli*

*E. coli* cells were grown either on agar plates in a 37°C incubator or as liquid cultures in a shaker. For liquid cultures, single colonies were picked from LB plates with a sterile toothpick, inoculated in 3mL media and grown over night at 37°C while shaking at 200-250 rpm. For growth of transgenic bacteria, the corresponding antibiotics were added for selection. Bacteria could be kept for several weeks at 4°C on YEB plates or at -80°C as glycerol culture (500 µL culture and 500 µL 65% Glycerol, 100 mM MgSO<sub>4</sub>, 25 mM Tris-HCl, pH 8.0).

### 2.2.2.1.3 Preparation of competent cells (*E. coli*)

A 5 mL culture was inoculated with a single *E. coli* colony and incubated over night in a 37°C shaker. The next day, 1mL of the overnight culture was used to inoculate a 100 mL culture which was grown until an OD<sub>550</sub> of 0.48 was attained. The culture was transferred into pre-cooled 50mL tubes, then incubated on ice for 15 min and the cells were spun down (375 g at 4°C for 10 min). All further steps were performed at 4°C. The supernatant was removed; the pellet was re-suspended in 15 mL Tfb1 and incubated on ice for 2 h. Then, the cells were centrifuged again (375 g at 4°C for 10 min) and the supernatant was removed. The cells were re-suspended in 4 mL Tfb2 and transferred in 100 µL aliquots into pre-cooled 1.5 mL tubes and immediately frozen in liquid nitrogen. The competent cells were then stored at -80°C until transformation. To test for transformation efficiency, one aliquot of competent cells was transformed with 10 pg PUC19 DNA and the number of grown colonies was determined on the next day.

Tfb1	100 mM	RbCl <sub>2</sub>
	50 mM	MnCl <sub>2</sub> *4 H <sub>2</sub> O
	30 mM	KAc
	10 mM	CaCl <sub>2</sub>
	15% (v/v)	Glycerin

The pH was adjusted to 7.0 and the media was filter sterilized.

Tfb2	10 mM	RbCl <sub>2</sub>
------	-------	-------------------

75 mM	CaCl <sub>2</sub>
10 mM	MOPS
15% (v/v)	Glycerin

The pH was adjusted to 7.0 and the media was filter sterilized.

#### 2.2.2.1.4 Transformation of *E. coli*

Competent cells (100 µl) were thawed on ice, mixed with 100 ng of plasmid DNA, and incubated on ice for 15 min. The cells were then transformed by heat shock (45 to 60 sec at 42°C). After addition of 1 mL SOC, the cells were incubated in a shaker at 37°C for about 1 h, and then the cells were plated in different concentrations on selective media and incubated at 37°C over night.

### 2.2.2.2 Growth and transformation of *Agrobacterium tumefaciens*

#### 2.2.2.2.1 Media

YEB	5 g	Bacto Peptone
	5 g	Beef Extract
	1 g	Yeast Extract
	5 g	Sucrose
	0.5 g	MgSO <sub>4</sub> * 7 H <sub>2</sub> O
	ad 1 L	H <sub>2</sub> O <sub>bd</sub>
MGL	5 g	Bacto Tryptone
	2.5 g	Yeast Extract
	5 g	NaCl
	5 g	Mannitol
	1.16 g	Na glutamate
	0.25 g	KH <sub>2</sub> PO <sub>4</sub>
	0.1 g	MgSO <sub>4</sub> * 7 H <sub>2</sub> O
	1 mg	Biotin
ad 1 L	H <sub>2</sub> O <sub>bd</sub>	

The media were autoclaved and the required antibiotics were added after cooling of the media to about 40°C.

#### 2.2.2.2.2 Growth of *A. tumefaciens*

For liquid cultures, single colonies were picked from YEB plates with an inoculation loop, inoculated in 3mL media and grown for one to two days at 28°C while shaking with 200-250rpm. For growth of transgenic bacteria, the corresponding antibiotics were added for selection. Bacteria could be kept for several weeks at 4°C on plates or at -80°C as glycerol culture (500 µL culture and 500 µL 65% glycerol, 100 mM MgSO<sub>4</sub>, 25 mM Tris / HCl, pH 8.0).

### **2.2.2.2.3 Preparation of competent cells of *A. tumefaciens***

A 5 mL MGL pre-culture was inoculated with *A. tumefaciens* and grown over night, then the culture was diluted in 100 mL MGL and grown until a density of OD 600 of about 0.5 was reached. The culture was centrifuged (5 min at 4°C and 2500 g) and the cells were re-suspended in 40 mL cold buffer (1 mM HEPES pH 7.0) followed by another centrifugation step (5 min at 4°C and 5000 rpm). Then, the cells were washed in 2 mL cold buffer (1 mM HEPES pH 7.0 containing 10%(v/v) glycerol) and finally re-suspended in 200  $\mu$ L 1 mM HEPES pH 7.0 containing 10%(v/v) glycerol. 50  $\mu$ L aliquots were frozen directly in liquid nitrogen and stored at -80°C.

### **2.2.2.2.4 Transformation of *A. tumefaciens* by electroporation**

Competent cells were thawed on ice, mixed with 200 ng plasmid DNA, and kept on ice for 2min. Then, the cells were transferred into pre-cooled 0.2 cm cuvettes. The electroporation conditions were 25  $\mu$ F, 400  $\Omega$ , 2.5 kV pulse with a retention time of 8-9 msec. Following electroporation, 1mL room temperature YEB media containing the antibiotics used for selection was added and the culture was incubated at 28°C whilst shaking at 100-150 rpm. The cells were plated in different concentrations on antibiotics containing YEB plates and were grown at 28°C for two days.

## **2.2.3 Molecular biological methods**

### **2.2.3.1 Plasmid isolation**

#### **2.2.3.1.1 Mini preparation**

Plasmid DNA from *E. coli* in ‘miniprep’ scale was isolated using the QuantumPrep Kit (BIORAD) following the manufacturer’s protocols. A part of the overnight culture was used for storage as glycerol stock cultures at -80°C.

#### **2.2.3.1.2 Midi preparation**

Plasmid DNA from *E. coli* in ‘midiprep’ scale was isolated using the CompactPrep Plasmid Midi Kit (QIAGEN) following the manufacturer’s protocols. A part of the overnight culture was used for storage as glycerol stock cultures at -80°C.

### **2.2.3.2 Isolation of *A. thaliana* genomic DNA**

#### **2.2.3.2.1 Fast Prep (Edwards et al., 1991)**

One leaf from each plant was harvested into a 2 mL tube, frozen in liquid nitrogen, and stored at  $-80^{\circ}\text{C}$  until isolation. The tissue was pulverized with 400  $\mu\text{L}$  extraction buffer. Cell debris was removed by centrifugation and the supernatant was transferred into a new 1.5 mL tube. The DNA was precipitated with Isopropanol in 1:1 ratio, pelleted by centrifugation and the supernatant was discarded. The resulting pellet was dried and re-suspended in 50-100  $\mu\text{L}$   $\text{H}_2\text{O}_{\text{bd}}$  and stored at  $-20^{\circ}\text{C}$ .

<b>Extraction Buffer</b>	200 mM	Tris HCl pH 7.5
	250 mM	NaCl
	25 mM	EDTA
	0.5%	SDS

#### 2.2.3.2.2 Standard Prep (Liu et al., 1995)

For isolation of genomic DNA with a higher purity, tissue (usually flowers and buds) from single plants was harvested into reaction tubes, frozen in liquid nitrogen, and stored at  $-80^{\circ}\text{C}$  until isolation. Samples were pulverized and mixed with 500  $\mu\text{L}$  extraction buffer. 400  $\mu\text{L}$  PCI (phenol, chloroform, and isoamyl alcohol in a ratio of 25:24:1) was added and the samples were mixed. The samples were centrifuged for 15 min at 10000 g to remove proteins and plant material from the aqueous phase, which was transferred into a new tube. Following addition of 300  $\mu\text{L}$  Isopropanol to the aqueous phase, the samples were incubated at room temperature for 10min, and then DNA was pelleted by centrifugation (20 min, 10000 g). The pellet was washed twice with 70% ethanol, dried, and re-suspended in 50  $\mu\text{L}$  RNase containing water (1:100 RNase dilution).

2x Buffer	0.6 M	NaCl
	100 mM	Tris HCl pH 7.5
	40 mM	EDTA
	4%(w/v)	Sarkosyl
	1%(w/v)	SDS
Extraction Buffer	25 mL	2x Buffer
	20 mL	12M Urea
	2.5 mL	Phenol
	2.5 mL	$\text{H}_2\text{O}$

#### 2.2.3.3 Expression analysis

##### 2.2.3.3.1 RNA isolation (Trisure method)

For RNA isolation, about 100 mg plant tissue was harvested into 1.5 mL tubes and directly frozen in liquid nitrogen. The samples were homogenized with 1 mL TRisure reagent and incubated at room temperature for 5 min. Then, 200  $\mu\text{L}$  chloroform was added to the samples, which were kept at room temperature for 2 min and then centrifuged at  $4^{\circ}\text{C}$  for 10 min at 10000 g. The supernatant was transferred into a new tube, mixed with 500  $\mu\text{L}$  Isopropanol,

incubated at room temperature for 10 min. The RNA was precipitated by centrifugation (4°C, 5 min, 10000 g), washed with 75% ethanol and air dried, then the RNA pellet was re-suspended in DEPC-H<sub>2</sub>O and the concentration was determined photometrically (2.2.3.3.5).

#### **2.2.3.3.2 RNA isolation (Qiagen method)**

For RNA isolation, about 100 mg plant tissue was harvested into 1.5 mL tubes and directly frozen in liquid nitrogen. The samples were homogenized using liquid nitrogen and the isolation of RNA was done using the RNeasy Plant Mini kit (Qiagen) according to manufacturer's protocol.

#### **2.2.3.3.3 DNase digestion**

To avoid false-positive results when testing the expression level of a gene, genomic DNA was removed by DNase digestion prior to cDNA synthesis. The DNase digestion was performed on quantified RNA using the DNA-free<sup>TM</sup> kit as per manufacturer's protocols (Ambion).

#### **2.2.3.3.4 Reverse transcription**

For cDNA synthesis, 10 µL DNase digested RNA and 1 µL oligo-dT primer were incubated for 5 min at 70°C and were then transferred onto ice. Further, 1 µL 10 mM dNTP's, 4 µL 5xRT-buffer, 2.75 µL DEPC-H<sub>2</sub>O and 0.25 µL BioScript Reverse Transcriptase (Bioline) were added. cDNA synthesis progressed at 37°C for 1 h and the enzyme was deactivated by heating to 70°C for 10 min.

#### **2.2.3.3.5 Photometric determination of nucleic acid concentration**

To determine the concentration of isolated nucleic acids (DNA and RNA), 1 µL of sample was used for photometric measurement using a Nanodrop ND-1000 (Pepqlab) photometer. The concentration of the sample was calculated from the absorption at a wavelength of 260 nm.

#### **2.2.3.3.6 Gel Electrophoresis**

DNA fragments of different size were separated using agarose gel electrophoresis and visualized by ethidium bromide staining under UV-light (254 nm wavelength). Agarose concentration was chosen depending on the fragment size, smaller fragments were separated using high percentage gels (3-5% agarose in TBE), larger fragments in low percentage gels (0.8-2.5% agarose in TAE). Agarose was boiled in the corresponding buffer in a microwave oven and ethidium bromide was added to the cooled liquid gel before pouring it onto

respective trays. For electrophoresis, size marker (1 kb ladder, Invitrogen or 20 bp ladder, MBI) was used and samples mixed with loading dye were pipetted into the gel slots and the gel was electrophoresced at an amperage of approximately 150 mA, corresponding to a voltage between 80 and 130 V, depending on the size and percentage of the gel.

<b>50x TAE</b>	2 M	Tris/ Acetic Acid, pH 7.5
	1 M	Sodium acetate
	50 mM	EDTA
<b>10x TBE</b>	0.89 M	Tris/NaOH, pH 8.3
	0.89 M	Boric Acid
	20m M	EDTA
<b>Ethidium bromide</b>	0.5% (w/v)	Ethidium bromide in methanol

<b>6x Loading Dye</b>	10 mM	Tris-HCl (pH 7.6)	
	60 mM	EDTA	
	60%	Glycerol	
Plus one or two of the following dyes	0.15%	Orange G	migrates in 1% gel at: 50-100bp
	0.03%	Bromophenol blue	200-300bp
	0.03%	Cresol Red	~3000bp
	0.03%	Xylene cyanol FF	~4000bp

## 2.2.3.4 Enzymatic analysis of DNA

### 2.2.3.4.1 Restriction Digestion

Restriction endonucleases recognize stretches of four or more nucleotides in a palindromic sequence and introduces double strand breaks specifically at these sites. A reaction containing DNA, one or several restriction endonucleases (0.5-3 U), the corresponding reaction buffer, and sterile water in a volume of 10  $\mu$ L to 50  $\mu$ L was used (MBI Fermentas). The enzyme activity per unit is defined as the amount of enzyme that is needed to digest 1  $\mu$ g of DNA in 60 min at the correct temperature and the corresponding buffer. The reaction temperature was dependent on the optimal reaction temperature of the enzyme; the reaction time was between 2 h and 16 h.

### 2.2.3.4.2 De-phosphorylation of cloning vectors

To the linearized vector post restriction digestion, 1 U SAP (shrimp alkaline phosphatase) and 1x de-phosphorylation buffer were added to a final volume of 10  $\mu$ l. For blunt-ended DNA fragments the reaction was incubated for 60 min at 65°C, for cohesive/sticky ended DNA

fragments the reaction was incubated for 10 min at 37°C. Finally, the SAP was inactivated for 15 min at 65°C.

#### 2.2.3.4.3 Ligation of DNA fragments

The T4 DNA Ligase catalyzes the formation of a phosphor-diester bond between juxtaposed 5'-phosphate and 3'-hydroxyl termini in duplex DNA or RNA with blunt or cohesive-end termini. The reaction takes place under ATP hydrolysis. For ligation into a linearized vector 100-200 ng of vector DNA were used. The DNA fragment and the vector were mixed in a molar ratio of 5:1 in a total volume of 20 µl 1x ligase buffer (Promega) and treated with 1-2 U T4 DNA ligase (Promega). The reaction was carried out overnight at 13 ° C.

#### 2.2.3.4.4 Gateway Cloning

GATEWAY<sup>®</sup>-Cloning uses the site-specific recombination activity of bacteriophage λ for all steps during cloning. The sequence of interest is amplified with either gene specific primers containing an *attB1* site 5' of the forward primer and an *attB2* site 5' of the reverse primer or primers containing a 5' CACC-sequence in the forward primer and the unmodified reverse primer. The PCR fragments are then recombined using BP-Clonase into a pDONR vector or via TOPO-Cloning into pENTR/D-TOPO<sup>™</sup> or pENTR SD/D-TOPO<sup>™</sup>. Positive clones of the *Entry Vectors* are then used for LR-recombination into the selected *Destination Vectors*.

For the TOPO-Cloning, 0.2 µL Salt Solution, 0.2 µL TOPO-pENTR<sup>™</sup>, 0.1 µL PCR fragment and 0.7 µL sterile water were mixed, incubated at room temperature for approximately 30 min and then transformed into *E.coli*.

**BP reactions :** 10 ng-50 ng PCR product, 50 ng Entry Vector, 1 µL 5xBP-Reaction Buffer and 1µL BP-Clonase and volume adjusted with sterile water to 5 µL.

**LR reactions :** 10 ng-50 ng Entry Clone, 50 ng Destination Vector, 1 µl 5x LR-Reaction Buffer and 1 µL LR-Clonase and volume adjusted with sterile water to 5 µL. The reaction were incubated at room temperature over night, stopped by addition of 1 µL Proteinase K, and then transformed into *E.coli*.

#### 2.2.3.4.5 Sequencing

Sequencing reactions were performed using the chain termination method (Sanger et al., 1977) , using the Big Dye<sup>®</sup> Terminator Cycle Sequencing Kit Version 3.1 (Applied Biosystems). A typical sequencing reaction contained 100 ng to 150 ng plasmid DNA or 0.5

ng to 25 ng PCR product as template, one primer with a final concentration of 1 mM and 2  $\mu$ L Big Dye v3.1 in a total volume of 10  $\mu$ L. This mix was volume adjusted with HPLC-H<sub>2</sub>O to 20  $\mu$ L after completion of the sequencing reaction.

The PCR program used for sequencing consists of the following steps:

<u>Step</u>	<u>Temperature</u>	<u>Time</u>
Denaturing	96°C	0:20 min
Denaturing	96°C	0:10 min
Annealing	50°C	0:05 min
Elongation	60°C	4:00 min
Elongation	60°C	5:00 min
	16°C	infinity

Sequence runs were performed at the Institute for Genetics, University of Cologne and the data was available via intranet.

## 2.2.3.5 Polymerase Chain Reaction

### 2.2.3.5.1 Standard PCR

PCR is a technique to exponentially amplify in vitro a small quantity of a specific nucleotide sequence in the presence of template sequence, two oligonucleotide primers that hybridize to opposite strands and flank the region of interest in the target DNA and a thermostable (taq) DNA polymerase. The reaction is cycled involving template denaturation, primer annealing, and the extension of the annealed primers by DNA polymerase until enough copies are made for further analysis.

The cycling conditions for PCR were as follows:

<u>Step</u>	<u>Temperature</u>	<u>Time</u>
Denaturing	95°C	5 min
Denaturing	95°C	0:30 min
Annealing	Primer dependent	0:30 min
Elongation	72°C (68°C for <i>Pfx</i> )	1 min/kb (2 min/kb for <i>Pfu</i> )
Elongation	72°C (68°C for <i>Pfx</i> )	7:00 min
	16°C	infinity

The annealing temperature ( $T_a$ ) was calculated from the GC content of the primers using the formula:  $T_a = 2\text{ }^\circ\text{C} \times (A + T) + 4\text{ }^\circ\text{C} \times (G + C)$

Commercially available polymerases were used with the buffer supplemented (as per manufacturer's protocol). For the homemade *Taq*; the following final concentrations were applied:

67 mM Tris HCl, pH 8.8

16 mM	(NH <sub>4</sub> ) <sub>2</sub> SO <sub>4</sub>
0.1%	Tween
1.5 mM	MgCl <sub>2</sub>
0.2 mM	dNTP's (each nucleotide)
0.2 mM	Primer 1
0.2 mM	Primer 2

#### 2.2.3.5.2 Colony PCR

Colony PCR is a method used to quickly screen for plasmid inserts directly from *E. coli* colonies without plasmid preparation. PCR reaction is assembled as standard PCR except the template DNA is a single bacterial colony. With a sterile pipette tip a single bacterial colony on the agar plate was picked and transferred into a PCR tube containing 20 µl H<sub>2</sub>O<sub>bd</sub>. The cells were denatured at 94°C for 20 min in a PCR cycler to release the DNA. The standard PCR (2.2.3.5.1) was conducted with 1 µL of sample as template.

#### 2.2.3.5.3 Semi-quantitative RT-PCR

For semi-quantitative RT-PCR analysis total RNA was isolated from different mutant lines (2.2.3.3.2). cDNA synthesis was performed as described in 2.2.3.3.4 and 1 µL of the cDNA was used as a template for PCR (2.2.3.5.1). A house-keeping gene Actin2 was used always as a control for normalization. The PCR products were loaded on a gel (2.2.3.3.6) and analyzed for expression.

#### 2.2.3.5.4 Real-Time PCR

Real-time analysis was done on a 7300 Real-Time PCR system (Applied Biosystems) using the Sequence Detection Software v1.4 with the Power SYBR Green mastermix (ABI Prism) according to manufacturer's instructions. Expression levels were normalized to Actin2 expression levels. Quantitative RT-PCR experiments were performed on three independent biological samples and three technical replicates.

### 2.2.4 Biochemical methods

#### 2.2.4.1 Protein extraction from *E. coli*

Gene (*ENO1*) expression was induced by the addition of 1 mM IPTG (isopropyl-b-D-thiogalactopyranoside) to the culture. The cells were pelleted by centrifugation at 4000 g for 15 min, re-suspended in solution containing 100 mM Tris-HCl (pH7.5), 1.5 M NaCl, 2 mM EDTA supplemented with 20 µL mL<sup>-1</sup> Protease Inhibitor Cocktail (Sigma, P2714). The suspension was lysed by sonication (20 cycles, duty cycle 50%, output control 4) with a

Branson sonifier 450. The lysate was centrifuged at 4000 g for 15 min and the supernatant was purified by Ni-NTA chromatography

#### **2.2.4.2 Protein extraction from *A. thaliana* seeds**

Ten Arabidopsis seeds were taken in a 1.5 mL tube and pulverized using a small pestle. 100  $\mu$ L of Seed Extraction Buffer (SEB) (Ruuska et al., 2002) was added to the tube and the contents were thoroughly mixed until a uniform suspension was formed. The protein in the suspension was quantified as described (2.2.4.7.1).

##### **Seed Extraction Buffer (SEB):**

25 mM	Tris-HCl, pH8.0
125 mM	NaCl
0.5 mM	EDTA
0.5% (w/v)	SDS

#### **2.2.4.3 Enrichment of proteins by Nickel-nitrilotriacetic acid affinity chromatography**

Nitrilotriacetic acid (NTA) is a tetra-dentate chelating adsorbent occupying four of the six ligand binding sites in the coordination sphere of the nickel ion, leaving two sites free to interaction with the 6xHis tag (Hochuli, 1989). This resin allows one-step purification of 6xHis-tagged proteins using high flow rates and pressures. The supernatant from the protein extraction was mixed with 0.5 mL of Ni-NTA agarose and pre-equilibrated with 50 mM NaCl and 100 mM Na-Pi (pH 7.8). The recombinant protein was allowed to bind to the Ni-NTA agarose for 1 h at 4°C, and after transfer to a column (i.e. a glasswool plugged pasteur pipette), the resin was washed twice with 800  $\mu$ L of 100 mM Na-Pi (pH 7.8), 8 mM imidazole and the recombinant protein was specifically eluted in four steps with 100  $\mu$ L each of 100 mM Na-Pi (pH 7.8) and 150 mM imidazole. The recombinant protein activity was enriched in the third fraction.

#### **2.2.4.4 Separation of proteins by SDS-PAGE**

For SDS-polyacrylamide gel electrophoresis (SDS-PAGE), the 2050 Midget Minigel apparatus system (Pharmacia, Freiburg, Germany) was used. The separation of proteins under denaturing conditions was carried out according to the method of Laemmli (1970). A 12.5% separating gel was overlaid with water saturated n-butanol, which was removed after

polymerization. Polymerization reaction was started by adding TEMED. The sample protein and molecular weight markers (Dalton Mark VII-L (Sigma) were applied into the wells of the stacking gel and electrophoresed at 40 mA for 5 min. The fractionation of the proteins was continued at 25 mA in the separating gel.

**4 x Stacking gel buffer:**

500 mM	Tris/HCl, pH 6.8
0.4%	SDS

**4 x Separating gel buffer:**

1.5 M	Tris/HCl, pH 8.8
0.4%	SDS

**Stacking gel:**

25% (v/v)	4 x Stacking gel buffer
15% (v/v)	Acrylamide-Bisacrylamide-Solution (37.5 : 1) (Roth, Gel 30)
0.06% (w/v)	APS
0.3% (v/v)	TEMED

**Separating gel (12.5% Acrylamide):**

25% (v/v)	4 x Separating gel buffer
42% (v/v)	Acrylamide-Bisacrylamide-Solution (37.5 : 1) (Roth, Gel 30)
0.05% (w/v)	APS
0.05% (v/v)	TEMED

**Sample Buffer (2x):**

125 mM	Tris/HCl, pH 6.8
20% (w/v)	Glycerin
5% (w/v)	SDS
5% (v/v)	$\beta$ -Mercaptoethanol
0.0025% (w/v)	Bromphenol blue

## 2.2.4.5 Staining of Proteins

### 2.2.4.5.1 Protein staining with Coomassie-Brilliant Blue

The protein staining was carried out according to Weber and Osborn (1969). In addition, the staining solution I and II were mixed in equal parts. The SDS-PAGE gel was stained for about 30 min with gentle shaking. For de-colorization and removal of excess stain from the background, the gel was shaken in de-colorization solution and documented photographically or vacuum dried for several days with heat.

Coomassie Solution I:

0.5% (w/v)	Coomassie Brilliant blue (Serva-Blue G250, Serva)
80% (w/v)	MeOH

Coomassie Solution II:

20% (v/v)	Acetic acid
-----------	-------------

De-colorization solution:

10% (v/v)	Acetic acid
40% (v/v)	MeOH

**2.2.4.5.2 Protein staining with Silver nitrate**

The staining was performed by the method of Blum *et al.*, 1987. It is approximately 5 to 10 times more sensitive than staining with Coomassie-Brilliant Blue (2.2.4.4.1). The gels were shaken for 2 h in the fixative solution, then washed 3 times for 20 min each with wash solution I and 1 min with wash solution II. After three washing steps with water for 20 s, the gels were incubated for at least 20 minutes in impregnating solution. After washing twice with water, each for 20 s, the gels were incubated in the developer solution until the appearance of distinct bands. The gel was then again washed twice briefly with water and incubated for 30 min in a stop solution. Subsequently, the gels were dried and documented.

**Fixing solution:**

50% (v/v)	Methanol
12% (v/v)	Acetic acid
0.019% (v/v)	Formaldehyde

**Wash solution I:**

50% (v/v)	Ethanol
-----------	---------

**Wash solution II:**

800 $\mu$ M	Sodium thiosulfate
-------------	--------------------

**Impregnating solution:**

0.2% (w/v)	Silvernitrate
------------	---------------

0.028% (v/v)                      Formaldehyde

**Developing solution:**

6% (w/v)                              Di-sodium carbonate

0.019% (v/v)                      Formaldehyde

18  $\mu$ M                                  Sodium thiosulfate

**Stop solution:**

50% (v/v)                              Methanol

12% (v/v)                              Acetic Acid

#### 2.2.4.6 Western Blotting

Western blotting or immune blotting is used to detect a target protein in a sample (containing a complex mixture of proteins) by using a polyclonal or monoclonal antibody specific to that protein. The transfer of proteins from poly-acrylamide gels to PVDF (Polyvinylidene Difluoride) membranes was done with a transfer chamber (Carbo Glass, Schleicher & Schuell) in the semi-dry blotting procedure as per KHYS-Andersen, 1984. The construction of the apparatus and the preparation of the solutions were made in accordance with the manufacturer. The cathode and anode buffer used was from RotiBlot<sup>®</sup> system (Roth, Karlsruhe). Before the construction of the system, the PVDF membrane was activated by submerging for 1 min in methanol. The electron transfer was carried out at 1 mA.cm<sup>-2</sup> for 60-90 min.

#### 2.2.4.7 Immunological detection of proteins on PVDF membrane

After transfer of proteins to a PVDF membrane, the area of the membrane containing the molecular weight marker was removed and stained in Coomassie Brilliant Blue. The rest of the membrane was transferred into blocking solution and incubated for 1 h at RT or overnight at 4°C. It was washed twice for 10 min in TBST-T and once in TBS for 10 min before the membrane was incubated with primary antibody (mouse anti-Penta-His IgG, Qiagen, Hilden, Germany) directed against the histidine tag of the protein addressed in a 1:2000 dilution in blocking buffer which was incubated for 2 h. This was followed by three washing steps with TBST-T and TBS, further, the secondary antibody (Goat anti-mouse IgG was alkaline-phosphatase conjugate, Pierce Biotechnology Inc., Rockford, IL) in a 1:2500 dilution in blocking buffer was added and membrane was incubated for 1-2 h. Thereafter, the membrane

was washed four times for 10 min in TBST-T. For the color development, the membrane was immersed in 10 mL of buffer with 33  $\mu$ L BCIP and 66  $\mu$ L of NBT, until color signals were visible. The staining solution was then briefly rinsed with water and the reaction was stopped by incubation for 5 min in 3% (w/v) TCA. The membrane was rinsed again with water, dried and wrapped in aluminum foil for better preservation.

**TBST-T:**

10% (v/v)	10 x TBS
0.2% (v/v)	Triton X-100
0.05% (v/v)	Tween 20

**TBS (10 x):**

0.1 M	Tris/HCl, pH 7.4
1.5 M	NaCl

**Buffer A:**

100 mM	Tris/HCl, pH 9.5
100 mM	NaCl
5 mM	MgCl <sub>2</sub>

**Blocking solution:**

3% (w/v)	BSA in 1 x TBS
----------	----------------

**BCIP-Stock solution:**

5% (w/v)	BCIP in DMF
----------	-------------

**NBT-Stock solution:**

5% (w/v)	NBT in 70% (v/v) DMF
----------	----------------------

**2.2.4.8 Determination of protein concentration****2.2.4.8.1 Standard method (Bradford 1976)**

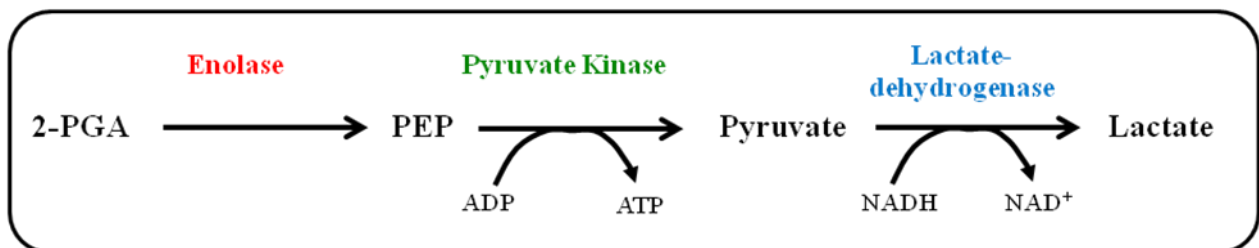
The protein quantification was carried out according to Bradford (1976). The reagent Rotiquant (Roth) in a 1:5 dilution was mixed with the sample and the absorbance was photometrically measured at  $\lambda = 595$  nm. As a calibration curve, a dilution series of 0.5-20  $\mu$ g BSA was used.

**2.2.4.8.2 Detergent-compatible protein assay**

DC protein Assay is a colorimetric assay for protein concentration determination following detergent solubilization. The assay is based on the reaction of protein with an alkaline copper tartrate solution and Folin reagent. The total protein content was measured from 100  $\mu$ L of the crude homogenate after detergent solubilization using the Bio-Rad detergent compatible protein assay system (BIO-RAD) using  $\gamma$ -globulin as a standard per manufacturer's instructions.

#### 2.2.4.9 Enzyme activity assay for enolase

Measurement of enolase activity was performed by a modified protocol from Miernyk and Dennis (1982) at 340 nm and a temperature of 25°C in a microtiter plate reader (Spectrafluor Plus, Tecan, Austria). The reaction sequence is illustrated below:



For the forward (glycolytic) reaction the assay mixture contained in 200  $\mu$ L, 100 mM Tricine–NaOH (pH 8.0) or 100 mM HEPES–NaOH (pH 7.0), 1mM MgSO<sub>4</sub>, 10 mM KCl, 5 mM 3-phosphoglyceric acid (3-PGA), 0.1 mM 2,3-diphosphoglyceric acid (2,3-DPGA), 1 mM ADP, 0.2 mM NADH, 3 U phosphoglycerate mutase (PGyM) from rabbit muscle (Boehringer, Mannheim, Germany), 2 U pyruvate kinase (PK) (Sigma–Aldrich, Steinheim, Germany) and 2.75 U lactate dehydrogenase (LDH) (Roche Diagnostics, Mannheim, Germany). Despite the lack of availability of 2-PGA by chemical supply companies, a residual batch of 2-PGA (Sigma–Aldrich, Steinheim, Germany) was used as the direct substrate at concentrations of up to 5 mM. In the case when 2-PGA was used 2,3-DPGA and PGyM were omitted. For the reverse (gluconeogenic) reaction the standard assay mixture contained 100 mM Tricine–NaOH (pH 8.0) or 100 mM HEPES–NaOH (pH7.0), 1 mM MgSO<sub>4</sub>, 10 mM KCl, 5 mM PEP, 0.1 mM 2,3-DPGA, 2 mM ATP, 0.2 mM NADH, 3 U PGyM, 6 U 3-phosphoglycerate kinase (PGK) from baker's yeast (Sigma–Aldrich, Steinheim, Germany) and 3 U glyceraldehyde 3-phosphate dehydrogenase (GAPDH) from rabbit muscle (Roche Diagnostics, Mannheim, Germany). Kinetic constants ( $K_m$ ,  $V_{max}$ ) were obtained from

hyperbolic curve fits to the experimental data implemented in SigmaPlot8.0 for windows (SPSS Inc.).

#### **2.2.4.10 Total fatty acid analysis in seeds**

Total fatty acids in seeds were quantified by gas chromatography after derivatization to fatty acid methyl esters using pentadecanoic acid (15:0) as internal standard (Browse et al., 1986). The de-saturation index was calculated as:

$$I_D = (18:1 + 2 \cdot 18:2 + 3 \cdot 18:3 + 20:1 + 22:1) / (14:0 + 16:0 + 18:0 + 20:0 + 22:0)$$

#### **2.2.4.11 Amino acid analysis in mature flowers**

Mature flowers were used for aromatic amino acid analysis, 6 flowers of mutants and their corresponding wild types were macerated to a fine powder using liquid nitrogen. 50  $\mu$ l of 1 M perchloric acid was added to the powder followed by the addition of 50  $\mu$ l of 0.1M perchloric acid. The pH was neutralized to pH 7.0 with 9.3  $\mu$ l of 5 M  $KCO_3$ . The mixture was centrifuged for 30 min at 14,000 rpm in low temperature of 4°C. The supernatant was taken in a fresh tube for HPLC analysis. Samples were pre-column- derivatized with o-phthalaldehyde (Lindroth and Mopper, 1979) and separated on a Hewlett Packard HP1100 HPLC system, using a Nucleodur 100-5 C18 ec column (Macherey & Nagel, Germany). An optimized stepwise gradient ranging from 7% buffer A (50% methanol, 50% acetonitrile) and 93% buffer B (40 mM sodium acetate, pH 6.5) to 80% buffer A was used for elution at 35°C for 33 min at a flow rate of 1 mL/min after injection of 5  $\mu$ l sample. Derivatives were detected by excitation at 230 nm and their fluorescence at 450 nm.

#### **2.2.4.12 Determination of flavonoids in mature flowers**

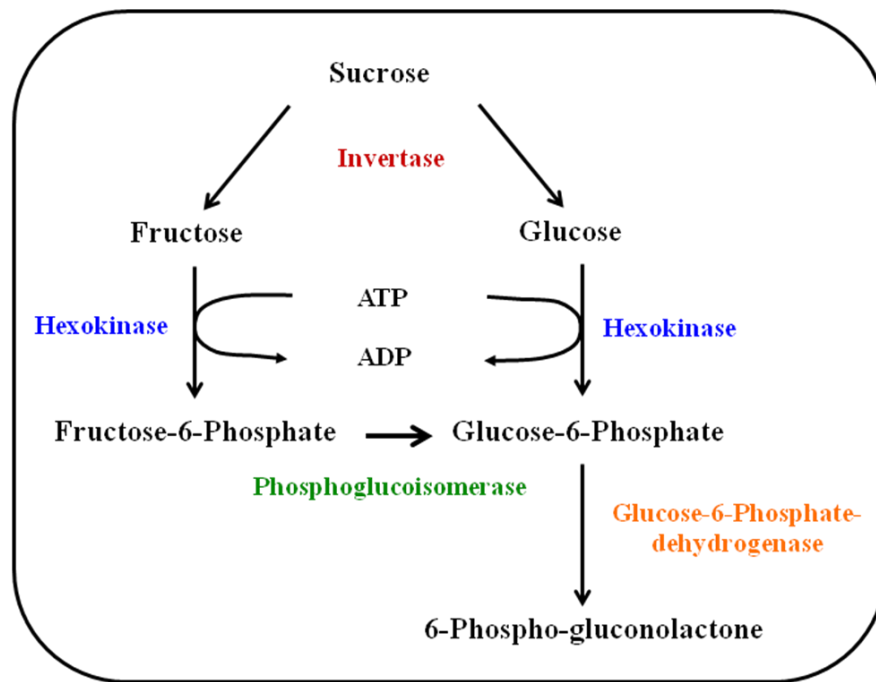
For flavonoid measurements, six mature flowers were pulverized using liquid nitrogen and extracted as described previously (Pinto et al., 1999) in 200 $\mu$ l of MeOH: H<sub>2</sub>O:HCl (70:20:1 by volume) at 60°C for 1 h (99.8 MeOH and 35.4% HCl) and the absorption at 310 nm was determined after cooling down the extracts at room temperature using a Tecan Infinite 200 reader equipped with the Magellan v6.3 software.

#### **2.2.4.13 Determination of anthocyanins in mature flowers**

For spectrophotometric determination of anthocyanin contents, six mature flowers were ground to powder using liquid nitrogen and extracted as described previously (Li et al., 2005) in 200  $\mu$ l of acidified methanol MeOH:H<sub>2</sub>O:HCl (70:29:1 by volume) for 48h at -20°C. Absorbance of the extracts was read using 535nm using a Tecan Infinite 200 reader equipped with the Magellan v6.3 software.

#### **2.2.4.14 Determination of soluble sugars and starch in seeds**

For the extraction of soluble sugars and starch, 35 seeds were homogenized in 200  $\mu$ L of 80% (v/v) ethanol and incubated at 70°C for 90 min. Following centrifugation at 16,000 g for 5 min, the supernatant was transferred to a tube. The pellet was extracted thrice with 100  $\mu$ L of 80% ethanol. The solvent of the combined supernatants was evaporated at room temperature under a vacuum. The residue was dissolved in 30  $\mu$ L of water, representing the soluble carbohydrate fraction. The pellet left from the ethanol extraction, which contained the insoluble carbohydrates including starch, was homogenized in 50  $\mu$ L of 0.2 M KOH, and the suspension was incubated at 95°C for 1 h to dissolve the starch. 8.75  $\mu$ L of 1 M acetic acid was added digested overnight at RT by adding 7 U of  $\alpha$ -amylase and 6 U of amyloglucosidase. The enzymes in the extract were inactivated the next day for 2-3h at 37°C. To quantify soluble sugars, 10  $\mu$ L of the sugar extract was added to 190  $\mu$ L of reaction buffer containing 100 mM HEPES pH7.5, 10 mM MgCl<sub>2</sub>, 0.8 mM NAD, 2 mM ATP, and 0.1 U of Glc-6-P dehydrogenase. For enzymatic determination of Glc, Fru, and Suc, 0.75 U units of hexokinase, 1 U of phosphoglucoisomerase, and 2  $\mu$ L of an Invertase solution (200 mg/mL) were added in succession. The production of NADPH was followed spectrophotometrically at a wavelength of 340 nm using Tecan Infinite 200 with the Magellan v6.3 software. Similarly, starch which was digested overnight to glucose and was assayed as shown above. The reaction sequence is represented in the diagram below:



## 2.2.5 Histochemical methods

### 2.2.5.1 Alexander's staining

Pollen viability of the mutants and corresponding wild types were assessed using Alexander staining (Alexander, 1969). The pollen grains released from the anthers were immersed in Alexander's stain and observed under the light microscope. The viable pollen cytoplasm stain red and the cell wall stains green.

### 2.2.5.2 DAPI staining

4'-6-Diamidino-2-phenylindole (DAPI) is known to form fluorescent complexes with natural double-stranded DNA, showing fluorescence specificity for AT, AU and IC clusters. Male gametophyte development was analyzed by DAPI staining (Park et al., 1998) on mature, dehiscent and indehiscent pollen.

### 2.2.5.3 ACN staining

Cross-sections of the stem 1 mm above the rosette were used to analyze lignified tissue in mutant and corresponding wild-type plant using 1:1:1 of astrablue, chrysoidin and neofuchsin at a concentration of 1 mg/mL each. With this method lignin stains red, suberin and cutin yellow and cellulose cell walls are contrasted blue. The cross-sections were immersed in the ACN stain and immediately analyzed by light microscopy.

### 2.2.5.4 Histochemical localization of secondary metabolites in pollen

For the histochemical localization of secondary metabolites, pollen from the wild-type and mutant plants were prepared with and without additives. After incubation for 15-30 min in the additive containing 0.25% Diphenylborate-2-aminoethyl (DPBA) + 0.005% Triton X-100, the pollen were viewed with an excitation of 330 nm  $<\lambda < 380$  nm and an emission filter  $\lambda > 420$  nm and documented photographically. With the help of DPBA, yellow or greenish-induced secondary metabolite fluorescence was observed.

All histochemical analyses were examined with a light microscope (Eclipse E800; Nikon, Düsseldorf, Germany) equipped for differential interference contrast and fluorescence microscopy. Images were captured using a 1-CCD color video camera (KY-F1030; JVC, Singapore) operated by the DISKUS software package (Technisches Büro Hilgers, Königswinter, Germany).

## 2.2.6 Microscopy

### 2.2.6.1 Transmission electron microscopy

Spurr's medium is a low viscosity epoxy embedding medium used for transmission electron microscopy work. Pollen and stamen were taken from different flower stages and fixed with 2% glutaraldehyde in 50 mM phosphate buffer, pH 7.2, overnight at 4°C. Samples were postfixed in 1% osmium tetroxide for 8 h on ice, dehydrated in a graduated acetone series, including a step with 1% uranylacetate (in 50% acetone, 2 h), embedded in Spurr's resin, and polymerized at 60°C for 72 h. Ultrathin sections (60 to 70 nm) were cut with a diamond knife (Diatome, Biel, Switzerland) on a Leica EM UC6 ultramicrotome (Leica Microsystems, Vienna, Austria) and mounted on pioloform-coated copper grids. The sections were stained with lead citrate and uranyl acetate (Reynolds, 1963) and viewed with a JEOL JEM-2100 transmission electron microscope (JEOL Ltd., Tokyo, Japan) operated at 80 kV. Micrographs were taken using a 4k x 4k Gatan UltraScan 4000 CCD camera (Gatan Inc, Pleasanton, CA, USA). The sections were also stained using toluidine blue stain (A 4:1 mixture of 1% Toluidine blue, 1% Borax and 1% Pyromin A) for light microscopy viewing.

### 2.2.6.2 Scanning electron microscopy

For scanning electron microscopy, mature dry seeds and young leaves with trichomes were mounted on stubs, and sputter coated with palladium gold. Specimens were examined with a scanning electron microscope (LEO 430i using the image analysis software sjs ver2.11).

### **2.2.6.3 Differential Interference Contrast (DIC) microscopy**

For DIC light microscopy, ovules were removed from the pistil or the silique and immersed in a droplet of water on a slide and covered with a cover-slip. The whole-mount ovules were examined with a light microscope (Eclipse E800; Nikon, Tokyo, Japan) equipped for differential interference contrast and fluorescence microscopy. Images were captured using a 1-CCD color video camera (KY-F1030; JVC, Singapore) operated by the DISKUS software package (Technisches Buero Hilgers, Koenigswinter, Germany) equipped with Nomarski optics.

### **2.2.6.4 Fluorescence microscopy**

Protein localizations were assayed using the fluorescent proteins GFP with optimal excitation and emission wavelengths of 488 nm/507 nm. Transformed Arabidopsis cells were pelleted by short centrifugation (5 min, 350 g) and then spread on a microscope slide and used for microscopy viewing (Eclipse E800; Nikon, Tokyo, Japan). Images were captured using a 1-CCD color video camera (KY-F1030; JVC, Singapore) operated by the DISKUS software package (Technisches Buero Hilgers, Koenigswinter, Germany)

## **2.2.7 Web Links used**

Aramemnon

<http://aramemnon.botanik.uni-koeln.de/>

NCBI

<http://www.ncbi.nlm.nih.gov/>

TAIR

<http://www.arabidopsis.org/>

eFP Browser

<http://bar.utoronto.ca/efp/cgi-bin/efpWeb.cgi>

SIGnAL

<http://signal.salk.edu/cgi-bin/tdnaexpress>

### 3 Results

#### 3.1 Identification and sub-cellular localization of *Arabidopsis thaliana* plastidic enolase (ENO1) and cytosolic enolase (ENOC)

The *A. thaliana* genome contains three genes annotated as putative enolases (ENOs) (At2g29560, At2g36530, At1g74030). According to the Aramemnon database (<http://aramemnon.botanik.uni-koeln.de/>; Schwacke et al., 2003), At1g74030 encodes a protein containing an N-terminal transit peptide for plastid targeting with a consensus prediction (i.e. its probability) of 15.8 compared to 0.6 and 0.0 for cytosolic forms At2g36530 and At2g29560, respectively (<http://aramemnon.botanik.uni-koeln.de/>). The protein function of At1g74030 is annotated as phosphopyruvate hydratase and the various biological processes to which the protein contributes are gluconeogenesis, glycolysis, anaerobic respiration, serine-isocitrate lyase pathway, aerobic glycerol catabolic process, non-phosphorylated glucose catabolic process, anaerobic glycolysis, glucose catabolic process to butanediol, acetate fermentation, glucose catabolic process to D-lactate and ethanol, and the glyceraldehydes 3-phosphate catabolic process (<http://aramemnon.botanik.uni-koeln.de/>). The sub-cellular localization of the putative plastidic ENO (i.e. ENO1) was investigated after fusion of 101 N-terminal amino acid fragments were to GFP, and transiently expressed in a heterotrophic *A. thaliana* cell culture. The ENO1-GFP fusion protein was localized within the plastids (Fig. 3.1). As a positive control for plastid targeting, GFP was fused to a fragment of the triose phosphate/phosphate translocator (TPT; At5g46110) and expressed in the same *A. thaliana* cell culture. The presence of GFP fluorescence within the plastids of *A.thaliana* cultures confirmed the existence of an active plastidic enolase and thus has been verified as annotated.

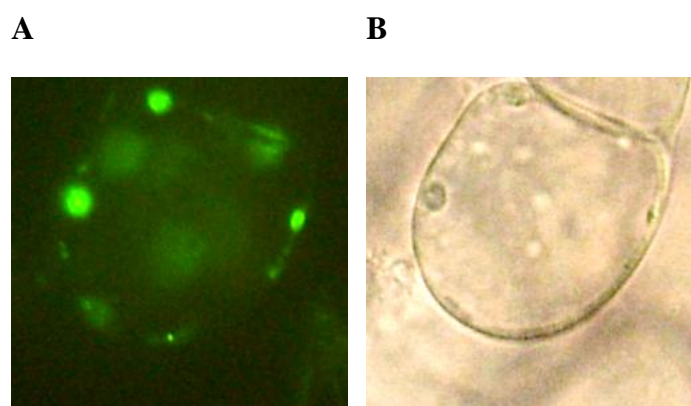


**Figure 3.1: Sub-cellular localization of ENO1.** The ENO1-GFP fusion protein was transiently expressed in a heterotrophic *A. thaliana* cell culture. A transformed cell is shown as a microscopic fluorescence image (exc, 485 nm; em, 530 nm) (A) compared to a bright field image (B) of the same cell.

Recently, a dual targeting has been shown for one of the two putative cytosolic ENO proteins (At2g36530, equivalent to AtLOS2), (Lee et al., 2002). A LOS2-GFP fusion protein was located both in the cytosol and in the nucleus. The second cytosolic enolase annotated as At2g29560 was identified in the Aramemnon database as a putative cytosolic enolase, which has a phosphopyruvate hydratase activity. Its sub-cellular localization was unconfirmed. At2g29560 does not encode a protein for plastid targeting shown with a consensus prediction (i.e. its probability) of 0.6 compared to the plastidic enolase having 15.8 (<http://aramemnon.botanik.uni-koeln.de/>). In order to verify the sub-cellular localization of ENOc, 107 N-terminal amino acid fragments were fused to GFP and the fusion protein was transiently expressed in *A. thaliana* cell culture. Green fluorescence of ENOc-GFP fusion protein was localized both in the cytosol and the nucleus (Fig. 3.2A and B) along with the cytoplasmic strings passing through the vacuole (Fig. 3.2A). The localization resembles the pattern of AtLOS2 (Lee et al., 2002).

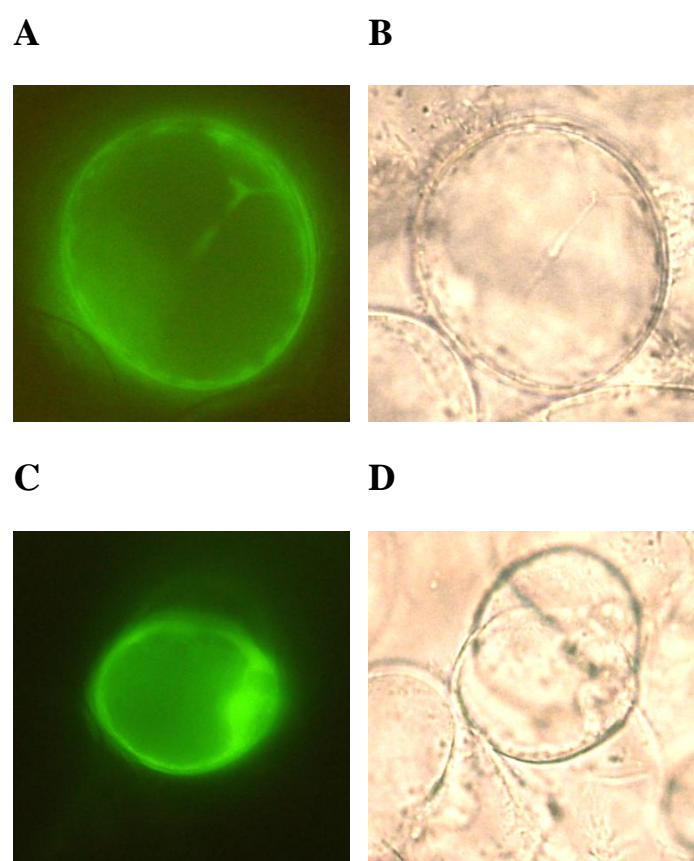


**Figure 3.2: Sub-cellular localization of ENOc (At2g29560).** The ENOc-GFP fusion protein was transiently expressed in a heterotrophic *A. thaliana* cell culture. A transformed cell is shown as a microscopic fluorescence image (exc, 485 nm; em, 530 nm) (A) and (C) compared to a bright field image (B) and (D) of the same cell.

### 3.2 Over-expression of ENO1 in *E. coli*

In order to functionally characterize the putative plastidic enolase, the cDNA of At1g74030 was fused to a C-terminal His-tag and the construct was expressed in *E. coli*. Over-expression of the recombinant protein was observed 1 h post induction by IPTG (Fig. 3.3). ENO1 protein was extracted under native conditions and separated by SDS-PAGE.

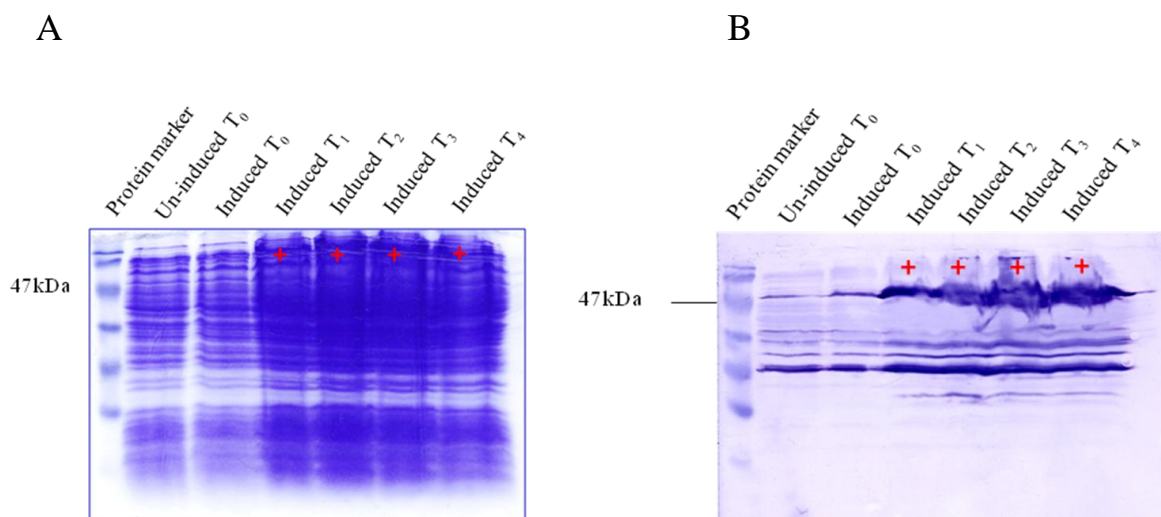


**Figure 3.3: Recombinant ENO1 expression and analysis.** Crude lysate of protein before and after induction by IPTG (Time points T<sub>0</sub> h to T<sub>4</sub> h) were loaded in a series and stained by Coomassie-Brilliant Blue R250 in the presence of a Protein Standard Marker. Western Blot analysis using Anti-hexa histidine antibody showed the protein of interest as visualized by a thick band above the 47kDa band of the protein marker in the induced samples. The increase in protein concentration was shown to be time-dependent in terms of induction.

In order to identify whether rENO1 protein was soluble or present in inclusion bodies, the crude lysate was centrifuged and aliquots of supernatant (soluble fraction) and pellet (insoluble fraction) were separated by SDS-PAGE and analyzed by Western Blot. It was observed that the lysate and the pellet fraction had the presence of various protein bands and the supernatant had a major band almost equivalent to the predicted ENO1 in size (Fig. 3.3). rENO1 was identified in the soluble fraction.

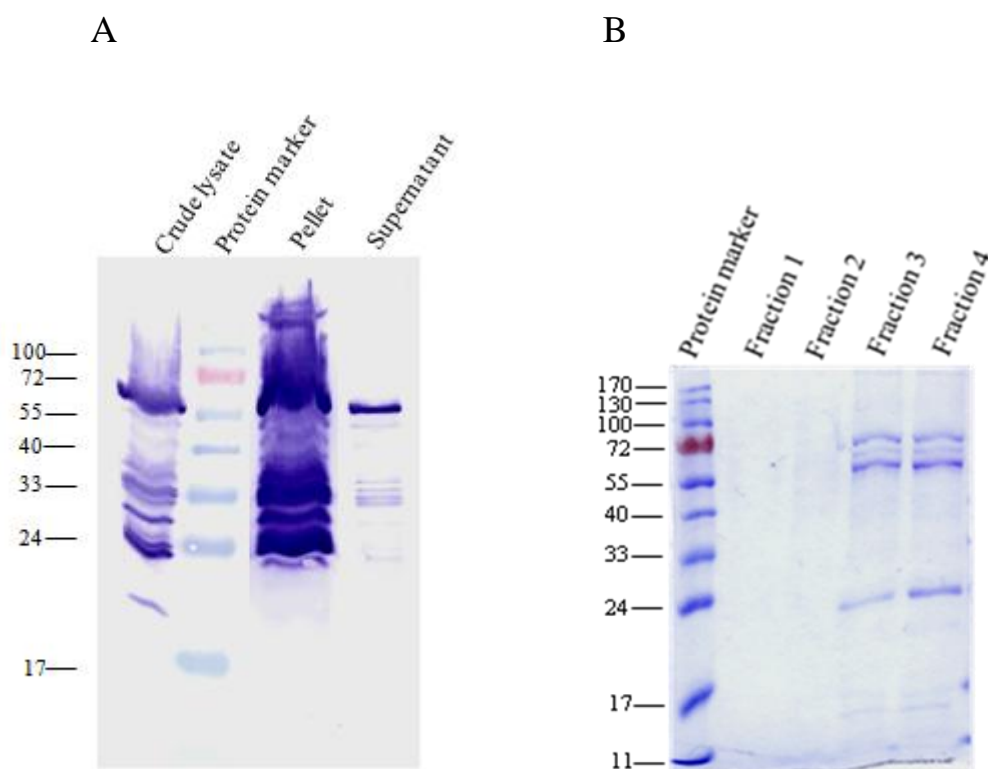


**Figure 3.4: rENO1 is a soluble protein.** Western Blot analysis of crude lysate, pellet fraction and supernatant fraction of protein with anti-hexahistidine tag antibody revealed that the rENO1 was present as a soluble protein in the supernatant fraction indicated by the thick band above the 55kDa band of the marker (A). Ni-NTA column purification of rENO1. Four fractions of the final elute were loaded on an SDS-PAGE gel and stained by Coomassie Brilliant-Blue stain. (B) rENO was shown to be completely eluted in the third and fourth fraction, which was then pooled and used for further analysis.

Since the supernatant fraction contained several other non-specific proteins, rENO1 protein was enriched by chromatography on nickel-NTA. Following purification different fractions of the eluate were separated by SDS-PAGE and the products were stained to identify the fraction containing the rENO1 protein for enrichment. The rENO1 protein was identified in the third and fourth fraction of the eluate. A SDS-PAGE gel with the final preparation revealed three major protein bands (Fig. 3.5A). The three bands had apparent molecular weights ( $M_r$ ) of 77.0 KDa, 61.2 KDa and 23.7 KDa respectively. On Western blots using an anti-hexa histidine tag antibody, only one band (Fig. 3.5B) corresponding to a  $M_r$  of 60.34 KDa (Fig. 3.5D) could be detected. This band was identical to the protein band on SDS gels corresponding to a  $M_r$  of 61.2 KDa, determined in independent experiments. It was estimated densitometrically that approximately 49% of the total protein separated on SDS gels consists of the rENO1.

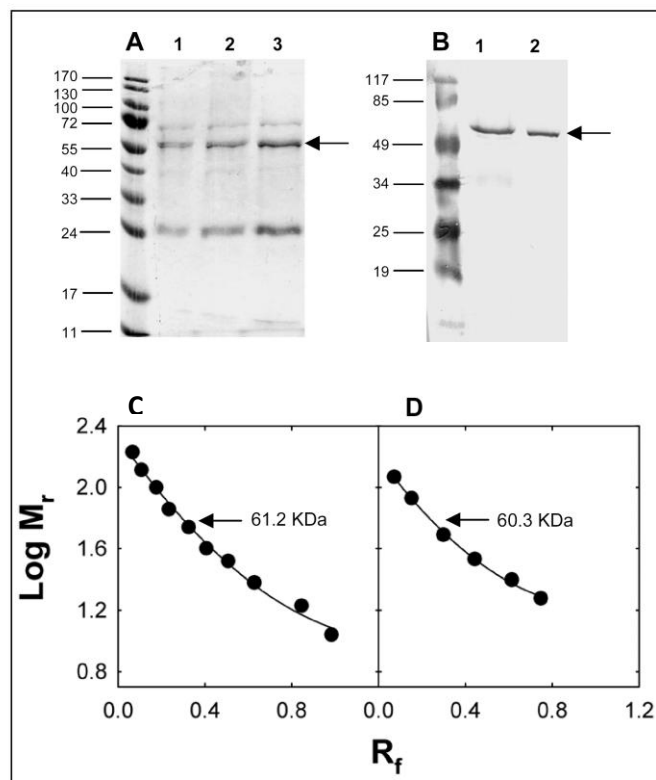


**Figure 3.5: Separation of a Ni-NTA purified ENO1 preparation on SDS-PAGE (A) and detection of the recombinant protein on a Western blot with an anti-hexahistidine-tag antibody.(B).** The relative migration distance ( $R_f$ ) of the corresponding ENO1 band was compared to different sets of molecular markers both on a SDS gel (C) or on a Western blot (D). The apparent molecular mass ( $M_r$ ) was calculated from polynomial regression curves fit to the  $\log M_r$  (markers) versus  $R_f$  plots. The numbers in (A) indicate concentration series (1-3  $\mu\text{g}$  of protein).

### 3.3 Recombinant ENO1 exhibits ENO activity; a kinetic characterization

The purified recombinant putative plastidic enolase was tested for its activity in a coupled enzymatic assay. 3-PGA (together with PGyM) or 2-PGA was used as a substrate in the reaction sequence (Fig. 3.6).

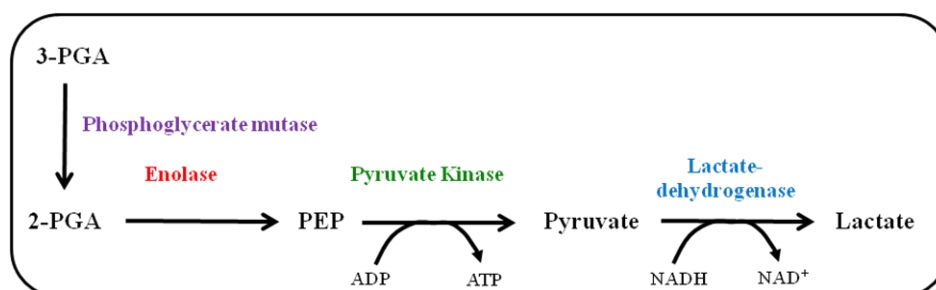


**Figure 3.6: Measurement of enolase activity (modified from Miernyk and Dennis 1982).**

In the standard assay, the enriched protein extract indeed exhibited an enolase activity with a specific activity between  $0.25$  and  $0.30 \text{ U}\cdot\text{mg}^{-1}$  protein. Considering about half of the protein

on the gel was the ENO1 protein band identified after SDS-PAGE and on Western blots, the maximum specific activity was calculated to be in the range between 0.5 to 0.6 U mg<sup>-1</sup> protein. As a control, lysates of wild-type or transformed *E. coli* cells, before induction of ENO1 expression by IPTG, were subjected to Ni-NTA chromatography and used for control enzymatic assays. ENO activity in crude cell lysates was increased to 8-fold and 11-fold upon induction with IPTG compared to lysates prepared from un-induced and wild-type *E. coli* cells, respectively. The specific ENO activity was further increased by a factor of 14 after Ni-NTA chromatography (data not shown). For further kinetic studies, the relative reaction velocity ( $v$ ) observed for saturating 2-PGA concentrations at pH 8.0 was referred to the highest ENO1 activity (100%). The pH response curves shown in Fig. 3.7 reveals distinct pH optima for the forward (PEP formation) and reverse (2-PGA formation) reaction. For the forward direction, there was a sharp pH-optimum between pH 7.5 and pH 8.5 compared to the reverse reaction, which exhibited a broader pH-optimum between pH 6.0 and pH 7.5.

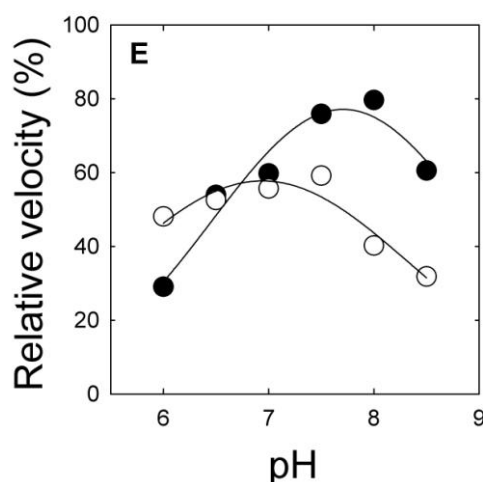


**Figure 3.7: pH dependency of the ENO1 reaction velocity.** ENO1 activity was determined at saturating substrate concentrations either in the direction of PEP- (●) or 2-PGA formation (○). The data are the mean of two independent measurements. The standard deviation was below 5% of the mean (not shown).

Substrate dependencies of ENO1 activity in the forward and reverse reaction obeyed Michaelis-Menten kinetics (Fig. 3.8), with apparent  $K_m$  values for the respective substrates in the submillimolar range (Table 3.1). At pH 8.0 the  $V_{max}$  of the forward direction was more than double compared to the  $V_{max}$  of the reverse reaction (Table 3.1, Fig. 3.7). In particular, the affinity for 2-PGA was high at pH 8, with a  $K_m$  in the upper micromolar range (Table 3.1). In general, the  $K_m$  values for both substrates were higher at pH 7.0 as compared to pH 8.0 (Table 3.1). The kinetic constants determined at pH 7.0 and pH 8.0 were used to calculate

the equilibrium constants for the ENO reaction at both pH values by applying the Haldane

$$\text{equation, e.g. (Segel, I.H, 1993)} K_{eq} = \frac{V_{\max(2-PGA)} \cdot K_m(PEP)}{V_{\max(PEP)} \cdot K_m(2-PGA)}$$

The thermodynamic equilibrium favors the formation of PEP from 2-PGA, with  $K_{eq}$ -values of 5.66 and 3.45 at pH 8.0 and pH 7.0, respectively (Table 3.1) and is hence close to the reported value of 6.7 (Bergmeyer, H.U, 1970). Moreover, from the ratios of the apparent  $K_m$  values for 3-PGA and 2-PGA, the thermodynamic equilibrium for the PGyM reaction could be estimated at both pH values (Table 3.1).

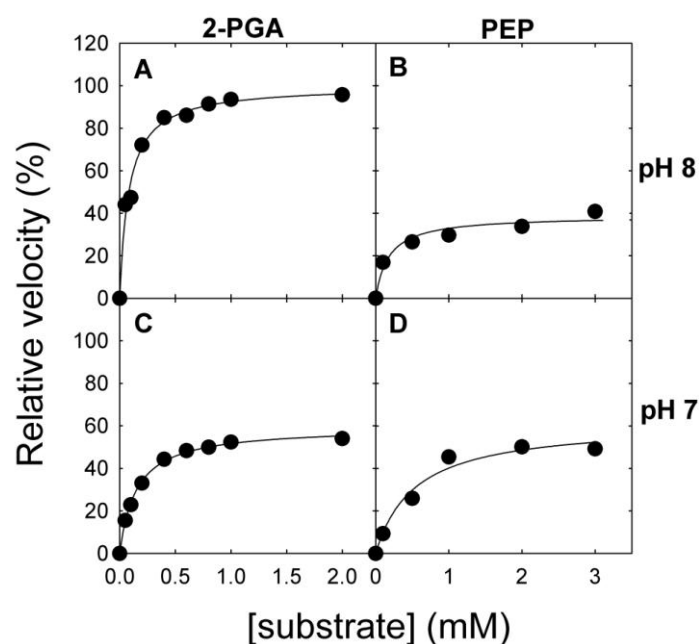


**Figure 3.8: Kinetic properties of recombinant ENO1.** The substrate dependencies of the reaction velocity of ENO1 were measured in the direction of PEP formation (forward reaction; A and C) or 2-PGA formation (reverse reaction; B and D), at pH 8 (A and B) or pH 7 (C and D).

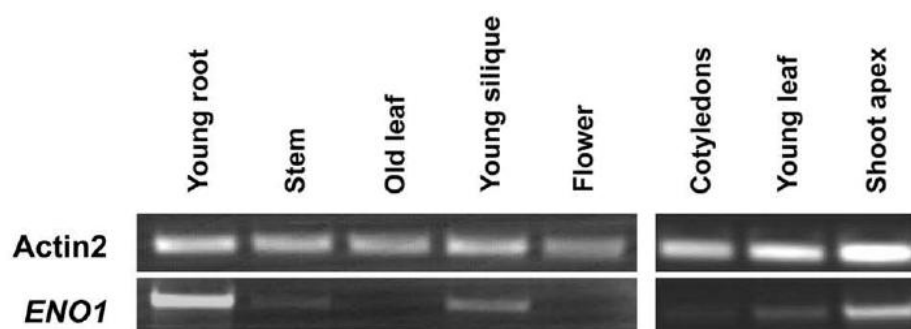
**Table 3.1 Kinetic constants of recombinant plastidic enolase in the forward (2-PGA consumption) and reverse reaction (PEP consumption).**

Substrate	pH 8			pH 7		
	$K_m$ (mM)	$V_{\max}$ (%)	$K_{eq}$	$K_m$ (mM)	$V_{\max}$ (%)	$K_{eq}$
3-PGA	$1.281 \pm 0.097$	$100 \pm 2.8$	$15.62^*$	$0.390 \pm 0.095$	$59.3 \pm 3.3$	$2.62^*$
2-PGA	$0.082 \pm 0.011$	$100 \pm 2.7$	<b>5.66</b>	$0.149 \pm 0.008$	$59.4 \pm 0.8$	<b>3.45</b>
PEP	$0.180 \pm 0.058$	$38.8 \pm 2.1$		$0.534 \pm 0.166$	$61.6 \pm 5.6$	

The equilibrium constants ( $K_{eq}$ ) were calculated according to the Haldane equation, whereas the  $K_{eq}$  for the PGyM reaction\* was estimated from the  $K_m$  (3-PGA)/ $K_m$  (2-PGA) ratios at both pH values.

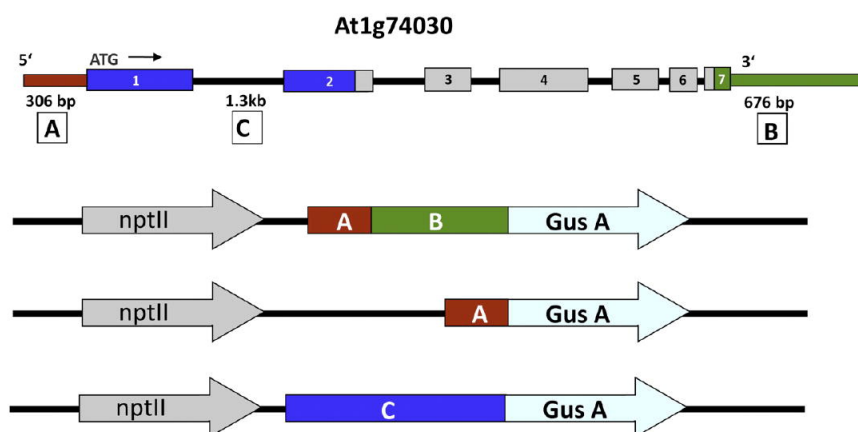
### 3.4 Tissue- and cell-specific expression profiles of *ENO1*

After verification of the catalytic activity and subcellular localization of *ENO1*, the temporal and spatial expression profile of *ENO1* was analyzed by both semi-quantitative RT-PCR and promoter::reporter gene fusions. For the semi-quantitative RT-PCR analysis various tissues of the wild type Col-0 plants four-week-old roots, stem, leaves, siliques, flowers, one-week-old roots, cotyledons, leaves, shoot apex and immature siliques were compared (Fig. 3.9)



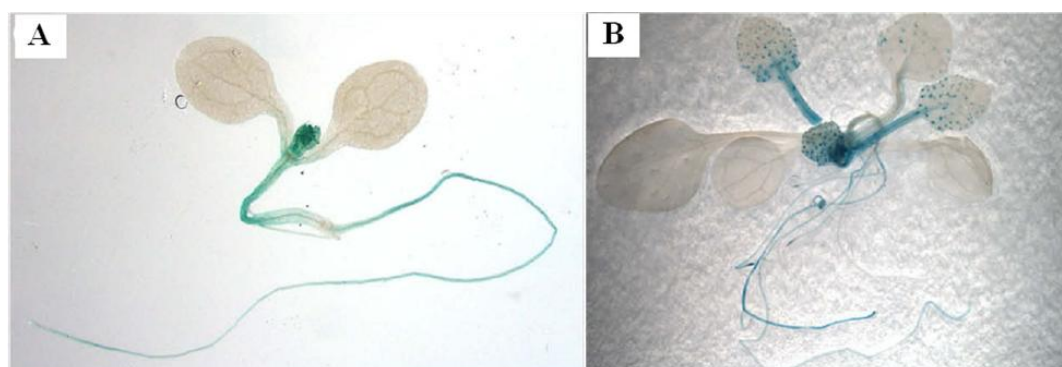
**Figure 3.9: Semi-quantitative RT-PCR analysis of *ENO1* expression in different parts of the plant.**

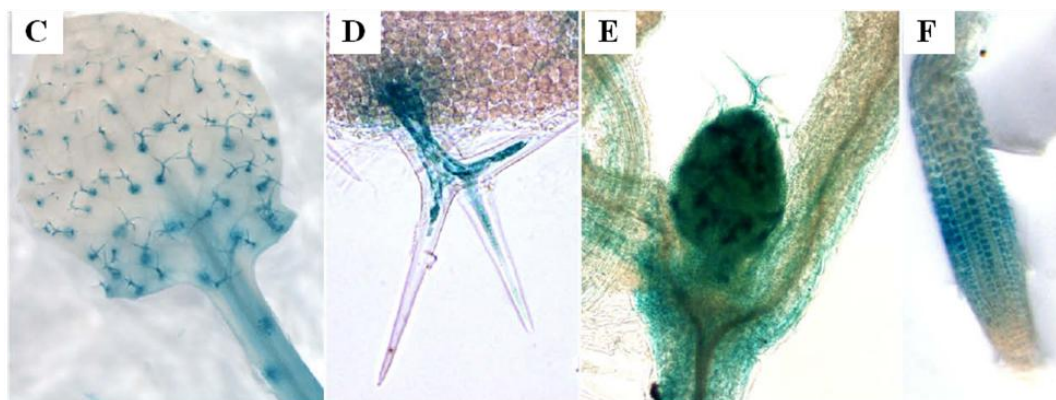
The mRNA abundance of *ENO1* was high in young roots and young siliques compared to the absence of transcript in the old roots and mature siliques (data not shown). The stem showed a very low abundance of transcript, and in the mature leaves and flowers the transcript was absent. It was also observed that the shoot apex had high abundance of transcript and surprisingly the young leaves showed presence of the transcript. *ENO1* expression was not reported in green tissues, so the only explanation that could be given is that the young leaves and the shoot apex have large numbers of mature trichomes on them. Trichomes are large colorless non-secreting epidermal cells where *ENO1* is expressed. In contrast, the cotyledons lacked transcript because of the absence of trichomes on them. The expression profile of the semi-quantitative RT-PCR matches the At1g74030 expression data in the eFP Browser. In order to study the expression of *ENO1* at the cellular level, transgenic *A. thaliana* plants were generated carrying three *ENO1* promoter::reporter gene (glucuronidase, GUS) fusion constructs of different lengths with kanamycin as the antibiotic resistance marker (Fig. 3.10). The promoter construct A consisted of a 306 bp fragment upstream of the translational start including the complete intergenic region in front of the At1g74040 and the 5' UTR. The fusion construct AB was generated by fusing construct A with a 646 bp fragment downstream of the translational stop including the 3' UTR (Bailey-Serres and Dawe, 1996; Larkin et al., 2003). The third fusion construct C included the fragment A, the first exon, first intron and a part of the second exon of At1g74030.



**Figure 3.10: Gene structure of At1g74030 and construction of various promoter-GUS constructs of At1g74030 for expression analysis.**

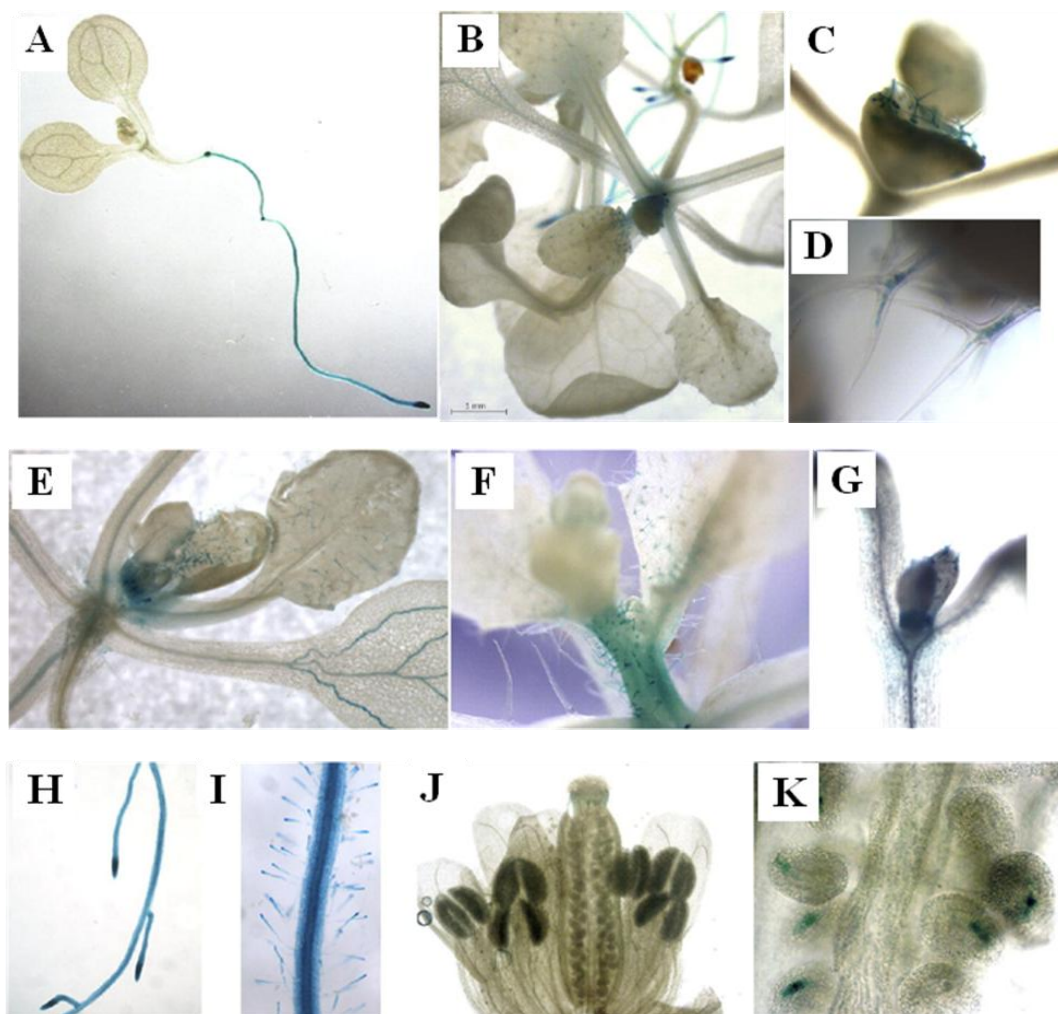
For the promoter construct A, there was no GUS staining detectable, indicating that relevant regulatory cis-acting elements were missing in this fragment (data not shown). The tissue-specific expression profile of the promoter-gene fusion-construct AB (Fig. 3.11) matched very well with RT-PCR data (Fig. 3.9) and the *in silico* expression profiles based on microarray data (i.e. <http://bar.utoronto.ca/efp/cgi-bin/efpWeb.cgi>). In particular, mature leaves were free of GUS activity (Fig. 3.11A), and in roots expression was found only in an early developmental stage (Fig. 3.11A). However, the shoot apex (Fig. 3.11A and E) and the hypocotyls (Fig. 3.11A) exhibited substantial GUS activity. Similar to the RT-PCR data, cotyledons were devoid of GUS activity (Fig. 3.11A and B). Apart from the spatial and temporal expression profiles of different organs, interesting insights into *ENO1* expression emerged at the cellular level. *ENO1* expression in roots was restricted to the cortex (in particular to the non-root-hair cells of the rhizodermis) and the central cylinder of the elongation zone (Fig. 3.11F). There was no expression at the root tip or basal parts of the roots. High GUS activity was found in trichomes of emerging leaves (Fig. 3.11B–E), whereas trichomes of mature leaves were devoid of any GUS activity (Fig. 3.11B). Moreover, GUS activity was also high in the meristematic regions of emerging leaves and the petioles (Fig. 3.11B and C).





**Figure 3.11: Analysis of *ENO1* expression in transgenic plants (A–F) expressing an *ENO1* promoter::GUS fusion construct AB** (Fig. 3.10). *ENO1* promoter activity is indicated by GUS staining of a seedling (A), a mature plant (B) trichomes on a young leaf (C), a mature trichome (D), the shoot apex (E) and the root elongation zone (F).

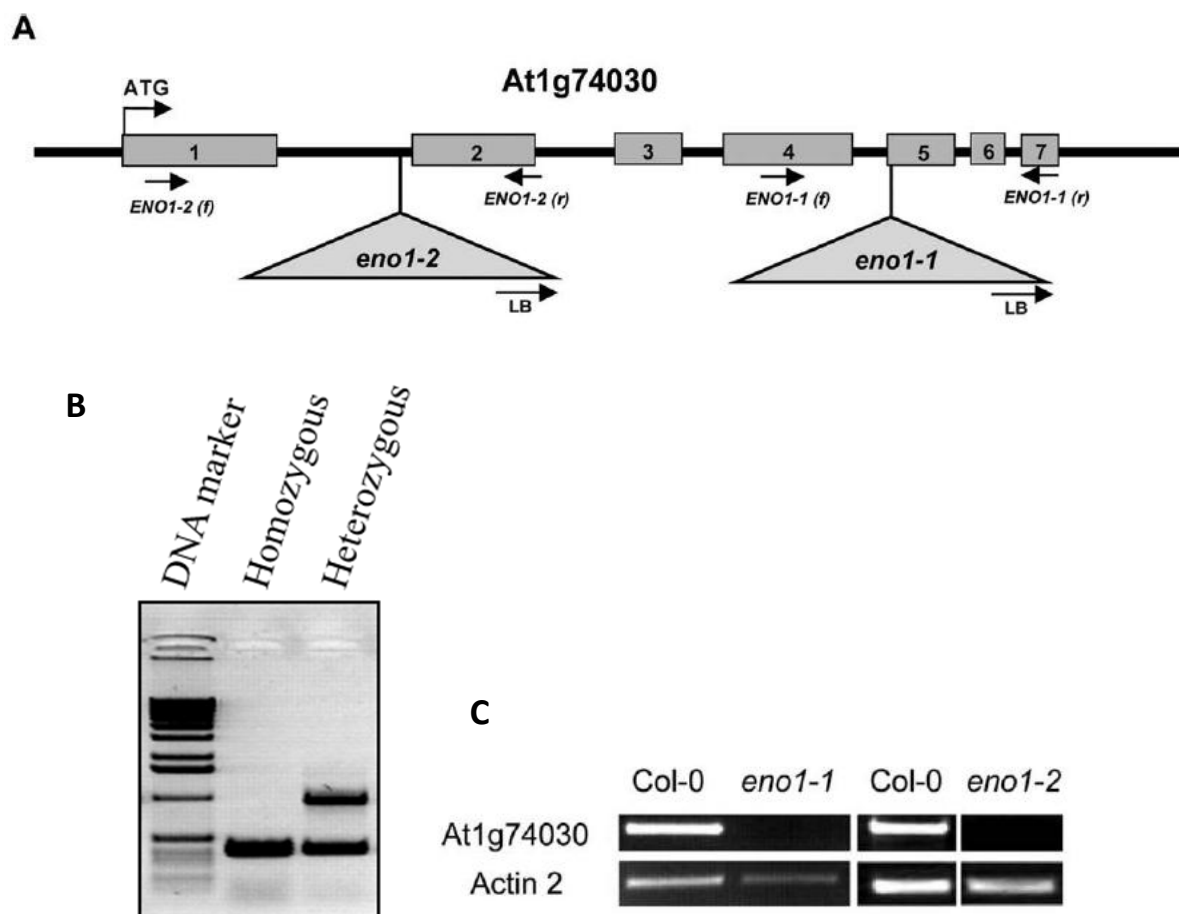
With the promoter construct C, a similar, but not identical, spatio-temporal expression profile was obtained as with the construct AB (Fig. 3.12). Again, mature leaves were free of GUS activity (Fig. 3.12B) and trichomes of young developing leaves exhibited an intense GUS staining (Fig. 3.12C, D, E and F). In contrast to promoter construct AB, promoter construct C also revealed high GUS expression in young and older roots (Fig. 3.12A and B), in particular at the root tips and in root hairs (Fig. 3.12H and I). Moreover, GUS expression was also found in the vasculature of cotyledons (Fig. 3.12B and E), which contrasts the lack of *ENO1* expression in cotyledons observed in RT-PCR experiments (Fig. 3.9). Furthermore, with promoter construct C, there was also some GUS staining in the style (Fig. 3.12J) and in the embryo sac (Fig. 3.12K). As revealed from RT-PCR data, flowers lack *ENO1* expression completely (Fig. 3.12J), whereas developing siliques showed a transient increase in *ENO1* expression. The expression profile of *ENO1* is consistent with the idea that photosynthetically active chloroplasts lack a complete glycolysis to PEP, whereas certain plastids of non-green tissues, in particular those of developing seeds or roots, are capable of generating PEP via glycolysis.



**Figure 3.12: Analysis of ENO1 expression in transgenic plants with the aid of different ENO1-promoter::GUS constructs** (Fig. 3.10). The construct C, which comprises the 5' fragment upstream of the translational start as well as the first exon, the first intron and parts of the second exon delivered similar, but not identical, tissue and cell-specific GUS staining (B to L) as compared to construct AB (compare Fig. 3.13). GUS staining of a seedling (A), a mature plant (B), trichomes on a young leaf (C), an individual trichome (D), in the veins of a mature leaf (E), of trichomes near the shoot apex (F), the shoot apex (G), young roots (H), root hairs of a young root (I), an immature flower (J) and in the embryo sac of the ovules (K).

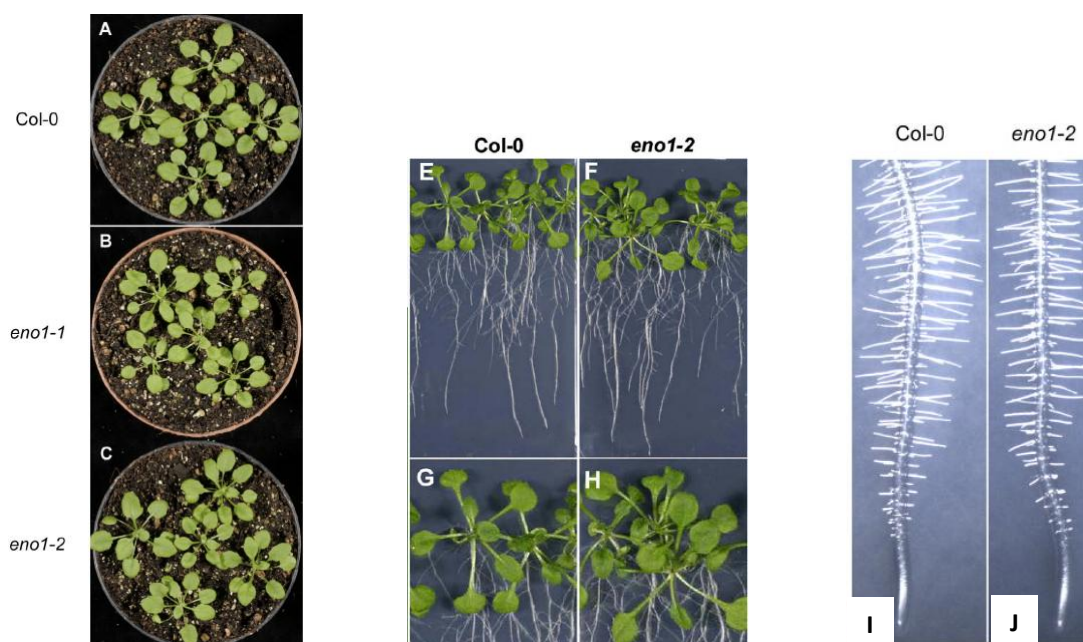
### 3.5 Identification and characterization of *ENO1* T-DNA insertion line *Atenol-2*

In order to test the consequence of a deficiency in ENO1, two *enol* mutant alleles were identified using the T-DNA express: Arabidopsis gene mapping tool from SIGnAL (Salk Institute Genomic Analysis Laboratory). The first *enol* T-DNA insertion mutant is the SALK line SALK\_021328 and this was named as *enol-1*. This T-DNA insertion mutant has an insertion in the fifth exon of At1g74030 (Löttgert, PhD thesis). The second *enol* T-DNA insertion mutant was the GABI-KAT 227D02 named as *enol-2* which has an insertion in the second exon of At1g74030 (Fig. 3.13).



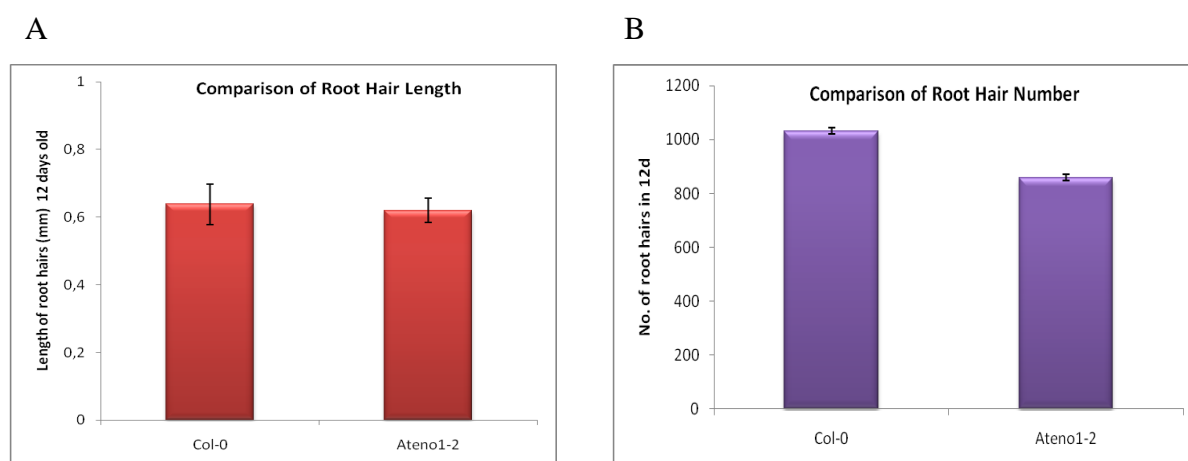
**Figure 3.13: Analysis of T-DNA insertion mutants of ENO1.** Two mutant alleles of *ENO1* (*eno1-1* and *eno1-2*) were isolated (A) and established as homozygous lines (B). The primer used for mutant screening are indicated by arrows (LB, T-DNA left border primer; ENO1-1(2) (f), forward = sense primer; ENO1-1(2) (r), reverse = antisense primer). Both lines lack ENO1-specific transcripts following RT-PCR (C)

These mutants were established as homozygous lines by amplifying the DNA fragments flanking the T-DNA insertion sites of individual plants with special PCR-based methods (Fig. 3.13B). The expression of *ENO1* in these mutants was determined by semi-quantitative RT-PCR method and it was observed that both mutant alleles lacked *ENO1* expression completely in the young roots (where there was prominent *ENO1* expression) (Fig. 3.13C). The phenotype of the *ENO1* mutants *eno1-1* and *eno1-2* were not different from the wild type in the macroscopic scale (Fig. 3.14A-C). They had normal germination and proliferation and flowered at the expected stage. The shoot and root growth was un-affected when the mutants were grown on MS medium supplemented with sucrose (Fig. 3.14 E-H).



**Figure 3.14:** Phenotypic comparison of four-week-old wild type (A), *eno1-1* (B) and *eno1-2* (C) plants as well as of roots of the wild-type (E) and *eno1-2* (F). On a macroscopic scale the *eno1* plants lacked any phenotype different from the wild type; in the microscopic scale root hair reduction was evident (I-J).

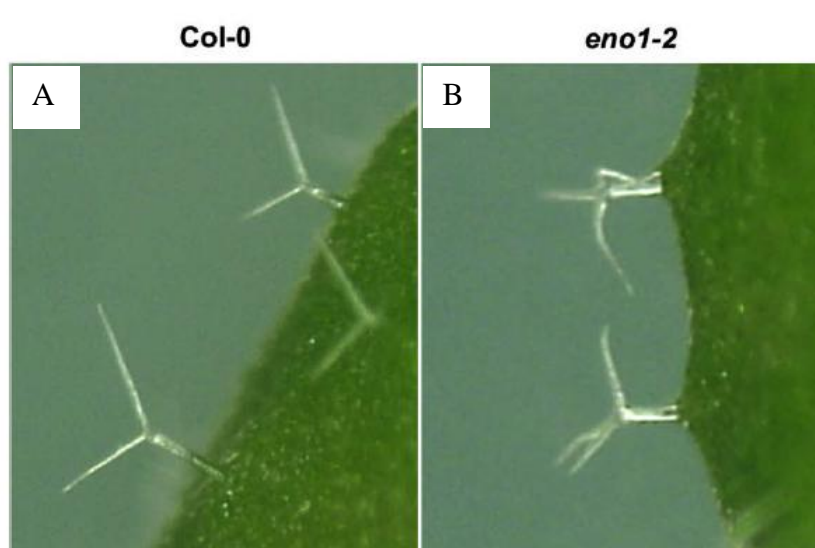
Since *ENO1* is expressed in the young roots of the plants, the plants were germinated on MS medium and inspected closely for differences in root morphology after 12 days. It was observed that there was no significant difference in the root hair lengths between the mutant and the wild type (Fig. 3.14 I and J), but the number of root hairs was reduced by 17% in 2-week-old plants (Fig. 3.14 I and J) compared to the wild type. This data might form a link to the expression of *ENO1* in non-root-hair cells which has been observed with the *ENO1* promoter::*GUS* construct AB (Fig. 3.11F)



**Figure 3.15:** Comparison of root hair length (A) and total number of root hairs (B) in 12-day-old seedlings of wild-type Col-0 and *Ateno1-2* mutant. The data are expressed as mean (n=5).

### 3.6 Distorted trichome morphology of homozygous *eno1-2*

The prominent expression of *ENO1* in the trichomes observed in the transgenic *ENO1* promoter::*GUS* plants lead to the close inspection of trichomes on young leaves in the *eno1* mutants. A common network of transcriptional regulators are known to influence the patterning of both the root hair and trichomes cell types (Kirik et al., 2004). Thus, after observing a phenotype of reduced root hairs in the *cue1/eno1(+/-)* plants, a closer look at the trichome phenotype was made. Under the light microscope, a visible difference between mutant and wild-type plants was observed when grown on MS medium supplemented with sucrose (Fig. 3.16A, B). Scanning electron microscopy also revealed trichome structure difference between the wild type (Fig. 3.16C, D) and the mutant trichomes which appeared less turgid and distorted (Fig. 3.16E, F). Since the epidermal cells of the leaves are usually transparent and lack chloroplasts (except for guard cells) scanning electron microscopy of the trichomes on young leaves was attempted to observe any abnormalities in the structure of epidermal cells. No changes in the epidermal cell phenotype was observed and cuticle structure on trichome remained unchanged except for the phenotype of the trichome on the whole. Thus, the occurrence of a trichome phenotype in both *eno1-1* and *eno1-2* underlines the expression pattern observed in *ENO1* promoter::*GUS* plants (compare Fig. 3.11C, D) and leads to the hypothesis that *ENO1* might play a role in proper trichome integrity.



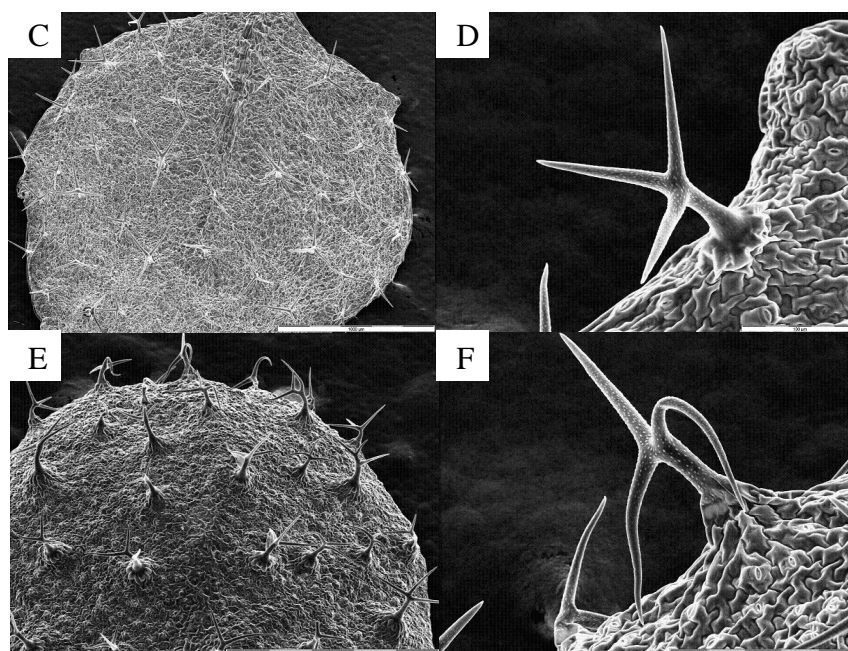


**Figure 3.16: Light and Scanning Electron Microscope images of leaves and trichomes.** A closer inspection of young leaves revealed an aberrant, distorted shape of trichomes in *eno1* plants (B) compared to the wild type (A). Scanning electron images of the leaves of Col-0 (C, D) and *Ateno1-2* (E,F) revealed no differences in the epidermal cell morphology on the leaves, but distortion of the trichomes was very evident.

### 3.7 Double knockout of *PPT1* and *ENO1* in genetic crosses of *cue1* and *eno1* mutant is lethal

The expression pattern of *PPT1* and *ENO1* indicated in the *in silico* expression profiles based on microarray data (i.e. <http://bar.utoronto.ca/efp/cgi-bin/efpWeb.cgi>) shows that both these genes are co-expressed during early embryo and seed development (Fig. 1.3, 1.4) and most likely share the provision of PEP to plastids for anabolic reaction sequences during this developmental stage. In order to elucidate the consequences of a restriction in PEP supply to plastids, the *eno1-1* mutant allele was crossed with the *cue1-1* mutant allele (Li et al., 1995), which represents a deletion of the *PPT1* gene locus by  $\gamma$ -rays (Streatfield et al., 1999). Amongst the F<sub>2</sub> generation, 300 plants homozygous for *cue1-1* were analyzed for the T-DNA insertion in the *ENO1* gene. In this screen no double homozygous mutants and only four plants (i.e. 1.3 %) heterozygous for *eno1* and homozygous for *cue1-1*, *cue1-1/eno1-1(+/-)* were found (Löttgert, PhD thesis). This low percentage was hence far below 50% as expected from a typical Mendelian inheritance. In the progeny of the *cue1-1/eno1-1(+/-)* plants (F<sub>3</sub> generation) again no double homozygous mutants (*cue1-1/eno1-1*) and only four heterozygous mutants [*cue1-1/eno1-1(+/-)*] with a retarded growth phenotype were found amongst the 74 tested plants. In order to confirm these results and to further reproduce this pattern, crosses of a second mutant allele defective in ENO1 (*eno1-2*) and three different

alleles of the *cue1* mutant (*cue1-1*, *cue1-3* and *cue1-6*) were carried out. Like *cue1-1*, *cue1-3* is in the background of the ecotype pOCA 108 (Bensheim) and is described as a weak allele of *cue1*, whereas *cue1-6* represents a strong allele in the Col-0 background (Streatfield et al., 1999). As for the crosses of *eno1-2* with *cue1-1*, no double homozygous mutants could be isolated which was also observed in the additional crosses and the percentage of heterozygous *eno1* mutants in the homozygous *cue1* backgrounds was again far below expectation (Table 3.2). These data clearly indicate that lethality of the double homozygous *cue1/eno1* mutants is due to a defect in both the PPT1 and ENO1 genes and is not caused by secondary insertions or mutations in the single mutant backgrounds.

**Table 3.2 Genetic analysis of crosses between *cue1* (male) and *eno1* (female) mutants.**

Mutant cross	<i>cue1-1/eno1-1</i> (+/-) plants (%)	Total number of homozygous <i>cue1</i> mutants analyzed
<i>cue1-1/eno1-1</i>	3.79 ± 0.18	66 - 71
<i>cue1-1/eno1-2</i>	1.43 ± 0.01	68 - 73
<i>cue1-3/eno1-2</i>	16.38 ± 0.22	53 - 57
<i>cue1-6/eno1-2</i>	13.08 ± 0.09	56 - 65

The frequency of heterozygous *eno1* mutants in the homozygous *cue1* background [*cue1-1/eno1-1*(+/-) plants] is shown as a percentage of plants analyzed in three independent harvests (mean ± SE).

### 3.8 Segregation pattern and transmission efficiency of *cue1/eno1* (+/-) mutants

Since no double homozygous plants were obtained from the *cue1/eno1* cross, the mutants were closely studied to scrutinize the segregation pattern of the individual genotypes in the F2 generation of crosses (i.e between *cue1-1* or *cue1-6* and *eno1-2*). The Punnett square represented in Table 3.3 shows the expected distribution of genotypes providing that a Mendelian inheritance is applicable.

**Table 3.3 Expected Mendelian distribution of genotypes in the segregating F2 generation of crosses between *cue1* and *eno1* mutants.** E and C represent the wild type and *e* and *c* the mutated loci of *ENO1* and *CUE1*, respectively.

Genotype	CE	<i>c</i> E	<i>C</i> <i>e</i>	<i>ce</i>
CE	CCEE	C <i>c</i> EE	CCE <i>e</i>	C <i>c</i> E <i>e</i>
<i>c</i> E	<i>c</i> CEE	<i>cc</i> EE	<i>c</i> CE <i>e</i>	<i>cc</i> E <i>e</i>
<i>C</i> <i>e</i>	CC <i>e</i> E	C <i>c</i> <i>e</i> E	CC <i>e</i> <i>e</i>	C <i>c</i> <i>e</i> <i>e</i>
<i>ce</i>	<i>c</i> C <i>e</i> E	<i>cc</i> <i>e</i> E	<i>c</i> C <i>e</i> <i>e</i>	<i>cc</i> <i>e</i> <i>e</i>

The hetero- and/or homozygous T-DNA insertion in the *ENO1* gene was analyzed by PCR on genomic DNA, whereas heterozygous mutations in the *PPT1* gene were tested in the progeny of the F2 plants after self-fertilization. Those plants that were heterozygous for *cue1* in the F2 generation segregated again in the F3 generation and exhibited homozygous *cue1* plants with its characteristic phenotype. Moreover, as mutant plants homozygous for the mutation in both genes could not be isolated, the occurrence of a heterozygous mutation in the *PPT1* gene in the homozygous *eno1* mutant background was analyzed by pollen viability tests in the F3 generation, after self-fertilization of the F2 plants. Only those plants showing a pollen abortion of more than 10% in the F3 generation were considered to have been heterozygous for *cue1* in the F2 generation. As shown in Table 3.4, the segregation pattern of the *cue1-1/eno1-2* plants were far away from a Mendelian distribution and exhibited a high percent of plants with a wild-type genotype (31%) and plants heterozygous for the mutation in the *PPT1* gene (41%). All other genotypes were severely diminished in number. As expected, no double homozygous plants could be detected. In order to determine female and male transmission efficiencies, reciprocal crosses between *eno1-2* and *cue1-1* were carried out. Interestingly, the segregation pattern of the reciprocal cross (i.e. *eno1-2* male with *cue1-1* female) exhibited a distribution, which was closer to the expected numbers of genotypes according to a Mendelian inheritance.

**Table 3.4 Distribution of genotypes in the segregating F2 population of crosses between *cue1-1* (male) and *cue1-6* (male) with *eno1-2* (female) as well as the reverse cross between *eno1-2* (male) and *cue1-1* (female). The right panel shows the expected Mendelian distribution of genotypes.**

<b>Genotype</b>	<i>cue1-1/eno1-2</i> (75 plants)	<i>eno1-2/cue1-1</i> (72 plants)	<i>cue1-6/eno1-2</i> (74 plants)	<b>Expected distribution (%)</b>
<b>CCEE</b>	23 (31)	15 (21)	4 (5)	6.25
<b>ccEE</b>	3 (4)	6 (8)	5 (7)	6.25
<b>CcEE</b>	31 (41)	17 (24)	7 (9)	12.5
<b>CCEe</b>	8 (11)	12 (17)	20 (27)	12.5
<b>CcEe</b>	2 (3)	10 (14)	20 (27)	25
<b>ccEe</b>	1 (1)	1 (1)	4 (5)	12.5
<b>Ccee</b>	2 (3)	4 (6)	0 (0)	12.5
<b>CCee</b>	5 (7)	7 (10)	14 (19)	6.25
<b>cc ee</b>	0 (0)	0 (0)	0 (0)	6.25

In particular, numbers of the *Ccee*, *CCEe*, *CcEE* and *ccEE* genotypes were similar to the expected distribution, suggesting differences in the male and female transmission efficiencies (TE) for the *cue1* and *eno1* mutation in the reciprocal cross. The TE was calculated according to Blanvillain et al. (2008) and is defined as the number of mutated alleles divided by the number of total alleles times 100. For the mutation in the *PPT1* gene both female and male TE were similar (30%), but lower than the expected value of 50% for each gametophyte (Table 3.5). In contrast the female TE for the mutation in the *ENO1* gene was about half (16.7%) compared to the male TE (31.3%), suggesting that a lesion in the *ENO1* gene in the background of the homozygous *cue1* mutant has a much stronger effect than a lesion in the *PPT1* gene in the homozygous *eno1* background, in particular on embryo sac development. This view was supported by the observation that *ccEe* plants lack any growth phenotype in the vegetative state and the lower percentage of seeds aborted, i.e.  $10.22 \pm 1.19$  % and  $13.3 \pm 2.68$  % for the *cue1-1/eno1-2* and *eno1-2/cue1-1* crosses, respectively, compared to more than 80% seed abortion in the *ccEe* plants (Table 3.6). Likewise the percentage of non-viable pollen of *Ccee* plants was reduced to  $9.0 \pm 1.0$  % and  $12.4 \pm 1.2$  % in *cue1-1/eno1-2* and *eno1-2/cue1-1* crosses, respectively, compared to 35% in the *ccEe* plants (Table 3.6). Interestingly, crosses of *cue1-6* and *eno1-2* also exhibited a segregation pattern (for some of the genotypes of the F2 generation i.e. CCEE, *ccEe*, CcEE and CcEe) closer to a Mendelian distribution. However, it is not clear as to why these differences in genotype distributions between the individual *cue1* alleles occur. It is conceivable that these differences are based on the individual ecotypes (i.e. Bensheim [pOCA] for *cue1-1* and Col-0 for *cue1-6*). Moreover,

the lesion of the *PPT1* gene in *cue1-6* is caused by a point mutation leading to a translational stop codon, whereas parts of chromosome 5 are deleted in *cue1-1*, which not only affects *PPT1* but also at least five additional expressed genes in the vicinity of *PPT1*.

**Table 3.5** Male and female transmission efficiency (TE) of the *eno1* and *cue1* mutations.

Parental genotypes	Male TE (%)	Female TE (%)
ENO1 x <i>eno1-2</i>	31.3	16.7
PPT1 x <i>cue1-1</i>	28.7	31.3

TE was estimated from reciprocal crosses of *cue1-1* and *eno1-2* mutants in the segregating F2 generation obtained from the self-crossed F1 generation. TE is defined as 'Number of mutated alleles' / 'Number of total alleles x 100'. For a typical Mendelian inheritance a TE of 50% for each gametophyte would be expected.

### 3.9 Phenotypic analysis of *cue1/eno1* (+/-) double mutants

The *cue1/eno1* (+/-) double mutants exhibited a stunted growth phenotype when compared to the wild-type Col-0 or *cue1*, *eno1* single mutants (Fig. 3.18). These mutants were much smaller in size compared to the others which was substantiated after a detailed investigation of the rosette diameter of the plants. A total of 308 plants were studied for rosette diameter, and all plants at the same age showed varying rosette diameters ranging from 0.9 to 3 cm as shown in the Fig. 3.17A, all the plants from the size class 0.9 to 1.3 cm and 3 representatives of plants from other size classes were analysed by PCR and it was found that plants in the size class 0.9 to 1.3 cm were *cue1/eno1* (+/-) mutants.



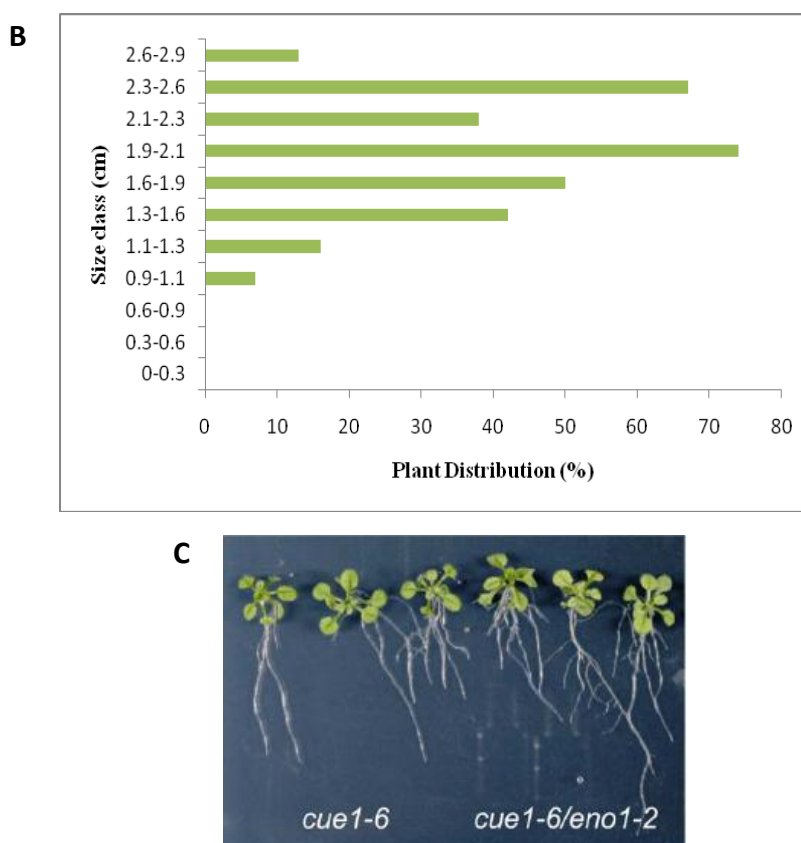


**Figure 3.17: Distribution of *cue1/eno1(+/-)* mutants in the F2 population.** Three-week-old *cue1/eno1* heterozygous mutant population when grown on soil displayed different rosette diameters (A). All the plants were analyzed for their rosette diameters and it was observed that the plants in the size class range of 0.9-1.5cm were the *cue1/eno1(+/-)* mutants (B). No difference in root growth observed between *cue1-6* and *cue1-6/eno1-2(+/-)* plants when grown on MS medium supplemented with sucrose (C).

Interestingly, growth retardation of these mutants became evident only when the plants were grown for three to four weeks on soil (Fig. 3.20A), whereas plants grown on MS agar plates for up to two weeks lacked any visible growth phenotype of the roots or the shoot. Besides the retarded growth of the shoot, the development of the first flowers was severely hampered and resulted in deformed, infertile and completely or partially aborted flowers with underdeveloped stamen (Fig. 3.18B, C). In the later stages, flower development was less affected and siliques were formed after pollination (Fig. 3.18D to F). However, the size of the siliques was diminished and its length was reduced by more than 50% compared to wild-type plants or the single mutants (Fig. 3.18G).

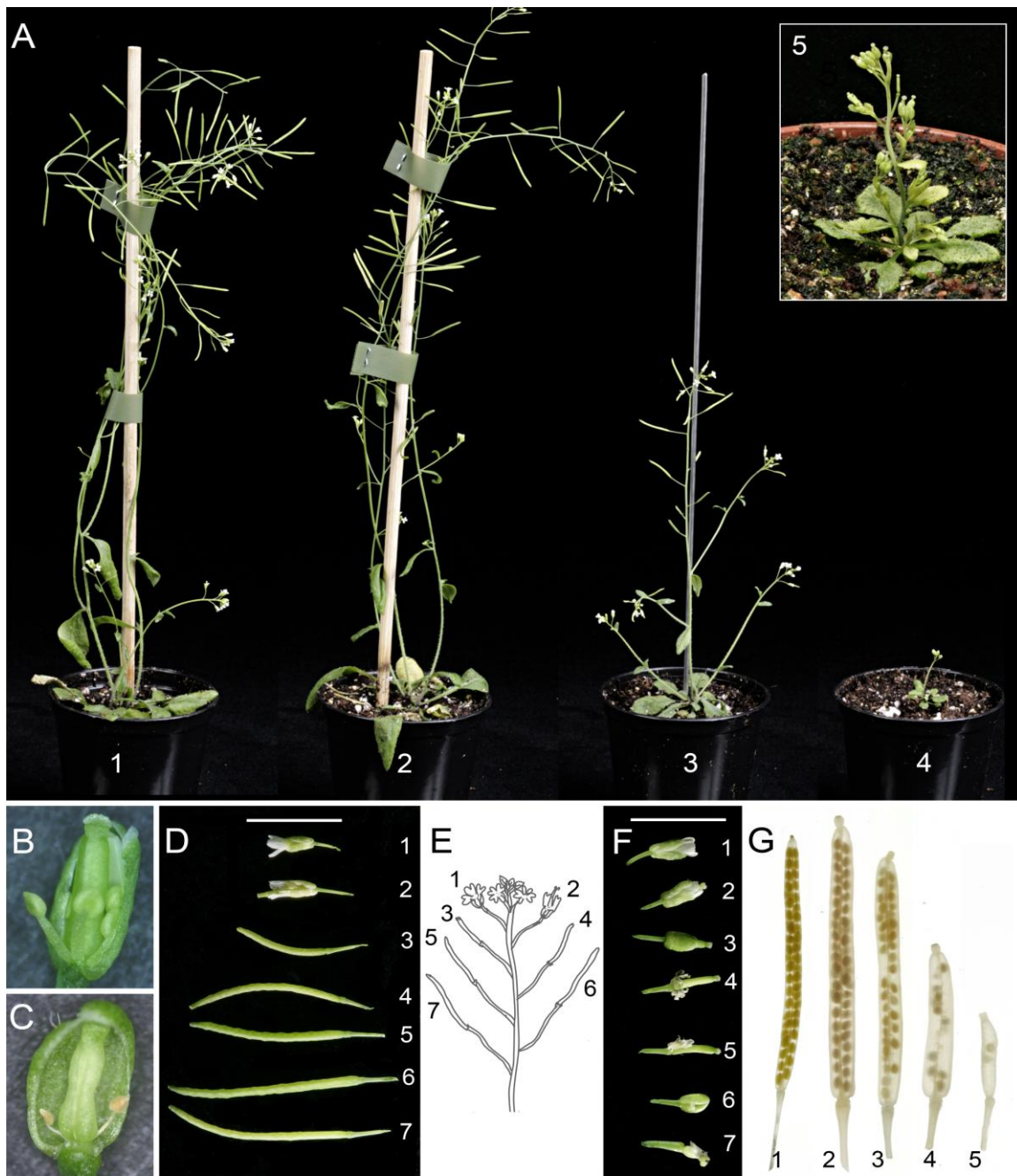


**Figure 3.18: Phenotypic appearance of heterozygous *eno1* mutants in the homozygous *cue1* background [*cue1/eno1(+/-)*] compared to wild-type and *cue1* plants grown for 8 weeks in the greenhouse.**

(A) Comparison of the growth phenotype of Col-0 (1), *Ateno1-2* (2), *cue1-1* (3) and *cue1-1/eno1-2* (4) plants. The inset shows a detailed view of *cue1-1/eno1-2* (5).

(B) Opened bud of an early (stage10) wild-type (Col-0) flower.

(C) Opened bud of an early (stage10) flower of *cue1-1/eno1-2* with degenerated stamen.

(D) Flower and silique development of *cue1-6*

(E) Schematic representation of the position of flowers and siliques shown in (D) and (F)

(F) Flower and silique development of *cue1-6/eno1-2* plants.

(G) Destained mature siliques of Col-0 (1), pOCA (2), *cue1-1* (3), *cue1-6/eno1-2* (4), and *cue1-1/eno1-2* (5)

Developmental stages of flowers and siliques shown in (D) and (F) are based on the position of the flowers/siliques at the raceme starting from the topmost to lower positions. The numbers in (E) represent the positions of flowers and/or siliques shown in (D) and (E). The bars in (D) and (E) are equivalent to 5 mm.

The number of seeds per silique was severely diminished in all *cue1-1/enol-2*(+/-) plants from about 50 seeds in Col-0 or pOCA to less than 10% in *cue1-1/enol-2* and between 30 and 40 in *cue1-3/enol-2* and *cue1-6/enol-2* (Table 3.6). There was also a decline in the seed number per silique in the *cue1* single mutant alleles, which was less marked for the *cue1-3* or *cue1-6* alleles. Based on the presence of gaps in the mature siliques of *cue1-1/enol-2*(+/-) (Fig. 3.21) an abortion frequency of seeds of more than 80 % was calculated for the progeny of *cue1-1/enol-2* crosses and about 45 % in both *cue1-3/enol-2* and *cue1-6/enol-2*.



**Figure 3.19: Silique phenotype of wild-type and mutant plants.** A comparison of the length of the siliques revealed that the *cue1-1/enol-2* (+/-) and *cue1-6/enol-2* (+/-) mutants were much reduced in size (~ 50%) compared to the wild type or single mutants. De-stained siliques revealed large number of gaps indicating the absence of a seed, leading to abortion.

**Table 3.6** Frequencies of seed abortions in wild-type *A. thaliana* (Col-0, pOCA), *eno1* and *cue1* alleles as well as heterozygous *eno1* mutants in the homozygous *cue1* background [*cue1/eno1*(+/-)]plants. Seeds and seed-gaps were counted in 6 -27 siliques per line (n).

Plant line	Seed abortion		
	Number of seeds per silique	Number of gaps	Abortion (%)
Col-0	50.3 ± 2.2	0.25 ± 0.13	0.5 (n = 12)
pOCA	47.9 ± 1.1	1.00 ± 0.29	2.0 (n = 9)
<i>eno1-1</i>	48.9 ± 0.8	1.44 ± 0.48	2.9 (n = 9)
<i>eno1-2</i>	43.8 ± 0.8	1.00 ± 0.37	2.2 (n = 9)
<i>cue1-1</i>	32.9 ± 1.1	8.89 ± 0.72	21.3 (n = 9)
<i>cue1-3</i>	45.3 ± 2.0	5.44 ± 0.84	10.7 (n = 9)
<i>cue1-6</i>	41.0 ± 2.2	1.30 ± 0.35	3.1 (n = 6)
<i>cue1-1/eno1-2</i> (+/-)	2.4 ± 0.6	12.40 ± 0.65	83.6 (n = 9)
<i>cue1-3/eno1-2</i> (+/-)	20.2 ± 2.3	16.50 ± 0.89	45.0 (n = 27)
<i>cue1-6/eno1-2</i> (+/-)	16.2 ± 2.3	13.20 ± 1.20	44.9 (n = 26)

### 3.10 Expression profile of *ENO1* in *cue1/eno1* (+/-) double mutant shoot apex and young roots

The cause for the developmental constraints in *cue1/eno1* (+/-) plants was further elucidated by expression studies of *ENO1*. It was shown that *ENO1* is highly expressed in non-root hair cells of the roots and in the shoot apex, but was absent in mature leaves. As revealed by real-time RT-PCR, *ENO1* expression in the roots of the *cue1/eno1* (+/-) lines was diminished with log<sub>2</sub>-ratios of  $-0.49 \pm 0.08$  (n = 3) and  $-1.96$  for the lines *cue1-6/eno1-2*(+/-) and *cue1-1/eno1-2*(+/-), respectively (Fig. 3.20). An even more pronounced repression of *ENO1* expression was observed for the shoot apex of the developing rosette. For *cue1-6/eno1-2*(+/-) and *cue1-1/eno1-2*(+/-) plants, log<sub>2</sub>- ratios were  $1.69 \pm 0.3$  (n = 4) and  $-3.47$ , respectively (Fig. 3.20). These data indicate that a heterozygous knockout of *ENO1* diminishes the expression level substantially and suggests that the growth retardation in the *cue1/eno1* (+/-) lines is based on a gene dosage effect.

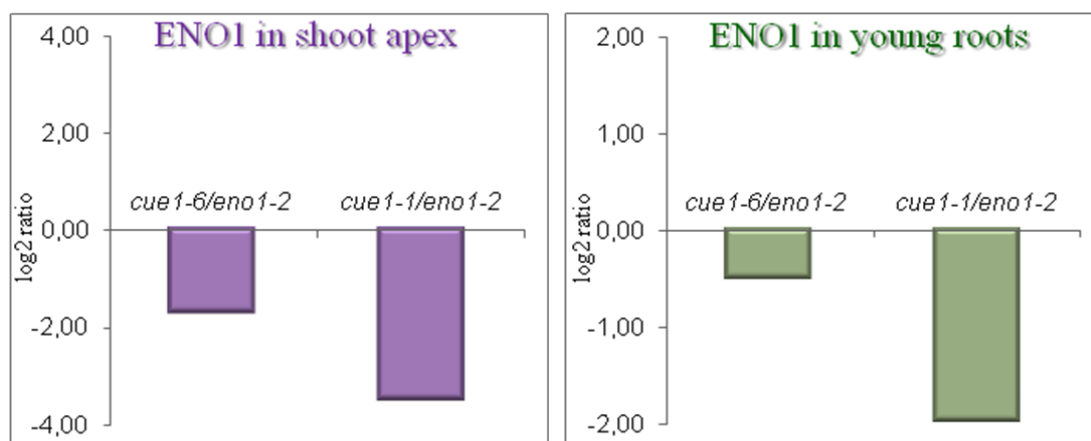


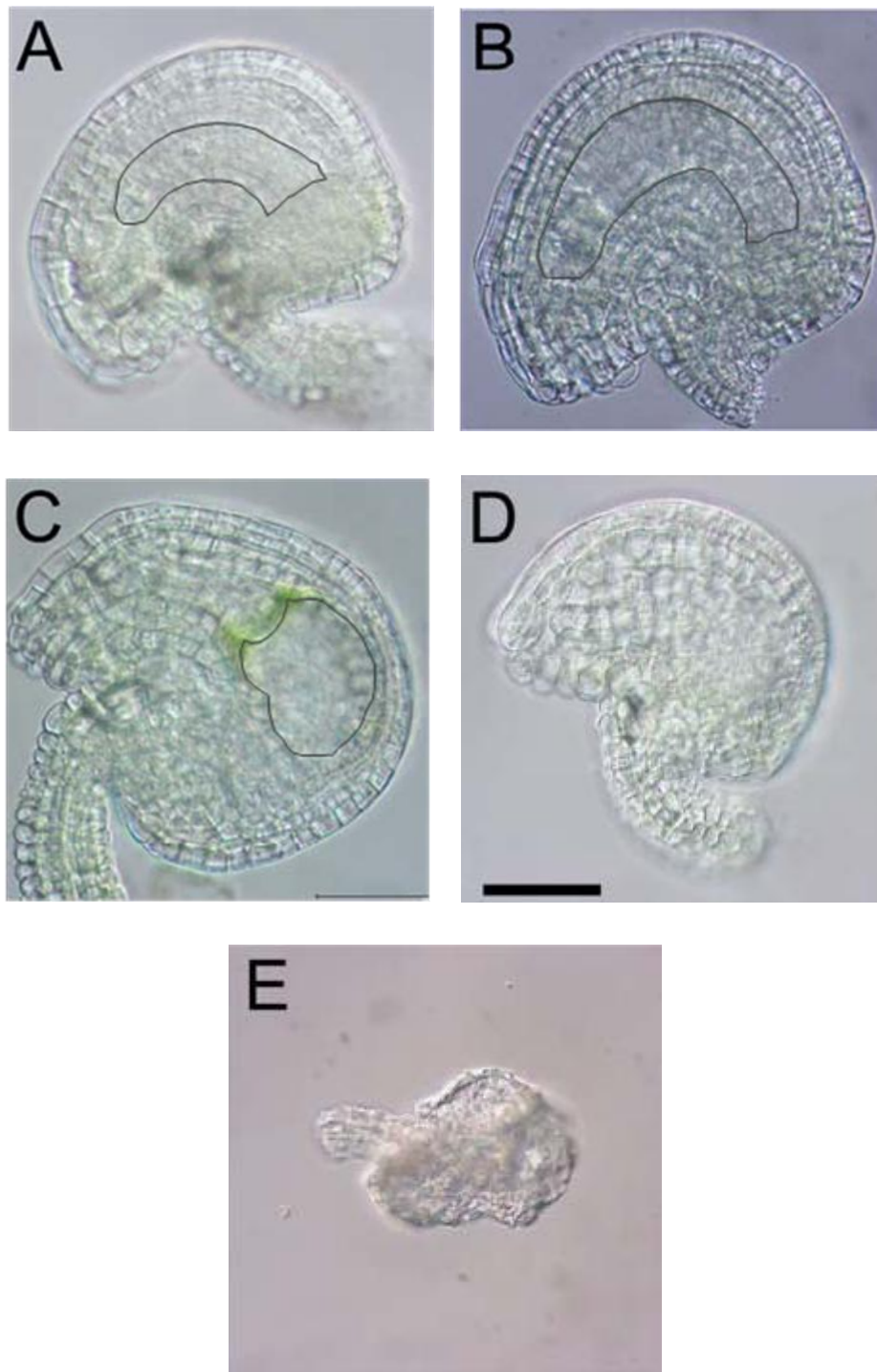
**Figure 3.20: Real-Time RT PCR expression analyses of ENO1 in the shoot apex and in young roots.** A down-regulation of ENO1 expression was observed in *cue1/eno1*(+/-) mutants, of which *cue1-1/eno1-2*(+/-) was more down-regulated, compared to *cue1-6/eno1-2*(+/-). This trend was similar in the shoot apex and young roots.

### 3.11 Phenotypic characterization of female gametophyte of the *cue1/eno1*(+/-) double mutants

Owing to the high percent of abortion in the double mutants, the question of whether or not female gametophyte development was hampered in *cue1/eno1*(+/-) plants was addressed. The gynoecium of the mutants in closed flower buds were analyzed at stage 12 when the ovules were ready for fertilization. The mature ovule consists of a central mass of tissue, the nucellus, surrounded by 1 or 2 protective layers, the integuments, which eventually give rise to the seed coat. Within the nucellus is a large oval structure, the embryo sac, which develops from the megaspore and contains the naked egg cell. The mature ovules from wild type and mutants were observed by Differential Interference Contrast microscopy (Normaski optics) and interestingly various phenotypes of ovules were observed in the *cue1/eno1* (+/-) mutants compared to the wild type and *cue1* and *eno1* single mutants.

#### 3.11.1 Ovule analysis

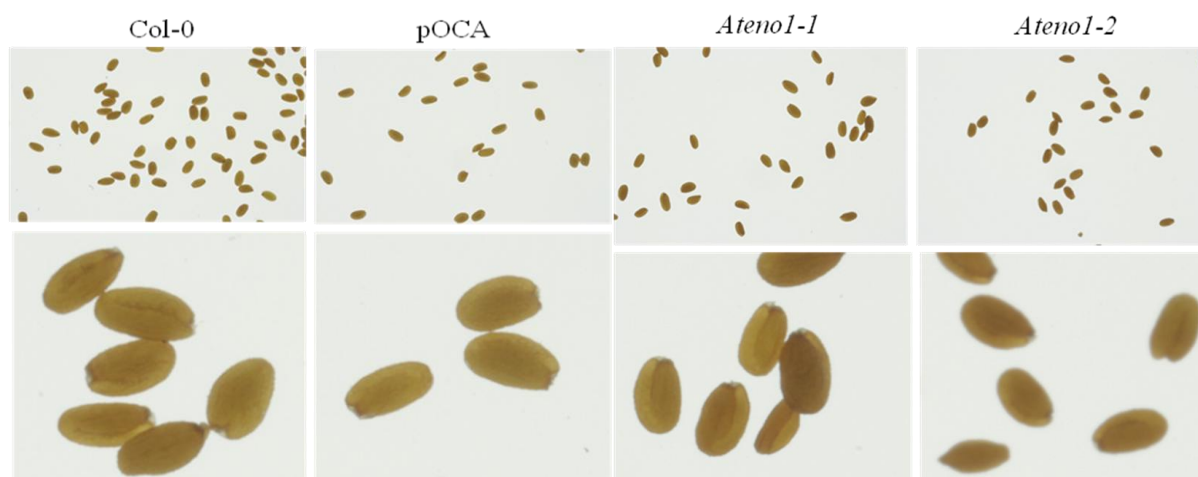
It was observed that 60% of the ovules in the *cue1/eno1* cross were wild-type like with intact integuments, nucellus and a well defined embryosac (Fig. 3.21B). Apart from this, the other ovules had different phenotypes, in approximately 40% of the ovules, the embryo sac was diminished in size and abnormally shaped (Fig. 3.21C). There was absence of embryosac in some ovules and only the nucellus could be visualized (Fig. 3.21D). Some of the ovules were completely halted in development and were non-viable (Fig. 3.21E). All these data indicated that combined knock-out of *PPT1* and *ENO1* results in partial lethality of the female gametophyte.



**Figure 3.21: Ovule phenotype of heterozygous *eno1* mutants in the homozygous *cue1* background [*cue1/eno1*(+/-)] compared to wild-type or *cue1* plants.** (A) Ovule of a wild-type (Col-0) plant. (B) Ovule of *cue1-1/eno1-2*(+/-) with a wild-type like appearance. (C) Ovule of *cue1-1/eno1-2*(+/-) with a swollen embryo sac. (D) Ovule of *cue1-1/eno1-2*(+/-) lacking an embryo sac. (E) Degenerated ovule of *cue1-1/eno1-2*(+/-).

### 3.12 Seed analysis

Post fertilization, the gynoecium elongates and develops into a silique which upon maturity dries and dehiscence occurs when the valves separate from the silique dispersing the seeds. Seed development comprises two major phases: embryo development and seed maturation. Embryogenesis, which is a morphogenesis phase, starts with the formation of a single-cell zygote and ends in the heart stage when all embryo structures have been formed (Mayer et al., 1991). It is followed by a growth phase during which the embryo fills the seed sac (Goldberg et al., 1994). Considering the partial lethality of the ovule, the phenotype of the mature, developed seeds were studied intensively. At the microscopic level, the seeds of the *cue1/enol* (+/-) mutants could be categorized into three different classes according to their size and phenotypic appearance. Class I seeds were indistinguishable from seeds of *cue1* (Fig. 3.22), which were slightly lighter in colour as compared to wild-type seeds, and hence resembled those from transparent testa mutants (Koornneef, 1990). In contrast, class II and class III seeds were intermediate and severely diminished in size, respectively (Fig. 3.22). Moreover, class II seeds exhibited a wrinkled and shrunken appearance with irregularly shaped testa cells as compared to wild type and single mutant seeds (Fig. 3.24). Table 3.7 shows the distribution of the individual seed classes between the different plant lines. There was also a higher percentage of class II and III seeds in the *enol* single mutant alleles as well as *cue1-1*. A genotypic analysis of all three seed classes revealed that class I seeds were wild-type like for *ENO1*, whereas both class II and class III seeds were heterozygous for the mutation in *ENO1* (Fig. 3.23). Class I and -II seeds were capable of germinating on MS-agar plates, whereas class III seeds were not (Fig. 3.23). Genotyping Class I, II and III seeds by PCR revealed that Class II and III seeds were heterozygous for *enol* and homozygous for *cue1*, and Class I seeds were wild type (Fig. 3.23).



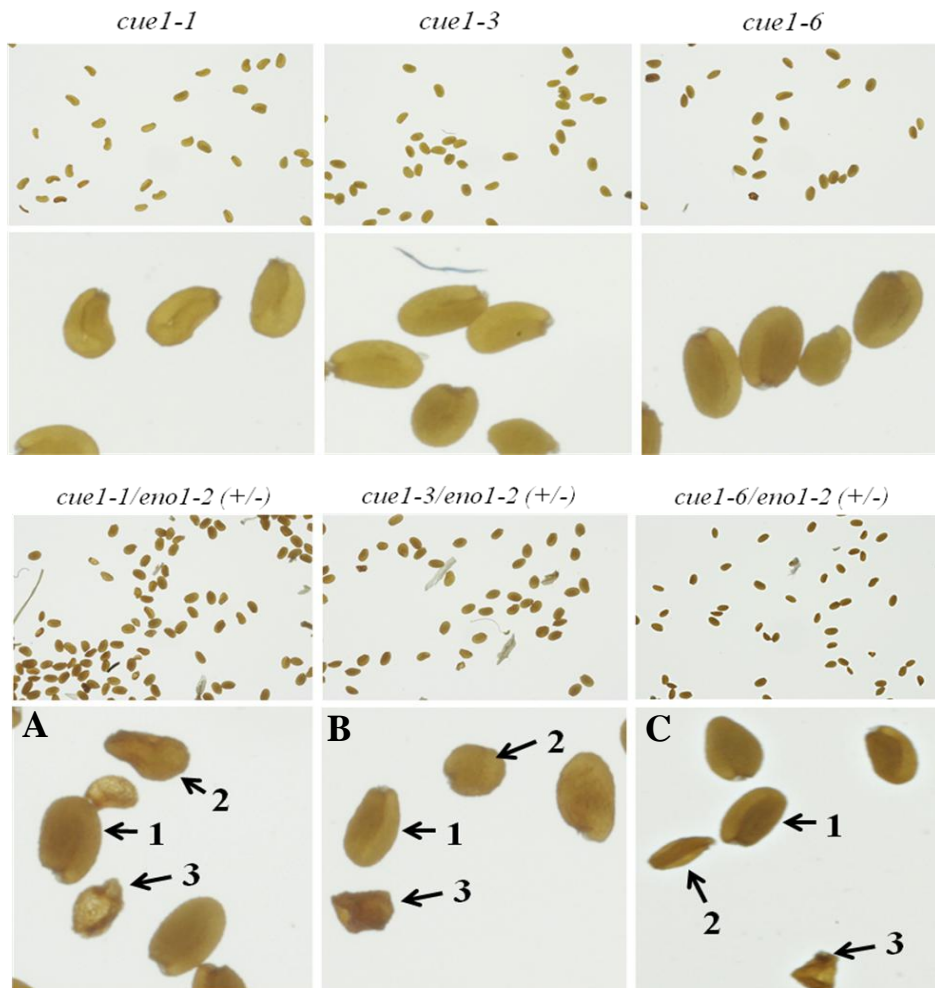


**Figure 3.22: Phenotypes of mature seeds of heterozygous *eno1* mutants in the homozygous *cue1* background (*ccEe*) compared to the wild-type or *cue1* plants. (A-C) Phenotype of seeds of *cue1/eno1(+/-)* showing either a wild-type like appearance (class I seeds; 1) or which were intermediately and strongly reduced in size (class II, 2 and class III seeds, 3).**

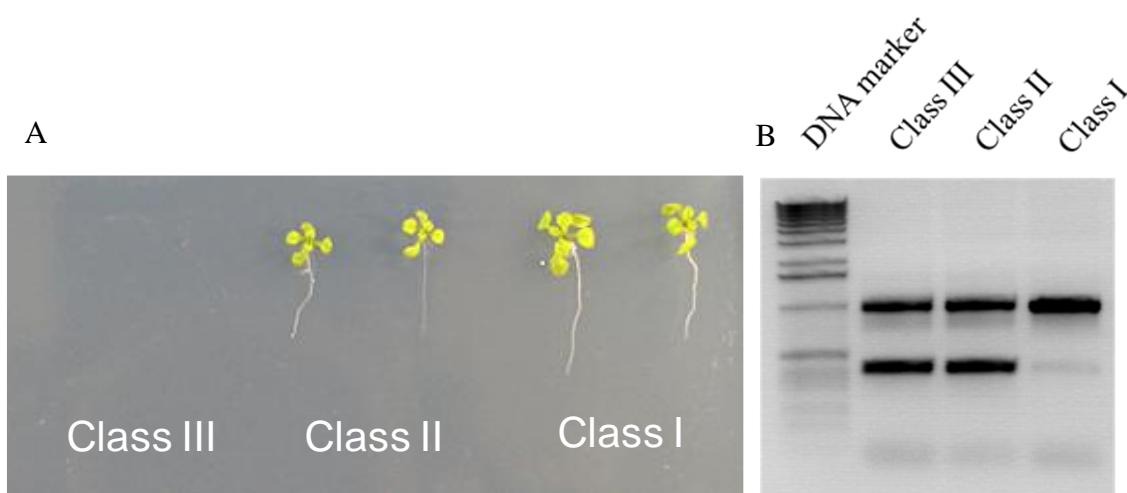


**Figure 3.23: Germination and genotyping of *cue1-1/eno1-2(+/-)* class I, II and III seeds. (A) Class III seeds of *cue1/eno1(+/-)* crosses does not germinate on MS medium supplemented with sucrose. (B) Genotyping of Class I, II and III seeds indicate that the Class II and III seeds are heterozygous for *eno1* and homozygous for *cue1*, Class III seeds are wild type.**

**Table 3.7: Seed phenotypes of wild type, single and *cue1/eno1*(+/-) mutants.**

Plant line	Seed phenotype (%)		
	Class I	Class II	Class III
Col-0	97.70	2.30	0.00
pOCA	95.00	5.00	0.00
<i>eno1-1</i>	80.00	17.00	3.00
<i>eno1-2</i>	76.00	20.00	4.00
<i>cue1-1</i>	70.00	25.00	5.00
<i>cue1-3</i>	91.10	8.90	0.00
<i>cue1-6</i>	91.10	8.90	0.00
<i>cue1-1/eno1-2</i> (+/-)	65.40	25.00	9.60
<i>cue1-3/eno1-2</i> (+/-)	86.20	10.30	3.50
<i>cue1-6/eno1-2</i> (+/-)	64.00	26.00	10.00

The developed seeds were classified into three classes according to their phenotypic appearance. Class I seeds were wild-type like, class II seeds showed an intermediate and class III seeds a strong reduction in size. The occurrence of Class III type seeds were predominant in the *cue1/eno1*(+/-) mutants, when compared to wild-type and single mutant seeds.

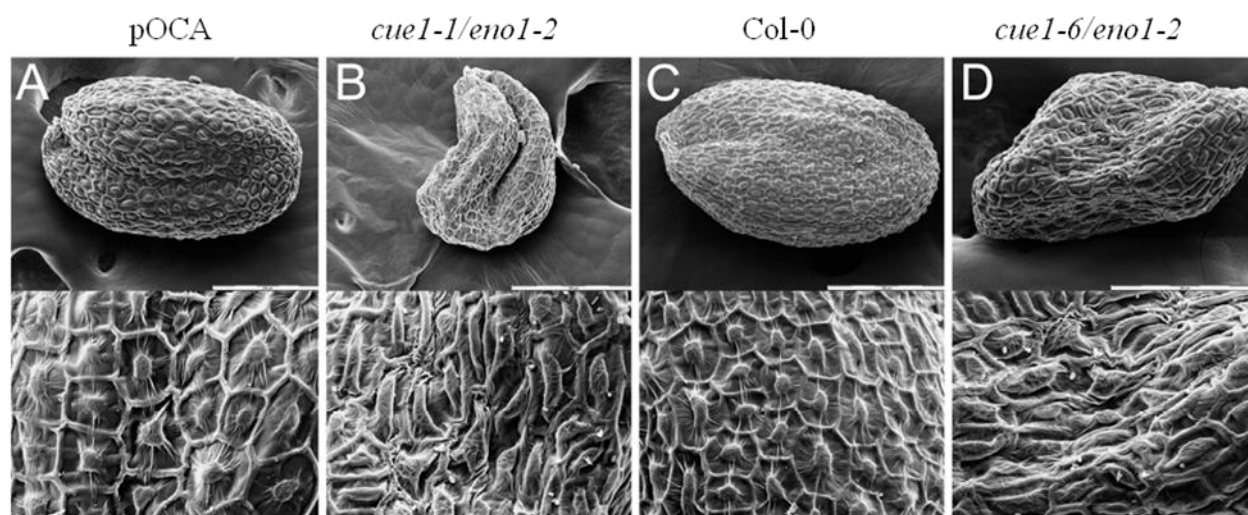


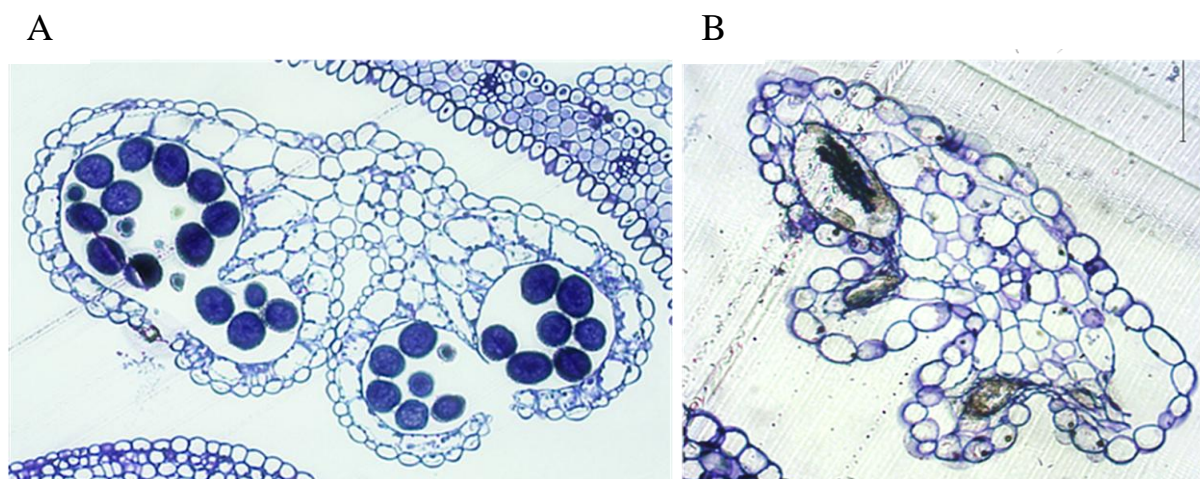
**Figure 3.24: Seed phenotypes of heterozygous *eno1* mutant in the homozygous *cue1* background [*cue1/eno1*(+/-)] analyzed by scanning electron microscopy.** The upper and lower panel shows overviews of individual seeds and the detailed structure of the testa, respectively. The bars represent 200 $\mu$ m and 50 $\mu$ m for the overviews and close-ups, respectively. (A) Mature seed of a wild-type plant (pOCA). (B) Mature type II seed of heterozygous *eno1* mutant in the homozygous *cue1* background (*cue1-1/eno1-2*) showing irregular structure of the testa cells. (C) Mature seed of a wild-type plant (Col-0). (D) Mature type II seed of heterozygous *eno1* mutant in the homozygous *cue1* background (*cue1-6/eno1-2*) showing irregular structure of the testa cells.

### 3.13 Phenotypic characterization of male gametophyte of *cue1/eno1* (+/-) double mutants

Pollen grains represent the highly reduced haploid male gametophyte generation in flowering plants consisting of just two or three cells when released from the anthers. Their role is to deliver twin sperm cells to the embryo sac to undergo fusion with the egg and central cell (Borg et al., 2009). This double fertilization is essential for fertility and proper plant development. It could be speculated that defects in pollen could be a reason for high rates of abortion in the *cue1/eno1*(+/-) cross. Thus, analyses of the effect of a double knockout of *PPT1* and *ENO1* on the development of the male gametophyte was carried out.

#### 3.13.1 Cross-section of anthers

The cross-sections of anthers in *cue1/eno1* (+/-) plants revealed reduced number of pollen compared to the wild type (Fig. 3.25). Also, dead pollen could be visualized as crescent shaped objects, which were present inside the intact pollen sac (Fig. 3.25B). The pollen sacs of the *cue1/eno1* (+/-) mutants were aberrantly shaped (Fig. 3.25B) and in extreme cases, indistinguishable from each other (Fig. 3.25C-D) unlike the spherical shaped pollen sacs of the wild type. Thus, a large portion of underdeveloped pollen in pollen sacs of *cue1-1/eno1-2* and *cue1-6/eno1-2* (+/-) plants could be one of the reasons for the abortion observed in the siliques.



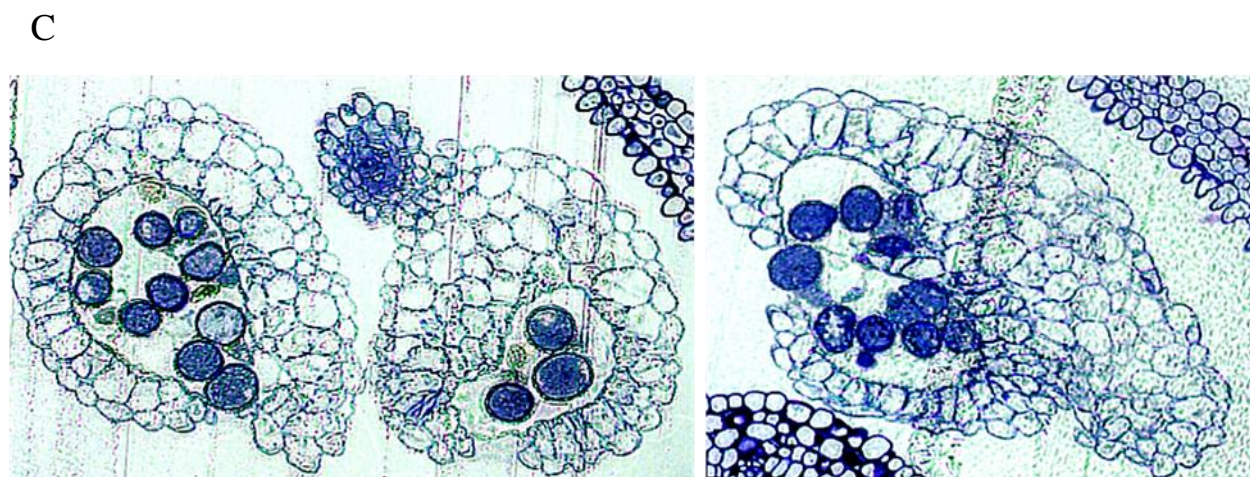


**Figure 3.25: Cross sections of anthers exposing the pollen sacs from heterozygous *eno1* mutants in the homozygous *cue1* background [*cue1/eno1(+/-)*] compared to the wild type. (A) Wild type (B) *cue1-1/eno1-2(+/-)* (C) *cue1-6/eno1-2(+/-)***

### 3.13.2 Analysis of pollen viability and structure

#### 3.13.2.1 Pollen viability analysis

The amount and quality of pollen produced by a flower is an important component of fitness. Pollen quality is often equated to pollen viability, i.e., the proportion of pollen grains that are viable. While viability can be measured in a number of ways (Stanley and Linskens, 1974; Heslop-Harrison et al., 1984) common method to assess both pollen load and pollen viability is by staining and direct count. Alexander's staining showed that the underdeveloped pollen of the *cue1-1/eno1-2 (+/-)* plants were not viable (Fig. 3.26). Alexander's stain stains the pollen wall green and the cytoplasm of the viable pollen grains red. The presence of numerous green colored pollen inside the intact pollen sac indicated cytoplasmic abnormality in pollen prior to anther dehiscence. Amongst the dehisced mature pollen the *cue1-1/eno1-2 (+/-)* mutants had the highest percentage of non-viable pollen,  $35 \pm 2.7\%$  followed by the *cue1-6/eno1-2 (+/-)* with  $29.0 \pm 2.0\%$ . The plants obtained from crosses of *eno1-2* with the weak *cue1-3* allele showed only 2% abortion suggesting that at least pollen viability can be rescued if PPT1 is present, albeit functionally impaired. Surprisingly, the ENO1 mutants, *eno1-1* and *eno1-2* showed a higher abortion percentage compared to the wild type, but the *cue1* single mutants were no different from their background. (Table 3.8)

**Table 3.8: Frequency of pollen viability in wild-type *A. thaliana* (Col-0, pOCA), *eno1* and *cue1* alleles as well as heterozygous *eno1* mutants in the homozygous *cue1* background [*cue1/eno1*(+/-)] plants. Pollen viability was tested by Alexander's stain and pollen were collected from three plants per line. The data are expressed as mean  $\pm$  SE.**

Plant line	Non-viable pollen (%)
Col-0	0.3 $\pm$ 0.3
pOCA	0.3 $\pm$ 0.3
<i>eno1-1</i>	6.3 $\pm$ 2.0
<i>eno1-2</i>	8.0 $\pm$ 1.0
<i>cue1-1</i>	0.6 $\pm$ 0.3
<i>cue1-3</i>	0.3 $\pm$ 0.3
<i>cue1-6</i>	0.3 $\pm$ 0.3
<i>cue1-1/eno1-2</i> (+/-)	35.0 $\pm$ 2.7
<i>cue1-3/eno1-2</i> (+/-)	2.0 $\pm$ 0.5
<i>cue1-6/eno1-2</i> (+/-)	29.0 $\pm$ 2.0

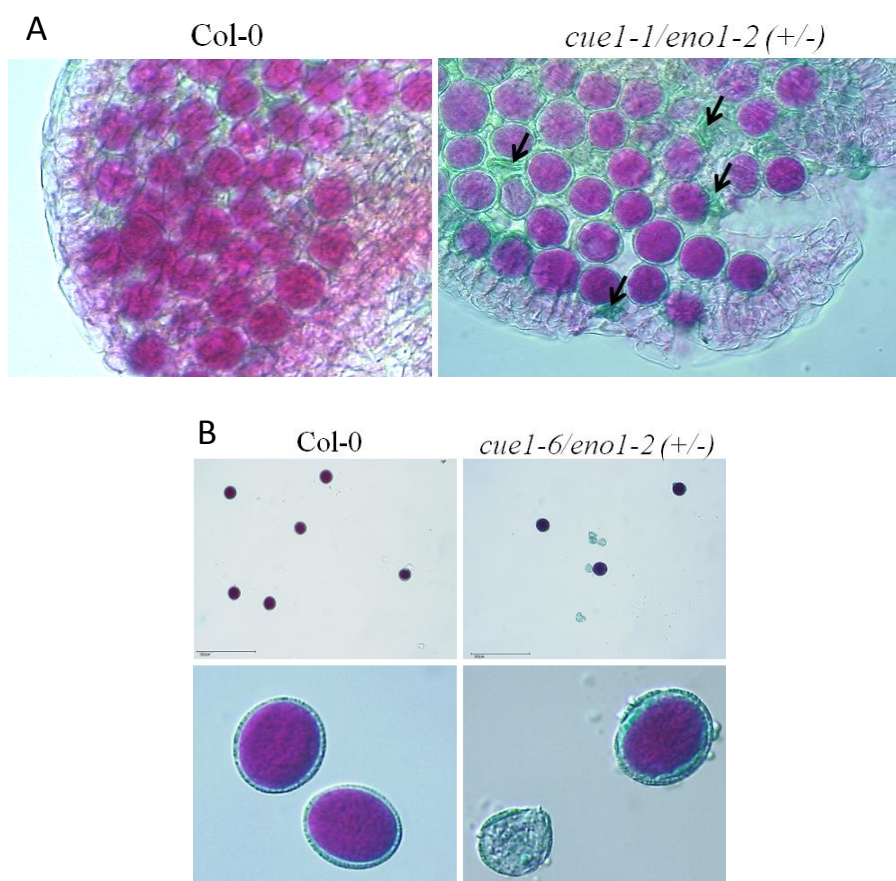
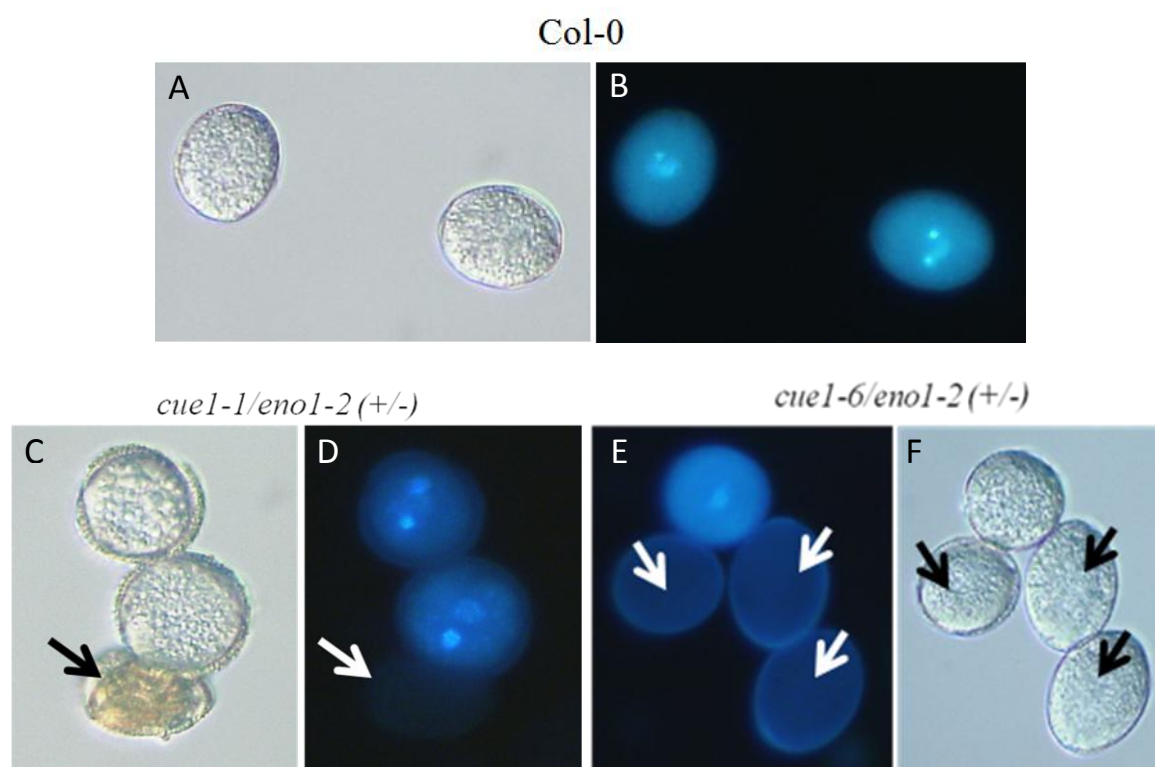


**Figure 3.26: Viability (Alexander's) staining of intact anther (A) and mature pollen (B) from heterozygous *eno1* mutants in the homozygous *cue1* background [*cue1/eno1*(+/-)] compared to the wild-type. Black arrows indicate the presence of green non-viable pollen inside intact anthers.**

To further validate the viability of pollen, DAPI staining was performed. The fluorescent dye DAPI binds selectively to DNA and forms strongly fluorescent DNA-DAPI complexes with high specificity. On adding DAPI to pollen it is rapidly taken up into cellular DNA yielding highly fluorescent nuclei and partially detectable cytoplasmic fluorescence. The pollen from wild-type and mutant plants were stained with DAPI and analyzed by fluorescence microscopy. The DNA of the viable pollen were clearly visible in the wild-type (Fig. 3.27A and B) and single mutant plants, but since the cellular structure of the underdeveloped pollen was disrupted in the *cue1/enol1(+/-)* plants, the DNA in the nuclei in the tri-cellular stage was not detectable by DAPI staining (Fig. 3.27 C-F).



**3.27: DAPI staining of mature pollen.** (A) Bright field image of a wild-type pollen (Col-0). (B) DAPI staining of the wild-type pollen shown in (A). (C) Bright field image of a wild-type like pollen and a degenerated pollen (arrow) of *cue1-1/enol1-2(+/-)*. (D) DAPI staining of the pollen grains shown in (C). The degenerated pollen is marked by an arrow. (E) DAPI of a wild-type like pollen and a degenerated pollen (arrow) of *cue1-6/enol1-2(+/-)*. (F) Bright field image of the pollen grains shown in (E). The non-viable pollen are marked by an arrow which shows the absence of DNA in the DAPI staining.

### 3.13.2.2 Pollen ultrastructure

To further elucidate the reason for pollen abortion, the ultrastructure of developing pollen grains of wild-type and *cue1/enol1-2(+/-)* plants were analyzed. As shown in Fig. 3.28 pollen grains from *cue1/enol1-2(+/-)* plants exhibit a variety of phenotypes different from wild-type pollen (Fig. 3.28A and B). The most prominent features of *cue1/enol1-2(+/-)* pollen grains were an irregularly shaped intine (Fig. 3.28, D, F, H, and L) and a strongly diminished exine

structure (Fig. 3.28, F to J). In some cases pollen development was completely disrupted (Fig. 3.28, K and L). Moreover, in some of the mutant pollen massive starch accumulation was found in the plastids (Fig. 3.28, D, G, and H), whereas starch granules in wild-type pollen were less abundant. Interestingly, lipid bodies and vacuoles were found at nearly the same density in *cue1/eno1-2(+/-)* pollen grains (Fig. 3.28, C to J) as compared to the wild type (Fig. 3.28A and B) suggesting that fatty acid biosynthesis appears not to be a major metabolic restriction during pollen maturation. Apart from aborted pollen (Fig. 3.28, K and L), deposition of exine material was severely restricted in pollen of *cue1/eno1-2(+/-)* plants. The exine structure consists mainly of sporopollonin, which is formed by the diploid cells of the pollen sac secretory tapetum (Ariizumi et al., 2004). Sporopollonin is an extremely rigid substance containing both long chain fatty acids and phenolic compounds derived from the phenylpropanoid metabolism (Guilford et al., 1988; Wiermann et al., 2001).

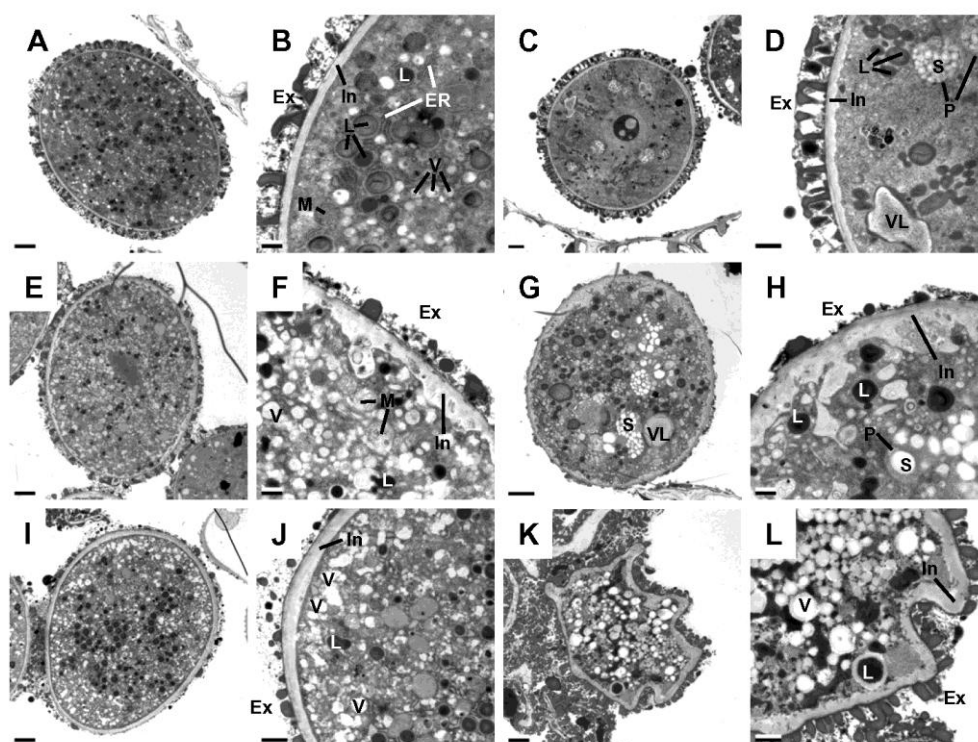


**Figure 3.28: Cross sections of differently affected pollen grains of heterozygous *eno1* mutants in the homozygous *cue1* background [*cue1/eno1(+/-)*] analyzed by transmission electron microscopy in the tri-cellular stage in comparison to the wild-type Col-0.** Ex, exine; In, intine; L, lipid body; ER, endoplasmatic reticulum; V, vacuoles; VL, vacuole like bodies; M, mitochondria; P, plastids; S, starch granules. The bars represent 2  $\mu\text{m}$  and 0.5  $\mu\text{m}$  for the overviews and close-ups, respectively. The pollen derived from anthers at stage 12 according to Sanders et al. (1999).

(A) Cross section of a wild-type (Col-0) pollen grain.

(B) Close-up of the wild-type pollen grain shown in (A).

(C-L) Phenotypic changes in the ultra-structure of pollen grains observed in pollen sacs of *ccEe* plants.

(C) Pollen grain of *cue1-1/eno1-2(+/-)* with a wild-type like appearance.

(D) Close-up of the pollen grain shown in (C) with increased numbers of starch granules in the plastids and a slightly deformed and swollen intine.

(E) Pollen grain of *cue1-1/eno1-2(+/-)* with a wild-type like size, but affected exine and intine structures.

(F) Close-up of the pollen grain shown in (E) with a focus on the underdeveloped exine structure and the strongly deformed intine.

(G) Pollen grain of *cue1-1/eno1-2(+/-)* with a deformed pollen wall, high numbers of starch granules and large vacuole-like structures.

(H) Close-up of the pollen grain shown in (G) with a focus on the impaired exine and intine structures.

(I) Pollen grain of *cue1-6/eno1-2(+/-)* with a wild-type like appearance, but an impaired exine structure.

(J) Close-up of the pollen grain shown in (I) with a focus on the underdeveloped exine structure.

(K) Strongly deformed pollen grain of *cue1-6/eno1-2(+/-)*.

(J) Close-up of the pollen grain shown in (K).

Hence the impaired exine formation observed in the majority of the pollen (80%) in *cue1/eno1-2(+/-)* plants is most likely due to a diminished gene dose of *ENO1* in the absence of *PPT1* in the tapetum cells rather than an absence of both proteins in the microspores. The heterozygous knockout of *ENO1* in the *cue1* background might thus hamper sporopollonin production by the tapetum cells due to diminished PEP provision for the shikimate pathway in the plastids therein.

### 3.13.2.3 Analysis of phenolic compounds in pollen

It has been reported previously that flavonoids are required for pollen viability in some species (Coe et al., 1981; Mo et al., 1992; Taylor and Jorgenson, 1992). In *Arabidopsis*, DPBA forms a highly fluorescent complex with quercetin and kaempferol, intermediates of the flavonoid pathway, generating golden and green fluorescence, respectively (Buer et al., 2007). The fluorescence emission from DPBA stained pollen grains revealed that phenolic compounds were less abundant in pollen grains of *cue1/eno1-2(+/-)* plants (Fig. 3.29). Wild-type pollen emit a bright gold/green fluorescence both from the wall and the cytoplasm of the pollen grains (Fig. 3.29B), whereas fluorescence emission from pollen grains of *cue1/eno1-2(+/-)* plants were considerably reduced (Fig. 3.29 D and F) suggesting that the level of phenolic compounds was decreased in the mutant.

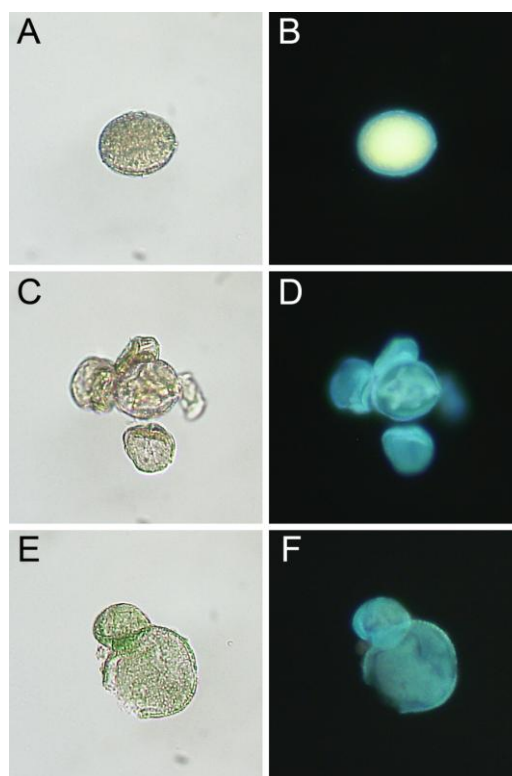


**Figure 3.29: Autofluorescence of pollen from a wild-type plant and heterozygous *eno1* mutants in the homozygous *cue1* background [*cue1/eno1*(+/-)].** The fluorescence was enhanced with DPBA (excitation: 330 nm >  $\lambda$  < 380 nm, emission:  $\lambda$  > 420 nm). The left and right panel represents bright field and fluorescence images, respectively. (A, B) Pollen grain of a wild-type plant (Col-0). (C-F) Pollen grains of *cue1-1/eno1-2*(+/-) double mutants.

### 3.14 Diminished content of aromatic and branched chain amino acids in flowers of *cue1/eno1* (+/-) mutants

One of the proposed functions of the PPT in vegetative tissues is the provision of PEP for the shikimate pathway. It has previously been reported that a mutation in the *PPT1* gene in the *cue1* mutants leads to lowered contents of phenylalanine in the leaves (Voll et al., 2003). Moreover, branched-chain amino acid synthesis commences from plastidic pyruvate via acetolactate synthase (Schulze-Siebert et al., 1984). In order to gain information on the steady state contents of amino acid during the early phase of gametophyte development, the amino acid composition in mature flowers (Stage 12-13) of *cue1/eno1*(+/-) plants, *cue1-6*, and both *eno1* alleles compared to wild type (Fig. 3.30). The content of total amino acids (i.e. the sum of all detected amino acids after HPLC separation) ranged between 3 and 4  $\mu\text{mol}\cdot\text{g}^{-1}$  fw and was not significantly affected in the individual mutant lines compared to the wild-type plants (Fig. 3.30A). Of the aromatic amino acids, phenylalanine (Phe) contents varied between the lines, but did not show a significant change in either of the mutants compared to wild-type plants (Fig. 3.30B). In contrast, tyrosine (Tyr) content was significantly increased in both

alleles of the *eno1* mutant, but only slightly decreased in *cue1-6* as well as in the *cue1/eno1* (+/-) plants (Fig. 3.30C). Similarly, the tryptophan (Trp) content was increased in both *eno1* mutant alleles, but decreased in the *cue1/eno1* (+/-) plants (Fig. 3.30D). As Trp serves as a precursor for auxin biosynthesis (Bartel, 1997), the stunted shoot growth and constraints of early flower development could be due to modified auxin availability (Vanneste and Friml, 2009; Pagnussat et al., 2009). Of the branched chain amino acids, the contents of valine (Val) and leucine (Leu) were not significantly altered between the lines (Fig. 3.30G), whereas isoleucine (Ile) content was diminished in *cue1-6* and the *cue1/eno1* (+/-) plants, but increased in both *eno1* mutant alleles (Fig. 3.30F).

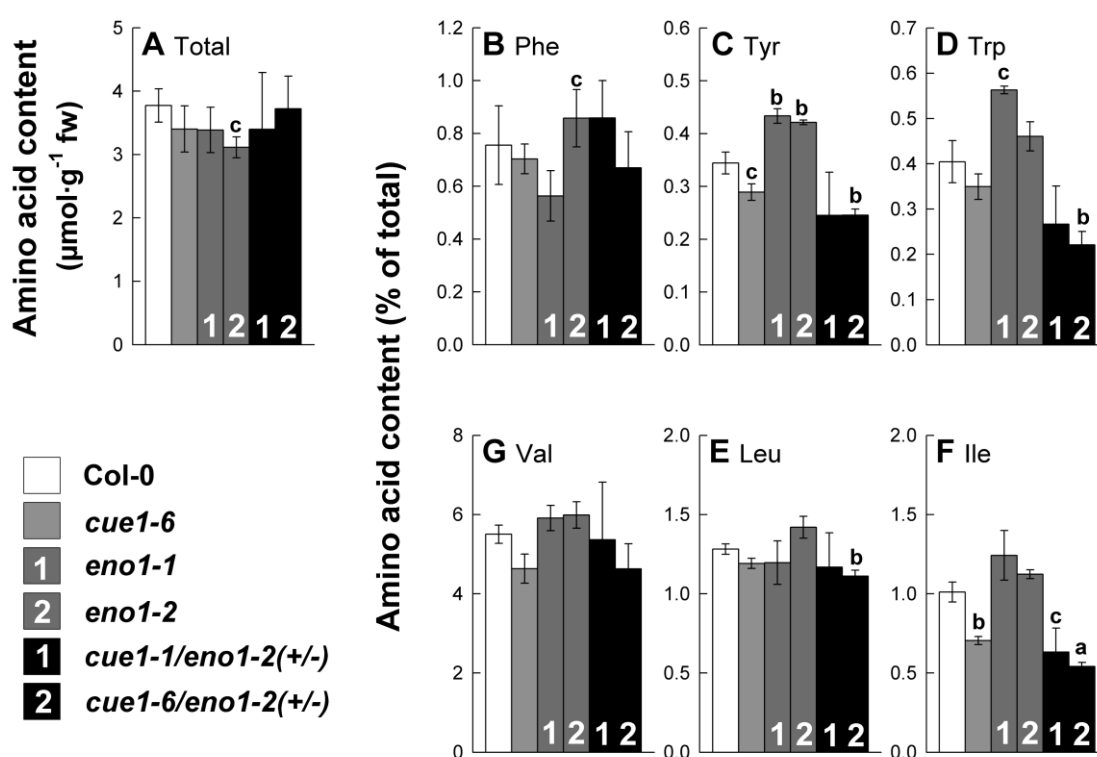


**Figure 3.30: Contents of selected amino acids extracted from flower buds of the wild-type (Col-0), the *cue1-6*, *eno1-1*, and *eno1-2* single mutants, as well as the heterozygous *eno1* mutants in the homozygous *cue1* background (*ccEe*).** The data represent the mean  $\pm$  SE,  $n = 5$  independent experiments. Statistical significance of differences between the parameters were assessed by the Welch-test with probability values of  $P < 0.001$  (a),  $P < 0.01$  (b),  $P < 0.02$  (c),  $P < 0.05$  (d) indicated above the respective bars. (A) Total amino acid content as estimated from the sum of all recognized proteinogenic amino acid after separation by HPLC. (B-D) The relative contents of the aromatic amino acids Phe, Tyr, Trp and (G-F) the branched chain amino acids Val, Leu, Ile were expressed as a percentage fraction of the total amino acid content (A) in flowers.

The contents of a broader range of proteogenic amino acids is displayed for the mutant compared to wild-type plants in Fig. 3.31. Of the major amino acids, glutamine (Gln) content

was significantly reduced by about 50% in both *eno1* mutant alleles and the *cue1/eno1* (+/-) plants (Fig. 3.31), whereas glutamate (Glu) content was unaffected (Fig. 3.31A). Threonine (Thr) and glycine (Gly) contents showed a trend for increase in both *eno1* alleles, but were diminished in *cue1-6* (Fig. 3.31 E and F), whereas serine (Ser) contents remained unaffected (Fig. 3.31D) The content of alanine (Ala) was increased in all mutant lines compared to the wild-type plants (Fig. 3.31G). Interestingly, both arginine (Arg) and lysine (Lys) contents were significantly increased in *cue1-6*, but exhibited wild-type levels in both *eno1* alleles and the *cue1/eno1* (+/-) plants (Fig. 3.31 I and J). An increased Arg content in *cue1* has previously been reported by Streatfield et al. (1999) and He et al. (2004). For the latter report a new *cue1* mutant allele (*nos1*) was isolated in a screen for nitric oxide (NO) overproducers. Arg has been proposed to act as a precursor for the synthesis of NO in plants (Guo et al., 2003), which exerts multiple effects on growth and development (del Rio et al., 2003). Furthermore, the histidine (His) content was significantly lowered by 30 % in *cue1/eno1* (+/-) compared to wild-type plants. It has recently been shown that His besides its role as essential amino acid for protein biosynthesis exerts control on developmental processes. A mutant of histidinalphosphate aminotransferase (HPA1) for instance leads to a short root phenotype but lacks other effects like an albino phenotype as in other His mutants (Mo et al., 2006) and, a complete knock out of HPA1 is embryo lethal.

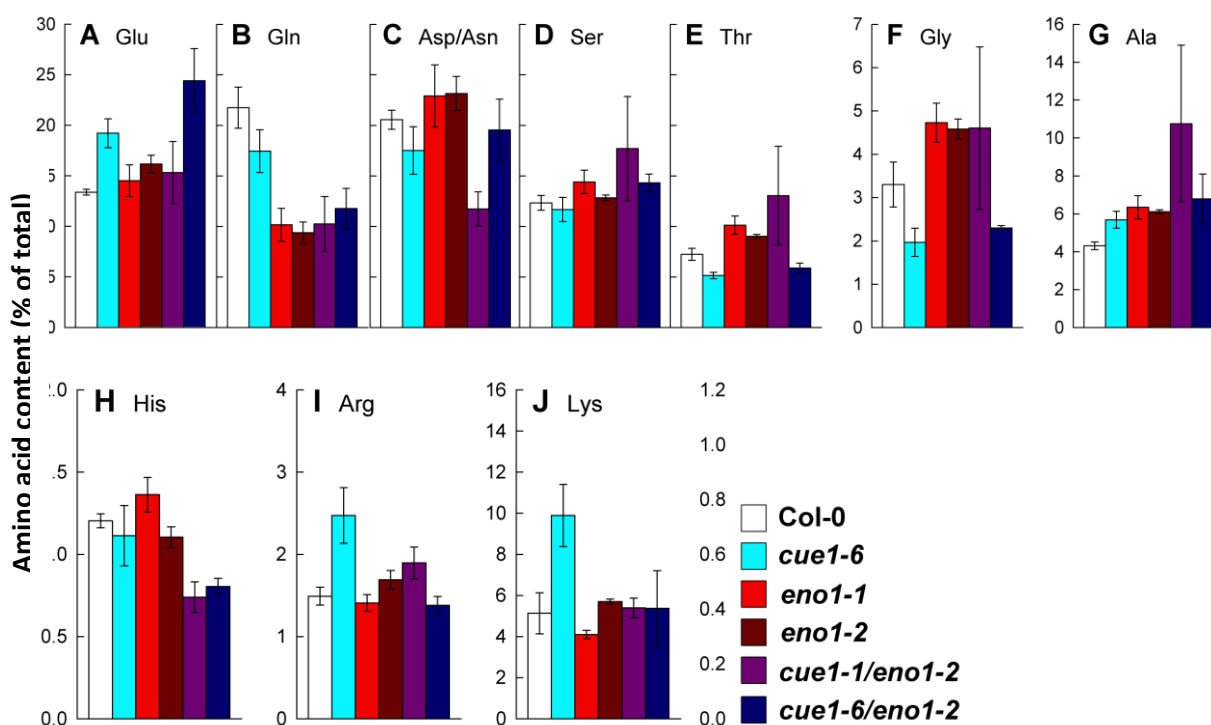


**Figure 3.31: Relative contents of amino acids (A-J) in flowers of the wild-type (Col-0), the *cue1-6*, *eno1-1*, and *eno1-2* single mutants as well as the heterozygous *eno1* mutants in the homozygous *cue1* background [*cue1/eno1* (+/-)].** The relative contents of amino acids were expressed as a percentage fraction of the total

amino acid content estimated from the sum of all recognized proteogenic amino acid after separation by HPLC (compare Figure 5A). The data represent the mean  $\pm$  SE, n = 5 independent experiments.

### 3.15 Analysis of secondary plant products in *cue1/eno1* (+/-) double mutants

Starting from amino acids phenylalanine or tyrosine, the phenylpropanoid pathway produces a majority of phenolic compounds found in nature. The main products of the various branches are lignin, flavonoids, anthocyanins, chlorogenic acid, salicylic acid and catecholamines (Aksamit-Stachurska et al., 2008). All the components of this pathway play an important role in plant physiology. Flavonoids play a key role in UV protection or as signal molecules (Li et al., 1993). It is conceivable that a decreased flux of PEP into aromatic amino acids and derived compounds (such as flavonoids) leads to disturbed development of the flowers as was observed for the *cue1/eno1*(+/-) plants (Fig. 3.18). Similar to the analysis of amino acid contents, flavonoids were extracted from mature flowers. Flavonoid contents were quite variable between the lines and ranged between 6.51 and 9.64 nmol·g<sup>-1</sup> FW (referred to the flavonoid, naringinin) in the wild-type control pOCA and in Col-0, respectively. There was no clear trend of reduced flavonoid contents in the *cue1* or *eno1* single mutants compared to the wild-type (Table 3.9). The flavonoid content in the *cue1/eno1*(+/-) plant (*cue1-6/eno1-2*) of 5.56 nmol·g<sup>-1</sup> FW was slightly, but not significantly less compared to the wild type or single mutant plants (Table 3.9).

**Table 3.9: Quantification of flavonoid content in mature flowers of wild type, *eno1*, *cue1* and *cue1/eno1*(+/-) mutants.** Naringinin was used as a reference standard for flavonoids.

Plant line	Flavonoid content (referred to naringinin) (nmol·g <sup>-1</sup> fw)
pOCA	6.51 $\pm$ 0.30
<i>cue1-1</i>	9.31 $\pm$ 0.42
<i>cue1-3</i>	10.82 $\pm$ 1.84
Col-0	9.64 $\pm$ 0.59
<i>cue1-6</i>	6.13 $\pm$ 0.60
<i>eno1-1</i>	8.01 $\pm$ 0.23
<i>eno1-2</i>	8.57 $\pm$ 0.98
<i>cue1-6/eno1-2</i>	5.56 $\pm$ 0.56

Lignin, as a constituent of cell walls, e.g. of the xylem elements, also derives from the phenylpropanoid metabolism. Staining with ACN dye reveals lignification in specific tissues of the inflorescence stem of *cue1-1/eno1-2(+/-)* plants, which appears to be reduced compared to the wild type or *cue1* single mutants (Fig. 3.32). (ACN dye stains the lignin in the cells red). Interestingly the inter-fascicular sclerenchyma cells in the stems of Col-0 (Fig. 3.32A), *cue1-6* (Fig. 3.32B) and *eno1* showed a strong lignification, whereas the xylem elements were only faintly stained. In contrast, there was almost no detectable lignification of the inter-fascicular cells in the stems of *cue1-6/eno1-2(+/-)* (Fig. 3.30C) or *cue1-1/eno1-2(+/-)* (Fig. 3.32D). In both lines the only lignified cells appeared to be those of the xylem elements. It is not clear, which factors control the degree of lignification in the individual cell types. However, the overall decline in lignification observed in the *cue1-1/eno1-2(+/-)* plants suggests again a limitation in the flux through the shikimate pathway.

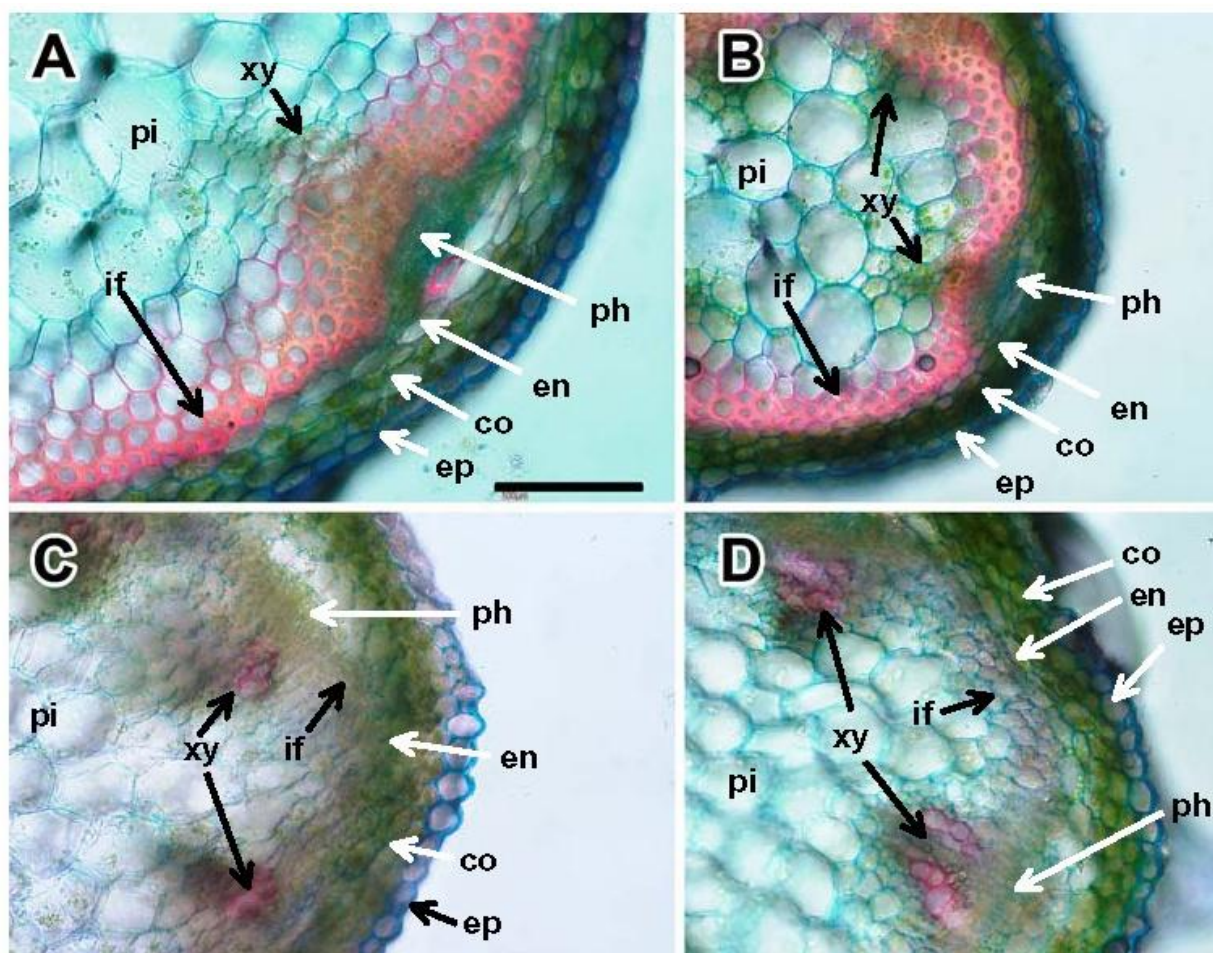


**Figure 3.32:** Cross sections of the inflorescence stem of heterozygous *eno1* mutants in the homozygous *cue1* background [*cue1/eno1(+/-)*] compared to wild-type and *cue1* plants stained with ACF to visualize lignin (red) or cellulose (blue) in cell walls. ep, epidermis; co, cortex (chlorenchyma); if, interfascicular cells (sclerenchyma); en, endodermis; ph, phloem; xy, xylem; pi, pith. The bar represents 100  $\mu$ m. (A) Col-0. (B) *cue1-6*. (C) *cue1-6/eno1-2(+/-)*. (D) *cue1-1/eno1-2(+/-)*.

### 3.16 Is cuticle wax integrity disturbed in *cue1/eno1* (+/-) double mutants ?

Beaudoin et al. (2009) observed a phenotype of shoots and flowers similar to the *cue1/eno1*(+/-) plants in the *kcr1* mutant (defective in  $\beta$ -ketoacyl-coenzyme A reductase) disturbed in fatty acid elongation. A knock out of this gene leads to embryo lethality. Interestingly, trichomes of *kcr1* exhibited a distorted phenotype similar to that of the *eno1* single mutant alleles, which is also evident for the *cue1/eno1*(+/-) plants. It has been proposed that KCR1 is involved in the synthesis of cuticular waxes or the composition of sphingolipids. Toluidine blue (TB) staining of the *kcr1* mutant revealed a loss of cuticle integrity. In some species, suberin, akin to cuticle can also contain flavonoids and phenylpropanoids (Jetter et al., 2006). Thus the cuticle integrity of the *cue1/eno1*(+/-) mutants was assessed by TB staining (Fig. 3.33). Interestingly, the *cue1/eno1*(+/-) plants exhibited a positive staining with TB (Fig. 3.33 C and D) as compared to wild-type (Fig. 3.31A) or *cue1-6* plants (Fig. 3.33B) indicating a lack of cuticle integrity when the expression of *ENO1* is reduced in the *cue1* background. In contrast, the TB treatment of *eno1* single mutant alleles pointed to an intact cuticle. The *cue1/eno1*(+/-) plants exhibited different degrees of cuticle damage.

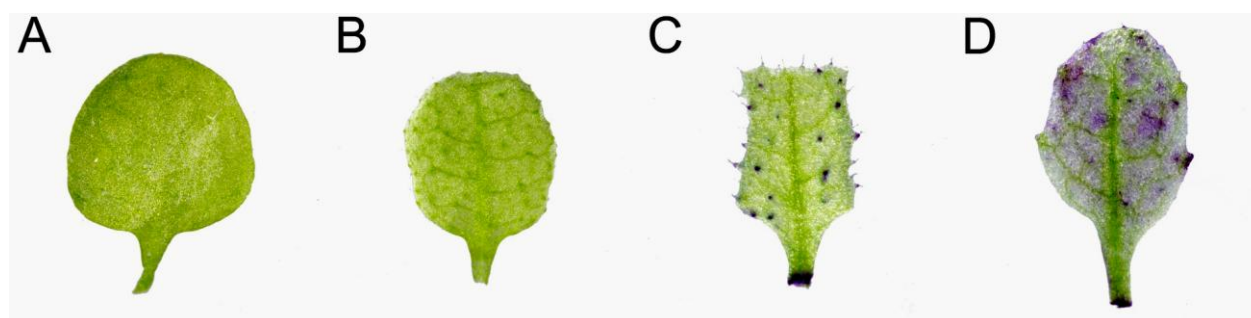


**Figure 3.33: Toluidine Blue (TB) staining as a test for the cuticle integrity of leaves from the heterozygous *eno1* mutants in the homozygous *cue1* background (*cue1/eno1*(+/-) compared to the wild type or the *cue1* single mutant grown for three weeks in the greenhouse. (A) TB stained leaf of the wild-type (Col-0). (B) TB stained leaf of *cue1-1*. (C) TB stained leaf of *cue1-1/eno1-2*(+/-) exhibiting a marked leakiness of the trichome cuticle. (D) TB stained leaf of *cue1-1/eno1-2*(+/-) with an irregular leakiness of the cuticle covering the leaf blade.**

Individual leaves showed only a TB staining of trichomes (Fig. 3.33C), whereas others exhibited a patchy TB staining throughout the leaf blade (Fig. 3.33D) resembling TB stained leaves of *kcr1* (Beaudoin et al., 2009). In particular, the damage of the trichome cuticle in the *cue1/eno1*(+/-) plants supports the distorted trichome phenotype of the *eno1* single mutants. However, *eno1* single mutants exhibited an intact trichome cuticle. Furthermore, *ENO1* is not expressed in mature leaves, but in the meristem of emerging leaves, suggesting that defects in cuticle integrity are determined at a very early stage of leaf development.

### 3.17 Expression of *KCR1* and *KCR2* in *cue1/eno1* (+/-) double mutants

As the deficiency in KCR is responsible for a similar phenotype in the *kcr1* mutant as in the *cue1/eno1*(+/-) plants, an experiment was designed to test the transcript abundance of *KCR1* and of its allele *KCR2* in the shoot meristem of *cue1-6/eno1-2*(+/-) in comparison to the wild-type by real time RT-PCR. Indeed both genes were down-regulated with a log<sub>2</sub>-ratio of -0.93 and -1.24 for *KCR1* and *KCR2*, respectively (Fig. 3.34). This pleiotropic down-regulation of both genes maybe at least partially responsible for the *cue1/eno1*(+/-) phenotype.

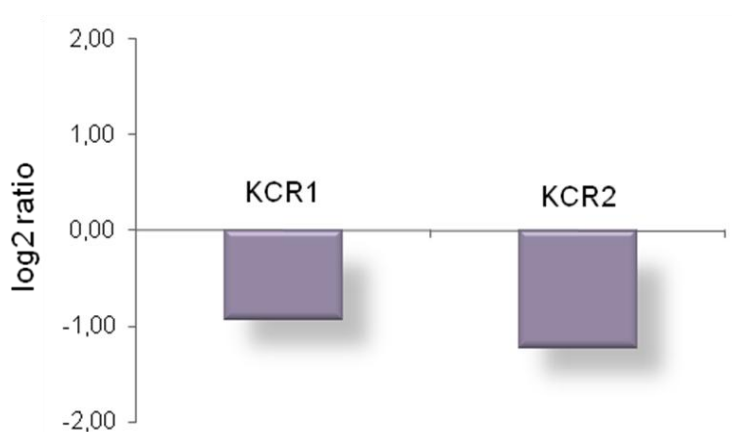


**Figure 3.34:** Down-regulation of gene expression of AtKCR1 and AtKCR2 in *cue1-6/eno1-2*(+/-) mutants observed with Real-Time RT PCR analysis.

### 3.18 Over-expression of *ENO1* rescues the *cue1* phenotype

Previously it was reported (Voll et al., 2003) that ectopic overexpression of a C<sub>4</sub>-type pyruvate, orthophosphate dikinase (PPDK) driven by the *CaMV* 35S promoter could rescue the *cue1* leaf phenotype. *PPDK* is capable of producing PEP from pyruvate and thus replenishes PEP in plastids of those tissues, where PPT1 is missing, e.g. in vascular cells of the leaf (Knappe et al., 2003). As *ENO1* is not expressed in mature leaves, PEP supply relies entirely on the import by the PPT and not on plastid glycolysis. So, the next step was to ascertain whether the ectopic over-expression of *ENO1* in the background of the *cue1-6* mutant was capable of rescuing the *cue1* phenotype. Out of the several transformed lines which over-expressed *ENO1*, *cue1-6* ENO1 line (4) and (5) showed the highest transcript abundance (Fig. 3.35B). As control, *ENO1* was also over-expressed in the Col-0 wild type yielding two lines (Col-0 ENO1 [A] and [C]) with an increased transcript level of *ENO1* (Fig. 3.35A). As shown in Fig. 3.36C and D, *ENO1* over-expressors in the *cue1-6* background had a wild-type like appearance, i.e. the reticulate leaf phenotype was completely rescued (Fig. 3.36D) and the rescue is gene dosage dependent. And, over-expression of *ENO1* could also

rescue the retarded growth phenotype of *cue1-6* (Fig. 3.36E) but had virtually no effect on the phenotypic appearance when over-expressed in wild-type plants (Fig. 3.36F). These data show that the only missing enzyme for a complete plastidic glycoytic pathway appears to be ENO1 and not plastidic PGyM, at least in those tissues where PPT1 is expressed in wild-type plants.

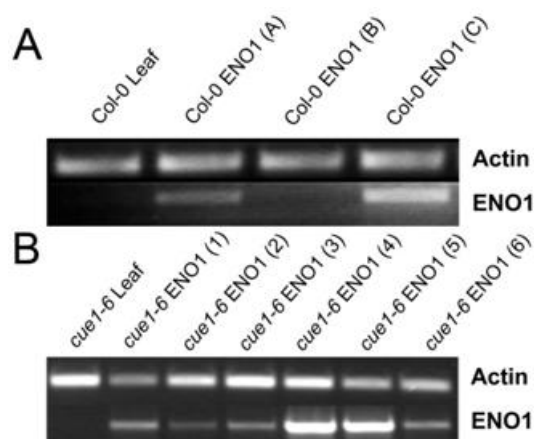


**Figure 3.35: Ectopic over-expression of ENO1 in the wild type (Col-0) and the *cue1-6* mutant.** Semi-quantitative RT-PCR with RNA extracted from leaves of wild-type (Col-0) or transformants over-expressing ENO1 in the Col-0 background. (B) Semi-quantitative RT-PCR with RNA extracted from leaves of *cue1-6* or transformants over-expressing ENO1 in the *cue1-6* background.

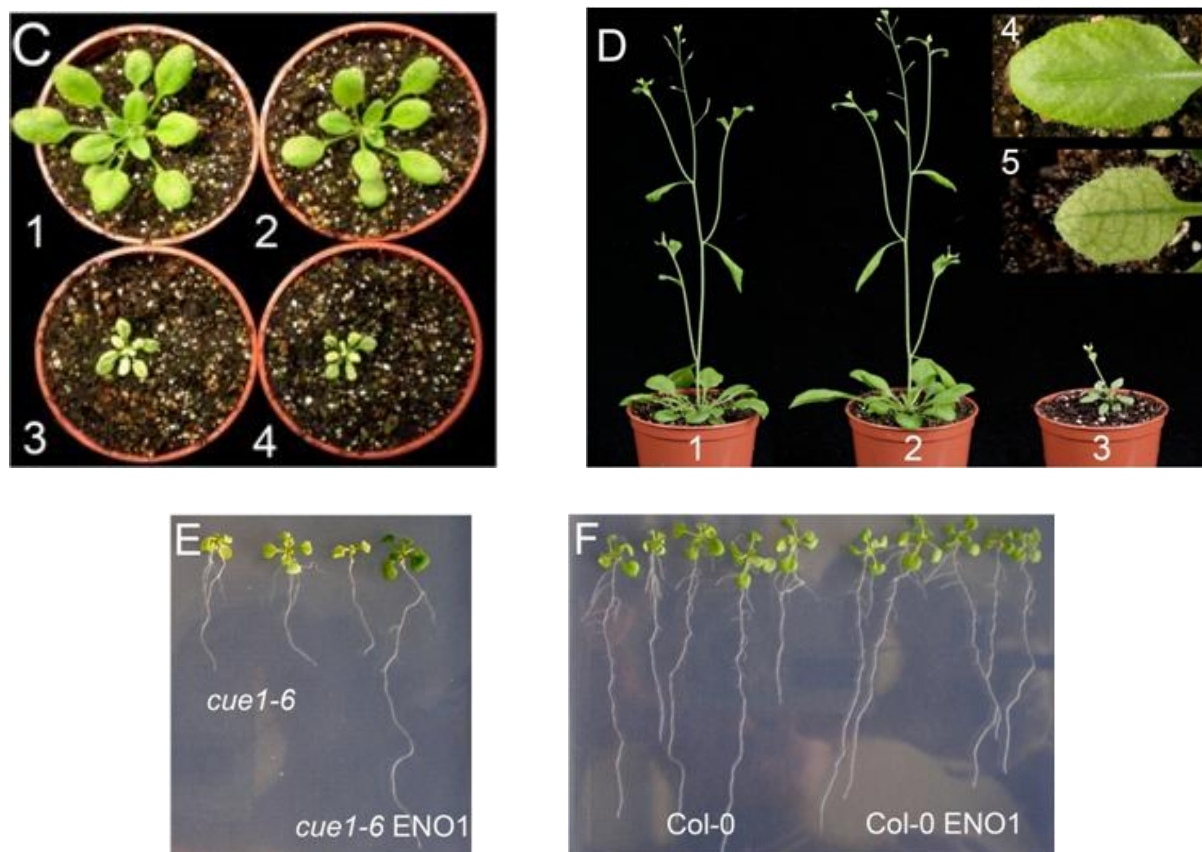


**Figure 3.36: Ectopic over-expression of ENO1 in the wild type (Col-0) and the *cue1-6* mutant.** (C) Rosette phenotypes of the wild type (1), an ENO1 over-expressing line (*cue1-6* ENO1 [4]) with a high transcript

abundance of ENO1 (2), of the *cue1-6* mutant (3) and an ENO1 over-expressing line (*cue1-6* ENO1 [1]) with a low transcript abundance of ENO1 (4). (D) Growth phenotype of flowering Col-0 wild-type (1), *cue1-6* ENO1 (2), and *cue1-6* (3) plants. The inset shows the rescue of the leaf phenotype of *cue1-6* over-expressing ENO1 (4) in comparison with *cue1-6* (5). (E) Rescue of the retarded root phenotype of the *cue1-6* mutant by over-expression of ENO1 in the *cue1-6* background. (F) Phenotypic comparison of wild-type Col-0 with Col-0 plants over-expressing ENO1.

### 3.19 Over-expression of *ENO1* in *los2* mutants has no effect

In order to address whether overexpression of *ENO1* could rescue the severe phenotype of the *los2* mutant (Lee et al., 2002), which is defective in one of the two cytosolic enolases (At2g36530), *ENO1* was over-expressed in heterozygous plants since the homozygous *los2* mutant was sterile. It is conceivable that the glycolytic flux in the cytosol could be diverted via the plastid stroma involving PPT1 and/or PPT2. Both transporters have been shown to be capable of a PEP/2-PGA counter exchange (Knappe et al., 2003). However, amongst the T0 generation of the transformed heterozygous *los2* mutants, there were no plants exhibiting a rescue or alleviation of the *los2* phenotype. Among the many *ENO1* over-expressors in *los2*, all of them showed a phenotype similar to the *los2* with underdeveloped roots and bleached leaves on medium supplemented with sucrose (Fig. 3.37A). When the plants were transferred and propagated on soil they were not complemented (Fig. 3.37B). One of the transgenic lines, line (2) produced extra lateral branches compared to the other transgenic lines and more flowers, but the flowers were sterile and did not develop into siliques. Thus, *LOS2*, besides its metabolic function, appears to be also involved in transcriptional regulation, the lack of any rescuing effect on the *los2* phenotype by this approach might be due to this latter function.



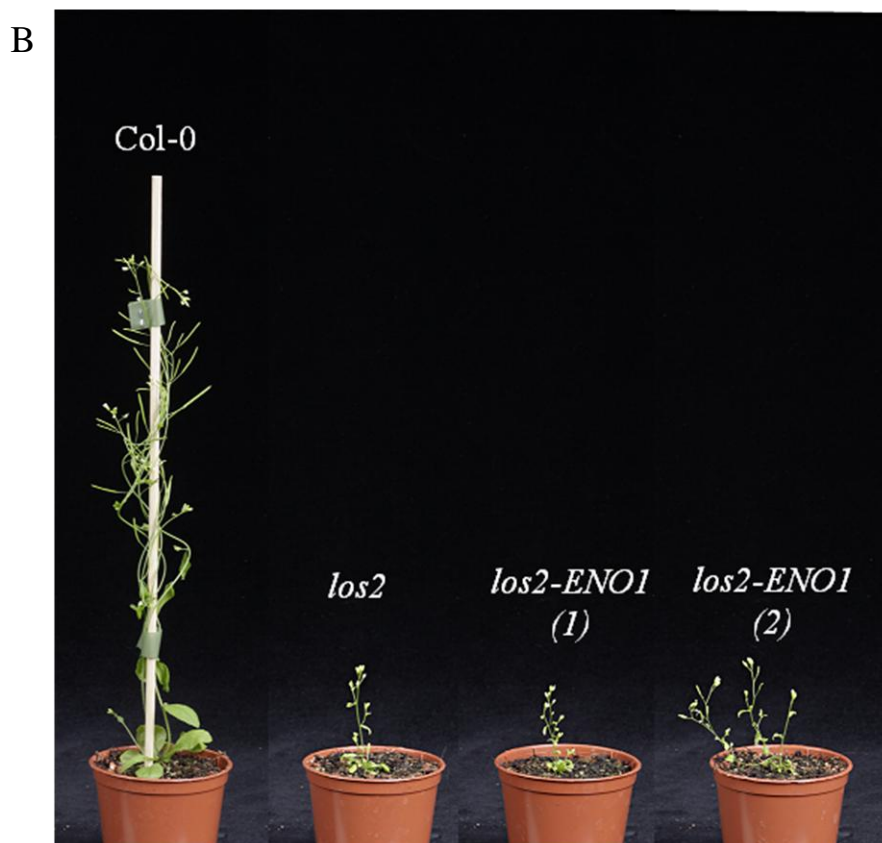


**Figure 3.37: Ectopic over-expression of ENO1 in the *los2* mutant.** (A) Phenotypic comparison of wild type plants (Col-0) with *los2* heterozygous mutants and *los2* homozygous mutants. Over-expression of ENO1 in *los2* mutants does not rescue the root and shoot phenotype. (B) Growth phenotype of wild-type Col-0 plants compared with the over-expressing lines of *los2* mutants.

### 3.20 *ENO1* over-expression restores photosynthetic electron transport in *cue1* but has no effect in wild-type plants

It has been shown previously that the rate of photosynthetic electron transport (ETR) is impaired in different alleles of the *cue1* mutant (Streatfield et al., 1999, Voll et al., 2003), most likely due to the decreased density of mesophyll cells characteristic for the leaf phenotype. Hence, the rescue of the *cue1* mutant phenotype by over-expressing *ENO1* might restore ETR. A complete glycolytic pathway in chloroplasts from 3-PGA to pyruvate would withdraw 3-PGA fixed by Rubisco in the light, which could result in a decreased replenishment of the Calvin cycle with intermediates and hence the regeneration of RubP as primary CO<sub>2</sub> acceptor. The overall withdrawal of 3-PGA might hence lead to a decline in ETR. This question was addressed by measuring the ETR by pulse amplitude modulation (PAM) fluorometry. As shown in Fig. 3.38, ETR in *cue1-6* plants overexpressing *ENO1* recovers to wild-type levels (Fig. 3.38B). Moreover, there was no effect on ETR in wild-type plants overexpressing *ENO1* (Fig. 3.38A), indicating that a complete glycolytic pathway in chloroplasts does not interfere with ETR.

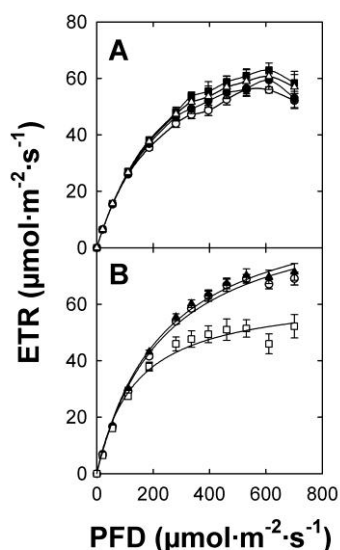


**Figure 3.38. Light saturation curves of photosynthetic electron transport rates (ETR) determined by PAM fluorometry.** (A) Comparison of light saturation curves between Col-0 (○), *eno1-2* (△), Col-0 ENO1 (A) (●) and Col-0 ENO1 (C) (■). (B) Comparison of light saturation curves between Col-0 (○), *cue1-6* (□), and *cue1-6* ENO1 (4) (▲). The data represent the mean  $\pm$  SE,  $n = 9$  measurements on individual plants per line.

### 3.21 Does *ENO1* overexpression lead to overall seed improvement?

*ENO1* together with *PPT1* is co-expressed during early embryo development and is most likely involved in the provision of PEP inside the plastid, as a precursor of fatty acid biosynthesis and for the shikimate pathway. Thus, different parameters with respect to the seed yield as well as metabolic end products in flowers and seeds in the mutant lines of *ENO1* over-expressing lines (*cue1* or Col-0 background) were determined. Table 3.10 shows a comparison of the number of siliques and seeds per plant determined for all lines used in this study. The individual mutant alleles of *cue1* and *eno1* as well the respective wild-type plants were grown in a temperature controlled greenhouse in September and October (Table 3.10A). For both the ecotypes Col-0 and Bensheim (pOCA) similar values for the number of siliques and total seed weight per plant were obtained. However, the number of seeds per plant was higher in pOCA resulting in a lower specific seed weight. For the *cue1* mutant alleles silique number, seed weight per plant, and number of seeds per plant was reduced significantly compared to the respective wild-type lines. The weak *cue1-3* allele had intermediate numbers of siliques and seed numbers per plant. The reduced harvest of the *cue1* mutant alleles is most likely a consequence of decreased maximum photosynthesis rates and retarded growth of the shoots. Interestingly, the number of siliques and seeds was increased in both alleles of the *eno1* mutant. However, the seed weight per plant was reduced, thus leading to an overall decline in the specific seed weight from about  $18.6 \mu\text{g}\cdot\text{seed}^{-1}$  in Col-0 to  $14.9 \mu\text{g}\cdot\text{seed}^{-1}$  in

*eno1-2*. Wild-type and *cue1-6* plants over-expressing *ENO1* were grown in the greenhouse during February and March (Table 3.10B). The overall yield of siliques and seeds was increased notably when the two harvests were compared. For Col-0, the number of siliques and seeds was increased by 54% from 135.6 siliques/plant to 208.5 siliques/plant and by 86% from 3895 seeds/plant to 7239 seeds/plant, respectively. Interestingly, the specific seed weight was decreased from 18.6  $\mu\text{g}\cdot\text{seed}^{-1}$  to 14.4  $\mu\text{g}\cdot\text{seed}^{-1}$ . Despite these differences in both harvests the overall trend in the *cue1-6* mutant allele was similar, i.e. less siliques and seeds per plant and reduced specific seed weight relative to the wild type. Two lines over-expressing *ENO1* in the Col-0 background exhibited no clear trend of a changed yield of siliques or seeds. Line Col-0 ENO1 (C) yielded similar numbers of siliques and specific seed weights, but exhibited lower number of seeds per plant, whereas Col-0 ENO1 (A) had similar seed numbers as the wild-type, but a slightly decreased specific seed weight. A comparison of *cue1-6* plants overexpressing *ENO1* with the *cue1-6* mutant revealed that the decreased number of siliques relative to the wild type was similar, despite a complete rescue of the *cue1* phenotype. Moreover, the number of seeds was considerably lower in *cue1-6* ENO1 than in the wild-type plants, but increased with respect to *cue1-6*, whereas the specific seed weight in *cue1-6* ENO1 plants was similar to wild-type plants. These data indicate that ectopic over-expression of *ENO1* had no effect on the harvest of wild-type *A. thaliana* plants. However, overexpression of *ENO1* could only partially rescue seed and silique production of the *cue1* mutant (expression driven by the CaMV 35 S promoter).

**Table 3.10: Harvest parameters of wild-type *A. thaliana* (Col-0, pOCA), *eno1* and *cue1* alleles as well as ENO1 overexpressing lines in the Col-0 or *cue1-6* background.** (A) Plants were grown in a temperature controlled greenhouse during September and October or (B) during February and March.

A

Plant line	Siliques/plant	Seed weight per plant	Specific seed weight	Number of seeds per plant
		(mg)	( $\mu\text{g}\cdot\text{seed}^{-1}$ )	
pOCA	133.8 $\pm$ 3.3 (100)	80.9 $\pm$ 3.0 (100)	16.8 $\pm$ 0.7 (100)	4821
<i>cue1-1</i>	95.9 $\pm$ 4.1 (72)	47.2 $\pm$ 2.9 (65)	15.2 $\pm$ 0.5 (91)	3105
<i>cue1-3</i>	117.2 $\pm$ 4.2 (88)	48.2 $\pm$ 2.2 (66)	12.3 $\pm$ 0.3 (73)	3907
Col-0	135.6 $\pm$ 7.1 (100)	72.5 $\pm$ 3.9 (100)	18.6 $\pm$ 0.9 (100)	3895
<i>cue1-6</i>	106.5 $\pm$ 4.6 (79)	31.0 $\pm$ 1.2 (43)	11.4 $\pm$ 0.7 (61)	2723
<i>eno1-1</i>	143.5 $\pm$ 3.5 (106)	75.3 $\pm$ 3.1 (104)	17.5 $\pm$ 0.7 (94)	4314
<i>eno1-2</i>	142.2 $\pm$ 3.6 (105)	76.4 $\pm$ 3.2 (105)	14.9 $\pm$ 1.0 (80)	5121

B

Plant line	Siliques/plant	Seed weight per plant	Specific seed weight	Number of seed per plant
		(mg)	( $\mu\text{g}/\text{seed}$ )	
Col-O	208.5 $\pm$ 10.2 (100)	104.2 $\pm$ 5.9 (100)	14.4 $\pm$ 0.7 (100)	7239
<i>cue 1-6</i>	188.7 $\pm$ 6.7 (91)	49.0 $\pm$ 2.4 (47) <sup>a</sup>	12.4 $\pm$ 0.5 (86)	3941
Col-O ENO1 (A)	201.7 $\pm$ 7.6 (97)	79.5 $\pm$ 5.9 (76) <sup>b</sup>	14.5 $\pm$ 1.1 (101)	5466
Col-O ENO1 (C)	199.4 $\pm$ 5.4 (96)	89.8 $\pm$ 7.7 (79)	12.4 $\pm$ 0.6 (86) <sup>d</sup>	7266
<i>cue 1-6</i> ENO1 (4)	180.5 $\pm$ 9.0 (87) <sup>d</sup>	79.1 $\pm$ 4.1 (76) <sup>b,a</sup>	13.2 $\pm$ 0.2 (92)	5989
<i>cue 1-6</i> ENO1 (5)	186.2 $\pm$ 12.4 (88)	82.1 $\pm$ 7.0 (86) <sup>c,a</sup>	14.0 $\pm$ 0.6 (97) <sup>d</sup>	5875

The data are expressed as mean  $\pm$  SE of 15 individual plants per line. The specific seed weight was estimated from 100-200 seeds counted. Statistical significance of differences between the parameters were assessed by the Welch-test with probability values of  $P < 0.001$  (a),  $P < 0.01$  (b),  $P < 0.02$  (c),  $P < 0.05$  (d). The letters in italics refer to *cue1-6* as a control

### 3.22 Analysis of seed storage compounds in *cue1/eno1* (+/-) double mutants

Analysis of storage compounds of seeds (fatty acid content and composition as well as protein and carbohydrate contents) of all lines was performed. Total fatty acids were quantified as a measure of seed oil content. The total lipid content in the wild-type plants Col-0 and Bensheim (pOCA) was 8.13  $\mu\text{g seed}^{-1}$  and 8.45  $\mu\text{g seed}^{-1}$ , respectively (Table 3.11). It was slightly reduced in the *cue1* and *eno1* mutant alleles. This decrease was significant according to Welch test for *cue1-6* and *eno1-1*, but less marked in *cue1-1* and *eno1-2*. Of the *cue1/eno1*(+/-) plants, class I seeds showed a high, wild-type like lipid content of 7-10  $\mu\text{g}\cdot\text{seed}^{-1}$ , while class II seeds (intermediate) were reduced to about 2.2-4.3  $\mu\text{g}\cdot\text{seed}^{-1}$ , and class III seeds contained strongly reduced amounts of oil (1.9-2.5  $\mu\text{g}\cdot\text{seed}^{-1}$ ). The strong reduction in oil content in class II and class III seeds was accompanied by an increase in the contents of saturated fatty acids, i.e. 16:0, 18:0 and 22:0, while the amounts of unsaturated fatty acids 18:3 and 20:1 decreased (Fig. 3.39). These changes are reflected in the strong decrease in the desaturation index ( $I_D$ ), which expresses the number of double bonds in all desaturated fatty acid classes divided by the number of all saturated fatty acid classes. Furthermore, the increase in 16:0 and the decrease in 18:3 affect the ratio of C16 to C18 fatty acids (for a complete comparison of fatty acid composition see (Fig. 3.39). Over-expression of *ENO1* in the Col-0 background had no severe effect on lipid content and composition. The average lipid content was slightly less in Col-0 ENO1, but the C16/C18 ratio increased and  $I_D$  decreased suggesting a reduced rather than an enhanced production of storage lipids.

**Table 3.11 Storage compounds in seeds of wild-type *A. thaliana* (Col-0, pOCA), *eno1* and *cue1* alleles, as well as ENO1 overexpressing lines in the Col-0 or *cue1-6* background and heterozygous *eno1* mutants in the homozygous *cue1* background [*cue1/eno1*(+/-)plants].**

Plant line	Total Lipid ( $\mu\text{g}$ per seed)	C16/C18 ratio	C20:1 (Mol %)	I <sub>D</sub>	n
pOCA	8.45 $\pm$ 0.29	0.123	13.60 $\pm$ 0.28	11.15	5
<i>cue1-1</i>	6.63 $\pm$ 0.73	0.112	13.08 $\pm$ 0.47	12.91	5
<i>cue1-3</i>	6.77 $\pm$ 0.44 <sup>c</sup>	0.109	13.96 $\pm$ 0.47	13.35	5
Col-0	8.13 $\pm$ 0.27	0.104	13.56 $\pm$ 0.23	10.71	10
<i>cue1-6</i>	5.70 $\pm$ 0.35 <sup>a</sup>	0.112	12.85 $\pm$ 0.32	12.41	5
<i>eno1-1</i>	5.53 $\pm$ 0.29 <sup>a</sup>	0.142	12.98 $\pm$ 0.27	10.02	10
<i>eno1-2</i>	7.77 $\pm$ 0.49	0.132	13.26 $\pm$ 0.18	10.28	10
Col-0 ENO1	7.17 $\pm$ 0.55	0.154	12.63 $\pm$ 0.27 <sup>d</sup>	9.37	10
<i>cue1-6</i> ENO1	7.21 $\pm$ 0.30 <sup>d, b</sup>	0.137	13.49 $\pm$ 0.29	9.88	10
<i>cue1-1/eno1-1</i> (class III)	2.51 $\pm$ 0.41 <sup>b</sup>	0.208	8.92 $\pm$ 0.72 <sup>b</sup>	5.56	5
<i>cue1-1/eno1-1</i> (class II)	3.98 $\pm$ 0.44 <sup>d</sup>	0.141	10.83 $\pm$ 0.66	8.54	5
<i>cue1-1/eno1-1</i> (class I)	10.40 $\pm$ 0.27 <sup>b</sup>	0.099	14.03 $\pm$ 0.29	13.02	5
<i>cue1-1/eno1-2</i> (class III)	2.10 $\pm$ 0.20 <sup>b</sup>	0.278	4.24 $\pm$ 0.52 <sup>a</sup>	3.45	5
<i>cue1-1/eno1-2</i> (class II)	2.25 $\pm$ 0.32 <sup>b</sup>	0.284	5.49 $\pm$ 0.55 <sup>a</sup>	3.26	5
<i>cue1-1/eno1-2</i> (class I)	6.50 $\pm$ 0.13	0.121	11.67 $\pm$ 0.25	8.75	5
<i>cue1-3/eno1-2</i> (class III)	2.18 $\pm$ 0.18 <sup>a</sup>	0.249	7.51 $\pm$ 0.61 <sup>a</sup>	3.98	5
<i>cue1-3/eno1-2</i> (class II)	4.26 $\pm$ 0.37 <sup>b</sup>	0.162	10.35 $\pm$ 0.74 <sup>c</sup>	6.52	5
<i>cue1-3/eno1-2</i> (class I)	7.00 $\pm$ 0.23	0.119	12.53 $\pm$ 0.20 <sup>d</sup>	9.76	5
<i>cue1-6/eno1-2</i> (class III)	1.91 $\pm$ 0.19 <sup>a</sup>	0.323	6.01 $\pm$ 0.95 <sup>b</sup>	2.8	5
<i>cue1-6/eno1-2</i> (class II)	2.62 $\pm$ 0.15 <sup>a</sup>	0.287	8.53 $\pm$ 0.73 <sup>c</sup>	3.9	5
<i>cue1-6/eno1-2</i> (class I)	7.07 $\pm$ 0.26 <sup>d</sup>	0.132	11.62 $\pm$ 0.05 <sup>c</sup>	8.76	5

Lipid contents and fatty acid composition were determined on individual seeds (n = 5-10) and C16/C18 ratios as well as the de-saturation index (I<sub>D</sub>) were calculated from the Mol% of individual fatty acid shown in Fig. 3.43. The data represent the mean value  $\pm$  SE. Statistical significance of differences between the parameters were assessed by the Welch-test with probability values of P < 0.001 (a), P < 0.01 (b), P 0.02 (c), P < 0.05 (d).

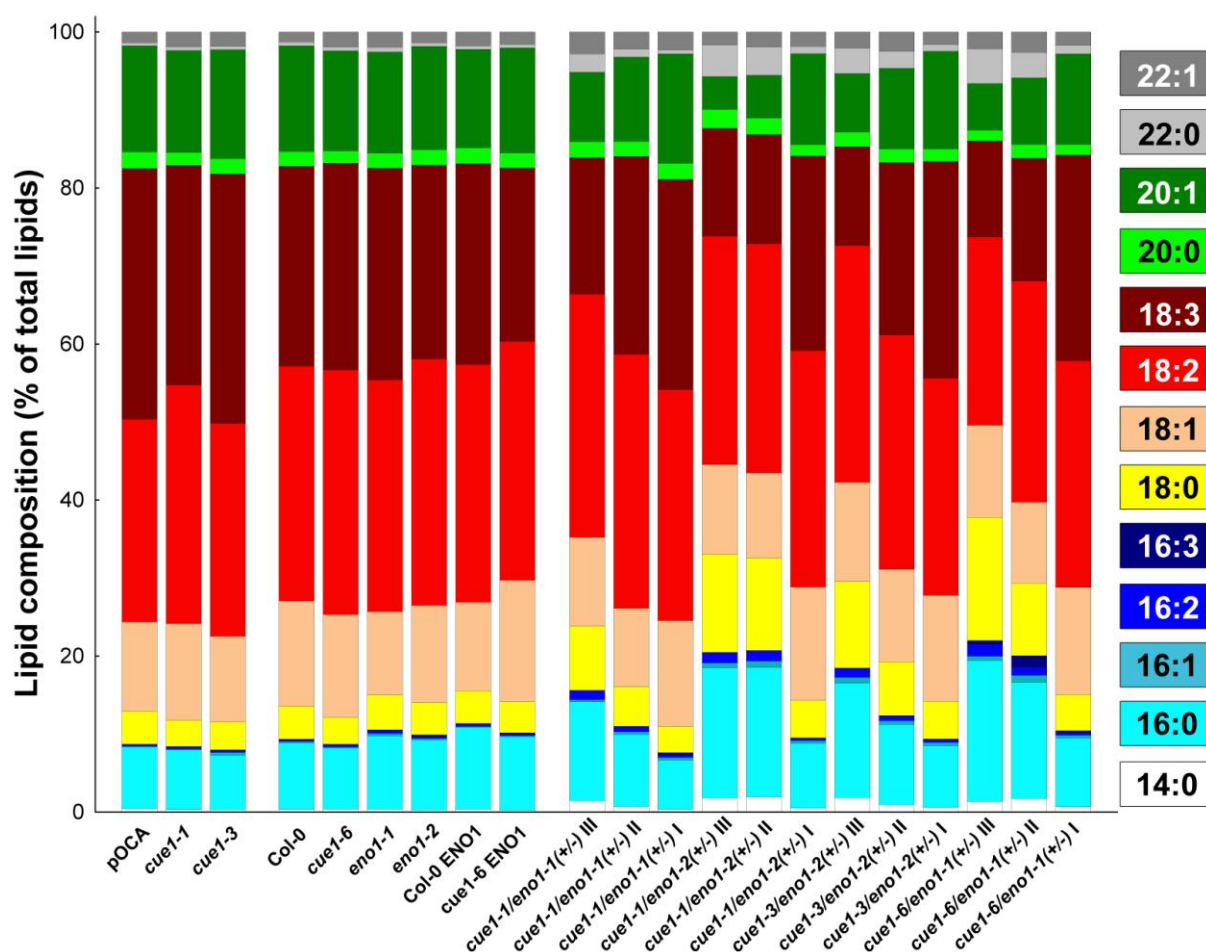


**Figure 3.39: Relative composition of saturated and desaturated fatty acids determined by gas chromatography after derivatization to fatty acid methyl esters.** The fatty acid composition was determined on single seeds ( $n = 5-10$ ) and referred to the total lipid content of the individual samples. The single mutants *cue1-1*, *cue1-3*, *cue1-6*, *eno1-1*, and *eno1-2* were compared to their respective wild-type (Col-0) or control plants (pOCA). For the wild-type as well as *cue1-6* plants overexpressing ENO1, data of the lines Col-0 ENO1 (A) and Col-0 ENO1 (C) as well as *cue1-6* ENO1 (4) and *cue1-6* ENO1 (5) were grouped. The roman numbers for the heterozygous *eno1* mutants in the homozygous *cue1* background represent measurement on individual class I, class II and class III seeds.

Mature *A. thaliana* seeds store similar amounts of protein and lipids when referred to percent of the dry weight (Chen et al., 2009). As shown in Table 3.12, total protein content was similar in the single *cue1* and *eno1* mutants compared to the respective wild-type or control plants, leading to a decline in the oil/protein (L/P) ratio by 10 to 20 % in the *cue1* alleles and up to 30% in the *eno1* alleles. These data indicate that oil content rather than protein content is controlled by PPT1 and ENO1. Similar to the seed oil content, protein content was severely diminished in class III seeds of the segregating *cue1/eno1(+/-)* plants, whereas class II seeds showed an intermediate decline in protein content. Likewise carbohydrate content was not severely affected in the single mutant alleles compared to the wild-type (Table 3.12). Mature

*A. thaliana* seeds comprise sucrose as major carbohydrate, whereas starch was below the detection limit of the coupled enzymatic assay applied. Total carbohydrate contents were not appreciably affected in the single mutants compared to the respective wild-type plants. Similar to seed oil and protein contents, sucrose content was severely decreased in class III and intermediately reduced in class II seeds of the *cue1/enol*(+/-) plants. Interestingly the levels of both hexoses (glucose and fructose) were appreciably increased in the strong *cue1* alleles as well as in both *enol* mutant alleles relative to the respective wild-type plants. Likewise, contents of both hexoses were enhanced in class III seeds of the *cue1/enol*(+/-) plants, whereas class II seeds contained diminished hexose contents relative to the wild-type like class III seeds. It is conceivable that a block in oil production leads to a reduced sucrose consumption by glycolysis and results in an enhanced hydrolytic cleavage of sucrose by invertase. However, this aspect has not been further addressed. Again, over-expression of ENO1 in the Col-0 or *cue1-6* backgrounds had no strong effect on seed protein and carbohydrate contents.

**Table 3.12 Storage compounds in seeds of wild-type *A. thaliana* (Col-0, pOCA), *enol* and *cue1* alleles, as well as ENO1 overexpressing lines in the Col-0 or *cue1-6* background and heterozygous *enol* mutants in the homozygous *cue1* background [*cue1/enol*(+/-)plants].**

Plant line	Total Protein ( $\mu\text{g}\cdot\text{seed}^{-1}$ )	Sucrose ( $\mu\text{g}\cdot\text{seed}^{-1}$ )	Glucose ( $\text{ng}\cdot\text{seed}^{-1}$ )	Fructose ( $\mu\text{g}\cdot\text{seed}^{-1}$ )	L/P ratio	L/C ratio
pOCA	10.28 $\pm$ 0.23	308 $\pm$ 31	5.10 $\pm$ 0.66	4.23 $\pm$ 0.44	0.82	32,4
<i>cue1-1</i>	10.60 $\pm$ 0.96	277 $\pm$ 10	7.61 $\pm$ 1.34	7.02 $\pm$ 1.01	0.63	36,3
<i>cue1-3</i>	10.98 $\pm$ 0.22	309 $\pm$ 4	4.99 $\pm$ 0.94	3.92 $\pm$ 1.72	0.62	34,5
Col-0	10.56 $\pm$ 0.31	249 $\pm$ 13	2.34 $\pm$ 0.60	2.39 $\pm$ 0.51	0.77	41,6
<i>cue1-6</i>	7.74 $\pm$ 0.18	374 $\pm$ 24	9.24 $\pm$ 4.14	7.58 $\pm$ 2.20	0.74	19,8
<i>enol-1</i>	10.95 $\pm$ 0.12	387 $\pm$ 24	9.42 $\pm$ 1.98	7.02 $\pm$ 2.30	0.51	27,1
<i>enol-2</i>	10.42 $\pm$ 0.29	317 $\pm$ 25	12.76 $\pm$ 1.07	8.23 $\pm$ 0.16	0.75	30,8
Col-0 ENO1	10.74 $\pm$ 0.44	341 $\pm$ 33	4.70 $\pm$ 0.60	3.91 $\pm$ 0.87	0.67	30,7
<i>cue1-6</i> ENO1	9.86 $\pm$ 1.07	307 $\pm$ 14	5.65 $\pm$ 0.91	4.21 $\pm$ 0.60	0.73	31,1
<i>cue1-1/enol-2</i> (class III)	1.50 $\pm$ 0.35	22 $\pm$ 1	6.88 $\pm$ 1.79	10.51 $\pm$ 1.70	1.67	38,1
<i>cue1-1/enol-2</i> (class II)	4.83 $\pm$ 0.55	177 $\pm$ 8	2.45 $\pm$ 0.64	3.17 $\pm$ 0.74	0.82	26,4
<i>cue1-1/enol-2</i> (class I)	12.14 $\pm$ 0.38	293 $\pm$ 10	6.59 $\pm$ 1.10	5.21 $\pm$ 1.21	0.86	39,8

The contents of protein and carbohydrates (sucrose, glucose, fructose) were referred to individual seeds of mutant and wild-type plants. The data represent the mean value  $\pm$  SE.

## 4 Discussion

The plastid localized enolase from *A. thaliana* (ENO1; At1g74030) was identified and functionally characterized and the central question, as to how the limitation of PEP availability inside the plastid stroma influences aspects of gametophyte and seed development of *A. thaliana* has been addressed.

### 4.1 Phosphoenolpyruvate enolase (ENO1) in *Arabidopsis thaliana* is plastid localized and functional

Earlier reports have indicated that chloroplasts, unlike most non-green plastids, are deficient in activities of enolase and/or phosphoglyceromutase (Bagge and Larsson, 1986; Borchert et al., 1993; Van der Straeten et al., 1991); hence triose phosphates cannot be converted to PEP in the plastid stroma and therefore these two enzymes may represent a missing link in the chain of glycolytic enzymes within the plastids. In this study, an *in silico* target prediction of At1g74030 indicated that this gene encodes a protein containing an N-terminal transit peptide for plastid targeting with values very much higher compared to its cytosolic forms. The localization of this putative plastidic enolase was confirmed by transient expression of an ENO1-GFP fusion protein, which verified its presence in the plastids of *A. thaliana* cell cultures (Fig. 3.1). Conversely, one of the two putative cytosolic enolases (ENOC; At2g36530) was found both in the cytosol and the nucleus (Fig. 3.2), which corresponds to the subcellular localization of the second putative cytosolic ENO (At2g36530), LOS2 (Lee et al., 2002). It has been proposed that LOS2 is involved both in metabolism and may act as positive regulator of gene transcription. The phenotype of the homozygous *los2* mutant was disturbed and exhibited a severe impairment in growth, pale green shoot development and its incapability to develop into flowers and accordingly siliques and seeds (Lee et al., 2002), underlining the importance of glycolytic PEP provision in the cytosol of plants. The localization of ENO1 in plastids lead to the first functional characterization of the protein. The activity of *rENO1* was confirmed using an enriched *rENO1* enzyme preparation obtained from the heterologous expression of the *rENO1* protein fused to a C-terminal His-tag in *E.coli*. Generally, the specific activity of ENO1 is different in diverse organisms (<http://www.brenda-enzymes.info/>) ranging from 1.1 U·mg<sup>-1</sup> protein in *Saccharomyces cereviceae* to 1118 U·mg<sup>-1</sup> protein in *Streptococcus rattus*. Specific activity of ENO1 in very few plants have been determined and are in the range of 197.4 to 252.4 U·mg<sup>-1</sup> protein in *Ricinus communis* and 22 U·mg<sup>-1</sup> protein in *Hevea brasiliensis* belonging to *Euphorbiaceae*, and 10.3 U·mg<sup>-1</sup> protein in *Zea mays* belonging to the family *Poaceae*. Specific activity of

ENO1 in *Brassicaceae* has not been reported so far, in this study, the specific activity of ENO1 in the direction of PEP formation of 0.5-0.6 U·mg<sup>-1</sup> protein was rather poor compared to the reported values discussed. However, ENO activity after purification with Ni-NTA chromatography was attributed to the plant enzyme specifically in comparison to control experiments with non-induced or wild-type *E. coli*. The pH dependency of the ENO1 reaction velocity displayed an optimum between pH 7.0 and pH 8.0 which adds to the apparent  $K_m$  values for both substrates in the upper micromolar range leading to the fact that ENO1 is possibly functional, both in heterotrophic plastids or in chloroplasts in the dark and light. It has been previously described that plastids of lipid storing seeds such as *Ricinus communis* harbour a complete glycolytic pathway starting from 3-PGA to pyruvate (Miernyk and Dennis 1982;1992;), in oil seed rape (*Brassica napus.L*) evidence for all enzymes required for hexose and hexose phosphate interconversion are present and functional (Kang and Rawsthorne 1994; 1996), in recent reports there are also evidences supporting the breakdown of Glc6P to PEP [Ruuska et al., 2002]), whereas in chloroplasts the absence of ENO1 hampers the conversion of 3-PGA to PEP (Fig. 4.1).

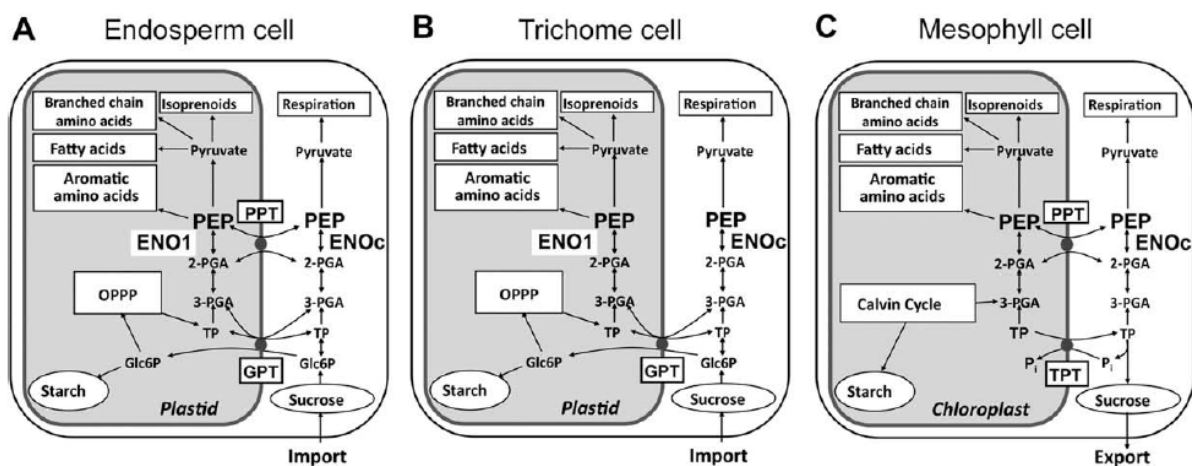


**Figure 4.1: Proposed paths of PEP supply to plastids and its fate in metabolism in different tissues of *A. thaliana*.** In plastids of seed endosperm cells, PEP can either be imported from the cytosol via a PPT or generated by the glycolytic conversion starting from imported Glc6P (A). Trichome cells have to rely entirely on PEP provision by glycolysis (B), whereas chloroplasts from green tissues depend on the provision of PEP by the PPT (C). For the sake of clarity additional ways to generate PEP inside plastids (i.e. by PPDK) have been omitted.

## 4.2 *ENO1* is also expressed in trichomes and non-root hair cells

*In silico* expression analysis based on microarray data (<http://bar.utoronto.ca/efp/cgi-bin/efpWeb.cgi>) has indicated that *ENO1* expression is highest in the young roots and developing siliques apart from vegetative shoot apex. This data is consistent with analysis of

wild-type *A. thaliana* plants expressing different *ENO1* promoter::reporter gene constructs. Apart from this, a number of additional features were revealed at a cellular level, such as expression in trichomes of young leaves (construct C and AB) or in non-root hair cells of the rhizodermis (construct AB) (Fig. 3.11). Particularly, the expression pattern of construct AB, (viz., the fusion of the small intergenic 5'-fragment with the 3'-fragment), coincided with the RT-PCR experiments and expression profiles obtained from microarrays (i.e. <http://bar.utoronto.ca/efp/cgi-bin/efpWeb.cgi>). In the analyses of plant promoters, most emphasis has been on sequences upstream of the transcription start site (Guilfoyle, 1998). However, in recent years, important regulatory sequences downstream of the transcription start site have been detected in an increasing number of plant promoters both in translated and untranslated regions (Sieburth and Meyerowitz, 1997). Stimulation of gene expression by downstream sequences of cell specific expression has already been reported for the *GLABROUS1* gene, a *MYB* gene homolog required for trichome initiation (Larkin et al., 1993) and *PAT1* gene, encoding phosphoribosylanthranilate transferase (Rose and Last 1997), nevertheless, for the transcriptional regulation of *ENO1*, presence of all regulatory *cis*-acting elements in construct AB needs to be studied at length. An analyses of *cis*-acting elements with the help of 'PLACE Web Signal Scan' (<http://www.dna.affrc.go.jp/PLACE/signalscan.html>; [Prestridge, D.S 1991; Higo et al., 1999]) uncovered a large series of regulatory elements all over the gene.

### 4.3 ENO mutants lack a pronounced phenotype in the macroscopic scale

The knockout mutants of *ENO1* (*eno1-1* and *eno1-2*) lack an altered phenotype when compared to wild-type plants on the macroscopic scale. They grew normally on soil as well as on MS medium supplemented with sucrose. This interesting finding led to the suggestion that *ENO1* is redundant for plant development and metabolism, also in those tissues where *ENO1* is highly expressed, such as roots, siliques, shoot apex and trichomes. Consequently, a closer look at roots and trichomes in the microscopic scale revealed a startling observation. Firstly, the trichomes of both *eno1* alleles displayed a distorted phenotype and secondly the root hairs in the *eno1* mutant plants were reduced by 17%. PEP can be supplied from the cytosol *via* both *PPTs*, which are differentially expressed both in green and non-green tissues (Knappe et al., 2003). The transcriptional profiling of mature trichomes revealed the importance of *ENO1* for PEP formation in plastids (Jakoby et al 2008). The expression of *PPT1*, *PPT2* or *PPDK* in trichomes could not be detected, but the expression of *ENO1* was strongly upregulated 3.8-fold compared to the residual epidermis cells (Jakoby et al., 2008). *PPT2* is expressed throughout the leaf blade, but is absent in the roots, whereas *PPT1* is highly

expressed in the vasculature of roots and leaves as well as in the root tip and lateral root formation zones (Knappé et al., 2003). Both *PPT* genes are expressed at distinct stages during seed development (<http://bar.utoronto.ca/efp/cgi-bin/efpWeb.cgi>). The observation of *ENO1* and *PPT1* co-expression during the early stage of embryo development, suggests that PEP supply is pooled by glycolytic conversion (e.g. from imported Glc6P [Kammerer et al., 1998]) and by import from the cytosol via a PPT (Fig. 4.1A). In non-green tissues such as root cells, a shared function of PEP import and synthesis within the plastids is also likely. The reduction in roots hairs in the *eno1* mutant plants indicates that a complete plastid glycolysis pathway partially determines root hair formation. In the past, trichome development has been closely associated with root hair cell development; The *FRA2 (FRAGILE FIBER2)/ERH3 (ECTOPIC ROOT HAIR3)* gene appears to be involved in the regulation microtubule assembly and disassembly (Burk et al., 2001; Webb et al., 2002). It encodes a katanin p60-like protein, displays mutants exhibiting pleiotropic phenotypes, including altered morphology of root and leaf trichome cells (Burk et al., 2001, Webb et al., 2002). Similarly, the expression pattern of *ENO1* in trichomes as well as in non-root hair cells (Fig. 3.11) is comparable to those of transcriptional regulators involved in trichome and root hair cell patterning (Schellmann et al., 2002; Kirik et al., 2004). Plastid glycolysis and developmental programs have no obvious links involved in cell patterning, but the distorted trichome phenotype observed in both alleles of the *eno1* mutants resembles in various aspects a group of mutants exhibiting aberrant trichome shapes based mainly on defective cytoskeleton formation (Hülkamp et al., 1994; Mathur et al., 1999; Schwab et al., 2003). The link between the distorted trichome phenotype in both *eno1* alleles and cytoskeleton development need to be elucidated since a direct relationship between the two is absent. It is likely that the glycolytic conversion of cytosolic Glc6P in trichomes might be the only way to produce PEP in the plastid stroma. This PEP can be used as a precursor for the shikimate pathway or, after conversion to pyruvate *via* PK, for fatty acid biosynthesis, the synthesis of branched-chain amino acids or the synthesis of isoprenoids via the MEP pathway.

#### **4.4 Importance of PEP in plants and the significance of ENO1 in plastidic PEP formation**

The import of PEP inside the plastid appears to be indispensable, as chloroplasts, and most non-green plastids have been reported to be incapable of producing PEP from 3-phosphoglycerate (3-PGA) via glycolysis. This is because of a deficiency in phosphoglycerate mutase and/or enolase (Bagge and Larsson, 1986; Journet and Douce, 1985; Stitt and ap Rees, 1979). In plastids, PEP can also act as a precursor for fatty acid biosynthesis (Kleinig and

Liedvogel, 1980; Qui et al., 1994) after conversion to pyruvate, which is quantitatively important in developing oil producing seeds (e.g. Voelker and Kinney, 2001; Rawsthorne, 2002; Ruuska et al., 2002) or for the biosynthesis of branched-chain amino acids (Schulze-Siebert *et al.*, 1984) and isoprenoids via the MEP pathway (Lichtenthaler *et al.*, 1997). The pre-chorismate part of the shikimate pathway is confined to the plastids (Herrmann, 1995; Schmid and Amrhein, 1995) and starts with the condensation of PEP with erythrose 4-P (Ery4P) catalysed by 3-deoxy-D-arabino-heptulosonate-7-phosphate synthase (DAHPS). Ery4P generated by the action of transketolase is an intermediate of both the Calvin cycle and the oxidative pentose phosphate pathway (OPPP).

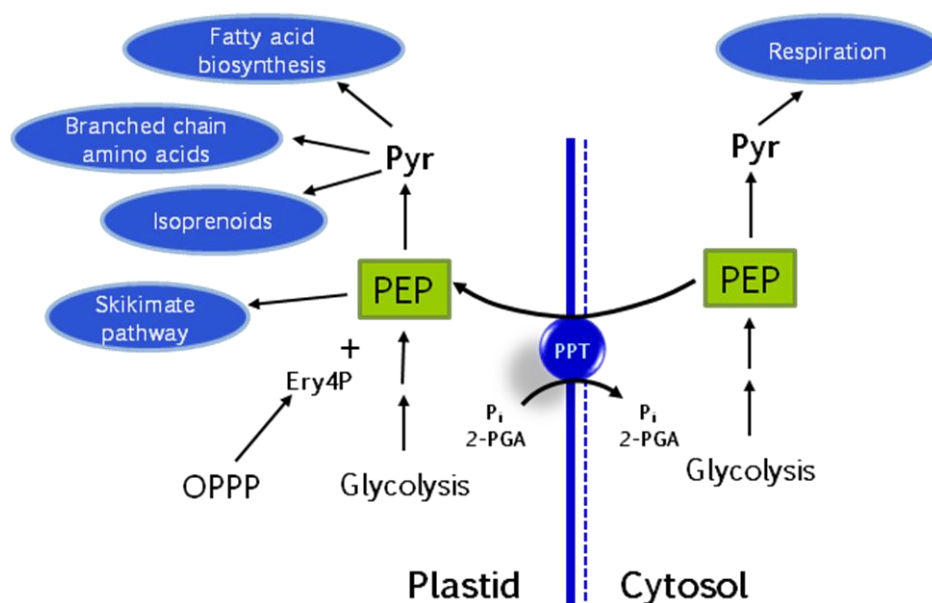


**Figure 4.2: Importance of PEP in plant glycolysis.** Pyr=Pyruvate PEP=Phosphoenolpyruvate Ery4P=Erythrose 4 phosphate 2-PGA=2 Phosphoglycerate OPPP=Oxidative pentose phosphate pathway

PEP is also required further downstream of the shikimate pathway for the conversion of 3-phosphoshikimate to 3-phospho-5-enolpyruvylshikimate (EPSP) catalysed by EPSP synthase (EPSPS). The primary product of the shikimate pathway, chorismate, is further metabolized to the aromatic amino acids Phe, Tyr and Trp, as well as folate precursors (Hanson and Gregory, 2002). In dicots, Phe is the starting point for the biosynthesis of a variety of secondary products like phenylpropanoids, e.g. hydroxycinnamic acid (HCA) derivatives and flavonoids, while prenylquinones like tocopherol, plastoquinone or vitamin K are synthesized from Tyr (Hofius et al., 2004) (Fig. 1.5). In various heterotrophic tissues like the roots or seeds, the plastid localized enolase (ENO1) can directly deliver PEP *via* glycolysis (Fig. 4.1), this is applicable to trichomes as well. In addition, PEP can also be produced from pyruvate by the activity of PPK (Chastain et al., 2002; Hibberd and Quick, 2002; Parsley and Hibberd,

2006). Apart from the glycolysis in the plastids, PEP can also be imported from the cytosol by the action of a PPT. *Arabidopsis* possesses two functional PPT genes, *PPT1* and *PPT2*. *PPT1* from cauliflower buds have shown to transport PEP in counter-exchange with inorganic phosphates (Fischer et al., 1997). The *PPT1* and *PPT2* show similar substrate specificities, but both *PPTs* show a differential and partially overlapping tissue specific expression pattern indicating that they are differentially expressed in *Arabidopsis*. Thus, the provision of PEP inside the stroma for various metabolic pathways is equally shared between the PPT and a complete glycolytic pathway (for e.g., in seeds). The transcriptional profiling of mature trichomes revealed the importance of *ENO1* for PEP formation in plastids (Jakoby et al 2008). The expression of *PPT1*, *PPT2* or *PPDK* in trichomes could not be detected, but the expression of *ENO1* was strongly upregulated 3.8-fold compared to the residual epidermis cells (Jakoby et al., 2008). This data is in agreement with the results of promoter::GUS studies of *ENO1* in trichomes, where GUS expression was strongly observed in constructs AB and C and furthermore in the RT-PCR experiments. Unlike heterotrophic plastids which produce triose phosphates via the oxidative pentose phosphate pathway, chloroplasts produce 3-PGA via Calvin cycle during CO<sub>2</sub> fixation by ribulose-1, 5-bisphosphate carboxylase/oxygenase. In the presence of a plastidic PGyM the conversion of 3-PGA to PEP rather than the reduction to TP during ongoing photosynthesis might hence be counter-productive for the export of photoassimilates from the chloroplasts or for the formation of transitory starch within the stroma (Fig. 4.1C). It can be hypothesized that a fine tuning of leaf primary and secondary metabolism (i.e. PEP provision for the shikimate pathway) could be achieved at the level of chloroplast 3-PGA, 2-PGA and Pi concentrations in combination with cytosolic ENO activity. The level of 3-PGA in the stroma could for instance determine the availability of 2-PGA via PGyM as a counter exchange substrate for the PPT, which in turn imports PEP generated from 2-PGA by cytosolic ENO (Fig. 4.3)

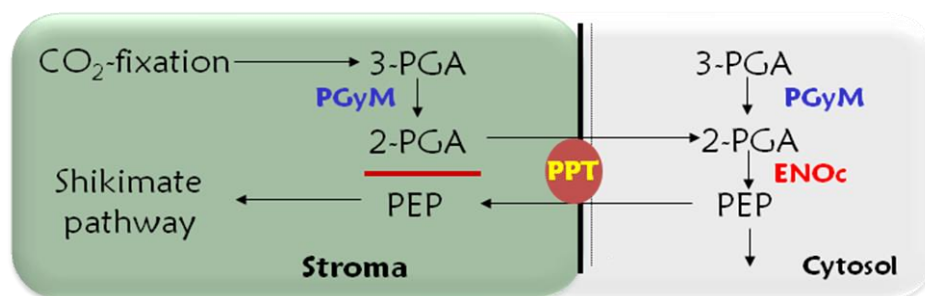


**Figure 4.3: Schematic representation of an alternate way of PEP provision inside the plastids in the absence of plastidic enolase.** 3-PGA=3-phosphoglycerate 2-PGA=2-phosphoglycerate PEP=phosphoenolpyruvate PGyM=phosphoglyceromutase ENOc=cytosolic enolase

The production of aromatic amino acids via the shikimate pathway might therefore be indirectly linked to 3-PGA in the chloroplasts. This theory could be tested by subcellular metabolite determinations in mutant or transgenic plants, which express ENO1 in chloroplasts.

As mentioned before, *ENO1* and *PPT1* are co-expressed during early embryo development (Fig. 1.3 and 1.4), hence it can be speculated that a double knockout of both functions (i.e. *ENO1* and the *PPT*) might impair the physiology and development of heterotrophic cells and tissues and probably the whole plant. This question was addressed in the next stage by generating double knockouts of *ppt1/enol*. One mutant allele of *cue1*, the *cue1-1* mutant was crossed with the first mutant allele of *enol*, *enol-1* (Löttgert, PhD thesis). This cross resulted in the absence of a homozygous double mutant which was consistent with the idea that a limitation of PEP availability inside the plastid stroma influences aspects of gametophyte and seed development of *A. thaliana* plants. To rule out the possibility that the absence of a homozygous double mutant of *cue1/enol* could also be perhaps due to secondary insertions or mutations in the single mutant background, other crosses of *cue1* alleles with second *enol* allele was carried out which led to an identical pattern confirming that the combined deficiency in ENO1 and PPT caused the lethal phenotype.

#### 4.5 ENO1 and PPT1 deficiency in plastids leads to partial lethality and aberrant segregation

A mutual constraint of PEP import by PPT1 and plastid glycolysis using ENO1 leads to lethality and unusual segregation pattern. No double homozygous lines could be obtained in the progenies of the crosses between the *cue1* and *enol* mutant alleles. Furthermore, heterozygous mutants *cue1/enol(+/-)* displayed aberrant female and male gametophyte development and surprisingly also constraints in vegetative development. The lethality of the *cue1/enol* mutants is also independent from the ecotypes (i.e. Col-0 or Bensheim) or secondary mutations as evident in *cue1-1*. The *Ccee* (heterozygous *cue1* mutants in the homozygous *enol* background) mutants were not severely compromised during vegetative development but the percentage of (*Ccee* plants) was less than half the expected number in the *cue1-1/enol-2*, *cue1-6/enol-2* crosses and the *enol-2/cue1-1* reciprocal cross. Likewise, the percentage of homozygous *cue1* mutants in the heterozygous *enol* background (*ccEe* plants) were far below expectation from the Mendelian segregation. From the results of the segregation analysis, a question arises as to why a high proportion of gametophytes survive regardless of the fact that *PPT1* and *ENO1* mutations are in haploid state. There are other

known genes such as *PPT2* and/or *PPDK* which could partially compensate the lack in *ENO1* and *PPT1*. In order to understand compensational effects, a comparison of the expression of different genes involved in PEP metabolism in plastids was carried out using publicly available microarray database (<http://bar.utoronto.ca/efp/cgi-bin/efpWeb.cgi>) (Table Appendix Table 1). The expression values of *ENO1* (At1g74030), *PPT1* (At5g33320), *PPT2* (At3g01550), *PPDK* (At4g15530), one of three putative plastid localized *PGyM* genes (At1g22170), three genes encoding  $\beta$  or  $\alpha$  subunits of the plastid localized PK (i.e. *PKp1* [At3g22960], *PKp2* [At1g32440] and *PKp3* [At1g32440]; Baud et al., 2007; Lonien and Schwender, 2009), a plastid-localized malic enzyme (*ME4* [At1g79750], Wheeler et al., 2005) and a recently identified  $\text{Na}^+$ -dependent pyruvate transporter (*PyT* [At2g26900]; Furumoto et al., 2009). *ENO1* expression is absent in the green tissues e.g. in leaf mesophyll (Appendix Table 2) quite similar to *PPT2*, *PGyM* expression, except for the vegetative shoot apex. In contrast, *PPT1* is highly expressed in all green tissues which are quite similar to *PKp1*, *PKp2*, *ME4* and *PyT*, whereas the *ENO1* and *PPT1* are highly expressed in roots compared to the other genes.

#### 4.6 Limitation of PEP inside plastids leads to gametophyte lethality

The expression of plastid genes involved in PEP production, especially during early flower development (Stage 9-10), shows that *ENO1* and *PPT1* transcripts are highly abundant, whereas *PPT2* is only weakly expressed or absent (i.e. in stamen of 'flower stage 12' and '15'). The expression level of *PPDK* exhibits some fluctuations during flower development, in particular with respect to stamen and carpel specific expression. Whereas *PPDK* transcripts are highly abundant in stamen of 'flower stage 12' and '15', they are almost absent in carpels of the same stage. In general, *PPDK* expression is absent in 'flower stage 9' and shows the highest levels at 'flower stage 15'. Interestingly, *PKp1* and *PKp2* as well as *PyT* are also expressed during flower development, in particular in the reproductive organs such as stamen and carpels. Moreover, the above genes exhibit a similar overall expression pattern during embryo development with the exception of *PPDK*, which is only faintly expressed (Appendix Table 1). On the basis of the above data, it appears unlikely that metabolic pathways commencing from stromal pyruvate are severely impaired in the absence of *PPT1* and *ENO1*, provided that the expressed *PyT* protein is capable of importing pyruvate efficiently into plastids from generative tissues. Moreover, pyruvate can also be supplied by oxidative decarboxylation of malate catalyzed by plastid-localized *ME4* (Wheeler et al., 2005). The transcripts of *ME4* are highly abundant both in generative and vegetative tissues (Appendix

Table 1 and 2). With the analysis of amino acid contents in flowers, it was obvious that there is a reduction in the aromatic amino acids Trp and Tyr whereas Phe was unaffected, which was consistent with the amount of flavonoids present in the flowers almost equivalent to wild type, a decrease of flavonoids were observed only in *cue1-6/eno1(+/-)* mutants compared to the single mutant *cue1-6* but not in the *cue1-1*. It is hence more likely that developmental constraints during flower development are based on a restriction of the shikimate pathway and downstream products rather than on a limitation of plastidic pyruvate availability. Similarly a restriction in the fatty acid provision cannot explain the partial abortion of the male gametophytes in the *ccEe* plants. A high percentage of pollen non-viability was observed in the *ccEe* mutants which lead to a closer analysis of the viable pollen by electron microscopy. The ultrastructural analysis of pollen revealed the the *ccEe* plants contained equal amounts of lipid bodies and vacuoles compared to wild-type pollen implying that fatty acid biosynthesis is not likely the limitation during male gametophyte development. Hence it can be debated that the partial abortion of pollen in the *ccEe* plants is due to a restriction in the shikimate pathway of the diploid cells in the tapetum. As observed in the ultrastructural analysis, the aberrant exine structure of the *ccEe* plants compared to the wild type may be due to the limitation in sporopollinin formation. Sporopollinin is a component of the pollen exine which is formed by the diploid cells of the pollen sac secretory tapetum (Ariizumi et al., 2004). It is an extremely rigid substance containing both long chain fatty acids and phenolic compounds which are derived from the phenyl propanoid metabolism (Wiermann et al., 2004). The heterozygous knockout of *ENO1* in the *cue1* background might affect the production of sporopollinin from the diploid tapetum cells because of the reduced supply of PEP in the plastids for the shikimate pathway. This can be substantiated further by the reduced dosage of *ENO1* in the absence of *PPT1* in the tapetum cells rather than the absence of both the proteins in the haploid microspores. Additionally, the *ccEe* pollen have reduced flavonoid content indicated by its autofluorescence enhanced by DPBA. Flavonoids are products of phenylpropanoid metabolism which then links the phenotype of the pollen in *ccEe* to a restriction in the shikimate pathway. The stromal PEP related gene expression during pollen and seed development offers picture similar to the flower development (Appendix Table 1). *PPT1* shows an intermediate to high transcript abundance during pollen development whereas *PPT2* is only weakly expressed. *ENO1* shows high transcript abundance in unicellular and bicellular pollen, but not in tricellular or mature pollen grains. In contrast, the expression of *PPDK* is almost absent in uni- and bicellular pollen, but increases to extremely high levels in tricellular and mature pollen grains. It is striking that *PyT* shows an inverse relation to the

stages of pollen development as compared to *PPDK* suggesting that both genes are not functionally coupled. Coexpression of both genes would be expected, if stromal PPDK entirely relies on imported pyruvate. However, PPDK has been shown to be dually targeted to the cytosol and the plastids (Parsley and Hibberd, 2006). Hence, transcript abundance of *PPDK* does not necessarily correlate with the localization of the PPDK protein.

#### 4.7 Absence of PEP/Pyruvate inside plastids leads to seed abortion

PEP import into plastids via the PPT is accomplished by the cytosolic glycolysis and/or gluconeogenesis, however, its formation inside the plastid initiates from the imported Glc6P or 3-PGA and the consequent conversion to PEP by plastid glycolysis which involves ENO1 and PGyM (Fig. 1.2). As reported earlier, Glc6P can enter the plastid via one of the two glucose6-P/phosphate translocators of *A. thaliana* (GPT1; Kammerer et al., 1998). The proposed physiological function of the GPT is the import of Glc6P into plastids of heterotrophic tissues for use as a precursor for starch (and fatty acid) biosynthesis and/or as a substrate for the OPPP. A GPT1 mutant of *A. thaliana* could not be established as homozygous line (Niewiedomski et al., 2005), and the heterozygous *gpt1* mutant was defective in both male and female gametophytes displaying high rates of abortion. A reduced formation of lipid bodies, small vesicles and the disappearance of dispersed vacuoles was observed in pollen. Glc6P is required for oxidative pentose phosphate pathway (OPPP, Kruger and von Schaewen, 2003; Lonien and Schwender, 2009), by which reducing equivalents in form of NADPH are supplied to anabolic reaction sequences, such as fatty acid biosynthesis. It was proposed that NADPH supply by the OPPP is necessary for early gametophyte development apparent in the *gpt1* mutants which had a deficiency in membrane formation and eventually abortion (Niewiedomski et al 2005). With regard to the *ccEe* plants a partial gametophyte abortion was observed and this relates to a restriction in the PEP supply to the plastids. It is tempting to speculate that at least in the female gametophytes and in developing seeds, PEP after conversion to pyruvate is the main substrate for fatty acid biosynthesis and is the primary reason for female gametophyte and seed abortion. There are other mutants of *A. thaliana* which support this notion. PK mutants are severely compromised in oil production suggesting that pyruvate, as a precursor for fatty acid biosynthesis is formed from PEP inside the plastids rather than import from the cytosol. The *WR11* gene encodes an APETALA2/ethylene-responsive element-binding protein transcription factor involved in the control of metabolism, particularly glycolysis, in the developing seeds (Focks and Benning, 1998; Ruuska et al. 2002). Both *pkp1/pkp2* double mutants and *wri1* exhibit a severe decrease

in seed oil contents. For Col-0 wild-type plants approximately 89% of plastidic pyruvate used for fatty acid biosynthesis was derived from PKp, the residual 11% might be shared by pyruvate import and oxidative decarboxylation by plastidic ME4 (Lonien and Schwender 2009). *ENO1* and *PPT1* are co-expressed in many silique and seed developmental stages (Stages 3-8). In contrast to *PPT1*, *ENO1* expression is reduced at seed stages 3 to 8. *PPT2* is highly expressed only in the early stage of seed development (stage 3) and interestingly the various subunits of the plastid localized PK are expressed during early seed development. Taking these expression data into account, it could be speculated that the PEP/pyruvate availability in the plastids is shared by the import from the cytosol and via glycolysis within the plastid.

#### 4.8 *ccEe* plants display constraints in vegetative development

The *ccEe* (homozygous *cue1* mutants in the heterozygous *eno1* plants) mutants were stunted in size and growth when compared to the single mutants or wild type. However, the growth retardation of these plants was not evident until grown on soil for 4 weeks when compared to the single mutants, where as younger plantlets were not affected in shoot and root growth. The leaves of the rosette were reticulate like *cue1*, but, smaller, thicker and showed distorted trichomes. A mutant defective in Trp biosynthesis shows a *cue1* leaf phenotype, however, Trp contents in the *cue1* single mutants were not significantly diminished, but reduced in the *ccEe* mutants. Since Trp serves as a precursor for auxin biosynthesis (Bartel, 1997), the stunted growth of *ccEe* plants could be linked to the auxin availability (Vanneste and Friml, 2009; Pagnussat et al., 2009). Additionally, the development of inflorescence was reduced along with the production of flowers. Flowers that eventually developed were malformed and either sterile or partially fertile leading to improper fertilization and reduction in silique size. In contrast to the reduction of Tyr and Trp contents in *ccEe* flowers, the contents of the anthocyanins and flavonoids were not decreased and were comparable to the wild type. *ENO1* and *PPT1* exhibit low and high transcript abundance in the whole stem, particularly at the bottom, close to the rosette, but there is also a weak expression of *PPT2* and *PPDK* in individual stem tissues. Differences in lignification of sclerenchyma cells and xylem elements observed in the *ccEe* stems points out to a restriction of PEP provision to plastids by *PPT1* and *ENO1* as shikimate pathway leads to the production of phenylpropanoids, which act as scaffold compounds for eg., lignin or suberin (Holloway, 1983; Lewis and Yakamoto, 1990). Moreover, xylem elements appeared to be the only significantly lignified cells in these plants. *PPT1* and *PPDK* are significantly expressed in the xylem (Knappe et al., 2003) suggesting

that the lignifications of xylem elements in the *ccEe* plants might derive from the PEP delivered by the activity of plastid localized *PPDK*. However, it cannot be excluded that precursors for lignin biosynthesis are transported via the transpiration stream. The root length of *ccEe* mutants was similar to *cue1* mutants when grown on media supplemented with sucrose, but highly reduced when compared to *eno1* single mutants or wild type. Apart from amino acids which are selectively diminished in flowers of *ccEe* or *cue1* plants (Tables 3.28, 3.29), the contents of Lys and Arg were significantly increased in *cue1*, but decreased to wild-type levels in the *ccEe* plants. An increased Arg content in *cue1* has previously been reported by Streatfield et al. (1999) and He et al. (2004). For the latter report, a new *cue1* mutant allele (*nos1*) was isolated in a screen for nitric oxide (NO) overproducers. Arg has been proposed to act as a precursor for the synthesis of NO in plants (Guo et al., 2003), which exerts multiple effects on growth and development (del Rio et al., 2003).

RT-PCR analysis of the *ccEe* mutants revealed that the expression of *ENO1* was decreased in the tissues where it was highly expressed (for eg., roots and shoot apex) in the *ccEe* plants, thus deformity in the vegetative development of these plants could be partially attributed to the diminished function of ENO1 protein in the background of PPT1 deficiency. Thus it is tempting to speculate that adequate PEP supply in the plastids is essential for appropriate vegetative development. It is interesting to note that there is no growth retardation in the *eno1* single mutants which resemble the wild type (Fig. 3.14) and lower growth retardation in the *cue1* mutants depending on their individual backgrounds. This observation could be due to the fact that ENO1 and PPT1 substitute each other during vegetative plant development. These vegetative growth constraints are reflected in male and female transmission efficiencies (Table 3.5). The male and female TE for the *cue1-1* mutation were quite similar, conversely the TE for the female in the *eno1-2* mutant was decreased by 15% compared to the male TE. This data suggests that the reduction in the female TE in the for the *eno1-2* mutation is a sporophytic effect rather than a gametophytic restriction. The TE was calculated from the genotype distribution in the offsprings of inverse crosses between the *cue1-1*(male) x *eno1-2* (female) and *eno1-1*(male) x *cue1-1*(female).

Summarizing all these factors together, the resulting data indicates that constraints during development and reproduction of *ccEe* are based on both a restriction in fatty acid biosynthesis and the shikimate pathway. Limitations in the MEP pathway or branched-chain amino acid biosynthesis due to a decline in pyruvate provision inside the plastids could also contribute to the phenotype of *ccEe* plants, however the individual contribution of the above pathways to the characteristic phenotype of *ccEe* needs to be elucidated. To distinguish

importance of one pathway from another for the synthesis of fatty acids, isoprenoids, branched chain amino acids or secondary compounds is the constitutive over-expression of a functional pyruvate transporter in the background of the segregating *ccEe* plants. The over expression of pyruvate transporter might lead to enhanced import of pyruvate from the cytosol, which could then compensate for the loss of stromal PEP in these mutants and rescue the plants. Similarly, the developmental constraints of *ccEe* due to the lack of secondary compounds ought to be rescued by a constitutive over-expression of a C<sub>4</sub> type PPDK targeted to the plastids as previously described by Voll et al. (2003).

#### 4.9 Link between cuticle wax biosynthesis and phenotype of *ccEe* plants

Cuticular waxes are complex mixtures of lipids and composed mainly of long chain aliphatic hydrocarbons derived from saturated very long-chain fatty acids (VLCFAs; chain length is >18 carbons). VLCFAs, the precursors for wax biosynthesis, are formed by a microsomal fatty acid elongation (FAE) system involving sequential additions of C<sub>2</sub> moieties from malonyl-coenzyme A (CoA) to pre-existing C<sub>16</sub> or C<sub>18</sub> fatty acids derived from the de novo fatty acid synthesis (FAS) pathway of the plastid (Millar et al., 1999). *A. thaliana* contains two orthologs of  $\beta$ -ketoacyl-coenzyme A reductases (*KCR1*; At1g67730 and *KCR2*; At1g24470). The mutants of *KCR1* and *KCR2* are defective in fatty acid elongation (Beaudoin et al., 2009) and phenotypically resemble the *ccEe* mutants. Homozygous mutants of *KCR1* could not be established because they were embryo lethal. Siliques of the heterozygous *kr1* mutants showed high rate of abortion and had the presence of brown, shrunken and deformed seeds whereas the *KCR2* mutants did not display any aberrant phenotype. RNAi plants of *KCR1* during vegetative development revealed stunted growth of shoots, deformed flowers, short and deformed siliques and a trichome phenotype comparable to *eno1* mutants (Fig. 3.16). The leaves of *KCR1* RNAi mutants upon Toluidine Blue (TB) staining revealed a disturbed cuticle (Beaudoin et al., 2009) which is comparable to the leakiness observed in the *ccEe* plants. By RT-PCR analysis of the *KCR1* gene in *ccEe* plants, it was observed that *KCR1* was pleiotropically down-regulated. The decrease in cuticular wax content in the *ccEe* mutants could be linked to a restriction in fatty acid biosynthesis in early leaf development based on limited PEP supply to the plastids which could then result in the relocation of fatty acids for the synthesis of cellular membranes rather than production of cuticle wax. It is likely that such a relocation is achieved if *KCR1* is down-regulated. Additionally, besides aliphatic and long chain fatty acids (Jetter et al., 2006; Samuels et al., 2008;), phenylpropanoids and anthocyanins are also constituents of the cuticle wax layers in tomato fruits (Mintz-Oron et al., 2008). Hence a lack in the production of these compounds might also lead to a

functionally impaired cuticle in the *ccEe* plants. Thus, adequate supply of PEP is required for proper development of plants, however, at this point it is not very clear which pathway is responsible for this constraint. It is debatable whether the restriction in the shikimate pathway or the plastidic pyruvate pathway leading to fatty acid biosynthesis, the MEP pathway or the synthesis of branched-chain amino acids is the cause for this developmental constraint.

#### 4.10 Constitutive overexpression of *ENO1* rescues the *cue1* phenotype

It has been demonstrated that both the *PPTs* of *A. thaliana* (*PPT1* and *PPT2*; Knappe et al., 2003) are capable of a 2-PGA/PEP counter exchange, thus the PEP import rather than its generation by a complete glycolytic pathway seems to be the main route for the provision of PEP to chloroplasts and most green plastids (Fischer et al., 1997). The two *PPTs* are expressed differently in *Arabidopsis*. *PPT1* is expressed in tissues of root such as the quiescent center of root tip, central cylinder and lateral root formation zones. *PPT1* expression is also found in the vascular bundle, particularly in the xylem parenchyma cells (Knappe et al., 2003), and this lead to the hypothesis that certain metabolic signals deriving from the phenylpropanoid pathway are generated in these cell types and may control correct mesophyll development. In contrast to the *PPT1* expression, *PPT2* is expressed throughout the leaf blade (Knappe et al., 2003) and also in very early stage of silique and seed development (*Arabidopsis* eFP browser). The lack in *PPT2* function has not been studied in plant development so far because of the absence of *PPT2* knockout mutants. The occurrence of a reticulate leaf phenotype in *cue1* mutants is unresolved as yet, considering the expression pattern of *PPT1*. Previous report of *cue1* phenotype complementation by a constitutive overexpression of a  $C_4$ -type *PPDK* of *Flaveria trinervia* targeted to plastids has shown that a limitation of PEP provision in the stroma via *PPT1* can be compensated by PEP generation from pyruvate inside the plastids (Voll et al., 2003). Since *ENO1* is not expressed in mature leaves, PEP provision by plastid localized glycolysis can be excluded, although the constitutive overexpression of *ENO1* could rescue the shoot and root phenotype of *cue1* mutants. Therefore *ENO1* appears to be the only missing enzyme in plastidic glycolysis, at least where *PPT1* is expressed. A sufficient flux through glycolysis exists to compensate the restriction of PEP import into the stroma by *PPT1*. It is probable that the conversion of 3-PGA to 2-PGA in heterotrophic tissues lacking *ENO1*, catalyzed by PGyM ceases. There are no PGyM mutants available so far to test the consequence of its absence. In *A. thaliana*, there are fifteen PGyM genes, out of which four encode a protein with predicted N-terminal transit

peptide for plastid targeting (At1g22170, At5g62840, At5g22620, and At1g78050). At1g22170 and At1g78050 are not expressed in photosynthetically active tissues, whereas the transcripts of At5g62840 and At5g22620 are highly abundant in leaves suggesting that 2-PGA can be formed also in chloroplasts. It is plausible that PPT could control the flow of substrates for secondary metabolism (i.e. shikimate pathway) by sensing the metabolic status within the mesophyll. 2-PGA/PEP counter-exchange by PPT would increase or decrease depending on the concentration of metabolites 2-PGA and 3-PGA within the plastid, which would then lead to the production of amino acids and other secondary metabolites. Overexpression of ENO1 in wild-type plants did not enhance any sporophytic or gametophytic effects. There was no obvious change in the photosynthetic capacity of these overexpressing lines in comparison to the wild type, conversely, the *ENO1* expression in *cue1* plants enhanced its ETR. A comprehensive analysis is required to understand whether a complete glycolytic pathway inside the plastids controls primary and secondary metabolism in plants. A limitation in the cytosolic PEP production results in a reticulate leaf phenotype quite similar to *cue1* which leads to the fact that cytosolic PEP supply in wild-type plants is sufficient (Voll et al., 2009). In *A. thaliana*, two cytosolic ENO have been reported, At2g36530 and At2g29560. A mutant of At2g36530 (ENOc), *los2*, shows bleached leaves and retarded growth like *cue1*. ENOc/LOS2 may be involved in transcriptional regulation besides its catalytic function in cytosolic glycolysis. In this study, the question as to whether an *ENO1* overexpression could complement the *los2* phenotype was addressed. It is conceived that a halt in the cytosolic glycolysis at the step of 3-PGA to 2-PGA conversion leads to the transport of 2-PGA to plastid via the PPT, subsequent conversion to PEP catalyzed by ENO1 and export to the cytosol via the PPT again for other metabolic pathways to take over. The *los2* phenotype could not be rescued by the overexpression of ENO1 indicating that a complete glycolysis in chloroplast is independent and cannot compensate for the loss of ENOc. The cause for the *los2* phenotype needs to be studied in more detail as *A. thaliana* has a second cytosolic ENO which could compensate for the loss of ENOc.

#### **4.11 Controlling seed production and oil content in *A.thaliana*: A biotechnological approach**

*A. thaliana* is an attractive system for studying oil production in seeds, a well studied plant model, it is also a close relative of *Brassica napus*, a major oilseed crop, Like *B. napus*, *A. thaliana* stores oil in its cotyledons as the major seed carbon reserve. It has similar seed phylogeny and development and on average, genes of these species share ca. 85% nucleotide

identity in their coding region (Cavell et al., 1998). Together, these factors facilitate the application of information obtained from Arabidopsis research to crops of the *Brassicaceae* family. In today's world, oil crops are not only essential as food supply, but also has its importance beyond nutrition. Vegetable oil, for instance is one of the most important lipid source for the production of lubricants, inks, paints and biodiesels (Carlsson 2009) The accumulation of storage reserve is a major differentiation event that takes place during *A.thaliana* seed development. The entire embryogenesis and maturation process of *A.thaliana* takes approximately 18–21 days (Wang et al., 2007). The fertilized zygote completes the major cell division and morphogenesis events within 4–5 days to form a torpedo stage embryo containing cotyledons and embryo axis. From this point until the seed mature, large amounts of storage products are accumulated in the cotyledon cells to occupy most of the space (Mansfield and Briarty 1992; Lin et al. 1999). The rate of net oil synthesis reaches a maximal level at 9–13 DAF whereas the rate of protein accumulation is relatively steady until almost the end of seed development (Mansfield and Briarty 1992; Goldberg et al. 1994; Focks and Benning 1998). In *A.thaliana* a limitation in the PK activity leads to a deficiency in seed storage oil accumulation, as seen in the *A. thaliana* mutant (*pkp1*) deficient in plastidic pyruvate kinase (PK<sub>p</sub>) (Andre and Benning 2007; Baud et al., 2007). Similarly, a constraint in the supply of PEP inside the plastids, leads to a severely compromised seed development. Firstly, the size of the seeds are highly reduced and can be categorized into three classes depending on its size and structure and secondly the class II and class III seeds of the *ccEe* mutants contained ca. 50% to 80% less lipids per seed (Table 3.11). As a matter of fact, protein and carbohydrate contents also followed the same tendency. Even though *ENO1* is highly expressed in developing siliques, overexpression of *ENO1* in the wild type background resulted in a slight increase in silique number, but unfortunately did not result in an increase in seed production or quality. The overexpression of *ENO1* in the *cue1* background could partially compensate the restriction in lipid production, indicating that only under conditions of limiting PEP import into the plastids during seed maturation, an improved glycolytic flux is capable of improving oil production in seeds. Previously, it was shown that an overexpression of heterologous PPT from cauliflower buds increased seed production in *cue1* plants (Voll et al., 2003), but the composition of the seeds are unknown to assess its quality. It is very unlikely that an overexpression of one gene could lead to an improvement in oil production in *A.thaliana*, as a very complex network of pathways seem to play a combined role. Further studies will unravel rate limiting steps in storage compound biosynthesis. A combined

increase in transport activities of GPT, PPT or PyT along with overexpression of ENO1 could perhaps lead to an enhancement in seed oil production.

## 5 References

- Adam, K. P., Thiel, R. and Zapp, J.** (1999) *Arch. Biochem. Biophys.* 369, 127–132.
- Alexander, M.P.** (1969). Differential staining of aborted and nonaborted pollen. *Stain Technol.* 44: 117-122.
- Andre, C., Froehlich, J.E., Moll, M.R., and Benning, C.A.** (2007), heteromeric plastidic pyruvate kinase complex involved in seed oil biosynthesis in *Arabidopsis*. *Plant Cell* 19: 2006-2022.
- ap Rees T.** (1990). *Plant Physiology, Biochemistry and Molecular Biology*. Singapore: Longman pp. 106–33.
- Arigoni, D., Sagner, S., Latzel, C., Eisenreich, W., Bacher, A. and Zenk, M. H.** (1997). *Proc. Natl. Acad. Sci. USA* 94, 10600–10605.
- Ariizumi, T., Hatakeyama, K., Hinata, K., Inatsugi, R., Nishida, I., Sato, S., Kato, T., Tabata, S., and Toriyama, K.** (2004). Disruption of the novel plant protein NEF1 affects lipid accumulation in plastids of the tapetum and exine formation of pollen, resulting in male sterility in *Arabidopsis thaliana*. *Plant J.* **39**: 170-181.
- Ausubel, F.M., Brent, R., Kingston, R.E., Moore, D.D., Seidman, J.G., Smith, J.A. and Struhl, K.** (1990) *Current Protocols in Molecular Biology*, Wiley, New York.
- Bagge, P. and Larsson, C.** (1986) Biosynthesis of aromatic-amino-acids by a highly purified spinach-chloroplasts – compartmentation and regulation of the reactions. *Physiol. Plant.* 68, 641–647.
- Bailey-Serres, J. and Dawe, R.K.** (1996) Both 50 and 30 sequences of maize *adh7* mRNA are required for enhanced translation under low-oxygen conditions. *Plant Physiol.* 112, 685–695.
- Bartel, B.** (1997). Auxin biosynthesis. *Annu. Rev. Plant Physiol. Mol. Biol.* 48: 51-66
- Baud S, Wuillème S, Dubreucq B, de Almeida A, Vuagnat C, Lepiniec L, Miquel M, Rochat, C.** (2007). Function of plastidial pyruvate kinases in seeds of *Arabidopsis thaliana*. *Plant J.* Nov;52(3):405-19. Epub 2007 Sep 24
- Baud, S., and Graham, I.A.** (2006). A spatiotemporal analysis of enzymatic activities associated with carbon metabolism in wild-type and mutant embryos of *Arabidopsis* using in situ histochemistry. *Plant J.* 46: 155-169.
- Baud, S., Mendoza, M.S., To, A., Harscoët, E., Lepiniec, L., and Dubreucq, B.** (2007a). WRINKLED1 specifies the regulatory action of LEAFY COTYLEDON2 towards fatty acid metabolism during seed maturation in *Arabidopsis*. *Plant J.* 50:825-838.

- Baud, S., Wuillème, S., Dubreucq, B., de Almeida, A., Vuagnat, C., Lepiniec, L., Miquel, M., and Rochat, C.** (2007b). Function of plastidial pyruvate kinases in seeds of *Arabidopsis thaliana*. *Plant J.* 52: 405-419.
- Beaudoin, F., Wu, X., Li, F., Haslam, R.P., Markham, J.E., Zheng, H., Napier, J.A., and Kunst, L.** (2009). Functional characterization of the *Arabidopsis thaliana*  $\beta$ -ketoacyl-Coenzyme A reductase candidates of the fatty acid elongase. *Plant Physiol.* 150: 1174-1191.
- Bechtold, N., Ellis, J., and Pelletier, G.** (1993). In planta *Agrobacterium* mediated gene transfer by infiltration of adult *Arabidopsis thaliana* plants. *C. R. Acad. Sci. Paris, Sciences de la vie/Life Sciences* 316: 1194-1199.
- Bergmeyer, H.U.** (1970) in: *Methoden der enzymatischen Analyse* (Bergmeyer, H.U., Ed.), Verlag Chemie, Weinheim.
- Blakeley SD, Dennis DT.** (1993). Molecular approaches to the manipulation of carbon allocation in plants. *Can. J. Bot.* 71:765–78.
- Blanvillain, R., Boavida, L.C., McCormick, S., and Ow, D.W.** (2008). Exportin1 genes are essential for development and function of the gametophytes in *Arabidopsis thaliana*. *Genetics* 180: 1493-1500.
- Blum, H., Beier, H. and Gross, H.J.** Improved silver staining of plant proteins, RNA and DNA in polyacrylamide gels. *Electrophoresis* 8: 93-99.
- Boerjan, W., Ralph, J. and Baucher, M.** (2003). **Lignin biosynthesis.** *Annu. Rev. Plant Biol.* 54:519–546
- Bonner, C.A., Jensen, R.A.** (1997) Recognition of specific patterns of amino acid inhibition of growth in higher plants, uncomplicated by glutamine-reversible, general amino acid inhibition. *Plant Science* 130: 133-43
- Borchert, S., Harborth, J., Schünemann, D., Hoferichter, P. and Heldt, H.W.** (1993) Studies of the enzymatic capacities and transport-properties of pea root plastids. *Plant Physiol.* 101, 303–312.
- Bradford, M.M.** (1976) Rapid and sensitive method for quantitation of microgram quantities of protein utilizing principle of protein-dye binding. *Anal. Biochem.* 72, 248–254.
- Browse, J., McCourt, P.J., and Somerville, C.R.** (1986). Fatty acid composition of leaf lipids determined after combined digestion and fatty acid methyl ester formation from fresh tissue. *Anal. Biochem.* 152: 141-145.
- Buer, C.S., Muday, G.K., and Djordjevic, M.A.** (2007). Flavonoids are differentially taken up and transported long distances in *Arabidopsis*. *Plant Physiol.* 145:478-490.

- Burk, D. H., Liu, B, Zhong, R, Morrison, W. H., Ye, Z-H.** (2001) *Plant Cell* 13: 807–827
- Canback, B., Andersson, S.G.E. and Kurland, C.G.** (2002) The global phylogeny of glycolytic enzymes. *Proc. Natl. Acad. Sci. USA* 99, 6097–6102.
- Carlsson, A. S.,** (2009). Plant oils as feedstock alternatives to petroleum – A short survey of potential oil crop platforms. *Biochimie* Volume 91, Issue 6, June, Pages 665-670
- Caspar, T., Huber., S.C., and Somerville, C.** (1985). Alterations in growth, photosynthesis, and respiration in a starchless mutant of *Arabidopsis thaliana* (L.) deficient in chloroplast phosphoglucomutase activity. *Plant Physiol.* 79:11-17.
- Caughey, I., and Kekwick, R. G.,** (1982). The characteristics of some components of the fatty acid synthetase system in the plastids from the mesocarp of avocado (*Persea americana*) fruit. *Eur. J. Biochem.* 123:553–561.
- Cavell, A.C., Lydiate, D.J. Parkin, I.A. Dean, C. and Trick, M.** (1998). Collinearity between a 30-centimorgan segment of *Arabidopsis thaliana* chromosome 4 and duplicated regions within the *Brassica napus* genome, *Genome* 41 (1998), pp. 62–69
- Cernac, A., and Benning, C.** (2004) WRINKLED1 encodes an AP2/ERE domain protein involved in the control of storage compound biosynthesis in *Arabidopsis*. *Plant J.* 40:575-585.
- Cernac, A., Andre, C., Hoffmann-Benning, S., and Benning, C.** (2006) WRI1 is required for seed germination and seedling establishment. *Plant Physiol.* 141:745-757.
- Chalker-Scott, L.** (1999). Environmental significance of anthocyanins in plant stress Responses. *Photochem. Photobiol.* 70: 1-9.
- Chang, S.-I., and Hammes, G. G.,** (1989) *Biochemistry* 28, 3781-3788.
- Chastain, C.J., Fries, J.P., Vogel, J.A., Randklev, C.L., Vossen, A.P., Dittmer, S.K., Watkins, E.E., Fiedler, L.J., Wacker, S.A., Meinhover, K.C., Sarath,G., and Chollet, R.** (2002). Pyruvate, orthophosphate dikinase in leaves and chloroplasts of C3 plants undergoes light-/dark-induced reversible phosphorylation. *Plant Physiol.* 128: 1368-1378.
- Chen, M., Mooney, B.P., Hajdich, M., Joshi, T., Zhou, M., Xu, D., and Thelen, J.J.** (2009). System analysis of an *Arabidopsis* mutant altered in de novo fatty acid synthesis reveals diverse changes in seed composition and metabolism. *Plant Physiol.* 150: 27-41.

- Chin, C.C.Q., Brewer, J.M., and Wold, F.** (1981). The amino acid sequence of yeast enolase. *J. Biol. Chem.* 256,1377-1384.
- Copeland, L., Turner, J. F.** (1987). The regulation of glycolysis and the pentose phosphate pathway. In *The Biochemistry of Plants*, ed. PK Stumpf, EE Conn, 11: 107–29.
- Davis, M.S., and Cronan, J.E.,** (2001). Inhibition of *Escherichia coli* acetyl coenzyme A carboxylase by acyl-acyl carrier protein, *J. Bacteriol.* 183 pp. 1499–1503
- del Rio, L.A., Corpasa, F.J., and Barroso, J.B.** (2004). Nitric oxide and nitric oxide synthase activity in plants. *Phytochemistry* 65: 783-792.
- Dennis DT, Miernyk JA.** (1982). Compartmentation of nonphotosynthetic carbohydrate metabolism. *Annu. Rev. Plant Physiol.* 33:27–50.
- Dennis, D.T.** (1989) Fatty acid biosynthesis in plastids in: *Physiology, biochemistry, genetics of non-green plastids* (Boyer, C.D., Shannon, J.C. and Hardison, R.C., Eds.), pp. 120-129, American Society of Plant Physiologists, Rockville, MD.
- Dewick, P. M.** (1998). The biosynthesis of shikimate metabolites. *Nat. Prod. Rep.* 15:17–58.
- Diaz, J. Merino, F.,** (1997). Shikimate dehydrogenase from pepper (*Capsicum annum*) seedlings. Purification and properties. *Physiol. Plant.* 100:147–52
- Dinkova-Kostova, A.T.** (2008). Phytochemicals as protectors against ultraviolet radiation: versatility of effects and mechanisms. *Planta Med.* 74:1548-1559.
- Disch, A., Hemmerlin, A., Bach, T. J. And Rohmer, M.** (1998) *Biochem. J.* 331, 615–621.
- Dobritsa, A.A., Shrestha, J., Morant, M., Pinot, F., Matsuno, M., Swanson, R., Moller, B.L., and Preuss, D.** (2009) CYP704B1 is a Long-chain fatty acid  $\omega$ -hydroxylase essential for sporopollenin synthesis in pollen of *Arabidopsis thaliana*. *Plant Physiol.* 151: 574-589.
- Duncan K, Chaudhuri S, Campbell M.S, Coggins J.R.** (1986). The overexpression and complete amino acid sequence of *Escherichia coli* 3-dehydroquinase. *Biochem. J.* 238:475–83.
- Eastmond, P.J., and Rawsthorne, S.** (2000). Coordinate changes in carbon partitioning and plastidial metabolism during the development of oilseed rape embryos. *Plant Physiol.* 122: 767-774.
- Edwards, G.E. and Nakamoto, H.** (1985) Pyruvate, Pi dikinase and NADP–malate dehydrogenase in C4 photosynthesis: properties and mechanism of light/dark regulation. *Annu. Rev. Plant Physiol.* 36, 55–86.
- Edwards, K., Johnstone, C., and Thompson, C.** (1991) A simple and rapid method for the preparation of plant genomic DNA for PCR analysis. *Nucl Acid Res* 19: 1349.

- Edwards, K., Johnstone, C., and Thompson, C.** (1991). A simple and rapid method for the preparation of plant genomic DNA for PCR analysis. *Nucl. Acid Res.* 19: 1349.
- Elias, B.A., and Givan, C.V.** (1979). Localization of pyruvate dehydrogenase complex in *Pisum sativum* chloroplasts. *Plant Sci. Lett.* 17: 115-122.
- Emes, M.J., Tobin, A.K.** (1993). Control of metabolism and development in higher plant plastids. *Int. Rev. Cytol.* 145:149-216.
- Fernie, A.S., Carrari, F. and Sweetlove, L.J.** (2004) Respiratory metabolism: glycolysis, the TCA cycle and mitochondrial electron transport. *Curr. Opin. Plant Biol.* 7, 254–261.
- Fischer, K., Kammerer, B., Gutensohn, M., Arbinger, B., Weber, A., Häusler, R.E., and Flügge, U.I.** (1997). A new class of plastidic phosphate translocators: a putative link between primary and secondary metabolism by the phosphoenolpyruvate/phosphate antiporter. *Plant Cell* 9: 453-462.
- Fisher, M., Kroon, J. T. M., Martindale, W., Stuitje, A. R., Slabas, A. R. and Rafferty, J. B.** (2000). The X-ray structure of *Brassica napus* beta-keto acyl carrier protein reductase and its implications for substrate binding and catalysis. *Structure* 8, 339-347
- Focks, N., and Benning, C.** (1998). *wrinkled1*: a novel, low-seed-oil mutant of Arabidopsis with a deficiency in the seed-specific regulation of carbohydrate metabolism. *Plant Physiol.* 118: 91-101.
- Fothergill-Gilmore LA, Michels PAM.** (1993). Evolution of glycolysis. *Prog. Biophys. Mol. Biol.* 59: 105–235.
- Franz, A., Makkouk, K. M., and Vetten, H. J.,** (1997). Host range of faba bean necrotic yellows virus and potential yield loss in infected faba bean, *Phytopathol. Mediterr.* 36, pp. 94–103
- Franz, J.E., Mao, M.K. and Sikorski, J.A.** (1997). Glyphosate: A Unique Global Herbicide, ACS Monograph 189, pp. 546–550, American Chemical Society, Washington, DC.
- Fraser H.I, Kvaratskhelia M, White M.F.** (1999). The two analogous phosphoglycerate from *Escherichia coli*: purification, cloning, and construction of overproducers of the enzyme. *Biochemistry* 23: 4470–75.

- Frisch, D.A., Tommey, A.M., Gengenbach, B.G., Somers, D.A.,** (1991) Direct genetic selection of a maize cDNA for dihydrodipicolinate synthase in an *Escherichia coli* *dapA* auxotroph. *Mol. Gen. Genet.* 228: 287-93.
- Frost J.W, Bender J.L, Kadonaga J.T, Knowles J.R.** (1984). Dehydroquinase synthase from *Escherichia coli*: purification, cloning, and construction of overproducers of the enzyme. *Biochemistry.* 23(19): 4470-4475.
- Furomoto, T., Yamaguchi, T., Ichie, Y., Takahashi, Y., and Izui, K.** (2009). Identification of a plastid Na<sup>+</sup> dependent pyruvate transporter in plants. Poster 38026, ASPB conference, Honolulu, Hawaii
- Galili, G.** (1995) Regulation of lysine and threonine synthesis. *Plant Cell* 7: 899-906.
- Genty, B., Briantais, J.M., and Baker, N.R.** (1989). The relationship between the quantum yield of photosynthetic transport and quenching of chlorophyll fluorescence. *Biochim. Biophys. Acta* 990: 87-92.
- Ghislain, M., Frankard, V., Vandenbossche, D., Matthews, B.F., Jacobs, B.** (1994) Molecular analysis of the aspartate kinase-homoserine dehydrogenase gene from *Arabidopsis thaliana*. *Plant Mol. Biol.* 24: 835-51
- Givan, C.V.** (1999) Evolving concepts in plant glycolysis: two centuries of progress. *Biol. Rev.* 74, 277–309.
- Goodwin, T.W.** (1977) in *Lipid and Lipid Polymers of Higher Plants* (M. Tevini and H.K. Lichtenthaler, eds.), Springer, Berlin. pp. 29–47.
- Gray, J.C.** (1989) *Adv. Bot. Res.* 14, 25–91.
- Gueguen, V., Macherel, D., Jaquinod, M., Douce, R. and Bourguignon, J.** (2000) *J. Biol. Chem.* 275, 5016-5025.
- Guilford, W.J., Schneider, D.M., Labovitz, J., and Opella, S.J.** (1988). High resolution solid state <sup>13</sup>C NMR spectroscopy of sporopollenins from different plant taxa. *Plant Physiol.* **86**:134-136.
- Guilfoyle, T. J.** (1998). Auxin-regulated genes and promoters. In K L Libbenga, M Hall, P J J Hooykaas, eds, *Biochemistry and Molecular Biology of Plant Hormones*. Elsevier Publishing Co., Leiden.
- Guo, F.-Q., Okamoto, M., and Crawford, N.M.** (2003). Identification of a plant nitric oxide synthase gene involved in hormonal signaling. *Science* 302: 100-103.
- Hannaert V, Brinkman H, Nowitzki U, Lee J. A, Albert M, Sensen C. W, Gaasterland T, Müller M, Michels P and Martin W.** (2000). Enolase from *Trypanosoma*

- brucei*, from the amitochondriate protist *Mastigamoeba balamuthi*, and from the chloroplast and cytosol of *Euglena gracilis*: pieces in the evolutionary puzzle of the eukaryotic glycolytic pathway, *Molecular Biology and Evolution* 17: 989–1000.
- Hanson, A. D., and Gregory III, J. F.**, (2002). Synthesis and turnover of folates in plants. *Curr. Opin. Plant Biol.* 5: 244-249
- Harborne, J. B.** (1991) in *Ecological Chemistry and Biochemistry of Plant Terpenoids*, eds. (Clarendon, Oxford), pp. 399–426.
- Hattori J, Baum BR, McHugh SG, Blakeley SD, Dennis DT, Miki BL.** (1995). Pyruvate kinase isozymes: ancient diversity retained in modern plant cells. *Biochem.Syst. Ecol.*
- He, Y., Tang, R.-H., Hao, Y., Stevens, R.D., Cook, C.W., Ahn, S.M., Jing, L., Yang, Z., Chen, L., Guo, F., Fiorani, F., Jackson, R.B., Crawford, N.M., and Pei, Z.-M.** (2004). Nitric oxide represses the Arabidopsis floral transition. *Science* 305: 1968-1971.
- Henze K, Schnarrenberger C, Kellermann J, Martin W.** (1994). Chloroplast and cytosolic triosephosphate isomerases from spinach: purification, microsequencing and cDNA cloning of the chloroplast enzyme. *Plant Molecular Biology* 26: 1961-1973.
- Herrmann, K.M.** (1995) The shikimate pathway: early steps in the biosynthesis of aromatic compounds. *Plant Cell* 7: 907–919.
- Herrmann, K.M. and Weaver, L.M.** (1999) The shikimate pathway. *Annu. Rev. Plant Physiol. Plant Mol. Biol.* 50: 473–503.
- Hibberd, J.M. and Quick, W.P.** (2002) Characteristics of C4 photosynthesis in stems and petioles of C3 flowering plants. *Nature* 415: 451–454.
- Higo, K., Ugawa, Y., Iwamoto, M. and Korenaga, T.** (1999) Plant cis-acting regulatory DNA elements (PLACE) database:1999. *Nuclear Acids Res.* 27: 297–300.
- Hirai, N., Yoshida, R., Todoroki, Y. and Ohigashi, H.** (2000) *Biosci. Biotechnol. Biochem.* 64: 1448–1458.
- Hofius, D., Hajirezaei, M. R., Geiger, M., Tschiersch, H., Melzer, M., and Sonnewald, U.**(2004). RNAi-mediated tocopherol deficiency impairs photoassimilate export in transgenic potato plants. *Plant Physiol* 135: 1256-1268.
- Holloway, P.J.** (1983). Some variations in the composition of suberin from the cork layers of higher plants. *Phytochemistry*, 22: 495-502.

- Hülskamp, M., Misera, S. and Jürgens, G.** (1994) Genetic dissection of trichome cell development in Arabidopsis. *Cell* 76, 555–566.
- Hülskamp, M., Misera, S. and Jürgens, G.** (1994). Genetic dissection of trichome cell development in Arabidopsis. *Cell*, 76, 555-566.
- Huppe H. C, Turpin D. H.** (1994). Integration of carbon and nitrogen metabolism in plant and algal cells. *Annu. Rev. Plant Physiol. Plant Mol. Biol.* 45: 577–607.
- Jakoby, M.J., Falkenhan, D., Mader, M.T., Brininstool, G., Wischnitzki, E., Platz, N., Hudson, A., Hülskamp, M., Larkin, J. and Schnittger, A.** (2008) Transcriptional profiling of mature Arabidopsis trichomes reveals that NOECK encodes the MIXTA-like transcriptional regulator MYB106. *Plant Physiol.* 148, 1583–1602.
- Jefferson, R.A., Kavanagh, T.A. and Bevan, M.W.** (1987) GUS fusions:  $\beta$ glucuronidase as a sensitive and versatile gene fusion marker in higher plants. *EMBO J* 6, 3901–3907.
- Jetter, R., Kunst, L., and Samuels, L.** (2006). Composition of plant cuticular waxes. In: Riederer, M., and Müller, C., eds. *Biology of the Plant Cuticle*. Oxford, UK: Blackwell, pp.145-181.
- Journet, E.P. and Douce, R.** (1985) Enzymic capacities of purified cauliflower bud plastids for lipid-synthesis and carbohydrate-metabolism. *Plant Physiol.* 79, 458–467.
- Kammerer, B., Fischer, K., Hilpert, B., Schubert, S., Gutensohn, M., Weber, A., and Flügge, U.I.** (1998). Molecular characterization of a carbon transporter in plastids from heterotrophic tissues: the glucose 6-phosphate/phosphate antiporter. *Plant Cell* 10: 105-117.
- Kaneko, T., Hashimoto, T., Kumpaisai, R., Yamada, Y.** (1990) Molecular cloning of wheat dihydrodipicolinate synthase. *J. Biol. Chem.* 265: 17451-5
- Kang, F. and Rawsthorne, S.** (1994) Starch and fatty acid biosynthesis in plastids from developing embryos of oil seed rape. *Plant J.* 6, 795–805.
- Kang, F. and Rawsthorne, S.** (1996) Metabolism of glucose-6-phosphate and utilization of multiple metabolites for fatty acid synthesis by plastids from developing oilseed rape embryos. *Planta* 199, 321–327.
- Kang, F., and Rawsthorne, S.** (1994). Starch and fatty acid biosynthesis in plastids from developing embryos of oil seed rape. *Plant J.* 6: 795–805.

- Kasahara, H., Takei, K., Ueda, N., Hishiyama, S., Yamaya, T., Kamiya, Y., Yamaguchi, S. and Sakakibara, H.** (2004) Distinct isoprenoid origins of cis and trans-zeatin biosyntheses in Arabidopsis. *J Biol Chem.* 279:14049-14054.
- Kinsman, E.A., and Pyke, K.A.** (1998). Bundle sheath cells and cell-specific plastid development in Arabidopsis leaves. *Development* 125: 1815-1822.
- Kirik, V., Simon, M., Hülskamp, M. and Schiefelbein, J.** (2004) The ENHANCER OF TRY AND CPC1 gene acts redundantly with TRIPTYCHON and CAPRICE in trichome and root hair cell patterning in Arabidopsis. *Dev. Biol.* 268, 506–513.
- Klee, H. J., Muskopf, Y. M., Gasser, C. S.,** (1987). Cloning of an *Arabidopsis thaliana* gene encoding 5-enolpyruvylshikimate 3-phosphate synthase: sequence analysis and manipulation to obtain glyphosate tolerant plants. *Mol. Gen.Genet.* 210:437–42
- Kleinig, H.** (1989) *Annu. Rev. Plant Physiol. Plant Mol. Biol.* 40, 39–59.
- Knappe, S., Löttgert, T., Schneider, A., Voll, L., Flüge, U.-I. and Fischer, K.** (2003) Characterization of two functional phosphoenolpyruvate/phosphate translocator (PPT) genes in Arabidopsis – AtPPT1 may be involved in the provision of signals for correct mesophyll development. *Plant J.* 36, 411–420.
- Koornneef, M.** (1990). Mutations affecting the testa color in Arabidopsis. *Arabidopsis Inf. Serv.* 27: 1 4.
- Koroleva, O.A., Tomlinson, M.L., Leader, D., Shaw, P. and Doonan, J.H.** (2005) High-throughput protein localization in Arabidopsis using Agrobacterium mediated transient expression of GFP-ORF fusions. *Plant J.* 41, 162–174.
- Kruger, N.J., and von Schaewen, A.** (2003). The oxidative pentose phosphate pathway: Structure and organisation. *Curr. Opin. Plant Biol.* 6: 236-246.
- Kubis, S.E., Pike, M.J., Everett, C.J., Hill, L.M., and Rawsthorne, S.** (2004). The import of phosphoenolpyruvate by plastids from developing embryos of oilseed rape, *Brassica napus* (L.), and its potential as a substrate for fatty acid synthesis. *J. Exp. Bot.* 55: 1455-1462.
- Laemmli, U.K.** (1970) Cleavage of structural proteins during assembly of head of bacteriophage-T4. *Nature* 227: 680–685.
- Larkin, J.C., Oppenheimer, D.G., Pollock, S. and Marks, M.D.** (1993) Arabidopsis GLABROUS1 gene requires downstream sequences for function. *Plant Cell* 5: 1739–1748.

- Lee, H., Guo, Y., Ohta, M., Xiong, L., Stevenson, B. and Zhu, J.K.** (2002) LOS2, a genetic locus required for cold-responsive gene transcription encodes a bifunctional enolase. *EMBO J.* 21: 2692–2702.
- Leegood, R.C. and Walker, R.P.** (2003) Regulation and roles of phosphoenolpyruvate carboxykinase in plants. *Arch. Biochem. Biophys.* 414: 204–210.
- Lernmark, U., and Gardstrom, P.** (1994). Distribution of pyruvate dehydrogenase complex activities between chloroplasts and mitochondria from leaves of different species. *Plant Physiol.* 106: 1633-1638.
- Lewis, N. G., and Yamamoto, E.** (1990). Lignin: occurrence, biogenesis and biodegradation. *Annu. Rev. Plant Physiol. Plant Mol. Biol.* 41:455-496.
- Li, H., Culligan, K., Dixon, R.A., and Chory, J.** (1995). CUE1: A mesophyll cell specific positive regulator of light-controlled gene expression in *Arabidopsis*. *Plant Cell* 7: 1599-1610.
- Lichtenthaler, H. K., Schwender, J., Disch, A. & Rohmer, M.** (1997) *FEBS Lett.* 400: 271–274.
- Lichtenthaler, H.K.** (1977) in *Lipids and Lipid Polymers of Higher Plants* (M. Tevini and H.K. Lichtenthaler, eds.), Springer, Berlin. pp. 231–258
- Lichtenthaler, H.K.** (1993) in *Lipid Metabolism in Plants*. (T.S. Moore, ed.) CRC Press, Boca Raton, FL. pp. 427–470
- Lichtenthaler, H.K.** (1999) The 1-deoxy-D-xylulose-5-phosphate pathway of isoprenoid biosynthesis in plants. *Annu. Rev. Plant Physiol. Plant Mol. Biol.* 50: 47–65.
- Liedvogel, B., Kleinig, H.** (1980). Phosphate translocator and adenylate translocator in chromoplast membranes. *Planta* 150: 170–173
- Lin, T.P., Caspar, T., Somerville, C., and Preiss, J.** (1988). Isolation and characterization of a starchless mutant of *Arabidopsis thaliana* (L.) lacking ADPglucose pyrophosphorylase activity. *Plant Physiol.* 86: 1131-1135.
- Lindroth, P., and Mopper, K.** (1979). High-performance liquid-chromatographic determination of subpicomole amounts of amino-acids by precolumn fluorescence derivatization with ortho-phthaldialdehyde. *Anal. Chem.* 51:1667-1674.
- Liu, S.-C., Webster, D.A. and Stark, B.C.** (1995). *Appi. Microbiol. Biotechnol.* 44: 419-424.
- Lonien, J., and Schwender, J.** (2009). Analysis of metabolic flux phenotypes for two *Arabidopsis* mutants with severe impairment in seed storage lipid synthesis. *Plant Physiol.* 151: 1617-1634.

- Mansfield, S. G., Briarty, L. G.** (1992) Cotyledon cell development in *Arabidopsis thaliana* during reserve formation. *Can J Bot* 70: 151–164.
- Mathur, J., Spielhofer, P., Kost, B. and Chua, N.H.** (1999) The actin cytoskeleton is required to elaborate and maintain spatial patterning during trichome cell morphogenesis in *Arabidopsis thaliana*. *Development*. 126: 5559–5568.
- Mathur, J., Szabados, L., Schaefer, S., Grunenberg, B., Lossow, A., Jonas-Straube, E., Schell, J., Koncz, C. and Koncz-Kalman, Z.** (1998) Gene identification with sequenced T-DNA tags generated by transformation of *Arabidopsis* cell suspension. *Plant J.* 13: 707–716.
- Miernyk, J.A. and Dennis, D.T.** (1982) Isozymes of the glycolytic-enzymes in endosperm from developing castor-oil seeds. *Plant Physiol.* 69: 825–828.
- Miernyk, J.A. and Dennis, D.T.** (1992) A developmental analysis of the enolase isozymes from *Ricinus communis*. *Plant Physiol.* 99: 748–750.
- Milborrow, B. and Lee, H.** (1998) *Aust. J. Plant Physiol.* 25: 507–512.
- Millar, A.A., Clemens, S., Zachgo, S., Giblin, E.M., Taylor, D.C., and Kunst, L.** (1999). *CUT1*, an *Arabidopsis* gene required for cuticular wax biosynthesis and pollen fertility, encodes a very-long-chain fatty acid condensing enzyme. *Plant Cell* 11: 825–838
- Mintz-Oron, S., Mandel, T., Rogachev, I., Feldberg, L., Lotan, O., Yativ, M., Wang, Z., Jette, R., Venger, I., Adato, A., and Aharoni, A.** (2008). Gene expression and metabolism in tomato fruit surface tissues. *Plant Physiol.* 147: 823-851.
- Mo, X., Zhu, Q., Li, X., Li, J., Zeng, Q., Rong, H., Zhang, H., and Wu, P.** (2006). The *hpa1* mutant of *Arabidopsis* reveals a crucial role of histidine homeostasis in root meristem maintenance. *Plant Physiol.* 141: 1425–1435.
- Moore T** (1976) Phosphatidylcholine synthesis in castor bean endosperm. *Plant Physiol* 57: 383-386
- Mousdale, D. M., Campbell, M. S., Coggins, J. R.,** (1987). Purification and characterization of bifunctional dehydroquinaseshikimate: NADP oxidoreductase from pea seedlings. *Phytochemistry* 26: 2665–70
- Mousdale, D. M., Campbell, M. S., Coggins, J. R.,** (1987). Purification and characterization of bifunctional dehydroquinase-shikimate: NADP oxidoreductase from pea seedlings. *Phytochemistry.* 26 (10): 2665-2670.

- Muehlbauer, G.J., Somers, D.A., Matthews, B.F., Gengenbach, B.G.** (1995) Molecular genetics of the maize (*Zea mays* L.) aspartate kinase-homoserine dehydrogenase gene family. *Plant Physiol.* 106: 1303-12
- Niewiadowski, P., Knappe, S., Geimer, S., Fischer, K., Schulz, B., Unte, U.S., Rosso, M.G., Ache, P., Flügge, U.I., and Schneider, A.** (2005). The Arabidopsis plastidic glucose 6-phosphate/phosphate translocator GPT1 is essential for pollen maturation and embryo sac development. *Plant Cell* 17: 760-775.
- Ohlrogge, J. B., Kuhn, D. N., Stumpf, P. K.,** (1979). Subcellular localization of acyl carrier protein in leaf protoplasts of *Spinacia oleracea*. *Proc Natl Acad Sci U S A.* Mar;76(3):1194–1198
- Ohlrogge, J.B. and Jaworski, J.G.** (1997) Regulation of fatty acid synthesis. *Annu. Rev. Plant Physiol. Plant Mol. Biol.* 48, 109–136.
- Ohlrogge, J.B., Kuhn, D.N., and Stumpf, P.K.** (1979). Subcellular-Localization of Acyl Carrier Protein in Leaf Protoplasts of *Spinacia-Oleracea*. *Proc. Natl. Acad. Sci. U. S. A.* 76: 1194-1198.
- Ohnishi, J.I., Flügge, U.-I., Heldt, H.W. and Kanai, R.** (1990) Involvement of  $\text{Na}^+$  in active uptake of pyruvate in mesophyll chloroplasts of some C4 plants:  $\text{Na}^+$ /pyruvate cotransport. *Plant Physiol.* 94, 950–959.
- Pagnussat, G.C., Alandete-Saez, M., Bowman, J.L., and Sundaresan, V.** (2009). Auxin-dependent patterning and gamete specification in the Arabidopsis female gametophyte. *Science.* 324: 1684-1689.
- Park, S.K., Howden, R., and Twell, D.** (1998). The *Arabidopsis thaliana* gametophytic mutation *geminipollen1* disrupts microspore polarity, division asymmetry and pollen cell fate. *Development.* 125: 3789–3799.
- Parsley, K. and Hibberd, J.M.** (2006) The Arabidopsis PPDK gene is transcribed from two promoters to produce differentially expressed transcripts responsible for cytosolic and plastidic proteins. *Plant Mol. Biol.* 62: 339–349.
- Plaxton, W.C.** (1996) The organization and regulation of plant glycolysis. *Annu. Rev. Plant Physiol. Plant. Mol. Biol.* 47: 185–214.
- Prestridge, D.S.** (1991) SIGNAL SCAN: a computer program that scans DNA sequences for eukaryotic transcriptional elements. *CABIOS* 7: 203–206.
- Proudlove, M.O. and Thurman, D.A.** (1981). The uptake of 2-oxoglutarate and pyruvate by isolated pea chloroplasts. *New Phytol.* 88: 255–264.

- Proudlove, O., Thurman, D.A.** (1981) The uptake of 2-oxoglutarate and pyruvate by isolated pea chloroplasts. *New Phytol.* 88: 255-64
- Qi, Q.G., Kleppingersparace, K.F., and Sparace, S.A.** (1995). The utilization of glycolytic intermediates as precursors for fatty acid biosynthesis by pea root plastids. *Plant Physiol.* 107: 413-419.
- Rawsthorne, S.** (2002). Carbon flux and fatty acid synthesis in plants. *Prog. Lipid Res.* 41: 182-196.
- Reid, E.E., Thompson, P., Lyttle, C.R., and Dennis, D.T.** (1977). Pyruvate dehydrogenase complex from higher plant mitochondria and proplastids. *Plant Physiol.* 59: 842-848.
- Reynolds, E.S.** (1963). The use of lead citrate at high pH as an electron-opaque stain in electron microscopy. *J. Cell. Biol.* 17: 208-212.
- Rock C. O., Cronan, J. E., Jr, Armitage, I. M.,** (1981). Molecular properties of acyl carrier protein derivatives. *J Biol Chem.* 256(6): 2669–2674.
- Rosso, M.G., Li, Y., Strizhov, N., Reiss, B., Dekker, K., and Weisshaar, B.** (2003). An *Arabidopsis thaliana* T-DNA mutagenized population (GABI-Kat) for flanking sequence tag-based reverse genetics. *Plant Mol. Biol.* 53: 247-259.
- Ruegger, M., and Chapple, C.,** (2001). Mutations that reduce sinapoylmalate accumulation in *Arabidopsis thaliana* define loci with diverse roles in phenylpropanoid metabolism. *Genetics* 159: 1741–1749
- Ruuska, S.A., Girke, T., Benning, C. and Ohlrogge, J.B.** (2002) Contrapuntal networks of gene expression during *Arabidopsis* seed filling. *Plant Cell.* 14: 1191–1206.
- Samach, A., Broday, L., Hareven, D., Lifschitz, E.** (1995) Expression of an amino acid biosynthesis gene in tomato flowers: developmental upregulation and MeJa response are parenchyma-specific and mutually compatible. *Plant J.* 8: 391-406
- Samuels, L., Kunst, L., and Jetter, R.** (2008). Sealing plant surfaces: cuticular wax formation by epidermal cells. *Annu. Rev. Plant Biol.* 59: 683-707.
- Sanger, F., Nicklen, S., Coulson, A. R.** (1977): DNA sequencing with chain-terminating inhibitors. *Proceedings of the National Academy of Sciences U.S.A.* 74: 5463-5467.
- Sathasivan, K., Haughn, G.W., Murai, N.** (1990) Nucleotide sequence of a mutant acetolactate synthase gene from an imidazolinone-resistant *Arabidopsis thaliana* var. Columbia. *Nucleic Acids Res.* 18: 2188

- Schellmann, S., Schnittger, A., Kirik, V., Wada, T., Okada, K., Beermann, A., Thumfahrt, J., Jürgens, G. and Hülskamp, M.** (2002) TRIPTYCHON and CAPRICE mediate lateral inhibition during trichome and root hair patterning in *Arabidopsis*. *EMBO J.* 21: 5036–5046.
- Schmid, J. and Amrhein, N.** (1995) Molecular organization of the shikimate pathway in higher plants. *Phytochemistry* 39: 737–749.
- Schmidt, C. L., Danneel, H. J., Schultz, G., Buchanan, B. B.,** (1990). Shikimate kinase from spinach chloroplasts. Purification, characterization, and regulatory function in aromatic amino acid biosynthesis. *Plant Physiol.* 93: 758–66.
- Schnarrenberger C, Pelzer Reith B, Yatsuki H, Freund S, Jacobshagen S, Hori K.** (1994). Expression and sequence of the only detectable aldolase in *Chlamydomonas reinhardtii*. *Arch. Biochem. Biophys.* 313: 173–78.
- Schreiber, U., Schliwa, U., and Bilger, B.** (1986). Continuous recording of photochemical and non-photochemical chlorophyll fluorescence quenching with a new type of modulation fluorometer. *Photosynth. Res.* 10: 51–62.
- Schulze-Siebert, D., Heineke, D., Scharf, H. and Schultz, G.** (1984) Pyruvate-derived amino-acids in spinach-chloroplasts - synthesis and regulation during photosynthetic carbon metabolism. *Plant Physiol.* 76: 465–471.
- Schwab, B., Mathur, J., Saedler, R., Schwarz, H., Frey, B., Scheidegger, C. and Hülskamp, M.** (2003) Regulation of cell expansion by the DISTORTED genes in *Arabidopsis thaliana*: actin controls the spatial organization of microtubules. *Mol. Gen. Genom.* 269: 350–360.
- Schwacke, R., Schneider, A., van der Graaff, E., Fischer, K., Catoni, E., Desimone, M., Frommer, W.B., Flügge, U.-I. and Kunze, R.** (2003) ARAMEMNON: a novel database for *Arabidopsis thaliana* integral membrane proteins. *Plant Physiol.* 131: 16–26.
- Schwender, J., and Ohlrogge, J.B.** (2002). Probing *in vivo* metabolism by stable isotope labeling of storage lipids and proteins in developing *Brassica napus* embryos. *Plant Physiol.* 130: 347–361.
- Schwender, J., Ohlrogge, J.B., and Shachar-Hill, Y.** (2003). A flux model of glycolysis and the oxidative pentosephosphate pathway in developing *Brassica napus* embryos. *J. Biol. Chem.* 278: 29442–29453.
- Schwender, J., Zeidler, J., Groner, R., Müller, C., Focke, M., Braun, S., Lichtenthaler, F. W. and Lichtenthaler, H. K.** (1997) *FEBS Lett.* 414: 129–134.

- Segel, I.H.** (1993) *Enzyme Kinetics. Behavior and Analysis of Rapid Equilibrium and Steady-state Enzyme Systems*, John Wiley and sons Inc., New York.
- Sieburth, L.E., and Meyerowitz, E.M.** (1997). Molecular dissection of the *AGAMOUS* control region shows that cis elements for spatial regulation are located intragenically, *Plant Cell* 9: 355-365.
- Sinha, S., and Brewer, J.M.** (1984). Purification and comparative characterization of an enolase from spinach. *Plant Physiol.* 74: 834-840.
- Slabas, A.R., and Hellyer, A.,** (1985). *Plant Sci.* 39: 177–182.
- Smith, R.G., Gauthier, D.A., Dennis, D.T., and Turpin, D.H.** (1992). Malate dependent and pyruvate dependent fatty acid synthesis in leukoplastids from developing castor endosperm. *Plant Physiol.* 98: 1233-1238.
- Smith, S.,** (1994). The animal fatty acid synthase: one gene, one polypeptide, seven enzymes. *FASEB J.* 8: 1248–1259.
- Smyth, D.R., Bowman, J.L., and Meyerowitz, E.M.** (1990). Early flower development in *Arabidopsis*. *Plant Cell* 2: 755-767.
- Stitt, M. and Ap Rees, T.** (1979) Capacities of pea chloroplasts to catalyze the oxidative pentose–phosphate pathway and glycolysis. *Phytochemistry* 18: 1905–1911.
- Streatfield, S.J., Weber, A., Kinsman, E.A., Häusler, R.E., Li, J., Post-Beittenmiller, D., Kaiser, W.M., Pyke, K.A., Flügge, U.-I. and Chory, J.**(1999) The phosphoenolpyruvate /phosphate translocator is required for phenolic metabolism, palisade cell development, and plastid-dependent nuclear gene expression. *Plant Cell* 11: 1609–1622.
- Sung, S.-J.S., Dian-Peng Xu, D.-P., Galloway, C.M. and Black, C.C.** (1988) A reassessment of glycolysis and gluconeogenesis in higher plants. *Physiol. Plant.* 7: 650–654.
- Towbin, H., Staehelin, T. and Gordon, J.** (1979) Electrophoretic transfer of proteins from polyacrylamide gels to nitrocellulose sheets: procedure and some applications. *Proc. Natl. Acad. Sci. USA* 76: 4350–4354.
- Turner, S., and Sieburth, L.E.** (2002). Vascular Patterning. *The Arabidopsis Book* 5, 1-23  
Online publication date: 1-Feb-2002.
- Van der Straeten, D., Rodriguespousada, R.A., Goodman, H.M. and Van Montagu, M.** (1991) Plant enolase – gene structure, expression, and evolution. *Plant Cell* 3: 719–735.

- Vanneste, S., and Friml, J.** (2009). Auxin: a trigger for change in plant development. *Cell* 136: 1005-1016.
- Vickers, C. E., Gershenzon, J. Lerdau, M. T., Loreto, F.** (2009). A unified mechanism of action for isoprenoids in plant abiotic stress. *Nature Chemical Biology*. 5: 283–291.
- Voelker, T., and Kinney, A.J.** (2001) Variations in the biosynthesis of seed-storage lipids. *Annu. Rev. Plant Physiol. Plant Mol. Biol.* 52: 335-361.
- Voll, L., Häusler, R.E., Hecker, R., Weber, A., Weissenböck, G., Fiene, G., Waffenschmidt, S., and Flügge, U.I.** (2003). The phenotype of the *Arabidopsis* *cue1* mutant is not simply caused by a general restriction of the shikimate pathway. *Plant J.* 36: 301-317.
- Voll, L.M., Hajirezaei, M.R., Czogalla-Peter, C., Lein, W., Stitt, M., Sonnewald, U., and Börnke, F.** (2009). Antisense inhibition of enolase strongly limits the metabolism of aromatic amino acids, but has only minor effects on respiration in leaves of transgenic tobacco plants. *New Phytol.* 184: 607-618.
- Wakil, S. J.,** (1989 ). Fatty acid synthase, a proficient multifunctional enzyme. *Biochemistry* 28: 4523-4530.
- Walker, R.P. and Chen, Z.-H.** (2002) Phosphoenolpyruvate carboxykinase: structure, function and regulation. *Adv. Bot. Res.* 38: 93–189.
- Wang, H., Guo, J., Lambert, K. and Lin, Y.** (2007) Developmental control of *Arabidopsis* seed oil biosynthesis. *Planta.* 226: 773–783
- Webb, M., Jouannic, S., Foreman, J., Linstead, P. and Dolan, L.** (2002) Cell specification in the *Arabidopsis* root epidermis requires the activity of *ECTOPIC ROOT HAIR 3*– a katanin-p60 protein. *Development.* 129: 123–131
- Weber and M. Osborn** (1969). The reliability of molecular weight determinations by dodecyl sulfate-polyacrylamide gel electrophoresis, *J. Biol. Chem.* 244: 4406–4412.
- Weisemann, J.M., Matthews, B.F.,** (1993) Identification and expression of a cDNA from *Daucus carota* encoding a bifunctional aspartokinase-homoserine dehydrogenase. *Plant Mol. Biol.* 22: 301-12
- Welch, B. L.** (1947). "The generalization of "student's" problem when several different population variances are involved", *Biometrika* 34: 28-35.
- Weng, M., Makaroff, C.A., and Zalkin, H.** (1986). Nucleotide sequence of *Escherichia coli pyrG* encoding CTP synthetase. *J. Biol. Chem.* 261: 5568-5574.

- Wheeler, M.C., Tronconi, M.A., Drincovich, M.F., Andreo, C.S., Flügge, U.I., and Maurino, V.G.** (2005) A comprehensive analysis of the NADP-malic enzyme gene family of Arabidopsis. *Plant Physiol.* 139: 39-51.
- Wiermann, R., Ahlers, F., and Schmitz-Thom, I.** (2001). Sporopollenin. *In* A. Stenbüchel, and M. Hofrichter, eds, *Biopolymers*, Vol 1. Wiley-VCH Verlag, Weinheim, Germany, pp 209-227.
- Winter, D., Vinegar, B., Nahal, H., Ammar, R., Wilson, G.V., and Provart N.J.** (2007). An “Electronic Fluorescent Pictograph” browser for exploring and analyzing large-scale biological data sets. *PLoS ONE* 2: e718.

## Appendix

**Table 1:** Spatial and temporal expression profiles of genes involved in the metabolism of PEP and pyruvate in plastids of generative tissue.

Generative tissues	ENO1 At1g74030		PPT1 At5g33320		PPT2 At3g01550		PPDK At4g15530		PGyMp At1g22170	
	E	SD	E	SD	E	SD	E	SD	E	SD
<b>Flowers</b>										
Flower Stage 9	296.3	5.2	717.4	5.2	89.5	2.8	3.8	2.3	90.7	0.8
Flower Stage 10/11	169.4	8.1	566.9	50.6	109.1	6.4	59.6	2.0	86.8	3.9
Flower Stage 12	164.8	6.4	681.6	39.0	89.6	9.2	208.9	13.2	86.2	6.7
Flower Stage 12. Carpels	150.6	11.4	591.6	31.5	84.8	8.4	10.7	3.5	70.7	5.0
Flower Stage 12. Stamens	111.7	4.9	468.5	60.0	15.0	0.7	605.3	31.5	57.1	7.9
Flower Stage 12. Petals	379.8	8.3	1287.3	89.3	16.0	1.7	28.8	0.8	265.1	10.4
Flower Stage 12. Sepals	38.9	1.8	456.6	28.1	113.3	3.7	831.5	57.7	24.7	5.0
Flower Stage 15	55.5	5.8	297.4	20.0	55.0	2.4	758.2	17.0	53.4	9.9
Flower Stage 15. Carpels	117.7	12.9	507.8	38.3	76.0	1.1	74.1	2.8	74.6	1.5
Flower Stage 15. Stamen	50.3	5.7	171.6	9.4	13.0	3.4	1519.4	45.6	25.7	8.4
Flower Stage 15. Petals	29.1	4.1	160.4	14.9	10.9	4.4	1039.9	43.1	39.5	2.7
Flower Stage 15. Sepals	27.5	1.1	216.7	6.2	36.9	6.6	1817.0	108.9	18.5	3.0
Flowers Stage 15. Pedicels	57.4	7.4	494.1	15.0	386.1	9.7	122.0	2.9	40.9	5.3
<b>Pollen</b>	<b>E</b>	<b>SD</b>	<b>E</b>	<b>SD</b>	<b>E</b>	<b>SD</b>	<b>E</b>	<b>SD</b>	<b>E</b>	<b>SD</b>
Uninucleate Micropore	517.8	12.2	523.5	20.8	34.8	8.9	9.1	3.3	40.8	5.8
Bicellular Pollen	414.1	53.6	510.0	5.2	30.3	9.5	45.4	13.8	52.5	0.9
Tricellular Pollen	37.9	4.9	187.8	23.7	28.3	3.7	2135.8	82.2	37.5	8.4
Mature Pollen Grain	84.9	0.0	117.6	0.0	37.4	0.0	6505.7	0.0	33.0	0.0
<b>Carpels</b>	<b>E</b>	<b>SD</b>	<b>E</b>	<b>SD</b>	<b>E</b>	<b>SD</b>	<b>E</b>	<b>SD</b>	<b>E</b>	<b>SD</b>
Stigma tissue	88.8	19.7	547.6	31.5	70.1	42.3	265.8	105.9	148.2	25.7
Ovary tissue	196.4	26.9	1064.0	164.7	241.0	20.9	162.9	56.4	97.8	10.4
<b>Embryo development</b>	<b>E</b>	<b>SD</b>	<b>E</b>	<b>SD</b>	<b>E</b>	<b>SD</b>	<b>E</b>	<b>SD</b>	<b>E</b>	<b>SD</b>
Globular - Apical	290.2	85.9	196.9	122.4	142.6	48.9	17.1	5.7	47.4	43.0
Globular - Basal	120.2	140.0	66.8	12.0	174.3	10.1	27.6	5.1	92.1	28.0
Heart - Cotyledon	1878.1	1209.4	140.9	89.0	105.7	60.7	14.5	8.5	81.2	20.7
Heart - Root	1765.1	1195.2	212.5	55.7	75.8	22.7	16.0	12.8	164.3	138.2
Torpedo - Cotyledon	240.0	288.1	153.7	34.5	105.9	13.2	47.2	21.5	191.1	192.0
Torpedo - Root	201.7	120.1	135.7	93.3	154.4	83.5	18.5	10.5	86.8	92.8
Torpedo - Meristem	310.0	236.0	321.1	243.0	99.0	42.5	15.0	4.1	92.7	48.5
Torpedo - Apical	1128.4	195.9	209.4	71.6	20.1	12.3	30.1	10.2	105.1	16.7
Torpedo - Basal	1194.6	547.3	191.2	130.7	29.7	5.0	13.1	9.4	144.2	41.7
<b>Seed development</b>	<b>E</b>	<b>SD</b>	<b>E</b>	<b>SD</b>	<b>E</b>	<b>SD</b>	<b>E</b>	<b>SD</b>	<b>E</b>	<b>SD</b>
Seeds Stage 3 w/ Siliques	88.0	6.1	382.4	41.2	294.7	7.6	178.9	6.3	60.0	4.2
Seeds Stage 4 w/ Siliques	479.4	2.3	839.4	57.9	69.2	5.4	354.7	14.6	185.4	1.0
Seeds Stage 5 w/ Siliques	558.4	13.0	781.4	1.0	48.5	4.2	348.6	9.1	296.1	2.6
Seeds Stage 6 w/o Siliques	730.0	28.7	946.8	47.1	9.4	2.4	261.9	6.7	385.2	33.7
Seeds Stage 7 w/o Siliques	589.4	22.0	638.4	40.1	11.4	1.4	455.7	23.1	366.1	32.6
Seeds Stage 8 w/o Siliques	67.4	5.0	138.0	17.6	14.2	3.4	1708.0	105.9	55.2	6.3
Seeds Stage 9 w/o Siliques	24.7	3.5	83.6	6.9	11.9	2.6	1663.8	32.6	36.4	7.6
Seeds Stage 10 w/o Siliques	13.5	9.6	77.6	6.0	13.8	3.8	1549.2	37.6	26.3	1.1
Dry seed	3.4	1.8	130.3	31.6	6.4	6.0	958.7	79.1	7.6	4.9
Imbibed seed. 24 h	97.8	24.3	456.1	8.5	6.4	2.2	1078.3	54.6	29.8	1.6

Generative tissues	PKp1 At3g22960		PKp2 At5g52920		PKp3 At1g32440		ME4 At1g79750		PyT At2g26900	
	E	SD	E	SD	E	SD	E	SD	E	SD
<b>Flowers</b>	<b>E</b>	<b>SD</b>	<b>E</b>	<b>SD</b>	<b>E</b>	<b>SD</b>	<b>E</b>	<b>SD</b>	<b>E</b>	<b>SD</b>
Flower Stage 9	532.8	2.7	510.2	32.5	95.2	6.1	466.5	3.8	765.6	9.1
Flower Stage 10/11	481.8	8.1	496.8	30.3	85.8	6.2	530.9	17.9	716.6	12.5
Flower Stage 12	534.2	19.8	513.1	8.5	95.5	2.9	512.3	25.0	672.4	31.1
Flower Stage 12. Carpels	560.8	19.0	489.6	4.1	63.9	3.6	513.7	7.4	671.4	10.7
Flower Stage 12. Stamens	291.0	8.6	223.0	9.2	81.0	7.0	412.1	25.3	242.0	15.2
Flower Stage 12. Petals	1042.5	17.6	1084.3	41.9	118.6	7.0	726.2	12.7	842.4	16.2
Flower Stage 12. Sepals	253.7	5.3	197.1	6.7	121.1	6.7	341.7	7.6	610.7	16.4
Flower Stage 15	368.8	8.4	255.6	12.4	87.1	5.0	312.0	13.4	483.5	10.2
Flower Stage 15. Carpels	542.1	9.4	449.1	11.3	74.1	8.1	392.8	18.3	768.2	36.1
Flower Stage 15. Stamen	178.4	9.5	115.9	7.8	120.1	6.2	246.6	23.5	356.8	12.6
Flower Stage 15. Petals	85.9	4.0	53.9	3.1	88.3	14.8	274.3	10.9	418.5	8.3
Flower Stage 15. Sepals	235.5	6.6	111.9	2.9	91.5	1.5	259.1	10.1	227.1	13.5
Flowers Stage 15. Pedicels	578.3	10.4	312.4	48.6	127.4	8.8	413.1	11.4	928.6	18.9
<b>Pollen</b>	<b>E</b>	<b>SD</b>	<b>E</b>	<b>SD</b>	<b>E</b>	<b>SD</b>	<b>E</b>	<b>SD</b>	<b>E</b>	<b>SD</b>
Uninucleate Micropore	224.9	35.0	493.0	11.6	476.9	45.1	298.6	9.4	291.5	4.7
Bicellular Pollen	254.3	8.8	456.9	13.5	419.2	31.1	373.8	16.9	249.2	44.5
Tricellular Pollen	109.4	10.2	18.8	1.3	86.2	11.9	618.9	20.7	58.7	2.9
Mature Pollen Grain	49.0	0.0	42.1	0.0	104.8	0.0	697.0	0.0	71.2	0.0
<b>Carpels</b>	<b>E</b>	<b>SD</b>	<b>E</b>	<b>SD</b>	<b>E</b>	<b>SD</b>	<b>E</b>	<b>SD</b>	<b>E</b>	<b>SD</b>
Stigma tissue	367.7	51.6	741.4	36.9	122.8	14.1	504.6	91.5	912.3	165.2
Ovary tissue	594.4	148.8	953.0	118.1	171.0	14.7	794.2	118.2	2011.8	124.9
<b>Embryo development</b>	<b>E</b>	<b>SD</b>	<b>E</b>	<b>SD</b>	<b>E</b>	<b>SD</b>	<b>E</b>	<b>SD</b>	<b>E</b>	<b>SD</b>
Globular - Apical	264.7	67.9	140.5	58.9	78.7	20.4	157.7	47.9	179.3	32.8
Globular - Basal	151.8	78.0	497.7	375.1	138.7	20.8	252.6	48.1	100.1	38.0
Heart - Cotyledon	3447.3	3271.7	890.7	671.4	74.0	28.8	3302.8	3951.0	677.1	474.6
Heart - Root	274.0	180.4	4418.1	2522.4	73.5	15.2	190.7	123.7	711.9	407.1
Torpedo - Cotyledon	765.1	575.1	3087.4	2470.9	75.8	42.2	216.4	146.2	461.8	202.0
Torpedo - Root	207.7	148.0	61.4	70.7	164.6	165.3	249.6	68.9	281.8	173.1
Torpedo - Meristem	335.4	162.2	3139.7	2086.5	83.1	52.5	360.6	168.4	247.8	195.3
Torpedo - Apical	1317.2	128.4	2473.1	298.6	37.1	26.6	345.7	49.4	158.9	8.9
Torpedo - Basal	841.4	427.8	1576.9	717.4	84.0	31.3	328.8	156.8	301.6	96.9
<b>Seed development</b>	<b>E</b>	<b>SD</b>	<b>E</b>	<b>SD</b>	<b>E</b>	<b>SD</b>	<b>E</b>	<b>SD</b>	<b>E</b>	<b>SD</b>
Seeds Stage 3 w/ Siliques	409.0	10.4	365.6	9.6	67.9	4.1	245.5	3.1	647.8	18.2
Seeds Stage 4 w/ Siliques	675.9	12.4	881.7	20.2	126.8	13.8	381.5	4.0	575.1	49.3
Seeds Stage 5 w/ Siliques	976.8	14.6	1221.5	53.4	91.5	4.5	468.3	15.8	497.0	17.3
Seeds Stage 6 w/o Siliques	1485.9	40.6	1556.5	89.3	104.8	3.8	647.9	20.9	394.9	17.1
Seeds Stage 7 w/o Siliques	1320.9	25.3	1247.4	34.0	111.7	0.4	476.3	22.4	323.1	3.2
Seeds Stage 8 w/o Siliques	444.6	29.6	392.2	10.2	64.0	6.0	297.3	34.0	66.7	5.8
Seeds Stage 9 w/o Siliques	282.6	3.7	221.5	15.4	72.6	3.8	322.3	8.1	29.7	3.1
Seeds Stage 10 w/o Siliques	183.4	14.9	120.2	3.4	74.7	6.1	305.3	26.7	22.7	9.3
Dry seed	217.2	13.3	211.2	14.6	29.5	3.4	214.0	32.1	21.7	1.7
Imbibed seed. 24 h	523.4	37.3	271.7	44.1	30.6	9.4	269.8	6.9	492.0	22.1

The data were extracted from the eFP-browser platform (<http://bar.utoronto.ca/efp/cgi-bin/efpWeb.cgi>; Winter et al., 2007) and are based on microarray analyses. E expression; SD, standard deviation.

**Table 2:** Spatial and temporal expression profiles of genes involved in the metabolism of PEP and pyruvate in plastids of vegetative tissue.

Vegetative tissues	ENO1 At1g74030		PPT1 At5g33320		PPT2 At3g01550		PPDK At4g15530		PGyM At1g22170	
	E	SD	E	SD	E	SD	E	SD	E	SD
<b>Shoot</b>										
Hypocotyl Col-0	55.1	6.7	256.1	3.7	9.6	2.8	30.6	5.0	20.2	3.1
Mesophyll cells	8.8	2.2	230.8	197.6	100.2	65.6	308.2	152.2	30.9	4.8
Stem epidermis. top of stem	36.4	1.2	319.2	11.5	70.9	11.8	69.0	4.5	50.7	2.0
Stem epidermis. bottom of stem	27.7	0.3	318.6	1.2	54.9	7.8	223.0	4.5	29.3	2.5
Whole stem. top of stem	50.2	7.6	731.3	28.9	116.9	4.6	66.4	13.4	61.4	3.4
Whole stem. bottom of stem	111.0	0.3	1288.9	181.3	145.6	11.1	578.0	9.6	56.5	9.9
Xylem Col-0	25.2	3.3	254.4	32.5	10.2	1.5	116.2	1.5	11.8	0.7
Cork Col-0	24.9	4.0	236.1	2.7	12.0	0.5	246.9	8.8	12.5	3.5
Shoot Apex. Vegetative	303.5	11.5	808.7	13.8	65.1	8.0	5.4	2.3	69.2	4.0
Shoot Apex. Transition	208.1	10.6	633.4	28.9	65.9	4.1	1.0	0.3	61.2	4.4
Shoot Apex. Inflorescence	213.6	20.5	573.6	20.8	81.1	10.7	1.9	0.2	46.7	2.4
<b>Root</b>										
Root Stage III Stele	401.63	0	322.4	0	11.54	0	4.46	0	44.35	0.0
Root Stage III Endodermis	469.41	0	267.43	0	15.97	0	4.26	0	42.81	0.0
Root Stage III Cortex + Endodermis	506.28	0	475.27	0	8.96	0	2.9	0	49.02	0.0
Root Stage III Epidermal Artrichoblasts	725.9	0	364.82	0	6.04	0	3.86	0	54.74	0.0
Root Stage III Lateral Root Cap	421.52	0	265.21	0	12.74	0	13.51	0	48.23	0.0
Root Stage II Stele	538.59	0	472.62	0	15.63	0	3.37	0	62.99	0.0
Root Stage II Endodermis	629.48	0	392.03	0	21.63	0	3.22	0	60.81	0.0
Root Stage II Cortex + Endodermis	678.93	0	696.71	0	12.14	0	2.2	0	69.63	0.0
Root Stage II Epidermal Artrichoblasts	973.44	0	534.8	0	8.19	0	2.92	0	77.76	0.0
Root Stage II Lateral Root Cap	565.26	0	388.77	0	17.25	0	10.22	0	68.52	0.0
Root Stage I Stele	444.74	0	427.6	0	11.75	0	54.52	0	69.78	0.0
Root Stage I Endodermis	519.8	0	354.69	0	16.25	0	52.16	0	67.36	0.0
Root Stage I Cortex + Endodermis	560.63	0	630.34	0	9.12	0	35.55	0	77.13	0.0
Root Stage I Epidermal Artrichoblasts	803.82	0	483.86	0	6.15	0	47.18	0	86.14	0.0
Root Stage I Lateral Root Cap	466.77	0	351.74	0	12.96	0	165.13	0	75.9	0

Vegetative tissues	PKp1 At3g22960		PKp2 At5g52920		PKp3 At1g32440		ME4 At1g79750		PyT At2g26900	
	E	SD	E	SD	E	SD	E	SD	E	SD
<b>Shoot</b>	<b>E</b>	<b>SD</b>	<b>E</b>	<b>SD</b>	<b>E</b>	<b>SD</b>	<b>E</b>	<b>SD</b>	<b>E</b>	<b>SD</b>
Hypocotyl Col-0	739.4	37.9	253.1	18.9	81.8	5.9	346.5	14.3	107.2	8.4
Mesophyll cells	621.1	493.3	816.2	494.4	158.5	34.0	206.5	122.7	302.1	40.3
Stem epidermis. top of stem	765.0	59.3	513.9	4.5	128.0	14.9	511.2	3.4	614.2	17.7
Stem epidermis. bottom of stem	658.1	23.6	282.8	35.8	89.3	8.5	408.2	37.5	419.6	17.0
Whole stem. top of stem	773.1	75.5	410.9	58.4	90.0	1.2	393.8	31.4	1167.8	131.7
Whole stem. bottom of stem	577.9	65.2	293.7	20.3	141.1	5.1	380.6	24.9	591.2	1.8
Xylem Col-0	494.7	25.7	156.6	6.3	82.4	5.1	571.0	32.7	35.5	3.3
Cork Col-0	681.2	78.1	200.8	9.0	68.9	2.7	488.9	26.0	120.7	7.3
Shoot Apex. Vegetative	681.3	33.6	632.4	2.7	85.9	3.1	432.9	6.5	1016.2	17.3
Shoot Apex. Transition	526.6	17.5	519.5	8.6	65.5	7.8	445.3	3.9	856.9	45.1
Shoot Apex. Inflorescence	509.1	25.1	413.1	25.0	71.2	6.3	396.3	9.7	714.3	19.6
<b>Root</b>	<b>E</b>	<b>SD</b>	<b>E</b>	<b>SD</b>	<b>E</b>	<b>SD</b>	<b>E</b>	<b>SD</b>	<b>E</b>	<b>SD</b>
Root Stage III Stele	242.6	0.0	103.4	0.0	102.1	0.0	298.2	0.0	98.28	0
Root Stage III Endodermis	192.2	0.0	154.9	0.0	105.3	0.0	422.1	0.0	129.47	0
Root Stage III Cortex + Endodermis	209.0	0.0	201.1	0.0	119.2	0.0	415.2	0.0	131.4	0
Root Stage III Epidermal Artrichoblasts	304.7	0.0	208.5	0.0	98.8	0.0	414.2	0.0	99.48	0
Root Stage III Lateral Root Cap	127.8	0.0	112.8	0.0	71.2	0.0	390.8	0.0	65.36	0
Root Stage II Stele	447.4	0.0	325.0	0.0	113.7	0.0	310.4	0.0	134.57	0
Root Stage II Endodermis	354.4	0.0	486.8	0.0	117.2	0.0	439.4	0.0	177.27	0
Root Stage II Cortex + Endodermis	385.4	0.0	632.3	0.0	132.6	0.0	432.3	0.0	179.91	0
Root Stage II Epidermal Artrichoblasts	561.9	0.0	655.4	0.0	109.9	0.0	431.2	0.0	136.21	0
Root Stage II Lateral Root Cap	235.6	0.0	354.5	0.0	79.2	0.0	406.8	0.0	89.49	0
Root Stage I Stele	411.4	0.0	306.6	0.0	168.0	0.0	319.9	0.0	149.73	0
Root Stage I Endodermis	325.9	0.0	459.3	0.0	173.3	0.0	452.7	0.0	197.24	0
Root Stage I Cortex + Endodermis	354.4	0.0	596.6	0.0	196.0	0.0	445.4	0.0	200.18	0
Root Stage I Epidermal Artrichoblasts	516.8	0.0	618.4	0.0	162.5	0.0	444.3	0.0	151.56	0
Root Stage I Lateral Root Cap	216.7	0.0	334.5	0.0	117.1	0.0	419.1	0.0	99.57	0

The data were extracted from the eFP-browser platform (<http://bar.utoronto.ca/efp/cgi-bin/efpWeb.cgi>; Winter et al., 2007) and are based on microarray analyses. E expression; SD, standard deviation.

Table 3: List of primers

Primer name	Sequence
<b>Subcellular localization</b>	
ENO1-GFP sense	5' TCA TGG CTT TGA CTA CAA AAC CTC ACC ATC TT 3'
ENO1-GFP antisense	5' CAC CTT TAC CAC CAT AGA CGC TCT 3'
ENOC-GFP sense	5' TCA TGT CGT TGC AAG AGT ATT TAG ACA AGC A 3'
ENOC-GFP antisense	5' CAA GAT ACA TTC CTT TGT CTC CAT CA 3'
<b>Gateway Cloning</b>	
ENO1 GW-F	5' CAC CAT GGC TTT GAC TAC AAA ACC 3'
ENO1 GW-R	5' TGG TGA TCG GAA AGC TTC ACC G 3'
ENO1 GWstop-R	5' TCA TGG TGA TCG GAA AGC TTC ACC 3'
<b>GUS expression analysis</b>	
ENO1(A) sense	5' ACG GCA CAG TGT CTC TGG TTA CTA CTT TGC TAG TG 3'
ENO1(A) antisense	5' CCT CTT CGA TAC GGC AAA GCC ATT ACA CGA TAC CT 3'
ENO1(B) sense	5' CAC CGT AAT GGC TTT GCC GTA TCG AAG AGG AAC TCG 3'
ENO1(B) antisense	5' GAA CTT GCT CAC AGC TCC ACA TAA TTT CCT TCA 3'
ENO1(C) antisense	5' CAT AAA CTC TTG CAT AGC CAA ACT ATT CCC AGC ATG 3'
<b>T-DNA insertion screening</b>	
GABI LB pAC161 08409	5' ATA TTG ACC ATC ATA CTC ATT GC 3'
ENO1-1for	5' CAG GAT GAT TGG AGC TCA TGG 3'
ENO1-1rev	5' CGA CAT ATC TCT GAG CAT CTG 3'
ENO1-2for	5' ATC ATG TCT GAG ATT CCG TCG 3'
ENO1-2rev	5' CTG ACC TTC ACT TCC CAT CTG 3'
<b>Semi-quantitative RT-PCR analysis</b>	
ActinF-Lg	5' TAA CTC TCC CGC TAT GTA TGT 3'
ActinR-Lg	5' CCA CTG AGC ACA ATG TTA CCG TAC 3'
<b>Real-Time RT-PCR Analysis</b>	
Actin RL Fw	5' ATG GAA GCT GCT GGA ATC CAC 3'
Actin RL Rv	5' TTG CTC ATA CGG TCA GCG ATG 3'
ENO1 RL fw1	5' TGA ACT TGT GGC TCC AAA AC 3'
ENO1 RL_rv1	5' CTA ATA TCG CAT TAG CCC CGA GT 3'
KCR1 qPCR_for	5' CTC TCA TGG GTG CAG TTG TCT C 3'
KCR1 qPCR_rev	5' TTC TTT CTT CAT GGA GTC TTT TTG G 3'
KCR2 qPCR_for	5' CGC AGA TCG GAA TTG GAT C 3'
KCR2 qPCR_rev	5' ATA AAC TTC TTC TGC GAA GTC CG 3'

## Abbreviations

%	Percent
°C	Temperature (in Grad Celsius)
μ	micro-
½ MS	half strength MS medium
2,3-DPGA	2,3-Diphosphoglyceric acid
2-PGA	2-Phosphoglyceric acid
3-PGA	3-Phosphoglyceric acid
<i>A. thaliana</i>	<i>Arabidopsis thaliana</i>
ACCase	acetyl-CoA carboxylase
ACN	Astrablue, chrysoidin and neofuchsin
ACP	acyl carrier protein
Arabidopsis	<i>Arabidopsis thaliana</i>
Arg	Arginine
ATP	Adenosine triphosphate
bd	distilled twice
bp	base pairs
BSA	bovine serum albumin
C	carbon
c	Concentration
ca.	circa
CAM	Crassulacean acid metabolism
cDNA	copy DNA
CHC	cyclohexane carboxylic acid
CoA	Co-enzyme A
<i>cue1</i>	<i>chlorophyll a/b binding protein underexpressed</i>
DAF	days after flowering
DAHPS	3-deoxy-D-arabino-heptulosonate-7-phosphate synthase
DAPI	4'-6-diamidino-2-phenylindole
dATP	2-Desoxyadenosintriphosphate
DEPC	Diethylpyrocarbonate
DHCHC	Dihydroxycyclohexane carboxylic acid
DIC	Differential interference contrast
DMAPP	Dimethylallyl pyrophosphate
DMF	Dimethylformamide
DMSO	Dimethylsulfoxide
DNA	Desoxyribonucleic acid
dNTP	2-Desoxynucleoside triphosphate
DPBA	Diphenylborate-2-aminoethyl
DTT	1,4-Dithiothreitol
<i>E. coli</i>	<i>Escherichia coli</i>
EDTA	Ethylendiamine tetra acetate
ENO	Enolase
ER	Endoplasmic reticulum

Ery4P	Erythrose 4-phosphate
F <sub>2</sub>	second generation from crossings
FAE	Fatty acid elongation
FAS	Fatty acid synthesis
FPP	Farnesyl diphosphate
Fru	Fructose
FW	Fresh weight
g	Gram
GFP	Green fluorescent protein
Glc	Glucose
Glc6P	Glucose 6-phosphate
GPT	Glucose 6-phosphate/phosphate translocator
GUS	Glucouronidase
HCA	Hydroxy cinnamic acid
HEPES	N-2-Hydroxyethylpiperazin-N'-2-ethansulfonic acid
His	Histidine
HPLC-H <sub>2</sub> O	pure water
IPP	Isopentenyl pyrophosphate
IPTG	Isopropyl-β-D-thiogalactopyranoside
kb	kilo base
kDa	kilo Dalton
Km	Michaelis constant
L	Litre
LB	T-DNA Left border
LB	Luria/Bertani medium
Lys	Lysine
M	Molar (mol/l)
m	milli-
mA	Milliampere
MeOH	Methanol
MEP	2-C-methyl-D-erythritol 4-phosphate
min	Minutes
MOPS	4-morpholinopropane-sulphonic acid
mRNA	messenger RNA
MS-Medium	Murashige & Skoog-Medium
MVA	Mevalonate
n	nano
N	nitrogen
NAD	Nicotine amide
NAD(H)	Nicotine amide adenine dinucleotide (reduced)
NADP(H)	Nicotine amide adenine dinucleotidephosphate (reduced)
Ni-NTA	Nickel-nitrilotriacetic acid
nm	Nanometer
NO	Nitric oxide

OD	Optical density
OPPP	Oxidative pentose phosphate pathway
p	Pico
PAGE	polyacrylamide gel electrophoresis
PCR	polymerase-chain reaction
PEP	phosphoenolpyruvate
PEPCK	phosphoenolpyruvate carboxy kinase
PGyM	Phosphoglycero mutase
Phe	Phenylalanine
pI	Isoelectric point
PK	Pyruvate kinase
PK <sub>c</sub>	cytosolic pyruvate kinase
PK <sub>p</sub>	plastidic pyruvate kinase
PPDK	pyruvate, orthophosphate dikinase
PPT	phosphoenolpyruvate phosphate translocator
PVDF	polyvinylidene difluoride
PyT	Pyruvate transporter
RB	T-DNA right border
RNA	Ribonucleic acid
rpm	rounds per minute
rRNA	ribosomal RNA
RT	Reverse Transcription
RT	Room temperature
RT-PCR	Reverse Transcription Polymerase Chain Reaction
SAP	Shrimps Alkaline Phosphatase
SDS	sodium dodecylsulfate
SEB	seed extraction buffer
Suc	Sucrose
Ta	annealing temperature
TAE	Tris acetate EDTA
Taq	DNA polymerase (from <i>Thermophilus aquaticus</i> )
TB	Toluidine blue
TBE	Tris borate EDTA
TCA	Citric acid cycle
T-DNA	Transfer-DNA
TP	Triose phosphate
TPT	Triose phosphate/phosphate translocator
Tris	Tris-(hydroxymethyl)-aminomethane
Trp	Tryptophan
Tyr	Tyrosine
UV	ultraviolet
VLCFA	Very long chain fatty acids
w/v	Weight per volume
WT	Wild type
X-Gluc	5-bromo-4-chloro-3-indoyl-β-D-glucuronic acid

XPT	Xylulose phosphate/phosphate translocator
YEP	Yeast extract peptone medium

## Abstract

Phosphoenolpyruvate (PEP) plays an essential role in plant metabolism. In catabolic direction, it delivers ATP and pyruvate by the action of pyruvate kinase, which can be fed into mitochondrial respiration. PEP and pyruvate also represent essential precursors for anabolism i.e. PEP is the precursor for the synthesis of aromatic amino acids, secondary plant products and pyruvate is important for the production of fatty acids, branched-chain amino acids or isoprenoids *via* the mevalonate-independent way. These pathways are exclusively localized to the plastid stroma. PEP may be imported into the plastids via a PEP/phosphate translocator (PPT) of the inner envelope membrane or it may also be generated inside the stroma by complete plastid glycolysis starting from hexose phosphates. Glycolysis as the main route for PEP production involves the enzymatic sequence of 3-phosphoglycerate to PEP conversion catalyzed by phosphoglyceromutase (PGyM) and enolase (ENO). However, biochemical studies indicate that chloroplasts and a number of non-green plastids lack ENO and/or PGyM. The present study shows for the first time, the identification and functional characterization of the putative plastid localized ENO (ENO1) of *Arabidopsis thaliana*. The effect of a deficiency in PEP provision to plastids was investigated with the aid of double mutants defective in ENO1 and PPT1. Crosses between different alleles of *eno1* and the *chlorophyll a/b binding protein underexpressed (cuel)* mutant defective in PPT1 could not be obtained as double homozygous lines due to partial lethality of the gametophytes and constraints in sporophyte development, including a largely reduced oil production in the seeds, thus highlighting the essential role of PEP in plastids. The heterozygous *eno1* mutants in the homozygous *cuel* background (*cuel/eno1*[+/-]) revealed an aberrant segregation pattern, retarded vegetative growth and disturbed flower development attributed to a reduced *ENO1* gene dosage. Constitutive overexpression of *ENO1* could rescue the reticulate leaf and the stunted root phenotype of *cuel* and alleviate the diminished seed and oil production in the mutant. In contrast, wild-type plants overexpressing *ENO1* alone, could not improve seed quality and oil content.

## Zusammenfassung

Phosphoenolpyruvate (PEP) spielt eine zentrale Rolle im pflanzlichen Stoffwechsel. In kataboler Richtung liefert PEP über die Pyruvatkinase ATP und Pyruvat, welches als Substrat für die mitochondriale Atmung dient. PEP und Pyruvat stellen aber auch wichtige Vorstufen für anabole Prozesse dar, z.B. fließt PEP in die Synthese von aromatischen Aminosäuren und davon abgeleiteten sekundären Pflanzenstoffen ein, und Pyruvat wird für die Synthese von Fettsäuren, verzweigt-kettigen Aminosäuren oder Isoprenoiden über den Mevalonat-unabhängigen Weg benötigt. Diese Stoffwechselwege sind ausschließlich im Stroma der Plastiden lokalisiert. PEP kann über einen PEP/Phosphat Translokator der inneren Hüllmembran aus dem Cytosol in die Plastiden transportiert werden oder innerhalb der Plastiden über Glykolyse, ausgehend von Hexosephosphaten bereitgestellt werden. Die Glykolyse als Hauptweg zur Produktion von PEP beinhaltet die Umwandlung von 3-Phosphoglycerat zu PEP, die von der Phosphoglyceromutase (PgyM) und Enolase (ENO) katalysiert wird. Biochemische Studien zeigten, dass in Chloroplasten und in einer Reihe nicht-grüner Plastiden ENO und/oder PgyM. In der vorliegenden Arbeit wird erstmalig die Identifizierung und funktionelle Charakterisierung der putativen plastidären ENO (ENO1) aus *Arabidopsis thaliana* vorgestellt. Der Effekt einer PEP Defizienz in Plastiden wurde mithilfe von Doppelmutanten untersucht, denen ENO1 und PPT1 fehlte. Kreuzungen unterschiedlicher Allele der *eno1* und der *chlorophyll a/b binding protein underexpressed (cue1=ppt1)* Mutanten konnten nicht als doppelt-homozygote Linien erhalten werden, da sie eine partielle Letalität der Gametophyten sowie eine beeinträchtigte Entwicklung des Sporophyten aufwiesen, die mit einer deutlich verminderten Ölproduktion in den Samen einherging. Dieser Befund unterstützt die essentielle Rolle von PEP in Plastiden. Die heterozygoten *eno1* Mutanten im homozygoten *cue1* Hintergrund (*cue1/eno1*[+/-]) zeigten ein abnormes Segregationsmuster, eine Hemmung des Sprosswachstums und eine beeinträchtigte Blütenentwicklung bedingt durch eine Verminderung der ENO1 Gen dosis. Durch eine konstitutive Überexpression von ENO1 konnte der retikulierte Blatt-Phänotyp sowie die Wachstumshemmung der Wurzel der *cue1* Mutante gerettet werden. Die verminderte Produktion von Samen und des darin enthaltenen Öls wurde

aber nur partiell aufgehoben. Eine Überexpression von *ENO1* in Wildtyp-Pflanzen bewirkte hingegen weder eine Erhöhung der Samenproduktion noch der Ölgehalte.

## Acknowledgements

This is perhaps the easiest and hardest chapter that I have to write. It will be simple to name all the people that helped to get this done, but it will be tough to thank them enough. I will nonetheless try...

Foremost, I would like to express my sincere gratitude to my advisor Prof. Ulf-Ingo Flügge for his continuous support in my PhD research, for his patience, motivation, and immense knowledge. His guidance helped me at all times of research and writing of this thesis.

Dr. Rainer Häusler, my group leader, for his enthusiastic supervision, guidance, trenchant critiques, fruitful discussions throughout my PhD. I cannot thank him enough. Simply put: Rainer Rocks !!

### **I owe my gratitude to.....**

the IGS-GFG for funding, especially Dr. Isabell Witt for believing in me and for her insight and guidance through the years, Dr. Brigitte v.Wilcken-Bergmann for her support in official and 'un-official' matters, Ms. Gabrielle Thorn and Ms. Kathy Joergens for their timely help.

Prof. Dr. Sabine Waffenschmidt and Prof. Ute Höcker, for serving on my thesis committee. Thank you for your support and guidance.

Mr. Sigfried Werth, for his excellent support in photographic documentation of data and I would like to give due credit to the gardeners of the Institute of Botany for all their help.

### **My heartfelt thanks to.....**

PD Dr. Veronica Maurino, my source of enthusiasm and inspiration, whose constant encouragement in my thesis writing days enabled me to successfully complete the process !!

Dr. Markus Gierth, whose expertise, scientific know-how and lots of 'wise words' got me going till completion.

Vinod Vijayakumar, my confidant, for scientific help, continual love, support, brainstorming and for bearing my vent out frustrations with patience, as I travelled through this journey of PhD. I could not have made it through without him by my side.

My close friends Charles, Suresh, Ram and Murali for making me feel so good about my PhD ☺ and all my colleagues and friends that I have met in this home far away from home called 'Botanik Köln', without whose help and translations (Deutsch-English)....life would have been difficult !! I would also like to thank our Post-Docs Tamara, Frank, Rainer and Stephan for their advise, Anke for helping me start the work at AG Flügge. Kirsten, Diana, Sonja and Iris for all their technical help and my group mates Pia and Jessi for giving moral support and bearing with the *cue1* story ☺. Thank you one and all !

Lastly, I would like to thank God for his blessings, my parents and entire family especially my grandfather and uncle Udaya for encouraging my studies since childhood.

## Erklärung

Ich versichere, dass ich die von mir vorgelegte Dissertation selbständig angefertigt habe, die benutzten Quellen und Hilfsmittel vollständig angegeben und die Stellen der Arbeit - einschließlich Tabellen, Karten und Abbildungen -, die anderen Werken im Wortlaut oder dem Sinn nach entnommen sind, in jedem Einzelfall als Entlehnung kenntlich gemacht habe; dass diese Dissertation noch keiner anderen Fakultät oder Universität zur Prüfung vorgelegen hat; dass sie abgesehen von der unten angegebenen Teilpublikation noch nicht veröffentlicht worden ist sowie, dass ich eine solche Veröffentlichung vor Abschluss des Promotionsverfahrens nicht vornehmen werde. Die Bestimmungen dieser Promotionsordnung sind mir bekannt. Die von mir vorgelegte Dissertation ist von Prof. Dr. Ulf-Ingo Flügge betreut worden.

(Veena Prabhakar)

Köln

### Teilpublikation:

**Prabhakar, V., Löttgert, T., Gigolashvili, T., Bell, K., Flügge U.I., and Häusler R.E.** (2009). Molecular and functional characterization of the plastid-localized phosphoenolpyruvate enolase ENO1 from *Arabidopsis thaliana*. FEBS Letters 583: 983-991.

### Beiträge in Mitteilungsbänden von Tagungen

Prabhakar et al., (2009) 22. Tagung Molekularbiologie der Pflanzen, Dabringhausen, Germany.

Prabhakar et al., (2009) Plant Biology 2009, Honolulu, Hawaii, USA.

## Lebenslauf

### Veena Prabhakar

Geboren am 11.09.1978 in Bangalore, Indien.

Staatsangehörigkeit: Indisch

Familienstand: Verheiratet

### Schulbildung

June 1984 – März 1991

St. John's High School, Bangalore, Indien.

June 1991 – März 1994

Goodwills Girl's High School, Bangalore, Indien.

### Hochschulstudium

June 1994 – März 1996

Pre-University Examination, St.Anne's College, Bangalore, Indien.

June 1996 – März 1999

Bachelor of Science (Chemie, Botanik, Mikrobiologie) St.Anne's College, Bangalore University, Bangalore, Indien.

June 1998 – März 1999

Certificate in plant tissue culture, St.Joseph's Post Graduate and Research Centre, Bangalore University, Bangalore, Indien.

November 1999 – Juli 2001

Post Graduate Diploma in Biotechnology, Jain Institute of Vocational Studies, A division of Sri Bhagavan Mahaveer Jain Educational Trust, Bangalore, Indien.

Thema: Identification of cDNA involved in stress tolerance from an etiolated seedling library of salt stressed rice variety, Rasi.

November 2001 – Mai 2003

Master of Science in Botany, Annamalai University, Chidambaram, Tamil Nadu, Indien.

### Berufserfahrung

Juli 2001 – Juli 2004

Research Fellow, Avestha Gengraine Technologies Pvt. Ltd., Bangalore, Indien.

Juli 2004 – September 2006

Project Leader, Asian Centre for Genotyping, Avestha Gengraine Technologies Pvt. Ltd., Bangalore, Indien.

Ab März 2007

Doctorandin, AG Flügge, Universität zu Köln.